

**CRANFIELD UNIVERSITY**

**CLIVE M. ALABASTER**

**COLLEGE OF DEFENCE TECHNOLOGY**

**THE MICROWAVE PROPERTIES  
OF TISSUE AND OTHER LOSSY  
DIELECTRICS**

**PhD**

**CRANFIELD UNIVERSITY**

**COLLEGE OF DEFENCE TECHNOLOGY**

**DEPARTMENT OF AEROSPACE, POWER AND  
SENSORS**

**PhD THESIS**

**Academic Year 2003 - 2004**

**Clive M. Alabaster**

**THE MICROWAVE PROPERTIES OF TISSUE AND  
OTHER LOSSY DIELECTRICS**

**Supervisor: Prof. J. S. Dahele**

**Date of submission: March, 2004**

## ABSTRACT

This thesis describes work on the theoretical modelling and experimental measurement of the complex permittivity of dielectrics. The main focus of research has been into the characterisation of permittivity of planar and layered samples within the millimetre wave band. The measurement method is based on the free-space measurement of the transmission and reflection coefficients of samples. A novel analytical method of determining the transmission and reflection coefficients as functions of frequency arising from a generalised structure of planar dielectric layers is also described and validated. The analytical method is based on signal flow techniques. The measurement and analytical techniques have been applied in two main areas: firstly, the acquisition of new data on human skin in the band 57 to 100GHz and secondly, the detection and location of defects in composite materials for which a band of 90 to 100GHz was used.

Measurements have been made on the complex permittivity of a single sample of excised human skin fixed in formaldehyde. The experimental results have been corrected to account for the fixing process in formaldehyde and are projected to body temperature. This data is, to the best of the author's knowledge, the first of its kind to be published. Predicted skin permittivity based on various relaxation models varies widely and only partially fits the measured data. The experimental results have been used to determine the parameters of a Cole-Cole function which gives the best fit to the measured data. The measured skin data has also been used to calculate power deposition in skin exposed to millimetre wave radiation. This work concludes that a skin surface temperature rise of only  $0.2^{\circ}\text{C}$  results from a thirty second exposure to signals of  $100\text{W/m}^2$ .

Experimental work with fibreglass composite samples has shown that defects such as delaminations, voids, matrix cracks and improper cure result in resolvable differences in the dielectric properties of the samples at 90 – 100GHz. The measurement technique is particularly sensitive to the detection of cracks and its spatial resolution is 20mm or better. Whilst confirming the general conclusions of previously published work, the specific findings of this study are novel.

*Keywords:* millimetre-wave, millimeter-wave, free-space, skin, dielectrics, permittivity, layered dielectrics, measurement of permittivity, composites, defect detection.

**ACKNOWLEDGEMENTS**

I am indebted to the following for their help and support:

Professor J. S. Dahele, my PhD supervisor, for his help, encouragement and advice.

Mr P. Haskins for his help around the microwave laboratory.

Dr R. A. Badcock, for his help and advice concerning the work on composite materials.

Dr P. Ziopoulos, for his help and advice with the biological samples

Ms V. Wise, for her help with the biological samples and manufacture of the composites.

Dr E. J. Hughes, for his help with MATLAB and for his general advice.

Mr R. S. Picton, head of the radar group, for protecting my time to work on this thesis.

Dr R. Zbikowski, for the translation of the Russian text of reference 123.

Birmingham University electrical engineering department, for access to their VNA facilities.

Anritsu Corporation for the loan of the 65GHz VNA.

Mr B. Duguid and the staff of the workshops for the manufacture of various parts.

The NDRI, PA, USA and an anonymous, white, 50 year old female for the provision of the human skin sample.

## CONTENTS

CHAPTER ONE: INTRODUCTORY REVIEWS .....	1
1.1 INTRODUCTION .....	1
1.1.1 Brief Overview of Work.....	1
1.1.2 Brief Overview of Thesis .....	2
1.2 REVIEW OF POLAR DIELECTRIC BEHAVIOUR.....	4
1.2.1 Dielectrics.....	4
1.2.2 General Theory Concerning Dielectrics .....	5
1.2.3 The Theoretical Model of Dielectric Relaxation.....	6
1.3 REVIEW OF MICROWAVE AND MMW PROPERTIES OF TISSUES .....	13
1.3.1 Biological Tissues.....	13
1.3.2 The Microwave Properties of Tissue.....	15
1.3.3 Millimetre Wave Permittivity of Tissue .....	17
1.4 REVIEW OF APPLICATIONS .....	20
1.4.1 Introduction .....	20
1.4.2 RF Hyperthermia & Safety Assessment of Power Deposition.....	21
1.4.3 Passive MMW Imaging .....	24
1.4.4 Automobile Radar.....	25
1.4.5 Wireless LANs .....	26
1.4.6 Wearable Computing.....	26
1.4.7 Dielectric Imaging of Composites .....	27
1.5 REVIEW OF PERMITTIVITY MEASUREMENT TECHNIQUES AT MMW FREQUENCIES.....	28
1.5.1 Introduction .....	28
1.5.2 Free-space techniques .....	28
1.5.3 Waveguide techniques .....	31
1.5.4 Termination of a coaxial line probe.....	33
1.5.5 Perturbation of resonant structures .....	35
1.5.6 Other methods.....	38
1.5.7 Comparison of methods.....	38

1.6 CHAPTER SUMMARY .....	39
---------------------------	----

CHAPTER TWO: THE ANALYSIS OF LAYERED DIELECTRICS .....	41
--	----

2.1 INTRODUCTION .....	41
2.2 GENERAL ANALYSIS OF N-LAYERS OF ARBITRARY THICKNESS .....	42
2.2.1 Single Dielectric Layer in Free Space .....	43
2.2.2 Two Dielectric Layers in Free Space .....	47
2.2.3 General Case of $n$ Dielectric Layers.....	51
2.2.4 Specific Formulation of Three Dielectric Layers .....	51
2.3 VALIDATION OF THE THREE DIELECTRIC LAYER MODEL .....	56
2.4 CHAPTER SUMMARY .....	58

CHAPTER THREE: THE MEASUREMENT OF PERMITTIVITY IN THE MILLIMETRE WAVE BAND .....	59
---	----

3.1 INTRODUCTION .....	59
3.2 SELECTION OF EXPERIMENTAL METHOD.....	59
3.3 THEORY .....	61
3.4 EXPERIMENTAL SET UP .....	63
3.5 DATA PROCESSING .....	65
3.6 VALIDATION OF EXPERIMENTAL METHOD.....	67
3.7 EXPERIMENTAL TOLERANCE .....	70
3.8 CHAPTER SUMMARY .....	71

CHAPTER FOUR: THE PERMITTIVITY OF HUMAN SKIN IN THE MILLIMETRE WAVE BAND .....	73
4.1 INTRODUCTION .....	73
4.2 PREDICTIONS OF DATA TO THE MMW BAND .....	74
4.2.1 Introduction .....	74
4.2.2 Permittivity of Water in the MMW Band.....	74
4.2.3 Modelling the Dielectric Properties of Human Skin .....	77
4.2.3.1 Predicted Data From 4-Term Cole-Cole Function of Gabriel.....	78
4.2.3.2 Single and Double Term Debye Predictions of Kuznetsov.....	82
4.2.3.3 Predicted Data From Single Debye Relaxation.....	83
4.2.3.4 Single Debye Relaxation Parameters of Ghodgaonkar and Daud.	87
4.2.3.5 Comparison Between Data of the Various Models .....	89
4.3 PERMITTIVITY MEASUREMENTS ON HUMAN SKIN IN THE MMW BAND .....	90
4.3.1 Introduction .....	90
4.3.2 Initial Tests on Bovine Pericardium and Porcine Skin (57 to 63 GHz) .....	90
4.3.3 Human Skin Sample Preparation.....	91
4.3.4 Measurements on Human Skin (76 to 100 GHz) .....	92
4.3.5 Measurements on Human Skin (57 to 63 GHz) .....	93
4.3.6 Effects of Formaldehyde Fixing .....	93
4.3.7 Results & Discussion.....	94
4.3.7.1 Initial Results on Animal Tissues.....	94
4.3.7.2 Human Skin (76 to 100GHz).....	94
4.3.7.3 Error Analysis on Human Skin Data (76 to 100GHz).....	97
4.3.7.4 Human Skin (57 to 63GHz).....	99
4.3.7.5 Error Analysis on Human Skin Data (57 to 63GHz).....	101
4.3.7.6 Projecting Results to 37 <sup>0</sup> C, Unfixed.....	103
4.3.7.7 The Effects of Fixing in Formaldehyde.....	103
4.3.7.8 Summary of Results on Human Skin .....	104
4.3.8 Comparison Between Predicted and Measured Results .....	106
4.4 PROPOSED MODEL FOR HUMAN SKIN.....	107

4.5 POWER DEPOSITION IN HUMAN SKIN .....	109
4.6 CHAPTER SUMMARY .....	113

## CHAPTER FIVE: DETECTION AND LOCATION OF DEFECTS IN COMPOSITES .....

115

5.1 INTRODUCTION .....	115
5.2 SAMPLE PREPARATION.....	117
5.3 ULTRA-SOUND TESTING.....	118
5.4 EXPERIMENTAL TESTS .....	121
5.5 RESULTS / DISCUSSION .....	123
5.5.1 Composite Samples #1 to #18 .....	123
5.5.2 Experimental Tolerances and Repeatability (Samples #1 to #18).....	127
5.5.3 Three-Layered Structure .....	128
5.5.4 Error Analysis (Three Layered Structure) .....	129
5.5.5 Sensitivity Analysis of Three Layered Structure.....	130
5.5.6 Modelled Three Layer vs. Modelled Single Layer.....	131
5.6 CHAPTER SUMMARY .....	133

## CHAPTER SIX: CONCLUSIONS .....

135

6.1 CONCLUSIONS ARISING FROM CHAPTER ONE.....	135
6.2 CONCLUSIONS ARISING FROM CHAPTER TWO.....	137
6.3 CONCLUSIONS ARISING FROM CHAPTER THREE.....	138
6.4 CONCLUSIONS ARISING FROM CHAPTER FOUR .....	141
6.5 CONCLUSIONS ARISING FROM CHAPTER FIVE.....	144
6.6 FUTURE POSSIBILITIES .....	148

## REFERENCES .....

151

**APPENDIX A: PUBLISHED PAPERS .....** **A1**

Free Space Measurement of Permittivity .....	A3
Permittivity of Human Skin in the Millimetre Wave Band.....	A7
Damage and Defect Detection in Composites Using Millimetre Wave Permittivity Measurement .....	A9

**APPENDIX B: UNPUBLISHED REPORTS .....** **B1**

Final Report on Permittivity Measurements of Soil at Hurn and Barnsfield Heath Test Sites. ....	B3
Further Work Since M.Phil. to Ph.D. Transfer.....	B19

**APPENDIX C: PROGRAM LISTINGS .....** **C1**

Debye1.m.....	C3
TR3.m.....	C4
P3.m .....	C6
P5.m .....	C8
D3TR.m.....	C11
TR1.m.....	C14
FindEi.m.....	C15
CCfit.m.....	C17
Trise.m.....	C19

## LIST OF TABLES

Table 3-1: Permittivity Results at J Band.....	68
Table 3-2: Permittivity Results at 60GHz .....	69
Table 4-1: Measured Permittivity data for Water in the MMW band.....	75
Table 4-2: Temperature gradients.....	76
Table 4-3: Model Input Parameters for Water.....	76
Table 4-4: Modelled Results for Water .....	77
Table 4-5: Model Parameters <sup>[43]</sup> .....	79
Table 4-6: Modelled Relaxation Frequencies <sup>[43]</sup> .....	79
Table 4-7: Modelled Dielectric Data of dry skin from Gabriel <sup>[43]</sup> .....	80
Table 4-8: Modelled Dielectric Data of wet skin from Gabriel <sup>[43]</sup> .....	80
Table 4-9: Predicted Permittivity of Skin, Kuznetsov <sup>[123]</sup> .....	83
Table 4-10: Modelled Permittivity of Skin Based on Single Debye Relaxation.....	85
Table 4-11: Summary of Predicted Permittivity ( <i>Human skin, dry, 37°C</i> ) .....	89
Table 4-12: Initial Results of Animal Tissues .....	94
Table 4-13: Measured Data on Human Skin at 30°C (76 to 100GHz).....	95
Table 4-14: Permittivity Results for Human Skin at 30°C (76 to 100GHz).....	96
Table 4-15: Statistical Summary of Measured Data on Human Skin (57 to 63GHz) .....	99
Table 4-16: Statistical Summary of Permittivity Results on Human Skin (57 to 63GHz) .....	100
Table 4-17: Changes in Porcine Skin Due to Formaldehyde Fixing.....	103
Table 4-18: Summary of Permittivity Results on Dry Human Skin .....	105
Table 4-19: Target Data for Cole-Cole Fit .....	107
Table 4-20: Best Fit Cole-Cole Parameters.....	107
Table 4-21: Comparison of Model Parameters For Single Term Debye Function .....	108
Table 4-22: Power Deposition in Skin .....	109
Table 4-23: Surface Temperature Model Parameters.....	111

Table 5-1: Sample details .....	118
Table 5-2: Samples 1 to 11 & 13 to 18 Permittivity Results.....	123
Table 5-3: Sample 12 Permittivity Results.....	124
Table 5-4: Sensitivity Analysis of Modelled Results on Three Layered Structure.....	130

## LIST OF FIGURES

Figure 1-1: Complex Permittivity .....	5
Figure 1-2: Transient Response of Polar Dielectric .....	7
Figure 1-3: Locus of Complex Permittivity .....	10
Figure 1-4: $\frac{\varepsilon'_r - \varepsilon_\infty}{\varepsilon_s - \varepsilon_\infty}$ vs. $\log_{10}\left(\frac{f}{f_c}\right)$ .....	11
Figure 1-5: $\frac{\varepsilon_r''}{\varepsilon_s - \varepsilon_\infty}$ and $\frac{\sigma_s}{\omega\varepsilon_0}$ vs. $\log_{10}\left(\frac{f}{f_c}\right)$ .....	11
Figure 1-6: Equivalent Circuit.....	12
Figure 1-7: W-Band Unbalanced Bridge Spectrometer <sup>[90]</sup> .....	30
Figure 1-8: The Brewster Angle.....	31
Figure 1-9: Waveguide Method <sup>[21]</sup> .....	33
Figure 1-10: Coaxial Probe .....	34
Figure 1-11: Resonant cavity geometry.....	36
Figure 1-12: $ S_{11} $ response of empty cavity (black) and that with sample (red) .....	37
Figure 1-13: Open Resonator Experimental Set-Up <sup>[115]</sup> .....	37
Figure 2-1: Multiple Reflections Between Two Dielectric Boundaries .....	43
Figure 2-2a: Signal Flow Diagram (input on lhs) .....	46
Figure 2-2b: Signal Flow Diagram (input on rhs) .....	46
Figure 2-3: Flow Diagram for Two Dielectric Layers .....	47
Figure 2-4: Three Dielectric Layers .....	52
Figure 2-5: Three Layer Reflection Coefficients .....	53
Figure 2-6: Three-Layered Dielectric Structure .....	56
Figure 3-1: Experimental Set Up.....	63
Figure 3-2: MMW Equipment (60GHz).....	65
Figure 3-3a: Simulated and Measured Reflection Coefficients of PTFE .....	67
Figure 3-3b: Simulated and Measured Transmission Coefficient of PTFE .....	67

Figure 4-1: Modelled Dielectric Data of dry skin from Gabriel <sup>[43]</sup> .....	81
Figure 4-2: Modelled Dielectric Data of wet skin from Gabriel <sup>[43]</sup> .....	81
Figure 4-3: Single Debye Relaxation (Dry skin, 37 <sup>0</sup> C).....	85
Figure 4-4: Single Debye Relaxation (Dry skin, 20 <sup>0</sup> C).....	86
Figure 4-5: Single Debye Relaxation (Wet skin, 37 <sup>0</sup> C) .....	86
Figure 4-6: Single Debye Relaxation (Wet skin, 20 <sup>0</sup> C) .....	87
Figure 4-7: Skin Surface Temperature Rises.....	112
Figure 5-1: Samples 1 to 11 & 13 to 18 Ultra-Sound Images .....	119
Figure 5-2: Sample #12 Ultra-Sound Images .....	120
Figure 5-3: Sample #12 Map .....	121
Figure 5-4: Summary of Permittivities of Samples #1 to #11 .....	126
Figure 5-5: Measured (+) and Simulated Transmission and Reflection Coefficients (solid lines) of Three Layered Structure .....	128
Figure 5-6: Measured (red +) and Simulated Data (blue solid lines) for Nominal Values and Extremes of Tolerances for the Three Layered Structure .....	129
Figure 5-7: Modelled Reflection (Left) and Transmission (Right) Coefficients of Dielectric Structures.....	131

# GLOSSARY

## Abbreviations

EM	Electro Magnetic
dB	Decibel(s) ( $= 10 \log_{10}\{\text{ratio}\}$ )
FMCW	Frequency Modulated Continuous Wave
GHz	Giga Hertz ( $= 10^9$ cycles per second)
HF	High Frequency (= 3 to 30 MHz)
ICNIRP	International Commission on Non-Ionizing Radiation Protection
IEE	The Institute of Electrical Engineers
IEEE	The Institute of Electrical and Electronic Engineers
IR	Infra-Red
J-band	NATO frequency band of 10 to 20GHz
kHz	Kilo Hertz ( $= 10^3$ cycles per second)
LAN	Local Area Network
MATLAB®	Contraction of Matrix Laboratory, a mathematical programming language distributed by the MathWorks Inc.
MDF	Medium Density Fibre (a construction material).
MHz	Mega Hertz ( $= 10^6$ cycles per second)
MMW	Millimetre Wave (or Millimeter Wave)
NDRI	National Disease Research Interchange
NRPB	National Radiological Protection Board (UK regulatory body)
PTFE	Polytetrafluoroethylene, also known as Teflon®
Q-Factor	Quality Factor
RF	Radio Frequency (= 300kHz to 300GHz)
rms	root mean squared
s-parameters	Scattering Parameters (as used in the analysis of RF networks) e.g. S <sub>11</sub> and S <sub>21</sub>
SAR	Specific Absorption Rate
TI	Thermal Imaging/Imager
VHF	Very High Frequency (= 30 to 300 MHz)
VNA	Vector Network Analyser

## Medical Terminology

*Cell membrane* = Outer layer of cells. In separating the materials inside and outside the cell, the membrane exhibits capacitance.

*Chemotherapy* = Cancer therapy using drugs.

*Collagen* = A fibrous protein substance found in many tissues and a major constituent of the pericardium and skin.

*Epidermis* = The outer layer of the skin

*Hyperthermia* = Elevated body temperature, *RF Hyperthermia* = heating the body by application of an RF signal.

*In-vivo* = (experimentation on) living tissue still part of the larger organism.

*In-vitro* or *Ex-vivo* = (experimentation on) tissue excised from the organism.

*Oncology* = Medical study and treatment of tumours.

*Pericardium* = the sac which surrounds the heart.

*Phantom* = A material or structure made from such materials designed to mimic the properties of a biological tissue/structure.

*Radio therapy* or *Radiation therapy* = Cancer therapy using ionising radiation.

## Units

Standard International units have been used throughout, except where stated.

Standard multipliers are also used i.e.

$$\begin{array}{ll} m \text{ (milli)} = 10^{-3} & k \text{ (Kilo)} = 10^3 \\ \mu \text{ (micro)} = 10^{-6} & M \text{ (Mega)} = 10^6 \\ n \text{ (nano)} = 10^{-9} & G \text{ (Giga)} = 10^9 \\ p \text{ (pico)} = 10^{-12} & \end{array}$$

Ratios are often expressed in Decibels (dB).

## Symbols

Standard symbols have been used throughout and are summarised below. There are a few instances whereby the same symbol is used to represent two quantities. This results from some unfortunate coincidences in which certain letters from the Latin and Greek alphabets are the commonly accepted symbols for two or more quantities. Footnotes are included where necessary in order to clarify the meanings of these symbols.

C	specific heat	$\alpha$	attenuation constant
D	electric displacement	$\alpha$	Cole-Cole distribution parameter
D	dimension of antenna aperture	$\beta$	phase constant
E	electric field	$\gamma$	propagation constant
e, exp	the exponential function	$\gamma$	a dielectric dispersion
f	frequency	$\delta$	a dielectric dispersion
$I_0$	incident power density	$\delta$	skin depth
j	imaginary number = $\sqrt{-1}$	$\Delta$	difference
J	Joules	$\tan \delta$	the loss tangent
k	the propagation constant	$\epsilon$	permittivity
k	thermal conductivity	$\lambda$	wavelength
m	metre	$\mu$	magnetic permeability
Q	energy (see also Q-factor)	$\pi$	pi ( $\sim 3.141592654$ )
r (R)	reflection coefficient (in dB)	$\rho$	specific density
s	seconds	$\sigma$	electrical conductivity
s	Laplacian complex frequency	$\tau$	relaxation time constant
S	Seimens	$\tau$	thermal time constant
t	thickness	$\omega$	angular frequency
t (T)	transmission coefficient (in dB)		
T	temperature	$\infty$	infinity
W	Watts	$\nabla$	the del operator

Subscripts and superscripts may be used with the symbols above to modify their meaning or to represent specific quantities, as explained in the text.

## CHAPTER ONE: INTRODUCTORY REVIEWS

### 1.1 INTRODUCTION

#### 1.1.1 Brief Overview of Work

This thesis describes work on the theoretical modelling and experimental measurement of the complex permittivity of dielectrics. The main focus of research has been into the characterisation of permittivity of layered planar samples within the millimetre wave (MMW) band, formally defined as 30 to 300GHz. The measurement method is based on the free-space measurement of the transmission and reflection coefficients of samples. The measurement technique has been applied in two main areas: firstly, the acquisition of new data on human skin in the band 60 to 100GHz and secondly, the detection and location of defects in composite materials for which a band of 90 to 100GHz was used. An analytical technique to describe multi-layered dielectrics is also presented and has been used to model the frequency dependence of transmission and reflection coefficients arising from single and multiple layers of planar dielectrics. This analysis has been employed in the determination of the complex permittivity of single dielectric layers such as skin and composites and in the detection of a large void defect within a composite material. The skin data is supported by modelled data from standard relaxation functions to find the frequency dependence of the permittivity of skin. The experimental results are used to assess which models and model parameters result in a best fit to the measured data. The measured skin data has also been used to calculate power deposition in skin exposed to radiation in these bands and the resultant skin surface temperature rises. The work with composite materials has investigated the feasibility of detecting defects in such materials in a non-contacting manner. It is shown that the dielectric characteristics of defective composite materials in the MMW band may be resolved from nominally ideal material.

A brief summary of an early study of radio frequency (RF) hyperthermia and permittivity measurements at centimetric wavelengths using resonant cavities and coaxial probes is also presented.

### 1.1.2 Brief Overview of Thesis

The remainder of this Chapter contains literature reviews and reviews of the underlying theory. It starts with a review of some basic concepts of electromagnetics and permittivity and explains some of the physical characteristics of materials which determine their dielectric behaviour. A discussion of the relaxation phenomena of polar molecules/samples such as water and biological tissues then follows and the Debye and Cole-Cole equations are formulated. There then follows a review of the dielectric properties of biological materials and, in particular, human tissues in the microwave band. This includes recently published data for human skin in the MMW band. An interest in the MMW properties of tissue and the dielectric imaging of composite materials is then justified in a short series of reviews of the applications of such data. A brief review of the methods by which permittivity may be measured at microwave frequencies is then given.

Chapter Two describes an analytical method to model the transmission and reflection coefficients arising from a general structure of multiple dielectric layers. The specific case of three dielectric layers is formulated and validated. This analysis has been developed to support the work on the measurements of single and multiple planar dielectric layers of Chapters Four and Five.

Chapter Three is concerned with the measurement of permittivity in the MMW band. Various candidate techniques are considered and the choice of the free-space technique is justified. A theoretical section provides the theory which underpins the measurement technique. The experimental set-up, procedure, calibration and data processing techniques are then described.

Chapter Four reports on the measured permittivity of human skin in the MMW band. A variety of models based on relaxation phenomena published in the literature are also discussed and used to model the dielectric characteristics of skin in the MMW band. The modelled and measured data are compared in order to deduce which model and model parameters result in the best agreement. Further calculations are made using the measured data to calculate the power deposition in skin and surface temperature rises resulting from exposure to RF energy in the MMW band.

Chapter Five describes the work on the detection and location of defects within composite materials. This chapter is a further application of the theoretical and experimental methods described in the earlier chapters. Measured data in the 90 to 100GHz band is compared with ultra-sound images of the samples and the predictions from the three layered model (Chapter Two). This chapter concludes that in many cases the measurement technique is able to resolve defective material from nominally ideal material.

Chapter Six summarises the conclusions arising from the previous chapters and describes the future possibilities of this work.

A Chapter summary is provided at the end of each chapter.

Considerable use is made of Appendices which are referred to in the main body of the thesis. These Appendices contain copies of published papers and unpublished reports resulting from this work plus listings of the programs written and used.

## 1.2 REVIEW OF POLAR DIELECTRIC BEHAVIOUR

### 1.2.1 Dielectrics

Propagation of electromagnetic waves in materials such as dielectrics and conductors is determined by their electrical parameters. In the case of dielectrics, chief amongst these is the complex permittivity,  $\epsilon$ , of the dielectric material which describes its ability to support an electric field. An electric field results from a potential difference supported across a medium and is therefore not possible within a pure conductor. Free space has dielectric properties by virtue of the energy temporarily borrowed to create short lived virtual charges to support an electric field. Many other dielectrics exhibit phenomena which also contribute to their permittivity such as the ability to support current flow (both ionic and displacement currents) and molecular polarisation. It is normal to refer to the *relative permittivity*,  $\epsilon_r$ , of a dielectric as being its permittivity with respect to that of free space,  $\epsilon_0$ , such that:

$$\epsilon = \epsilon_r \cdot \epsilon_0 \quad (1.1)$$

The relative permittivity of a dielectric is defined as the factor by which the capacitance of a capacitor increases when the volume between and around its plates is filled with the dielectric as compared with free space. It is known that the permittivity of a dielectric is determined by its molecular/atomic structure but no theory exists to relate the two. It is also known that permittivity is often (but by no means always) frequency and temperature dependent, since certain phenomena which determine its permittivity are functions of frequency and temperature. Furthermore, the permittivity differs for the various phases of the material which is unsurprising since the concentration of particles and their bonding differs in each phase. Various theories have been proposed to describe the permittivity of mixed dielectrics from its constituent ingredients, concentration and particle size and shape. These have been useful in describing the behaviour of solutions, suspensions and complex structures of dielectrics.

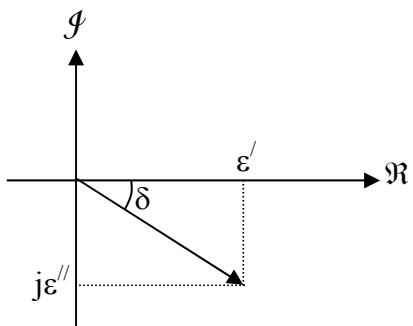
### 1.2.2 General Theory Concerning Dielectrics

The parameters of greatest interest are the conductivity,  $\sigma$ , and the permittivity,  $\epsilon$ , since these govern the dielectric attenuation. Permittivity is a complex quantity, whereby:

$$\epsilon = \epsilon' - j\epsilon'' = D/E \quad (1.2)$$

Where  $D$  is the electric flux density and  $E$  the electric field strength and  $\epsilon'$  is the dielectric constant,  $\epsilon_0 (= 8.854191 \times 10^{-12} \text{ Fm}^{-1})$  the permittivity of free space and  $\epsilon_r'$  the relative dielectric constant and  $\epsilon'' = \epsilon_0 \epsilon_r''$  is the dielectric loss factor and  $\epsilon_r''$  the relative dielectric loss factor of the dielectric.

The real and imaginary parts of permittivity may be depicted on a set of orthogonal axes, as in Figure 1-1, below:



Dielectric loss can also be expressed in terms of the loss tangent:

$$\tan \delta = \frac{\epsilon''}{\epsilon'} = \frac{\sigma}{\omega \epsilon_r' \epsilon_0} \quad (1.3)$$

and is high for a lossy dielectric.

Figure 1-1: Complex Permittivity

EM propagation is characterised by the propagation constant  $\gamma = \alpha + j\beta$  where  $\alpha$  (the real part of  $\gamma$ ) is the attenuation factor and  $\beta$  (the imaginary part of  $\gamma$ ) is the phase constant. From Maxwell's equations one can derive the wave equation which has a general solution given by:

$$\gamma = j\omega\sqrt{\mu\epsilon} \quad (1.4)$$

where  $\mu$  is the permeability, which is equal to that of free space in non-magnetic materials i.e.  $\mu = \mu_0 = 4\pi \times 10^{-7} \text{ Hm}^{-1}$ .

From (1.2) and (1.3) we have  $\varepsilon = \varepsilon' (1 - j \tan \delta)$  (1.5)

Substituting (1.5) into (1.4) gives

$$\begin{aligned} \gamma &= j\omega\sqrt{\mu\varepsilon'(1-j\tan\delta)} \\ \therefore \quad \gamma &= j\omega\sqrt{\mu\varepsilon'}(1-j\tan\delta)^{1/2} \end{aligned}$$

Performing a binomial expansion of the bracketed term on the right hand side and approximating the expansion by considering the first two terms only gives:

$$\begin{aligned} \gamma &\approx j\omega\sqrt{\mu\varepsilon'}\left(1-\frac{j\tan\delta}{2}\right) \\ &= j\omega\sqrt{\mu\varepsilon'} + \frac{\omega\sqrt{\mu\varepsilon'}}{2}\tan\delta \end{aligned}$$

Whose real part is:

$$\alpha = \frac{1}{2}\omega\sqrt{\mu\varepsilon'}\tan\delta \quad (1.6)$$

This term describes the attenuation of RF energy through a lossy dielectric.

### 1.2.3 The Theoretical Model of Dielectric Relaxation

The orientation of polar molecules changes in sympathy with an applied radio frequency (RF) E-field. This phenomenon has a significant effect in determining the permittivity of the material. The ability of the polar molecules to align with the applied E-field at RF frequencies is determined by the kinematics of the molecular structure and is described by relaxation theory. An excellent description of relaxation phenomena and its application to dielectric behaviour is given by Williams and Thomas<sup>[1]</sup>.

The theoretical analysis presented here is characterised, initially, by a single relaxation process centred around a single relaxation time constant. The description which follows is taken largely from Foster and Schwan<sup>[2]</sup>.

In the simplest case, the polarisation of a sample will relax towards the steady state as a first order process characterised by a single time constant,  $\tau$ . Thus the transient response looks like that of Figure 1-2 opposite:

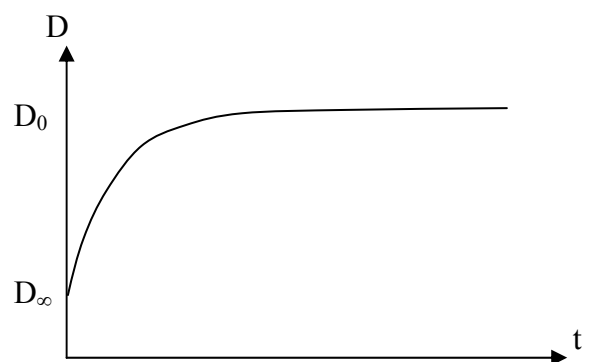


Figure 1-2: Transient Response  
of Polar Dielectric

This has the form:

$$D = D_{\infty} + (D_0 - D_{\infty}) \left(1 - e^{-t/\tau}\right) \quad (1.7)$$

where  $D$  = Electric displacement

$D_0$  = Final value of  $D$

$D_{\infty}$  = Initial value of  $D$

Since: where

$$D = \epsilon_r \epsilon_0 E$$

$\epsilon_r$  = complex relative permittivity

$$D_{\infty} = \epsilon_{\infty} \epsilon_0 E$$

$\epsilon_{\infty}$  = relative permittivity at infinite frequency

$$D_0 = \epsilon_s \epsilon_0 E$$

$\epsilon_s$  = static relative permittivity

We can re-write (1.7) in terms of permittivity:

$$\epsilon_r \epsilon_0 E = \epsilon_{\infty} \epsilon_0 E + (\epsilon_s \epsilon_0 E - \epsilon_{\infty} \epsilon_0 E) \left(1 - e^{-t/\tau}\right)$$

Cancelling  $\epsilon_0 E$  terms both sides leaves:

$$\epsilon_r = \epsilon_{\infty} + (\epsilon_s - \epsilon_{\infty}) \left(1 - e^{-t/\tau}\right)$$

$$\epsilon_r = \epsilon_{\infty} + (\epsilon_s - \epsilon_{\infty}) - (\epsilon_s - \epsilon_{\infty}) e^{-t/\tau}$$

Taking Laplace transforms both sides to convert to the frequency ( $s$ ) domain:

$$\frac{\varepsilon_r}{s} = \frac{\varepsilon_\infty}{s} + \frac{(\varepsilon_s - \varepsilon_\infty)}{s} - \frac{(\varepsilon_s - \varepsilon_\infty)}{s + 1/\tau}$$

Multiplying all terms by  $s$ :

$$\varepsilon_r = \varepsilon_\infty + (\varepsilon_s - \varepsilon_\infty) - \frac{(\varepsilon_s - \varepsilon_\infty)s}{s + 1/\tau}$$

Rearranging:

$$\varepsilon_r = \varepsilon_\infty + \frac{\tau(\varepsilon_s - \varepsilon_\infty)(s + 1/\tau) - (\varepsilon_s - \varepsilon_\infty)s\tau}{1 + s\tau}$$

$$\varepsilon_r = \varepsilon_\infty + \frac{s\tau\varepsilon_s - s\tau\varepsilon_\infty + \varepsilon_s - \varepsilon_\infty - s\tau\varepsilon_s + s\tau\varepsilon_\infty}{1 + s\tau}$$

$$\varepsilon_r = \varepsilon_\infty + \frac{\varepsilon_s - \varepsilon_\infty}{1 + s\tau}$$

Setting  $s = j\omega$  so as to transform back to the frequency domain gives:

$$\varepsilon_r = \varepsilon_\infty + \frac{\varepsilon_s - \varepsilon_\infty}{1 + j\omega\tau} \quad (1.8)$$

which is a single relaxation Debye equation.

The single relaxation Debye equation exhibits a relaxation frequency centred on:

$$f_c = \frac{1}{2\pi\tau} \quad (1.9)$$

and strictly,  $\varepsilon_s$  and  $\varepsilon_\infty$  refer to the permittivity well below and well above  $f_c$ , respectively.

(1.8) omits the currents flowing at infinite time such as would arise due to the movement of ions in a constant field. The model is expanded to include a static conductivity term,  $\sigma_s$ , where  $\sigma_s = j\omega\varepsilon_0\varepsilon_s$ . Note that the imaginary nature of  $\sigma_s$  is a consequence of the solution to the wave equation.

$$\therefore \varepsilon_s = \frac{\sigma_s}{j\omega\varepsilon_0} = -j\frac{\sigma_s}{\omega\varepsilon_0} \quad (1.10)$$

Including this within (1.8) results in:

$$\varepsilon_r = \varepsilon_\infty + \frac{\varepsilon_s - \varepsilon_\infty}{1 + j\omega\tau} - j\frac{\sigma_s}{\omega\varepsilon_0} \quad (1.11)$$

Since (relative) permittivity is a complex quantity,  $\varepsilon_r = \varepsilon'_r - j\varepsilon''_r$ , we expand (1.11) to give:

$$\varepsilon_r = \varepsilon_\infty + \frac{(\varepsilon_s - \varepsilon_\infty)(1 - j\omega\tau)}{1 + \omega^2\tau^2} - j\frac{\sigma_s}{\omega\varepsilon_0}$$

$$\varepsilon_r = \varepsilon_\infty + \frac{(\varepsilon_s - \varepsilon_\infty)}{1 + (\omega\tau)^2} - j\left[\frac{\omega\tau(\varepsilon_s - \varepsilon_\infty)}{1 + (\omega\tau)^2} + \frac{\sigma_s}{\omega\varepsilon_0}\right]$$

Separating real and imaginary parts, we obtain:

$$\Re\{\varepsilon_r\} = \varepsilon'_r = \varepsilon_\infty + \frac{(\varepsilon_s - \varepsilon_\infty)}{1 + (\omega\tau)^2} \quad (1.12a) \quad \text{and} \quad \Im\{\varepsilon_r\} = \varepsilon''_r = \frac{\sigma_s}{\omega\varepsilon_0} + \frac{\omega\tau(\varepsilon_s - \varepsilon_\infty)}{1 + (\omega\tau)^2} \quad (1.12b)$$

The first term on the right hand side of (1.12b) arises due to the static conductivity.

At  $f = f_c$  we obtain  $\omega\tau = 1$  and (1.12a) and (1.12b) become:

$$\varepsilon'_r = \frac{(\varepsilon_s + \varepsilon_\infty)}{2} \quad (1.13a)$$

$$\varepsilon''_r = \frac{\sigma_s}{\omega\varepsilon_0} + \frac{(\varepsilon_s - \varepsilon_\infty)}{2} \quad (1.13b)$$

where (1.13a) is the *mean* of the static and infinite frequency permittivity and the second term of (1.13b) is the value half way between the static and infinite frequency permittivity.

The locus of  $\left(\varepsilon''_r - \frac{\sigma_s}{\omega\varepsilon_0}\right)$  vs.  $(\varepsilon'_r)$  in the complex  $\varepsilon_r$  plane over a wide range of frequencies (centred on  $f_c$ ) is a semi-circle with apex at  $f = f_c$  corresponding to the value  $\varepsilon'_r = \frac{(\varepsilon_s + \varepsilon_\infty)}{2}$  on the real axis, as illustrated in Figure 1-3 below.

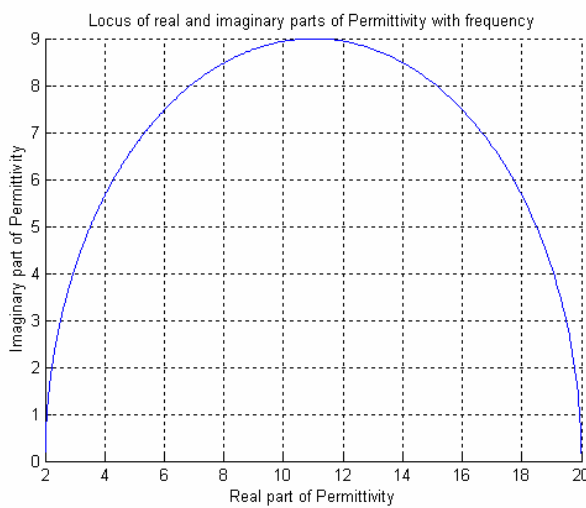


Figure 1-3: Locus of Complex Permittivity

(Based on  $\varepsilon_s = 20$ ,  $\varepsilon_\infty = 2$ ,  $\sigma_s = 5e-4$ ,  $f_c = 1\text{GHz}$  over  $f = 10\text{MHz}$  to  $100\text{GHz}$ )

A plot of  $\frac{\varepsilon'_r - \varepsilon_\infty}{\varepsilon_s - \varepsilon_\infty}$  vs.  $\frac{f}{f_c}$  yields a value of 0.5 at  $f = f_c$  and is illustrated in Figure 1-4.

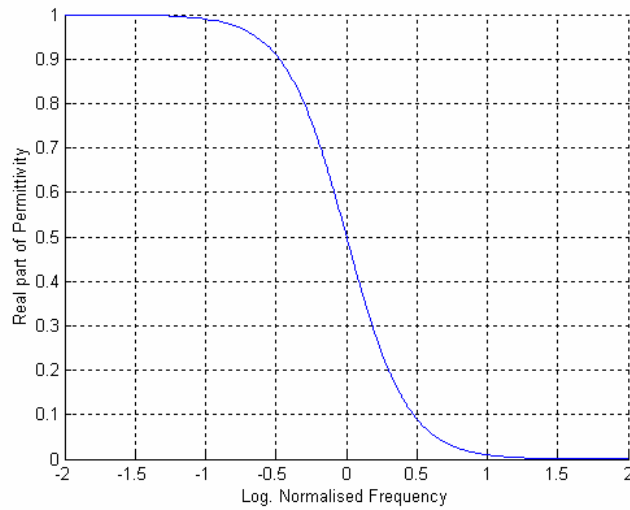


Figure 1-4:  $\frac{\epsilon_r' - \epsilon_\infty}{\epsilon_s - \epsilon_\infty}$  vs.  $\log_{10}\left(\frac{f}{f_c}\right)$

(Based on  $\epsilon_s = 20$ ,  $\epsilon_\infty = 2$ ,  $\sigma_s = 5e-4$ ,  $f_c = 1GHz$  over  $f = 10MHz$  to  $100GHz$ )

A plot of  $\frac{\epsilon_r''}{\epsilon_s - \epsilon_\infty}$  vs.  $\frac{f}{f_c}$  peaks at a value of 0.5 at  $f = f_c$  and is illustrated in Figure 1-5

(blue) together with a plot of  $\frac{\sigma_s}{\omega\epsilon_o}$  vs.  $\frac{f}{f_c}$  (green).

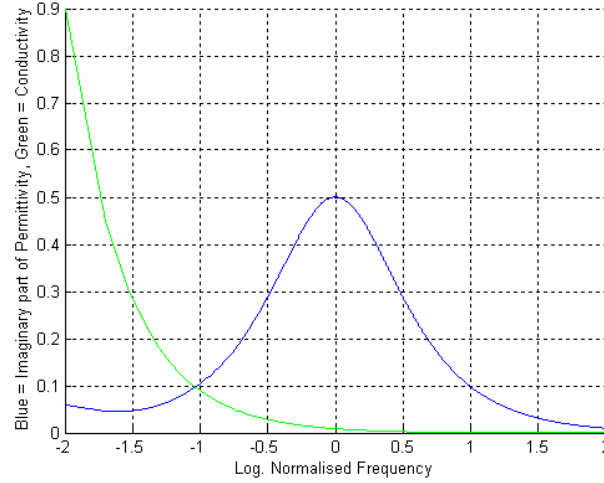


Figure 1-5:  $\frac{\epsilon_r''}{\epsilon_s - \epsilon_\infty}$  and  $\frac{\sigma_s}{\omega\epsilon_o}$  vs.  $\log_{10}\left(\frac{f}{f_c}\right)$

(Based on  $\epsilon_s = 20$ ,  $\epsilon_\infty = 2$ ,  $\sigma_s = 5e-4$ ,  $f_c = 1GHz$  over  $f = 10MHz$  to  $100GHz$ )

This behaviour suggests the equivalent circuit of Figure 1-6, below:

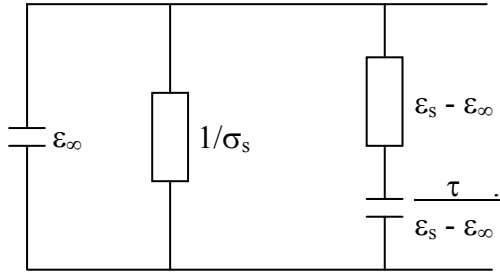


Figure 1-6: Equivalent Circuit

A MATLAB® program, Debye1.m, (see Appendix C) has been written to solve (1.11) and plot the graphs of Figure 1-3, Figure 1-4 and Figure 1-5.

An empirical function used for a distribution of relaxation times is the Cole – Cole equation:

$$\epsilon_r = \epsilon_\infty + \frac{\epsilon_s - \epsilon_\infty}{1 + \left( j \frac{f}{f_c} \right)^{1-\alpha}} - j \frac{\sigma_s}{\omega \epsilon_0} \quad (1.14)$$

This has been widely used since it fits the measured data well. The distribution parameter,  $\alpha$ , is indicative of the distribution of relaxation times<sup>a</sup>. A typical range for biological materials<sup>[2]</sup> is  $\alpha = 0.3$  to  $0.5$  (although it may be lower in the MMW band).

When  $\alpha = 0$  equation (1.14) becomes:

$$\epsilon_r = \epsilon_\infty + \frac{\epsilon_s - \epsilon_\infty}{1 + j \frac{f}{f_c}} - j \frac{\sigma_s}{\omega \epsilon_0}$$

and since  $f = \frac{\omega}{2\pi}$  and  $f_c = \frac{1}{2\pi\tau}$       then     $\frac{f}{f_c} = \omega\tau$

---

<sup>a</sup> Do not confuse the Cole-Cole distribution factor with the attenuation constant. Both typically use the symbol  $\alpha$ .

and equation (1.14) becomes equation (1.11). Therefore the Cole – Cole equation becomes that of a single relaxation Debye equation for  $\alpha = 0$ . It is suspected that  $\alpha \sim 0$  for water and wet tissues in the MMW band<sup>[3]</sup>. Other Debye-type functions have been used to describe the dielectric behaviour of polar materials as functions of frequency such as the Davidson-Cole, constant-phase-angle and that of Raicu<sup>[4]</sup> who related the dielectric properties of wet and dry skin measured in-vivo over the 100Hz to 100MHz band to a newly reported dispersion function. Further models such as the Maxwell-Wagner theory plus various extensions have been used to describe the permittivity of mixtures and suspensions of particles (a convenient representation of many tissue types)<sup>[2]</sup>, but are generally applicable well below the MMW band.

### 1.3 REVIEW OF MICROWAVE AND MMW PROPERTIES OF TISSUES

#### 1.3.1 Biological Tissues

The permittivity of biological tissues is determined by several important dispersion phenomena whose contributions are normally confined to specific bands. An excellent and highly comprehensive review of this topic has been written by Foster and Schwan<sup>[2]</sup>. The behaviour of biological tissues at RF and microwave frequencies is largely determined by the electro-chemical behaviour of cells and its cellular structure as well as the intra-cellular fluid in which the cells are suspended and the internal cellular materials, including the nucleus. The cell membrane exhibits capacitance and supports a potential difference across it such that at low frequencies current flows around the cells but at higher frequencies current flow may penetrate the cells. The application of an electric field within a medium causes a displacement of charge whose kinematics give rise to a frequency dependence of its bulk dielectric properties. For heterogeneous materials such as biological tissues, polarisations at the interfaces are established and then decay away in time.

Some of the physical processes can be described by a single time constant, whilst others are more complex; several such processes may occur in parallel. The dielectric behaviour of biological tissues and chemicals is therefore characterised by a number of relaxation phenomena which give rise to dispersions within the RF and microwave band. In fact, similar behaviour is also observed in various non-biological polar materials such as polymers<sup>[1]</sup>. Due to the complex nature of biological materials and of the relaxation processes, several such processes are believed to co-exist at frequencies throughout the RF and lower microwave band. Each relaxation process is characterised by its relaxation time(s) and so research effort has been directed at finding the distribution of relaxation times in any given tissue and frequency band. Some researchers have approached the problem by deducing the physical processes involved and relating these to the relaxation times and hence the dielectric properties. Measured data should then confirm/deny these properties and the processes giving rise to them. Others have started with measured data and then attempted to produce theories of relaxation distributions (with no regard to the physical processes) which best fit the measured data. Both approaches suffer from the fact that there is significant variability in biological tissues and that measured data has an experimental tolerance. The variability of the data permits several models to be accommodated. The tolerance on experimental data and the natural variability of tissues has lead to difficulties in confirming the theories of both approaches.

The electro-chemical properties of cells start to change soon after death or the removal of tissue and therefore the permittivity will also change. The chemical composition may also change when tissues are excised. Caution must be exercised to preserve the integrity of samples for in vitro research work.

### 1.3.2 The Microwave Properties of Tissue

The dielectric properties of tissue are determined by a number of dispersion phenomena which are described in the following sections. Additional, lower frequency, dispersions are known to exist but have little bearing at microwave frequencies and so are not reported on here, however, excellent reviews have been provided by Pethig<sup>[5][6]</sup>, Foster and Schwan<sup>[2]</sup>, Raicu et al<sup>[4]</sup> and Stuchly and Stuchly<sup>[7]</sup>.

**$\gamma$ -dispersion<sup>b</sup>**. The dielectric properties of tissues above 100MHz are determined by the intra-cellular electrolytes, principally, water (0.9% saline solution). These properties are consistent with those from suspensions of low conductivity, low permittivity particles (i.e. cells) in an aqueous electrolyte. In the microwave band, tissue properties can be attributed to their "free" water content and the dispersion for normal bulk water. Changes after death or tissue excision are attributable to the loss of tissue water content.

**$\delta$ -dispersion<sup>c</sup>**. Approximately 10% of water in tissues, dependent on organ/tissue type, is termed "bound" water i.e. it is rotationally hindered, and has a relaxation frequency some 50 to 100 times lower than that of free water. The relaxation of bound water leads to the  $\delta$ -dispersion, which is very much weaker than the  $\gamma$ -dispersion, and is centred at 100MHz. This effect results from the fact that, within suspensions, the electrical properties of water in the immediate vicinity of particles is perturbed by its proximity to the particles, and so differs slightly from those of free water. The differences in properties are dependent on the molecule to which the water is bound, its viscosity and temperature.

There appears to be a transition at around 100MHz, above which the capacitive impedance shorts out and the resistivity is approximately that of 0.9% saline solution, which is the ionic strength of cellular fluid. Above 100MHz the dielectric properties of tissues are consistent with those expected for a suspension of low conductivity particles

---

<sup>b</sup> Do not confuse the  $\gamma$ -dispersion with the propagation constant,  $\gamma$ .

<sup>c</sup> Do not confuse the  $\delta$ -dispersion with the skin depth ( $\delta$ ) or the loss tangent ( $\tan \delta$ ).

(cells) in an aqueous electrolyte and the distinction between tissue types becomes lost<sup>[5]</sup>.

The dielectric properties of tissues are not only frequency dependent but also temperature dependent. Pethig<sup>[6]</sup> quotes a change in permittivity of 1.2% /°C at 1MHz and a value of 0.3% / °C at 100MHz. Martin, Broquetas and Jofre<sup>[8]</sup> quote temperature variations of – 0.5%/ °C in  $\epsilon'$  and + 2%/ °C in  $\epsilon''$ . Table 4-2 summarises temperature gradients reported in the literature applicable to the MMW band. Since permittivity and conductivity ( $\sigma$ ) are related by:

$$\sigma = \sigma_s + \omega\epsilon_0\epsilon'' \quad (1.15)$$

where  $\sigma_s$  is the total conductivity resulting from processes other than the dispersion (such as ionic conduction).

Tissue conductivity is also temperature dependent, with a low frequency sensitivity of:

$$\frac{d\sigma}{dT} = 2\%/\text{°C} \quad (1.16)$$

being typically cited<sup>[9]</sup>. In the RF band, the temperature induced changes in conductivity map those of the dielectric loss factor.

It is possible that the physical processes in biological tissues can give rise to resonance behaviour, though none has been confirmed through experimental work. Nevertheless, medics in some east European countries have applied MMW at two very precisely defined frequencies, namely 42.25GHz and 53.57GHz, and at very low powers for therapeutic treatments on human patients<sup>[10][11]</sup>. These treatments are highly frequency dependent and cannot be explained by thermal effects and have lead some to suggest a resonance phenomenon. Such frequency specific behaviour seems contrary to high absorption characteristics of tissue water content. No experimental evidence has yet been found to support the existence of any related high Q-factor dielectric changes<sup>[12][13][14][15]</sup> and there remains no explanation for the therapeutic effects. Such non-thermal tissue effects are outside the scope of this thesis.

### 1.3.3 Millimetre Wave Permittivity of Tissue

Presently, there is little data on the permittivity of tissues in the millimetre wave (MMW) band, i.e. 30 to 300GHz. The paucity of such data has been noted by several authors over the years, namely, Ghandi (1983)<sup>[12]</sup>, Steel and Sheppard (1988)<sup>[16]</sup>, Tofighi and Daryoush (2000)<sup>[17]</sup> and, largely, remains the case today. The lack of data is due to technical difficulties in making the measurement rather than a lack of importance of such data<sup>[16][17]</sup>. Current interest is strongest at the atmospheric window frequencies of 35 and 94GHz, as well as frequencies of high atmospheric attenuation such as 60 and 77GHz since a number of radar, sensor and communications applications are exploiting these bands. The MMW band is generally above the frequencies of the relaxation phenomena in tissues but below the frequencies of the absorption spectra of biological chemicals and, therefore, tissues are thought to be relatively non-dispersive in this band. The highest frequency relaxation phenomenon is that of pure water which is centred on 25GHz at 37°C<sup>[6][18]</sup> (or 20GHz at 20°C). The assumption would seem to be that the dielectric behaviour of tissues through the MMW band is determined by its water content. There is, rather sparse, data for water through the MMW band (see section 4.2.2), which indicates a gradual reduction of  $\epsilon'$  and an increase in  $\sigma$  with increasing frequency, in keeping with the Kramers-Kronig relations. It therefore seems reasonable to assume that the permittivity of biological tissue in the band 60 to 100GHz will follow the trend of its water content i.e. a gradual reduction in  $\epsilon'$  and an increase in  $\sigma$  as the frequency continues to increase beyond the upper end of the single, pure water relaxation frequency. It is anticipated that most tissues, especially those of high water content, will be extremely lossy in the MMW band. Samples used for experimental work should preserve their in vivo water content as much as possible. Since human tissues are expected to be highly lossy, priority should be given to the measurement of skin, since, as the outermost layer, it will receive greatest exposure. Deeper tissues will be shielded by the skin. Skin has a water content of about 60 to 76%<sup>[6]</sup>.

When work on this thesis commenced in July 1998, there was, to the best of the author's knowledge, no data on the permittivity of human skin in the MMW band published in the open literature. During the course of this work a few examples have been published and have recently come to the author's attention. These, plus a few examples of experimental data obtained for animal tissues, are reviewed below.

Ghodgaonkar, Gandhi and Iskander have reported on permittivity measurements made on human skin *in vivo*<sup>[19][20][21]</sup>. They have used a waveguide technique to measure the permittivity of skin on a human finger at 32GHz and on the palm of a hand over the band 26.5 to 57GHz (see also section 1.5.3). The permittivity of the palm at 57GHz is given as  $\epsilon_r = 4 - j7$  with an error in  $\epsilon'_r$  of  $\pm 14\%$  and an error in  $\epsilon''_r$  of  $\pm 6\%$ . Their measured complex permittivity data together with that of Hey-Shipton et al<sup>[22]</sup> (palm, *in vivo*, 8 to 18GHz) has been fitted to a single relaxation Debye function having the following model parameters:

$$\epsilon_s = 26.47 \pm 1.2, \quad \epsilon_\infty = 1.5, \quad \tau = 9.57 \pm 0.6 \text{ ps}, \quad (f_c = 16.6 \text{ GHz}), \quad \sigma_s = 0.0092 \Omega/\text{cm}$$

They note that all these parameters are much lower than those reported by Cook<sup>[23]</sup> (excised human skin from breast and instep, 1.78 to 4.6GHz), see section 4.2.3.2. In general, both the real and imaginary parts of the complex permittivity of skin *in vivo* are expected to be significantly lower than for excised skin. They conjecture that this is due to the variations in water content, blood content and epidermal thickness.

Boric-Lubecke et al<sup>[24][25]</sup> present complex permittivity data of human skin (elbow, back of hand and palm of hand) measured *in vivo* using a 2.2mm coaxial probe across the band 30 to 40GHz. Their permittivity results are summarised below:

Elbow (1 subject):  $\epsilon_r \sim 19.5 - j10.7$  (30GHz) to  $\sim 17.0 - j11.7$  (40GHz)

Back of hand (3 subjects):  $\epsilon'_r = 18.0$  to  $19.5$  (30GHz) to  $16.0$  to  $17.0$  (40GHz)

$\epsilon''_r = 9.5$  to  $10.7$  (30GHz) to  $10.5$  to  $12.0$  (40GHz)

Palm of hand (3 subjects):  $\epsilon'_r = 11.5$  to  $13.5$  (30GHz) to  $11.3$  to  $13.0$  (40GHz)

$\epsilon''_r = 3.0$  to  $4.0$  (30GHz) to  $3.5$  to  $5.5$  (40GHz)

This data indicates increases in the imaginary part of the permittivity with increasing frequency which is contrary to expectation. They note that the results for the elbow and back of the hand are very similar and that they are probably representative of most of the human skin but that skin on the palm of the hand has a much lower permittivity. They attribute this to the fact that palm skin is thicker and more horny (without hair cells) which appears to be of lower water content. (*Author's note:* it seems that the same could also be said of the skin on the sole of the foot.)

Hwang et al [26] report on the use of 1 and 3 mm coaxial probes to measure the permittivity of the human epidermis on the palm and wrist up to frequencies of 110GHz. The 3 mm probe was used over the band 500MHz to 30GHz and the 1 mm probe from 500MHz to 110GHz. They ascertained that each probe had a penetration depth equal to its diameter. The permittivity of palm epidermis varied from approximately  $6.0 - j2.5$  at 60GHz to  $5.3 - j2.0$  at 94GHz and that of the wrist epidermis varied from approximately  $8.0 - j4.0$  at 60GHz to  $7.0 - j3.0$  at 94GHz. This data was used to parameterise a Cole-Cole function (1- 14). The model parameters were found to be:

Palm:  $\epsilon_s = 19.73$ ,  $\epsilon_\infty = 4.596$ ,  $\sigma_s = 0.2870$ ,  $f_c = 7.223\text{GHz}$  and  $\alpha = 0.2531$

Wrist:  $\epsilon_s = 21.86$ ,  $\epsilon_\infty = 4.581$ ,  $\sigma_s = 0.1895$ ,  $f_c = 15.54\text{GHz}$  and  $\alpha = 0.2672$

There are, however, significant discrepancies in the measured permittivity of the tissues in the 500MHz to 30GHz range using the two probe sizes. These are believed to be due to the fact that the greater penetration depth of the 3 mm probe enables the wetter tissues underlying the thin wrist epidermis to be coupled to the measurement more readily than for the 1 mm probe. They further remark that the lower permittivity of the palm skin is due to its thicker epidermal layer and that the wetter tissues beneath it have a reduced influence on the result.

Alison and Sheppard [27] have measured the complex permittivity of human blood over the band 29 to 90GHz and identified two dispersion processes from the data: a high frequency  $\gamma$  relaxation and a low frequency fractional power-law response. Their data

also afforded an estimate of the volume fraction of water in blood to be between 0.76 and 0.78 at 37°C.

Edrich and Hardee<sup>[13]</sup> have measured the permittivity and penetration depth of freshly excised rat muscle and fat tissues in the 40 to 54GHz and 85 to 90GHz bands. They noted that skin appeared to be a matching layer. Steel and Sheppard<sup>[16]</sup> have measured the permittivity of various rabbit tissues at 35GHz.

## 1.4 REVIEW OF APPLICATIONS

### 1.4.1 Introduction

Applications which are currently driving the requirement for dielectric data on human tissues in the MMW band are RF hyperthermia/safety assessment of power deposition, passive MMW imaging (35 and 94GHz), determining the radar cross section of human beings for 77GHz car cruise control and collision avoidance purposes and the propagation of 60GHz communication links (wireless LANs) in an indoor environment. Possible future applications could also include the RF links of wearable computing devices distributed around the human body. This is not an exhaustive list, however, it is outside the scope of this study to consider the applications of the therapeutic frequencies of 42.25GHz and 53.57GHz mentioned in section 1.3.2 and of the reputed systems which direct MMW to placate a crowd and influence one's state of mind. Further applications of time varying magnetic fields in medicine are reviewed by Stuchly<sup>[28][29]</sup>.

Currently, to the best of the author's knowledge, no one has published any requirement on the accuracy of tissue permittivity in the MMW band that these applications demand. Experimental accuracies published at centimetric wave frequencies tend to lie within the range of  $\pm 3\%$  to  $\pm 10\%$  with accuracies of around  $\pm 5\%$  being considered good at 10GHz. Experimentally determined permittivity values tend to have larger inaccuracies as frequency increases due to the increased complexity of the measurement. Furthermore, natural tissue variability between different subjects and from different

sites can be considerable. The data of Boric-Lubecke et al [24][25] presented in section 1.3.3 indicated a variation of up to  $\pm 7\%$  in  $\epsilon_r'$  and  $\pm 22\%$  in  $\epsilon_r''$  at 40GHz for the palm skin of three subjects. Significantly greater variations are reported in skin data from different sites. Ghodgaonkar, Gandhi and Iskander [19][20][21] reported errors in  $\epsilon_r'$  of  $\pm 14\%$  and an error in  $\epsilon_r''$  of  $\pm 6\%$  for palm skin at 57GHz. It is therefore suggested here that an experimental tolerance for measured skin permittivity in the MMW band of  $\pm 10\%$  should be considered desirable but that a tolerance of  $\pm 20\%$  would be of value to the scientific community.

In addition to the applications mentioned above, there is interest in the ability of RF signals to cure composite materials, monitor their cure state and detect defects within them; signals in the MMW band would appear to offer an interesting potential in these last two areas.

These application areas are now reviewed in more detail in the ensuing sub-sections.

#### **1.4.2 RF Hyperthermia & Safety Assessment of Power Deposition**

These topic areas are combined as both are concerned with deposition of RF power into the human body. RF hyperthermia was the subject of a lengthy review forming part of the author's M.Phil to PhD transfer thesis (an internal Cranfield University publication) and includes over 200 references. A very brief synopsis of some of the salient details taken from this review is given below.

RF hyperthermia is the heating of body tissues through the application of EM energy. Its primary application is as a cancer therapy, since tumours are damaged and killed at lower temperatures than normal healthy tissues. Although the efficacy of RF hyperthermia has been well established for some years, especially when used as an adjunct to chemotherapy and radiation therapy [30][31], it has yet to enter routine clinical practice. There remain several major technical and medical problems to be resolved before it gains widespread acceptance. Whilst RF hyperthermia has the potential of being a hugely beneficial form of therapy in oncology, medical professionals, in the UK

at least, remain sceptical regarding its viability for the time being. The main areas of technical difficulty are in the fields of dosimetry, control of power deposition and thermal monitoring<sup>[32][33][34][35][36][37]</sup>.

The Specific Absorption Rate (SAR) is the parameter used to quantify the rate of energy deposition in the human body between frequencies of 100kHz and 10GHz. SAR is formally defined as the rate of energy deposition in a unit mass of tissue due to a time varying electromagnetic field<sup>[28]</sup>.

$$SAR = \frac{\sigma E_{in}^2}{\rho} \quad (1.17)$$

where  $\sigma$  is the tissue conductivity,  $E_{in}$  is the induced electric field strength and  $\rho$  the specific density of the tissue. In spite of the apparent simplicity of this equation the exact determination of SAR is a very complex issue. Factors affecting SAR have been reviewed by Chou et al<sup>[32]</sup>. All three variables on the right hand side of (1.17) are temperature dependent and the conductivity and induced electric field are also frequency dependent.

Hyperthermia may also be delivered using ultrasound or warm water irrigation, both of which share many of the problems of RF hyperthermia, although Stuchly and Stuchly<sup>[7]</sup> contend that the biological response to EM induced heating can be significantly different to the responses to other thermal stimuli. Ultrasound delivered hyperthermia, in particular, has very similar problems to those of RF hyperthermia.

The transfer thesis also included a feasibility study into the use of 35GHz signals for non-invasive temperature profiling purposes using estimated values of permittivity based on measured data for rabbit tissues. This study concluded that tissues would be too lossy to permit penetration of the MMW energy to any appreciable depth. Clearly, as a medical therapy, the use of MMW energy for RF hyperthermia is not viable. Nevertheless, the radiation of the body by MMW energy will result in a surface heating effect. Current UK basic restrictions issued by the National Radiological Protection Board (NRPB) for non-ionising radiation in the band 10 to 300GHz is set at a maximum power density of 100W/m<sup>2</sup><sup>[38]</sup> and is made in response to the 1998 ICNIRP guidelines

<sup>[39]</sup>. This will be dissipated as heat in an increasingly thin surface layer as frequency and dielectric losses increase. It is therefore anticipated that higher skin temperatures will be attained in the MMW band than at lower frequencies, although this may be offset by greater surface cooling.

Dielectric losses are quantified by the real part of the propagation constant,  $\Re(\gamma) = \alpha$  where  $\alpha = \frac{1}{2} \omega \sqrt{\mu\epsilon'} \tan \delta$  (1.6). The penetration depth =  $1/\alpha$  may be defined as that depth at which the specific absorption rate has diminished to  $1/e^2$  of the surface value<sup>[40]</sup> (which is consistent with the definition of skin depth as a diminution of  $1/e$  in electric field strength).

Some work on the heating effects on phantom materials and the human body due to radiation in the MMW band has been reported in the literature. Khizhnyak and Ziskin<sup>[41]</sup> irradiated 0.1mm phantoms at 37 to 78GHz and recorded the surface SAR distribution using IR thermography. They observed localised hot spots which were highly frequency dependent having Q-factors > 500. They note that the wavelength of MMW is about the same as skin pore sizes and the thickness of the epidermis. The surface heating effects are difficult to judge due to cooling by evaporation. They further remark that some biological responses depend not only on the steady state temperature but also on the heating rate and temperature gradients. No dielectric data is given. Walters et al<sup>[42]</sup> determined the cutaneous pain threshold in ten human subjects exposed to three second bursts of radiation at 94GHz. They used IR thermography to measure the skin temperature. The nominal skin temperature was recorded as  $34.0 \pm 0.2^\circ\text{C}$  and the threshold for pricking pain was measured at  $43.9 \pm 0.7^\circ\text{C}$ , an increase of  $9.9^\circ\text{C}$ . They remark on the poorly established properties of skin at 94GHz and that it is undoubtedly variable. They assumed the permittivity of dry skin at 94GHz to be  $5.8 - j7.5$ , which is predicted from the model of Gabriel<sup>[43]</sup>, see also section 4.2.3.1.

### 1.4.3 Passive MMW Imaging

Passive MMW imaging has emerged in recent years as a useful sensor for security, search and rescue, anti-personnel mine detection and battlefield surveillance applications<sup>[44][45]</sup>. These sensors detect the natural radiation emitted and reflected by “hot” bodies in much the same way as thermal imagers (TI) do in the far infrared (IR) bands. Unlike thermal imagers, however, MMW imagers operate well below the wavelength of the maximum spectral power density described by Planck’s radiation law for bodies of room temperature. This apparent loss of sensitivity is compensated for by the fact that MMW are subject to lower propagation losses than the far IR band and can even penetrate obstacles such as clothing, internal wall materials, smoke, haze, fog, vegetation and even a thin layer of dry soil<sup>[44][45][46]</sup>. The contrast of a passive MMW image is determined by differences in the temperature, emissivity and reflectivity of bodies. Passive MMW images of an outdoors scene tend to be highly dominated by the reflection of cooler surroundings. Most systems operate over a wide bandwidth around the atmospheric window centred on 94GHz<sup>[47][48]</sup>. Passive MMW imagers have been built as cameras capable of outputting real-time video at a frame rate of 30Hz of 60 x 75 pixel images<sup>[46]</sup>. Modern MMW imagers can measure temperatures to a resolution of 1 degree Kelvin in an integration time of 10ms<sup>[45]</sup>. However, spatial resolution tends to be poor due to diffraction limitations and can only be overcome by using a large aperture.

One of the applications of primary concern is the use of a MMW imager in airport security and its ability to detect concealed weapons and explosives<sup>[49]</sup>. Detection at ranges up to 25 metres has been demonstrated<sup>[50]</sup>. Detection is based on the difference between the extraordinarily high emissivity of human skin and the much lower values of most other materials<sup>[51]</sup>.

It is clear, that the reflectivity and transmission characteristics of materials, including human skin, around 94GHz is crucially important to the image quality of passive MMW imaging.

In their review of biomedical applications of microwaves and MMW, Boric-Lubecke et al [24] describe the potential of passive MMW imaging in the 30 to 40GHz band to identify and classify burns in human patients by virtue of the differences in the dielectric properties of normal and burnt human skin. These differences are attributed to variations in skin water content which is dependent on the severity of the burn. The presence of blisters increases the skin water content whereas burnt skin typically has a lower water content than undamaged skin. Increased water content increases  $\epsilon_r'$  and reduces emissivity. Skin conductivity and penetration depth is a function of  $\epsilon_r''$  and the air/skin reflection coefficient and skin emissivity are functions of  $\epsilon_r'$  and  $\epsilon_r''$ . They conclude that there are resolvable differences between burnt and healthy skin. This review also describes the diagnosis and treatment of dental caries using active MMW techniques. Teeth affected by caries have a higher water content and hence higher absorption of EM energy than healthy enamel and dentin.

#### 1.4.4 Automobile Radar

Automobile radar systems are currently under development for the purposes of autonomous cruise control [52][53] and collision avoidance/warning [53][54]. These radars are being developed in the 76-77GHz band (Europe and America) and 60-61GHz (Japan) using pulsed Doppler [52][55] or FMCW waveforms [53][54]. The projected demands of millions of units a year generates problems of high-volume, low-cost, high-yield manufacturing and testing of these systems which are only just being recognised. In future applications of pedestrian avoidance, it is important that the radar should recognise a human “target”. It is anticipated that detailed characterisation of the radar cross section of the clothed human body will require knowledge of the permittivity of human skin and clothing materials in the bands occupied by automobile radars.

### 1.4.5 Wireless LANs

The drive to establish communications links of higher data rates (wider bandwidths) has led to the exploitation of the MMW band. This has been driven most strongly by the requirement for fast, short range wireless links forming a local area network (LAN). MMW wireless LANs have recently become viable since the technology has matured and is now affordable. The MMW band appears attractive because of its high bandwidth, the feasibility of manufacturing high gain, narrow beamwidth antennas of reasonable size and the high propagation losses which permit channel re-use. The band 59-64GHz has been assigned as it coincides with a peak of atmospheric absorbance due to oxygen<sup>[56]</sup>. There is now a substantial research effort in the modelling of propagation paths in an indoor environment at 60GHz<sup>[56][57][58][59][60]</sup>. This requires dielectric data on building materials<sup>[61]</sup> and was the primary motivation for the author's own measurements on building materials at 60GHz<sup>[62]</sup>.

Inevitably, questions arise regarding the fading of a channel path when it is intercepted by a human and of the potential exposure hazard to the human. This again provides further justification for the acquisition of the dielectric characteristics of building materials and of human skin in the 60GHz band.

### 1.4.6 Wearable Computing

Wearable computing devices are set to become an important aspect of personal communications, data recording/retrieval and interactive systems<sup>[63][64]</sup>. These systems are likely to include sensor and processors distributed about the human wearers, their clothing and surroundings which will communicate via wireless links. The propagation characteristics of wireless links around the human body will be highly dependent on the dielectric characteristics and geometry of human tissues and clothing materials. Some of the propagation problems have been considered by Hall et al<sup>[65]</sup> who suggested that a link from the shoulder to the hip was maintained by an energy flow travelling as a surface wave or diffracted ray around the outside of the body. This work quantified the variation in path loss at 2.45, 5.8 and 10GHz due to breathing movements and posture

changes. Path losses and variations were worse for the higher frequencies. The likely requirement is for secure, short range, high data rate (high bandwidth) links and this may dictate the use of MMW frequencies. This, in turn, will require knowledge of the dielectric characteristics of human skin and clothing, possibly into the MMW band.

#### 1.4.7 Dielectric Imaging of Composites

Composite materials are being used increasingly in applications requiring high strength and lightness of weight e.g. in the aerospace industry. However, their mechanical properties can be compromised if they are not properly cured or include defects such as delaminations, voids and matrix cracks. Defects may be induced by incorrect curing or by physical damage of the composite. There is concern that low levels of physical damage may grow into major defects as the material continues to be stressed during use. The initial damage may be too minor to detect and may only come to light after catastrophic failure.

Conventionally, composites are cured in a furnace and non-destructive evaluation techniques are based on ultra-sound imaging. The use of ultra-sound requires the sample to be immersed in a water bath and so is limited in its application. Increasingly, however, RF and microwave techniques are being considered for both curing and non-destructive evaluation purposes. Microwave curing of composites is considered as an attractive alternative to conventional conduction based methods since it offers a more uniform and controllable heating. This subject is reviewed in the works of Wei, Shidaker and Hawley <sup>[66]</sup>, Thostenson and Chou <sup>[67]</sup> and Mijovic and Wijaya <sup>[68]</sup>. Microwave heating for curing purposes could also be combined with dielectric imaging to monitor the curing process. RF measurements offer the potential to determine the structural integrity of composite materials in a non-destructive, non-contacting manner. Defects such as delaminations, voids, matrix cracks and improper cure result in changes in the dielectric properties of the composite <sup>[69][70][71][72]</sup>. The presence of such defects may be determined via a measurement of dielectric properties, such as permittivity, or by the absorption, scattering and reflections of an electromagnetic signal, propagating in the medium, which is incident on a discontinuity resulting from the defect. Ideally, one

would desire a diagnostic tool which is non-contacting and capable of achieving a spatial resolution in the order of the likely defect dimensions (in the order of 2 to 20mm). The non-contacting requirement dictates a free-space RF based measurement and the requirement for fine resolution dictates the use of MMW frequencies. The use of MMW in this role was discussed by Gopalsami, Bakhtiari et al [70][73] in which a 75 to 110GHz imaging system was developed and employed to detect sub-surface voids and disbonds in Kevlar/epoxy composite samples. Millimetric measurements also offer a high contrast between defective and nominally ideal material.

## **1.5 REVIEW OF PERMITTIVITY MEASUREMENT TECHNIQUES AT MMW FREQUENCIES**

### **1.5.1 Introduction**

Permittivity is not measured directly but may be deduced from measured data of some variable e.g. impedance, reflectivity, transmission losses etc. which is dependent on it. Several techniques for the measurement of permittivity are in routine use at microwave frequencies and are described in the following paragraphs. Special emphasis is given to those techniques which have been applied for the measurement of biological material and those suitable for use within the MMW band. For further information, the reader is referred to the reviews of Birch et al [74], Correia [75] and Jain and Voss [76].

### **1.5.2 Free-space techniques**

The permittivity of a sample may be deduced from the reflection and/or transmission coefficients measured in free-space [20][77]. Such methods generally require planar samples of a known constant thickness and which are sufficiently large to intercept the entire beam. A variety of methods on this general theme are reported in the literature. Ma and Okamura [78] measured the permittivity of damp saw dust samples within a container at 9.4GHz based on the amplitudes of reflection and transmission coefficients. The experimental set up and sample sizes required at centimetric wavelengths are large.

A typical set-up is illustrated in Figure 3-1 and Figure 3-2. The author's own work using this technique at 11 to 12GHz required a sample size some 50cm across and an antenna separation of 80cm. Kadaba <sup>[79]</sup> has made permittivity and permeability measurements at 56 and 94GHz (on a variety of dielectric materials used in the microwave industry) from the transmission and reflection coefficients at various angles of incidence. Dielectric focussing lenses were fitted over the waveguide horn apertures and were successful in reducing the necessary sample dimensions to just under 18cm and the overall separation between antennas to 47cm. Cullen et al <sup>[80][81]</sup> used a similar technique in the MMW band for the measurement for ferrite materials and Shimabukuro et al <sup>[82]</sup> employed it at 94GHz on Teflon and fused quartz samples and Zheng and Ziqiang <sup>[83]</sup> at 36GHz on polystyrene. Friedsam and Biebl <sup>[84]</sup> have used this technique to measure the permittivity of glass in the band 75 to 95GHz. They point out that utilising the phase of the transmission and reflection coefficients leads to greater accuracy than an 'amplitudes only' method. However, accurate phase measurements require a high degree of mechanical precision to be maintained and a highly stable signal source; the degree of difficulty in ensuring both of these increases with increasing frequency. The difficulties of accurate phase measurements were discussed by Iijima et al <sup>[85]</sup> who also proposed and implemented a method of phase correction. Other examples of the use of free space techniques are Koh <sup>[86]</sup> (ice at 75 to 110GHz), Lyaschenko and Zasetsky <sup>[87]</sup> (aqueous solutions at 80 to 120GHz), Jose et al <sup>[88]</sup> (alcohols and water at 8 to 40GHz) and Otsuka et al <sup>[89]</sup> in which samples of two thicknesses are used. Afsar, Tkachov and Kocharyan <sup>[90]</sup> reported on a free space transmission method utilising a precision waveguide reference run which combines coherently with the free-space path to generate an interferogram when the frequency is shifted. This was used to measure a ceramic material over the band 68 to 118GHz and is illustrated in Figure 1-7.

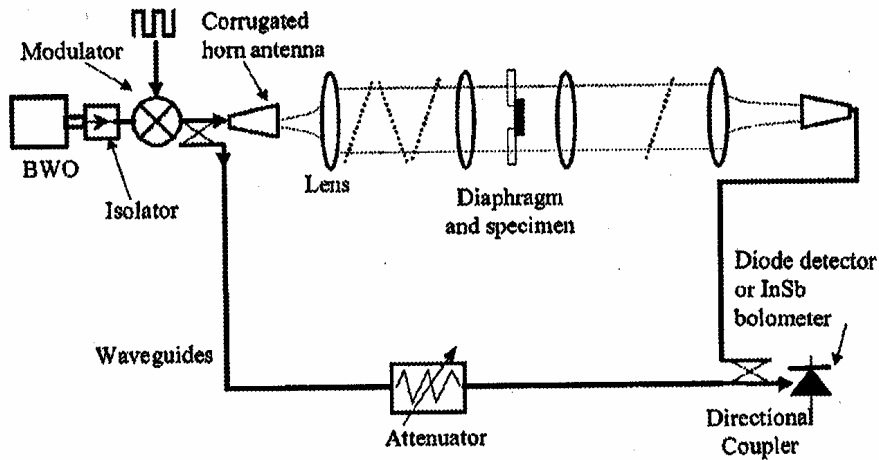


Figure 1-7: W-Band Unbalanced Bridge Spectrometer<sup>[90]</sup>

Lahteenmaki and Karttaavi<sup>[61]</sup> measured the dielectric properties of building materials at 60GHz by measuring the amplitude of the transmission coefficient through a double slab structure as a function of the separation between slabs. A numerical iteration based on signal flow analysis was used to find the best  $\epsilon'_r$ ,  $\epsilon''_r$  pair which resulted in the closest fit of computed data to measured data.

One final free-space technique is to measure the permittivity of a planar sample by identifying the Brewster angle. This has been used by Polivka<sup>[91]</sup> for the measurement of concrete at 51.3GHz and Gvozdev et al<sup>[92]</sup> at 70-71GHz. This technique generally assumes the sample to be highly lossy so as to avoid multiple reflections, and consequentially, modes of propagation, within the sample. In practice, it becomes difficult to identify the Brewster angle accurately for large samples of lossy material or when the sample surface is rough. The Brewster angle is illustrated in Figure 1-8.

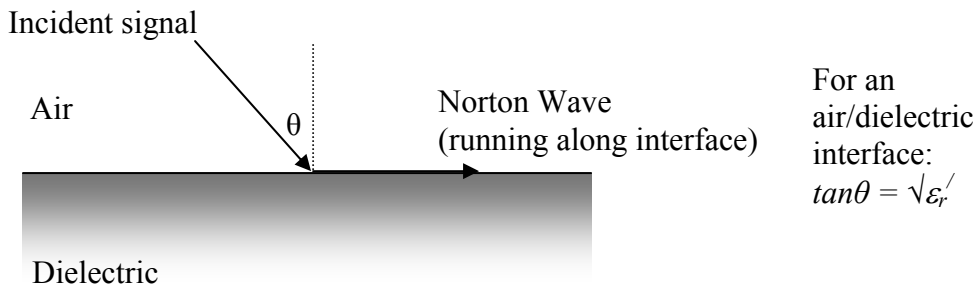


Figure 1-8: The Brewster Angle

One problem common to all these techniques is the processing of the measured data to solve for the permittivity (and/or permeability) of the sample. Most processing methods compute trial solutions which are fitted to measured data. Multiple solutions are possible and so several data points are required in order to overcome the ambiguity. Some processing methods seek to fit data at several frequencies, others at various angles of illumination and yet others as thickness or the relative position of samples varies. Several other authors point out the requirement to avoid diffraction around the edges of the sample. Another potential problem associated with low loss samples is the multiple reflections between sample and horns or between horns. This is usually overcome using time gating techniques to isolate the desired signal path. The tolerance on sample thickness is a major contribution to experimental error, particularly if phase is to be measured.

### 1.5.3 Waveguide techniques

A very popular method for the measurement of permittivity is based on the measurement of the reflection and/or transmission coefficients arising from a slice of the sample of known thickness fitted within a waveguide [13][14][3][93][94][95][96][97]. Alternatively, the measurement may be made from the reflection coefficient of an open ended waveguide terminated in the sample material [98][13][99][21]. These methods assume the dominant mode of propagation only and work well over the bandwidth of this mode (nearly an octave for rectangular waveguide). One practical difficulty associated with

this method is that the sample must make a firm all-round contact with the waveguide walls since in its analysis it is assumed that the surface currents in the waveguide walls flow at the (metal) wall/sample interface. Samples have to be prepared very carefully so as to provide a tight fit on all surfaces<sup>[76]</sup>. Lossy samples must be prepared in thin slices in order to ensure that the transmission coefficients are within a reasonable range. This method has been applied successfully in the MMW band (see above references) but requires small sample sizes, in keeping with the waveguide dimensions and poses practical difficulties, especially for biological materials<sup>[13][100]</sup>. Sample preparation can be problematic in the MMW band, especially for highly lossy materials<sup>[101]</sup>. Liquid samples must be contained by a window whose effects should be accounted for in the analysis of the measured data.

As with the free space methods, there are a variety of similar techniques. Alekseev and Ziskin<sup>[98]</sup> measured the reflection, transmission and absorption coefficients of absorbing films (water and water/alcohol solution) as a function of film thickness at 42.25 and 53.57GHz. Alison and Sheppard<sup>[27]</sup> measured the permittivity of human blood in the band 29 to 90GHz using a waveguide method with a moving plunger (short circuit) to vary the sample thickness. The permittivity was calculated from the reflection coefficient measured at two thicknesses. Steel and Sheppard<sup>[16][102]</sup> measured the permittivity of rabbit tissues at 35GHz using waveguide techniques in which the distance between the sample and a short circuit was varied. They claim experimental errors of  $\pm 7\%$  in both  $\epsilon_r'$  and  $\epsilon_r''$ . A similar technique is used by Van Loon and Finsy for liquid samples in the bands 5 to 40GHz<sup>[103]</sup> and 60 to 150GHz<sup>[101]</sup>. They point out the practical difficulties in using waveguide methods above 40GHz due to the degree of mechanical precision required and increasing waveguide losses. Jain et al<sup>[76]</sup>, however, set the limit at 140GHz.

Further variations on this theme are to introduce the sample as a discontinuity into a transmission line such as a dielectric waveguide<sup>[100]</sup> or microstrip line<sup>[95]</sup>. The s-parameters of the structure are modelled as a function of sample permittivity and a solution declared when the modelled and measured data match.

The most relevant application of waveguide techniques was that of Ghodgaonkar, Gandhi and Iskander<sup>[21]</sup> in which they measured the permittivity of human skin in vivo across the band 26.5GHz to 57GHz. The skin on the palm of the hand was used to terminate an open waveguide. A quarter wavelength Teflon impedance transformer was used and the magnitude and phase of the reflection coefficient was measured using a slotted line. The set-up is illustrated in Figure 1-9 below. The measured reflection coefficient is then related to the permittivity of the skin and impedance transformer terminating the waveguide. The computation of the skin permittivity from this arrangement is not trivial.

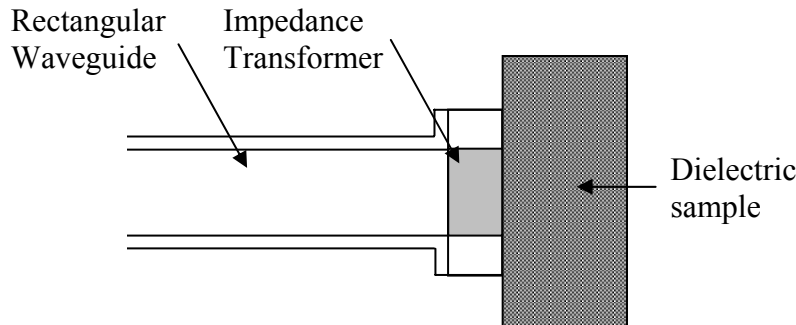


Figure 1-9: Waveguide Method<sup>[21]</sup>

#### 1.5.4 Termination of a coaxial line probe

The admittance at the end of a coaxial line probe is a function of the permittivity of the medium surrounding the probe tip and may be measured using a standard vector network analyser (VNA) or impedance analyser<sup>[4][43][104][105][106][107]</sup>. A typical experimental set-up is illustrated in Figure 1-10.

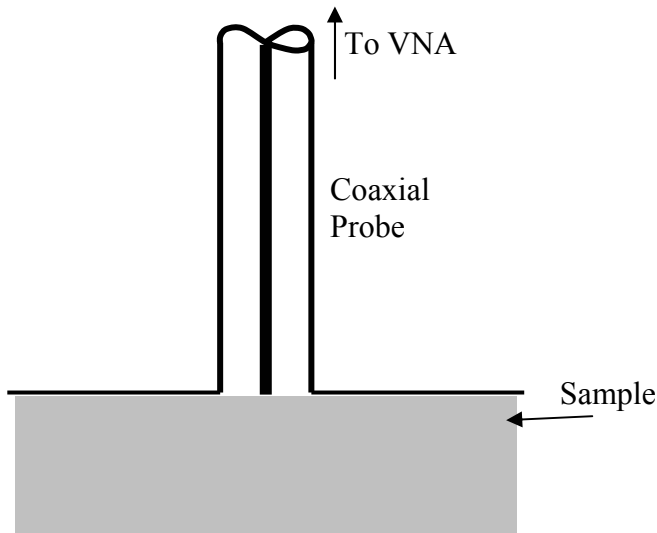


Figure 1-10: Coaxial Probe

This is perhaps one of the most convenient forms of making permittivity measurements at microwave frequencies since it requires almost no sample preparation and is also one of the few capable of making measurements on biological tissues *in vivo*. It has been widely used at microwave frequencies and on biological tissues<sup>[4][43]</sup>. The chief concerns are that the probe must be calibrated with respect to a reliable short circuit fitted at its end and a sample of known permittivity. The modelling of an open ended coaxial probe is not a trivial exercise and the processing of data must be calibrated with respect to known materials. It must also be assumed that the sample material bulk is sufficient to approximate to an infinite half-space; large discontinuities in the vicinity of the probe would couple to the probe and corrupt the measurement. Furthermore, the sample must be in good electrical contact with the whole of the end surface of the probe, which tends to preclude hard, rough surfaces. Practical difficulties in calibrating the probe and the absence of a reliable reference material limit the use of the coaxial probe technique to frequencies below 20GHz<sup>[17]</sup>, and are largely responsible for the scarcity of data on biological materials above this frequency. However, with higher frequency coaxial cables appearing on the market this frequency limitation is being challenged. Boric-Lubecke et al<sup>[24][25]</sup> have made measurements on human skin at 30 to 40GHz using a 2.2 mm coaxial probe and more recently (2003), Hwang et al<sup>[26]</sup> have

used a 1 mm coaxial probe for skin measurements to 110GHz. The measurement is calibrated using distilled water, methanol and air as standard materials, although no details are given, and is validated by reference to measurements made using a 3 mm coaxial probe in the band 500MHz to 30GHz. Nevertheless, it has to be acknowledged that the probes will be very delicate and difficult to calibrate at such frequencies.

Probe methods were used by Gabriel and Gabriel <sup>[43]</sup> to gather their own data on the dielectric properties of 44 human tissue types in the band 10Hz to 20GHz. This work has become one of the most comprehensive and highly respected databases of its kind.

The author has also used this technique to measure the permittivity of soil in the band 100MHz to 5GHz. Further details are given in the report ‘Final Report on Permittivity Measurements of Soil at Hurn and Barnsfield Heath Test Sites’ which forms the final report to DSTL under contract ZAA002E and is reproduced in Appendix B.

### 1.5.5 Perturbation of resonant structures

When a small sample of dielectric material is introduced into a resonant structure such as a cavity, the cavity is perturbed such that it resonates at a lower frequency and with a lower (unloaded) quality (Q-) factor. The shift in resonant frequency,  $\delta f$ , should be small compared with the resonant frequency,  $f_0$ , i.e.  $\delta f/f_0 < 0.001$  for the perturbation theory to be valid<sup>[108]</sup>.  $\delta f$  is a function of  $\epsilon_r'$  whereas the change in unloaded Q-factor is a function of  $\epsilon_r''$ . This technique has been used with biological materials<sup>[109][110]</sup> and has limited application in the MMW band<sup>[111][112][113]</sup>. Clearly, the cavity size reduces as frequency increases and this can again lead to practical problems in the MMW band since the sample volume must be small compared with the cavity volume, especially for high permittivity materials. This technique is one of the most accurate means of measuring permittivity<sup>[76]</sup> and is ultimately limited by the Q-factor of the cavity and the resolution with which  $\delta f$  may be measured. It is particularly well suited to the determination of the dielectric loss of low loss materials. One further limitation is the fact that the measurement is performed at a single spot frequency. The author has used this technique, largely at 3GHz, to make measurements on a number of solid and liquid

samples. The effect of the container material for liquid samples has been accounted for quite successfully. This work is reported on in extracts from the report ‘Further work since M.Phil to PhD Transfer’ which is reproduced in Appendix B. A typical experimental set-up is illustrated in Figure 1-11 below.

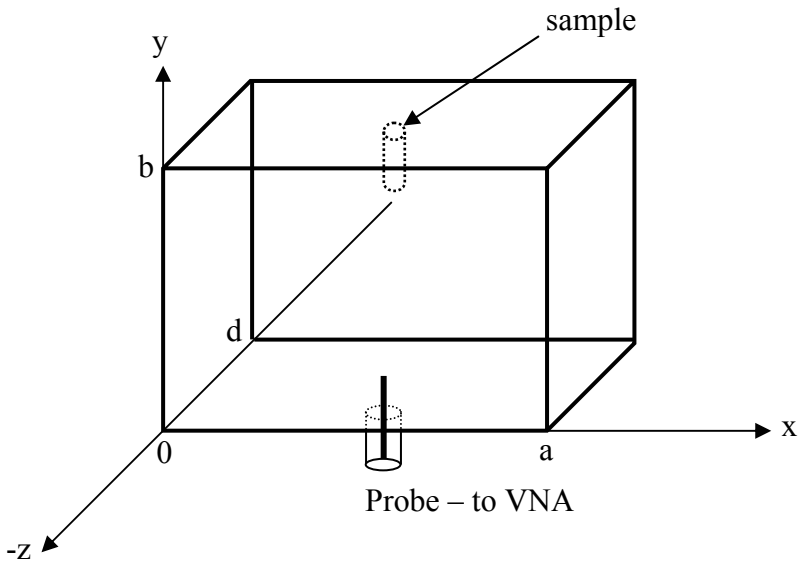


Figure 1-11: Resonant cavity geometry

It is important that the sample be placed in a region of near uniform E-field such as the centre of the broad surface of a rectangular cavity resonant in its dominant  $TE_{101}$  mode. The probe is used to couple a swept frequency RF energy signal from a network analyser. A single probe may be used to measure the reflection coefficient of the cavity and so determine its resonant frequency and Q-factor. It is also important that the probe couples to the cavity only very lightly, so as not to load the cavity and corrupt the measurement. A coupling factor  $\leq 1$  is generally required. The typical profiles of measured reflection coefficients are illustrated in Figure 1-12.

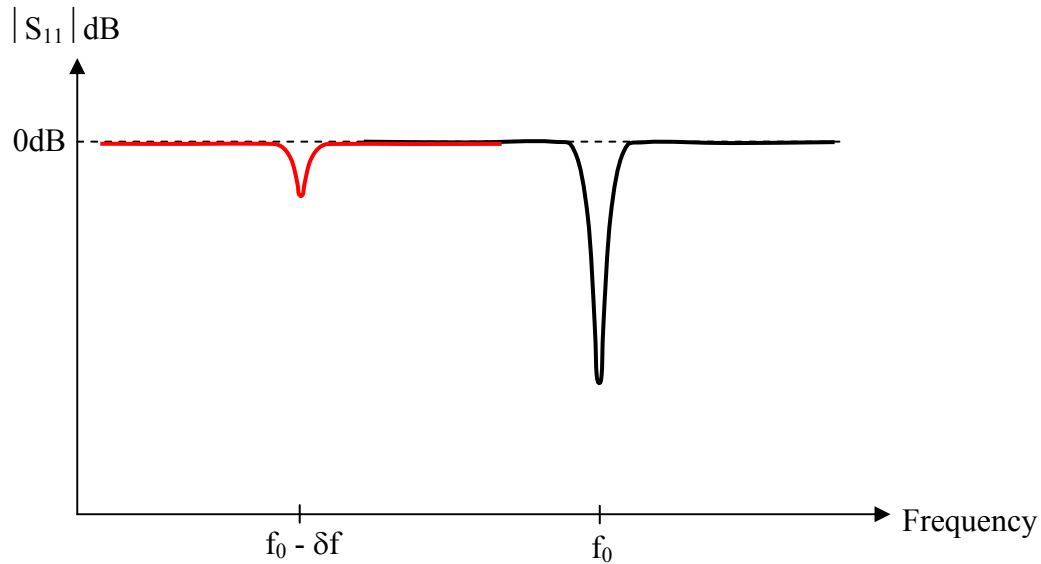


Figure 1-12:  $|S_{11}|$  response of empty cavity (black) and that with sample (red)

Open resonators operating in very high order modes have been used at 60GHz<sup>[114][115]</sup>, see Figure 1-13 below. Here again, the change in unloaded Q-factor is a function of  $\epsilon_r^{\prime\prime}$  whereas  $\epsilon_r'$  may be determined from the change in resonant frequency or by the distance by which the reflectors must be adjusted in order to restore the original resonant frequency. These measurements have been made at several closely spaced resonant peaks.

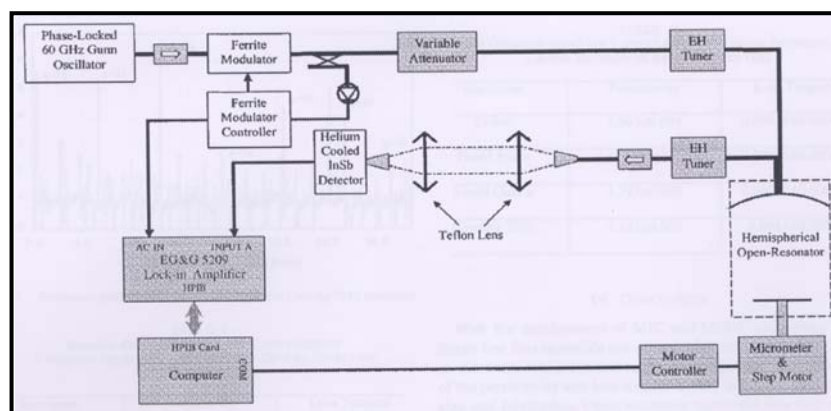


Figure 1-13: Open Resonator Experimental Set-Up<sup>[115]</sup>

### 1.5.6 Other methods

Various other methods have been used in the measurement of permittivity at microwave frequencies. These include time domain spectroscopy methods<sup>[116]</sup> and the dielectric fill of a coaxial line which is terminated in a short circuit<sup>[23]</sup> similar to the method of Roberts and Von Hippel<sup>[117]</sup>. However, none of these methods is suitable for use in the MMW band<sup>[76]</sup>. A review of methods suitable for use in the HF band (3 to 30MHz and VHF band (30MHz to 300MHz) is given by Bramanti and Salerno<sup>[71]</sup>.

### 1.5.7 Comparison of methods

Free space techniques offer a wideband, non-contacting measurement on planar samples with minimal sample preparation at frequencies above 8GHz, below which the equipment and sample sizes required become unfeasibly large. Free space techniques are not well suited to the accurate measurement of the dielectric losses of low-loss samples since this requires the measurement of very low levels of transmission coefficients with a high degree of accuracy. Furthermore, these methods require accurate knowledge of the sample thickness which should be constant over its surface area.

Waveguide methods are also wideband and are recognised as being very accurate. However, they suffer from practical problems of sample preparation and scaling to frequencies well into the MMW band. Sample thickness must be known accurately. The termination of open waveguide may be applied to in vivo measurements of human skin.

Coaxial probes are very convenient, wideband and require minimal sample preparation but are difficult to calibrate above 20GHz.

Resonant methods are highly accurate at a spot frequency. Cavities do not scale conveniently to the MMW band. Open resonators can be employed well into the MMW band but are expensive and require a high degree of mechanical precision to set up. Small samples of known volumes/dimensions are required.

## 1.6 CHAPTER SUMMARY

This chapter started with a brief description of the work reported in this thesis, namely, the measurement of permittivity in the millimetre wave band and its applications to the measurement of skin and defect detection in composite materials. It then provided a review of some of the relevant concepts of permittivity, relaxation phenomena and how these relate to the dielectric properties of biological tissues in the microwave and MMW bands. It has also been noted that there is very sparse measured dielectric data on human tissues in the MMW band. A few examples on the measurement of human skin have been published during the course of this study and have recently come to light and a summary of this data has been provided. Various methods of permittivity measurement methods have been reviewed and considered for their suitability in the millimetre wave band and on biological tissues. Finally, a brief review of the use of RF methods of the detection of defects in composite materials has been given. This indicated a growing interest in and the potential of millimetric wave dielectric imaging.

These reviews have highlighted several key issues and problems which will be addressed by this thesis:

- There is very sparse dielectric data on human tissues in the MMW band. Where it exists, such data is often inconsistent.
- Differences may exist between tissues *in vivo* and *ex vivo* and also by site.
- The spread of relaxation processes applicable to tissues in the microwave and MMW bands is not entirely clear. Several functions have been advanced, some of which are not founded on, or limited to, the physical processes known to exist.
- It is desirable to have measured data available but measured data is corrupted by tolerances and does not confirm the exact relaxation processes present in tissue. Tolerances within  $\pm 10\%$  would be desirable although  $\pm 20\%$  would still be useful.
- The requirement for dielectric data on human tissue is justified on account of various medical applications, the safety assessment of human exposure to MMW

radiation and several sensor, medical and communications applications which are currently emerging.

- There is great concern that lightweight composite materials may contain defects which would undermine their strength. Consequently, there is growing interest in the feasibility of RF signals, particularly in the MMW band, to detect defects and monitor the cure state of composites.
- On the whole, techniques commonly used to measure the permittivity in the microwave band do not scale conveniently to the MMW band. Some are not suitable for the measurement of tissue either because of its physical characteristics or its high losses.

One of the main challenges identified from the problems associated with both human tissues and defect detection in composites is the ability to measure the permittivity of a planar material well into the MMW band. These two applications have a common solution which is presented in Chapter Three.

## CHAPTER TWO: THE ANALYSIS OF LAYERED DIELECTRICS

### 2.1 INTRODUCTION

This Chapter describes a novel means of analyzing the transmission and reflection coefficients for a generalized structure of any number of planar dielectric layers, each of any thickness. The analysis assumes that the incident signal is a plane wave and is normally incident on the dielectric surfaces. It starts by considering the analysis of a single dielectric which is the basis of the permittivity measurements described in Chapter Three and then extends it to multiple layers. The multiple layered problem starts by examining how two neighbouring layers can be replaced by an equivalent single layer and then, by repeated combinations, how any number of layers can be considered. The specific case of a structure of three dielectric layers is then formulated. The analytical model describing the specific case of three dielectric layers is validated by the reproduction of previously published data pertaining to a simplified three-layered structure.

This analysis has been developed to support the experimental work on single and multiple dielectric layers. It forms the basis for the processing of measured data to find the permittivity of a single planar dielectric layer (see, sections 3.3 and 3.5) and of multiple layers. The analysis presented here has been applied in finding the permittivity of human skin (Chapter Four) and single composite layers (Chapter Five) and also to analyse a three-layered structure comprising composites and an air gap (Chapter Five).

In the past this kind of problem has been treated by considering the intrinsic impedance of each layer starting with that which is furthermost from the illuminated surface and transforming this impedance over the thickness of the layer to form the load impedance of the previous layer. Repeating this operation ultimately results in deducing the load impedance at the illuminated surface from which the reflection and transmission coefficients at this plane may be calculated. This is described in standard texts such as that by Ramo, Whinnery and Van Duzer<sup>[118]</sup>. The alternative method presented here, based on signal flow methods, is more in keeping with optical techniques which become

more relevant in the millimetre wave band. In particular, the signal flow techniques applied in this analysis are well suited to the millimetric wave analysis of layered composites since they can be related quite readily to the signal flow in and around a void within the material. This method also forms a useful tool supporting ray tracing methods of modelling the propagation of signals. Furthermore, the present analysis could be extended to consider illumination by a plane wave at any arbitrary angle of incidence. This extension would be a useful tool in several further applications such as the optimisation and design of wideband stealthy coatings and frequency selective surfaces, particularly in the MMW band.

## 2.2 GENERAL ANALYSIS OF n-LAYERS OF ARBITRARY THICKNESS

This analysis starts by considering the case of a single dielectric slab separating two semi-infinite regions of dielectrics as may be presented by a single dielectric in free-space. Signal flow methods are used to derive the transmission and reflection coefficients of the dielectric slab plus also the coefficients of incident signals on the two inner surfaces of the dielectric slab walls. The analysis is repeated by considering an applied signal from the opposite side of the dielectric slab and a parallel set of four coefficients are defined. The case of two dielectric slabs is then considered and the eight coefficients derived for the single slab (four for each direction of incidence) are used to describe the signal flow between the dielectric interfaces. It is shown that the two dielectric slabs may be reduced to a single slab and are described by a similar set of four coefficients for each direction of incidence. Thus two layers are reduced to one. By repeated application of the layer reduction technique any number of dielectrics may be reduced to a single layer. The equations for the transmission and reflection coefficients of the reduced structure are presented and take account of all the multiple reflections between all dielectric interfaces.

### 2.2.1 Single Dielectric Layer in Free Space

Consider the case of three dielectric layers ( $a$ ,  $b$  and  $c$ ). The two outermost layers ( $a$  and  $c$ ) are infinitely thick layers and surround the inner layer ( $b$ ) which has a thickness,  $t_b$  and propagation constant,  $k_b$ . A plane wave signal within layer  $a$  is normally incident on the  $ab$  boundary and following multiple reflections between the  $ab$  and  $bc$  boundaries is partially reflected back into  $a$ , partially transmitted into  $c$  and partially absorbed within  $b$ . The situation is illustrated in Figure 2-1, below, in which the signals and labels refer to the signal E-field.

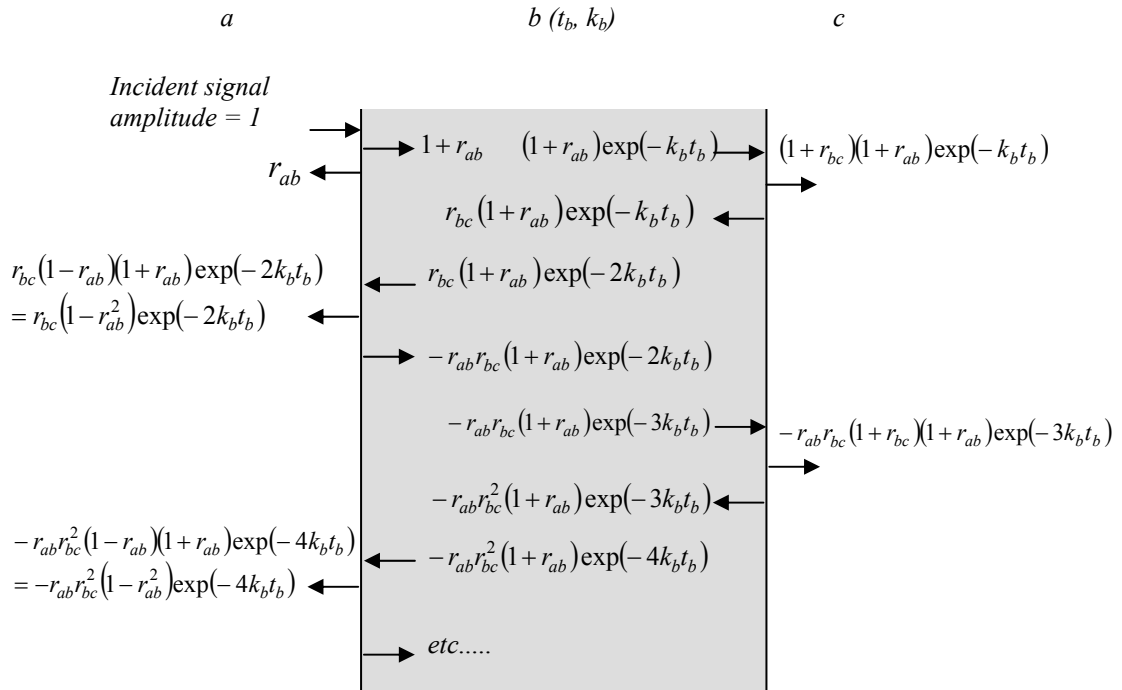


Figure 2-1: Multiple Reflections Between Two Dielectric Boundaries

Where  $r_{ab}$  is the reflection coefficient of the  $a$  to  $b$  boundary  
and  $r_{bc}$  is the reflection coefficient of the  $b$  to  $c$  boundary

Note that the arrows of Figure 2-1 refer to the direction of propagation and not the E-field orientation. The signs of the reflected and transmitted component at each boundary ensure that the E-field boundary condition is met; namely, that the E-field is continuous across the boundary between two dielectrics.

The total signal reflected from the  $ab$  boundary is<sup>d</sup>:

$$= r_{ab} + r_{bc} (1 - r_{ab}^2) \exp(-2k_b t_b) + (-r_{ab}) r_{bc}^2 (1 - r_{ab}^2) \exp(-4k_b t_b) + \dots$$

$$= r_{ab} + r_{bc} (1 - r_{ab}^2) \exp(-2k_b t_b) [1 + (-r_{ab}) r_{bc} \exp(-2k_b t_b) + \dots]$$

Using the result  $\frac{1}{1-x} = 1 + x + x^2 + \dots$

$$\begin{aligned} &= r_{ab} + \frac{r_{bc} (1 - r_{ab}^2) \exp(-2k_b t_b)}{1 + r_{bc} r_{ab} \exp(-2k_b t_b)} \\ &= \frac{r_{ab} (1 + r_{ab} r_{bc} \exp(-2k_b t_b)) + r_{bc} (1 - r_{ab}^2) \exp(-2k_b t_b)}{1 + r_{bc} r_{ab} \exp(-2k_b t_b)} \\ &= \frac{r_{ab} + r_{bc} \exp(-2k_b t_b)}{1 + r_{bc} r_{ab} \exp(-2k_b t_b)} \end{aligned} \quad (1)$$

The total transmitted signal from  $a$  to  $c$  is:

$$\begin{aligned} &= (1 + r_{bc})(1 + r_{ab}) \exp(-k_b t_b) + (-r_{ab}) r_{bc} (1 + r_{ab})(1 + r_{bc}) \exp(-3k_b t_b) + \dots \\ &= (1 + r_{bc})(1 + r_{ab}) \exp(-k_b t_b) [1 + (-r_{ab}) r_{bc} \exp(-2k_b t_b) + \dots] \\ &= \frac{(1 + r_{bc})(1 + r_{ab}) \exp(-k_b t_b)}{1 + r_{ab} r_{bc} \exp(-2k_b t_b)} \end{aligned} \quad (2)$$

---

<sup>d</sup> Throughout the analysis a specific system of equation numbering is used which, by necessity, differs from the format of other chapters; expressions developed in the early stages are imported into future stages. The later stages of the analysis develop equations which are formed from the earlier expressions and are referred to using the appropriate equation numbers.

The total signal incident on the  $ab$  boundary from the rhs is:

$$\begin{aligned}
 &= r_{bc} (1 + r_{ab}) \exp(-2k_b t_b) + (-r_{ab}) r_{bc}^2 (1 + r_{ab}) \exp(-4k_b t_b) + \dots \\
 &= r_{bc} (1 + r_{ab}) \exp(-2k_b t_b) [1 + (-r_{ab}) r_{bc} \exp(-2k_b t_b) + \dots] \\
 &= \frac{r_{bc} (1 + r_{ab}) \exp(-2k_b t_b)}{1 + r_{ab} r_{bc} \exp(-2k_b t_b)} \quad (3)
 \end{aligned}$$

The total signal incident on the  $bc$  boundary from the lhs is:

$$\begin{aligned}
 &= (1 + r_{ab}) \exp(-k_b t_b) + (-r_{ab}) r_{bc} (1 + r_{ab}) \exp(-3k_b t_b) + \dots \\
 &= (1 + r_{ab}) \exp(-k_b t_b) [1 + (-r_{ab}) r_{bc} \exp(-2k_b t_b) + \dots] \\
 &= \frac{(1 + r_{ab}) \exp(-k_b t_b)}{1 + r_{ab} r_{bc} \exp(-2k_b t_b)} \quad (4)
 \end{aligned}$$

Since the incident signal amplitude is normalized to 1, then equations (1), (2), (3) and (4) represent coefficients (of reflection, transmission and incidence) of the dielectric structure with infinite multiple reflections between interfaces taken into consideration. This situation is represented using the diagram and nomenclature of Figure 2-2a below, in which the broad arrow within dielectric  $b$  represents the multiple reflections and the bracketed numbers represent the coefficients defined by equations (1), (2), (3) and (4) above. The arrow labelled “1” top left indicates the application of a signal of amplitude normalised to unity from within dielectric  $a$  onto the  $ab$  interface.

If the incident signal had been from the other side i.e. from within layer  $c$ , then the situation is described using similar equations except that  $r_{cb}$  replaces  $r_{ab}$  and  $r_{ba}$  replaces  $r_{bc}$ . Making these replacements (1) to (4) become:

$$\frac{r_{cb} + r_{ba} \exp(-2k_b t_b)}{1 + r_{cb} r_{ba} \exp(-2k_b t_b)} \quad (1') \quad \frac{(1+r_{ba})(1+r_{cb})\exp(-k_b t_b)}{1+r_{cb}r_{ba}\exp(-2k_b t_b)} \quad (2')$$

$$\frac{r_{ba} (1+r_{cb})\exp(-2k_b t_b)}{1+r_{cb}r_{ba}\exp(-2k_b t_b)} \quad (3') \quad \frac{(1+r_{cb})\exp(-k_b t_b)}{1+r_{cb}r_{ba}\exp(-2k_b t_b)} \quad (4')$$

This parallel set of four equations also represents coefficients of reflection, transmission and incidence of the dielectric structure when the incident signal (amplitude normalised to unity) applied from dielectric  $c$  is incident on the  $cb$  interface. The dashes used in these equation numbers above indicate that forward propagation is taken to be from right to left, whereas the un-dashed equation numbers denotes forward propagation in the direction left to right. Similarly, this situation is represented in Figure 2-2b.

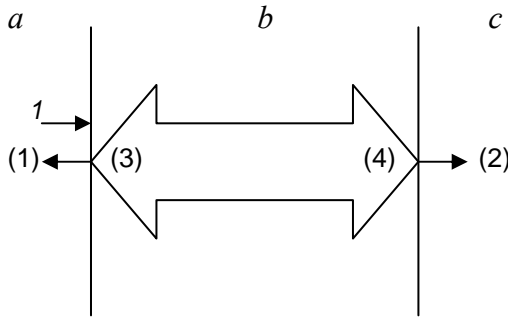


Figure 2-2a: Signal Flow Diagram  
(input on lhs)

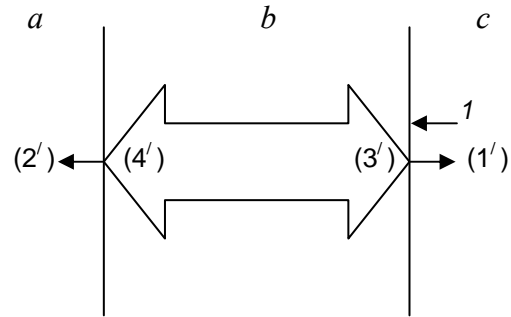


Figure 2-2b: Signal Flow Diagram  
(input on rhs)

The experimental set up to measure permittivity of a sample is a special case in which layers  $a$  and  $c$  are free space and layer  $b$  is a sample having a wave number  $k_s$  of known thickness,  $t_s$ . For this special case let  $r_{ab} = r_I$ ,  $r_{bc} = -r_I$ ,  $k_b = k_s$  and  $t_b = t_s$ . In which case equations (1) to (4) become:

$$\frac{r_1 - r_1 \exp(-2k_S t_S)}{1 - r_1^2 \exp(-2k_S t_S)} \quad (1S)$$

$$\frac{(1 - r_1^2) \exp(-k_S t_S)}{1 - r_1^2 \exp(-2k_S t_S)} \quad (2S)$$

$$\frac{- (r_1 + r_1^2) \exp(-2k_S t_S)}{1 - r_1^2 \exp(-2k_S t_S)} \quad (3S)$$

$$\frac{(1 + r_1) \exp(-k_S t_S)}{1 - r_1^2 \exp(-2k_S t_S)} \quad (4S)$$

Equations (1S) and (2S) above are identical to (3.1) and (3.2) presented in section 3.3 concerning the theory of the measurement of permittivity of a single dielectric layer.

### 2.2.2 Two Dielectric Layers in Free Space

In an attempt to analyse the general case of  $n$  dielectrics, consider first the case of two layers ( $n = 2$ ) plus a zeroth and third layer of free-space. The idea is to simplify the two layers into a single one (equivalent to the two). This is best shown using the signal flow diagram of Figure 2-3, below, which builds on those of Figure 2-2a and Figure 2-2b.

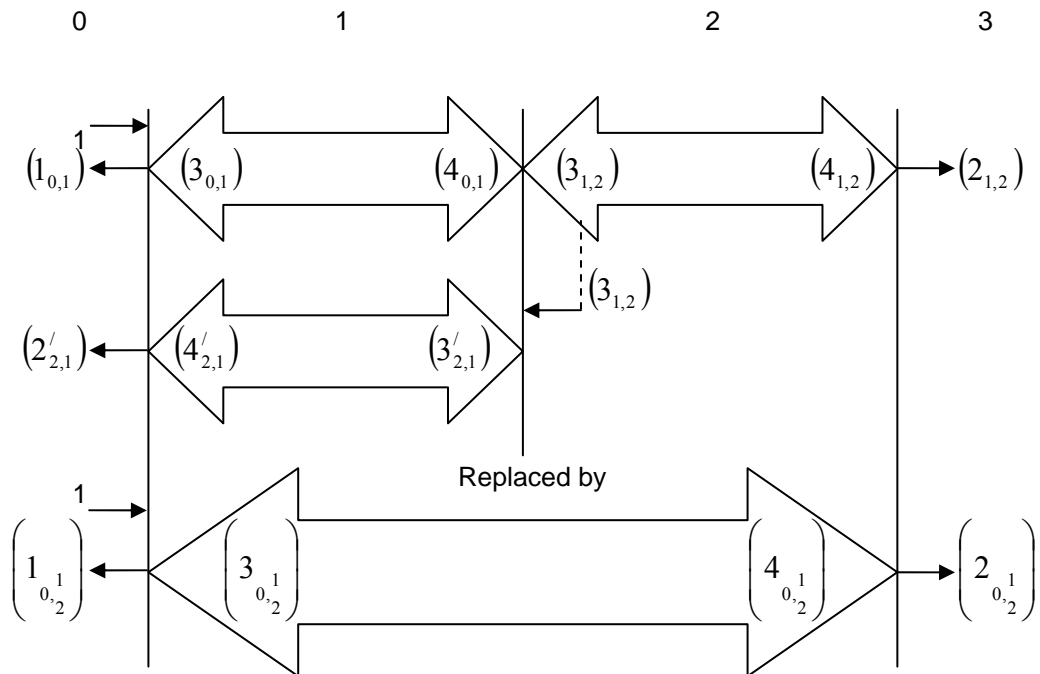


Figure 2-3: Flow Diagram for Two Dielectric Layers

The bracketed numbers denote the relevant equation numbers for the reflected, transmitted and incident coefficients. The first subscript denotes the layer number from which the incident signal arrives at a boundary and the second subscript denotes the layer number into which an incident signal is transmitted. The second subscript of  $\frac{1}{2}$  denotes the combination of layers 1 and 2. Un-dashed equation numbers denote an incident signal arriving from the left and the dashed superscript denotes an incident signal arriving from the right.

The coefficient  $(4_{0,1})$  forms the input into the second layer which is incident from the first. Similarly, when multiple reflections are taken into consideration, coefficient  $(3_{1,2})$  represents the signal incident on the right hand side of the first layer arriving from the second layer, as indicated by the dashed arrow. This signal is then subject to multiple reflections within the first layer, being partially reflected (back into the second), partially transmitted (on into the zeroth) and partially absorbed (within the first). That which is reflected back towards the second layer i.e.  $(3'_{2,1})$ , adds to the original component denoted by  $(4_{0,1})$  and is once again subject to an infinite series of multiple reflections within layer two. This component has followed the path  $(4_{0,1})$  cascaded with  $(3_{1,2})$  and then further cascaded with  $(3'_{2,1})$ . Each of these terms represents coefficients with multiple reflections taken into consideration. By a continuation of this argument it is evident that there exists an infinite series of multiple reflections between the two layers. The signal incident on the boundary between the first and second layer from the left is therefore the original  $(4_{0,1})$  plus the product of  $(4_{0,1})(3_{1,2})(3'_{2,1})$  plus an infinite series of additional terms due to further multiple reflections. In this way it is possible to develop expressions for the total overall coefficients of reflection, transmission and incidence for the double layer; each expression being the sum of an infinite series. This description is not as complex as it may first sound since it is remarkably similar to the case of a single dielectric. Once these coefficients have been derived and simplified they may be used to represent the double layer as if it were a single layer.

The total reflected signal back into the zeroth layer consists of an infinite sum of contributions:

$$\begin{aligned}
 &= (1_{0,1}) + (4_{0,1})(3_{1,2})(2'_{2,1}) + (4_{0,1})(3_{1,2})(3'_{2,1})(3_{1,2})(2'_{2,1}) + (4_{0,1})(3_{1,2})(3'_{2,1})(3_{1,2})(3'_{2,1})(3_{1,2})(2'_{2,1}) + \dots \\
 &= (1_{0,1}) + (4_{0,1})(3_{1,2})(2'_{2,1}) \left[ 1 + (3'_{2,1})(3_{1,2}) + (3'_{2,1})^2 (3_{1,2})^2 + \dots \right] \\
 &= (1_{0,1}) + \frac{(4_{0,1})(3_{1,2})(2'_{2,1})}{1 - (3'_{2,1})(3_{1,2})} \\
 &= \frac{(1_{0,1})(1 - [(3_{1,2})(3'_{2,1})]) + (4_{0,1})(3_{1,2})(2'_{2,1})}{1 - (3_{1,2})(3'_{2,1})}
 \end{aligned}$$

The total signal transmitted into layer 3 is:

$$\begin{aligned}
 &= (4_{0,1})(2_{1,2}) + (4_{0,1})(3_{1,2})(3'_{2,1})(2_{1,2}) + (4_{0,1})(3_{1,2})(3'_{2,1})(3_{1,2})(3'_{2,1})(2_{1,2}) + \dots \\
 &= (4_{0,1})(2_{1,2}) \left[ 1 + (3_{1,2})(3'_{2,1}) + (3_{1,2})^2 (3'_{2,1})^2 + \dots \right] \\
 &= \frac{(4_{0,1})(2_{1,2})}{1 - (3_{1,2})(3'_{2,1})}
 \end{aligned}$$

The total signal incident on the 0/1 boundary from the right is:

$$= (3_{0,1}) + (4_{0,1})(3_{1,2})(4'_{2,1}) + (4_{0,1})(3_{1,2})(3'_{2,1})(3_{1,2})(4'_{2,1}) + \dots$$

$$= (3_{0,1}) + (4_{0,1})(3_{1,2})(4'_{2,1}) [1 + (3_{1,2})(3'_{2,1}) + \dots]$$

$$= (3_{0,1}) + \frac{(4_{0,1})(3_{1,2})(4'_{2,1})}{1 - [(3_{1,2})(3'_{2,1})]}$$

$$= \frac{(3_{0,1})(1 - [(3_{1,2})(3'_{2,1})]) + (4_{0,1})(3_{1,2})(4'_{2,1})}{1 - [(3_{1,2})(3'_{2,1})]} \begin{pmatrix} 3 \\ 0, 1 \\ 1, 2 \end{pmatrix}$$

The total signal incident on the 2/3 boundary from the left is:

$$= (4_{0,1})(4_{1,2}) + (4_{0,1})(3_{1,2})(3'_{2,1})(4_{1,2}) + (4_{0,1})(3_{1,2})(3'_{2,1})(3_{1,2})(3'_{2,1})(4_{1,2}) + \dots$$

$$= (4_{0,1})(4_{1,2}) [1 + (3_{1,2})(3'_{2,1}) + (3_{1,2})^2(3'_{2,1})^2 + \dots]$$

$$= \frac{(4_{0,1})(4_{1,2})}{1 - [(3_{1,2})(3'_{2,1})]} \begin{pmatrix} 4 \\ 0, 1 \\ 1, 2 \end{pmatrix}$$

### 2.2.3 General Case of $n$ Dielectric Layers

Having combined two neighbouring layers it is now possible to repeat this process as many times as necessary to combine all layers into one and so to derive the overall transmission and reflection coefficients from a general structure of  $n$  dielectric layers, each of any thickness,  $t_n$ , and wave number,  $k_n$ , and hence permittivity,  $\varepsilon_n$ . The sequence of the algorithm is to:

- Input the  $k$  and  $t$  values of each layer (or input  $\varepsilon$  and calculate  $k$ )
- Calculate the reflection coefficient ( $r_{xy}$ ) at each boundary, x/y
- Calculate  $(1_{x,y})$ ,  $(2_{x,y})$ ,  $(3_{x,y})$ ,  $(4_{x,y})$ ,  $(1'_{x,y})$ ,  $(2'_{x,y})$ ,  $(3'_{x,y})$  and  $(4'_{x,y})$  for each boundary
- Combine layers in pairs successively, calculating the combinatory set of coefficients at each level of combination until the structure is reduced to a single layer
- Reflection coefficient =  $\begin{pmatrix} 1 & \\ & \ddots & 1 \\ & 0, : & n \end{pmatrix}$  and transmission coefficient =  $\begin{pmatrix} 2 & \\ & \ddots & 1 \\ & 0, : & n \end{pmatrix}$ .

### 2.2.4 Specific Formulation of Three Dielectric Layers

The general analysis of multiple layers described above has been applied to solve the transmission and reflection coefficients of three dielectric layers. A three layer model has a number of practical applications e.g. a liquid dielectric between two layers of container material, a solid composite material containing a void within it, the three discrete layers of skin. The model has been implemented in the MATLAB program, D3TR.m, a complete listing of which is given in Appendix C. This model is validated in the next section.

The signal flow chart and layer reductions are shown in Figure 2-4 below.

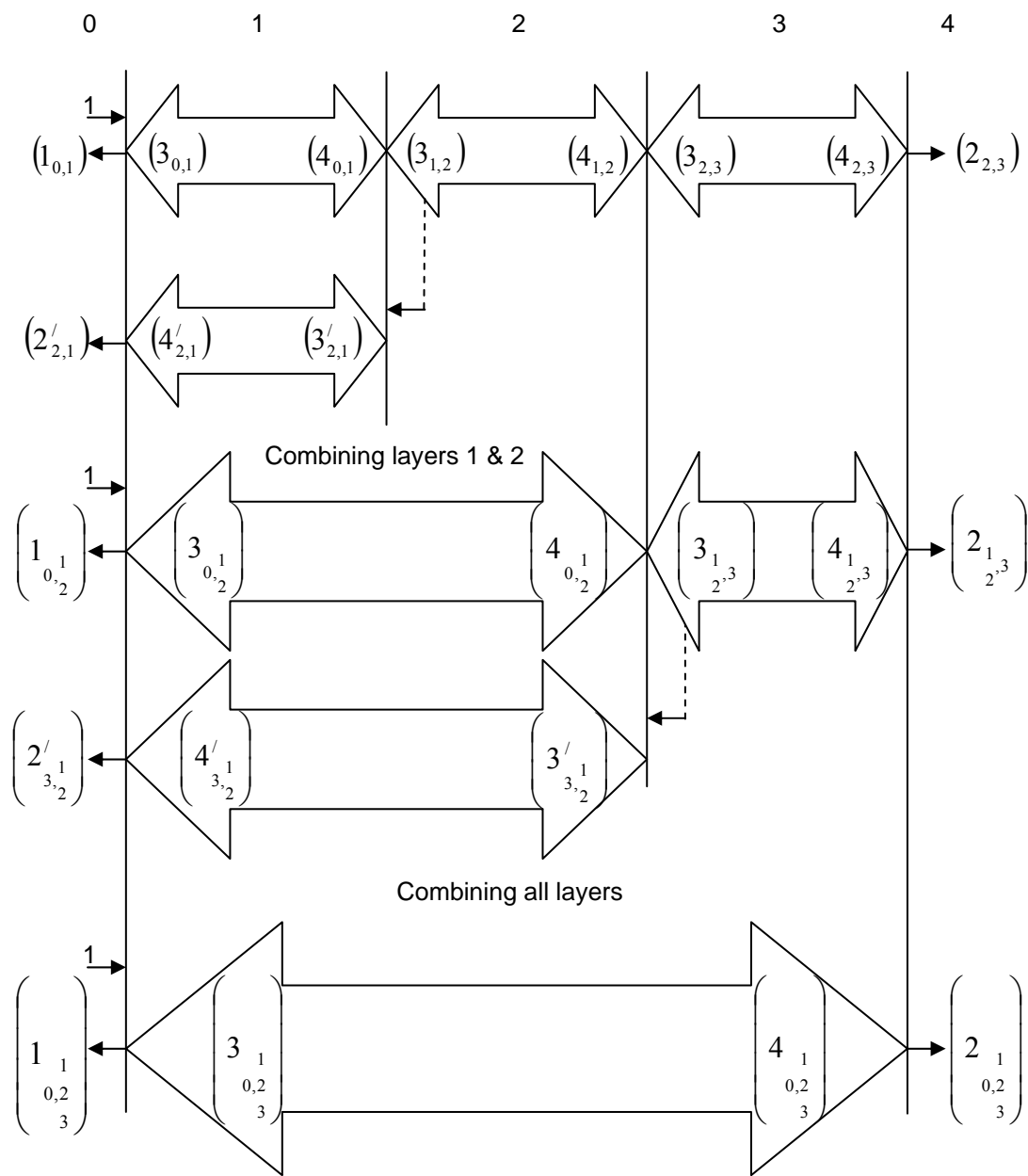


Figure 2-4: Three Dielectric Layers

The reflection coefficients at each boundary are shown in Figure 2-5 below.

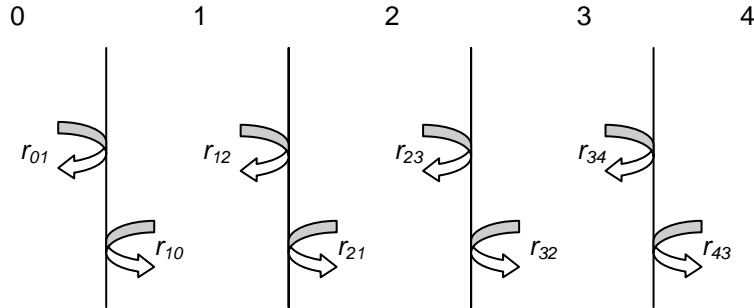


Figure 2-5: Three Layer Reflection Coefficients

Note  $r_{10} = -r_{01}$ ,  $r_{21} = -r_{12}$ ,  $r_{32} = -r_{23}$  and  $r_{43} = -r_{34}$ .

The coefficients of reflection, transmission and incidence for each of the individual layers are given below. These are the cases of equations (1), (2), (3) and (4) for signals incident from the left and equations (1'), (2'), (3') and (4') for signals incident from the right with the appropriate reflection coefficients for each layer applied.

First Layer.

$$\frac{r_{01} + r_{12} \exp(-2k_1 t_1)}{1 + r_{01} r_{12} \exp(-2k_1 t_1)} \quad (1_{0,1}) \quad \frac{(1+r_{12})(1+r_{01})\exp(-k_1 t_1)}{1+r_{01}r_{12}\exp(-2k_1 t_1)} \quad (2_{0,1})$$

$$\frac{r_{12}(1+r_{01})\exp(-2k_1 t_1)}{1+r_{01}r_{12}\exp(-2k_1 t_1)} \quad (3_{0,1}) \quad \frac{(1+r_{01})\exp(-k_1 t_1)}{1+r_{01}r_{12}\exp(-2k_1 t_1)} \quad (4_{0,1})$$

$$\frac{r_{21} + r_{10} \exp(-2k_1 t_1)}{1 + r_{21} r_{10} \exp(-2k_1 t_1)} \quad (1'_{0,1}) \quad \frac{(1+r_{10})(1+r_{21})\exp(-k_1 t_1)}{1+r_{21}r_{10}\exp(-2k_1 t_1)} \quad (2'_{0,1})$$

$$\frac{r_{10}(1+r_{21})\exp(-2k_1 t_1)}{1+r_{21}r_{10}\exp(-2k_1 t_1)} \quad (3'_{0,1}) \quad \frac{(1+r_{21})\exp(-k_1 t_1)}{1+r_{21}r_{10}\exp(-2k_1 t_1)} \quad (4'_{0,1})$$

## Second Layer

$$\frac{r_{12} + r_{23} \exp(-2k_2 t_2)}{1 + r_{12} r_{23} \exp(-2k_2 t_2)} \quad (1_{1,2})$$

$$\frac{(1+r_{23})(1+r_{12})\exp(-k_2 t_2)}{1+r_{12}r_{23}\exp(-2k_2 t_2)} \quad (2_{1,2})$$

$$\frac{r_{23}(1+r_{12})\exp(-2k_2 t_2)}{1+r_{12}r_{23}\exp(-2k_2 t_2)} \quad (3_{1,2})$$

$$\frac{(1+r_{12})\exp(-k_2 t_2)}{1+r_{12}r_{23}\exp(-2k_2 t_2)} \quad (4_{1,2})$$

$$\frac{r_{32} + r_{21} \exp(-2k_2 t_2)}{1 + r_{32} r_{21} \exp(-2k_2 t_2)} \quad (1'_{3,2})$$

$$\frac{(1+r_{21})(1+r_{32})\exp(-k_2 t_2)}{1+r_{32}r_{21}\exp(-2k_2 t_2)} \quad (2'_{3,2})$$

$$\frac{r_{21}(1+r_{32})\exp(-2k_2 t_2)}{1+r_{32}r_{21}\exp(-2k_2 t_2)} \quad (3'_{3,2})$$

$$\frac{(1+r_{32})\exp(-k_2 t_2)}{1+r_{32}r_{21}\exp(-2k_2 t_2)} \quad (4'_{3,2})$$

## Third Layer

$$\frac{r_{23} + r_{34} \exp(-2k_3 t_3)}{1 + r_{23} r_{34} \exp(-2k_3 t_3)} \quad (1_{2,3})$$

$$\frac{(1+r_{34})(1+r_{23})\exp(-k_3 t_3)}{1+r_{23}r_{34}\exp(-2k_3 t_3)} \quad (2_{2,3})$$

$$\frac{r_{34}(1+r_{23})\exp(-2k_3 t_3)}{1+r_{23}r_{34}\exp(-2k_3 t_3)} \quad (3_{2,3})$$

$$\frac{(1+r_{23})\exp(-k_3 t_3)}{1+r_{23}r_{34}\exp(-2k_3 t_3)} \quad (4_{2,3})$$

$$\frac{r_{43} + r_{32} \exp(-2k_3 t_3)}{1 + r_{43} r_{32} \exp(-2k_3 t_3)} \quad (1'_{4,3})$$

$$\frac{(1+r_{32})(1+r_{43})\exp(-k_3 t_3)}{1+r_{43}r_{32}\exp(-2k_3 t_3)} \quad (2'_{4,3})$$

$$\frac{r_{32}(1+r_{43})\exp(-2k_3 t_3)}{1+r_{43}r_{32}\exp(-2k_3 t_3)} \quad (3'_{4,3})$$

$$\frac{(1+r_{43})\exp(-k_3 t_3)}{1+r_{43}r_{32}\exp(-2k_3 t_3)} \quad (4'_{4,3})$$

Strictly, the last four equations are not required but are included for completeness.

Combining layers 1 and 2, the coefficients of reflection, transmission and incidence for each direction of incidence are given below.

$$\begin{array}{lll}
 \left(1_{0,1}\right) + \frac{\left(4_{0,1}\right)\left(3_{1,2}\right)\left(2'_{2,1}\right)}{1 - \left(3'_{2,1}\right)\left(3_{1,2}\right)} & \left(1_{0,2}\right) & \frac{\left(4_{0,1}\right)\left(2_{1,2}\right)}{1 - \left(3'_{2,1}\right)\left(3_{1,2}\right)} \\
 \left(3_{0,1}\right) + \frac{\left(4_{0,1}\right)\left(3_{1,2}\right)\left(4'_{2,1}\right)}{1 - \left(3'_{2,1}\right)\left(3_{1,2}\right)} & \left(3_{0,2}\right) & \frac{\left(4_{0,1}\right)\left(4_{1,2}\right)}{1 - \left(3'_{2,1}\right)\left(3_{1,2}\right)} \\
 \left(1'_{3,2}\right) + \frac{\left(4'_{3,2}\right)\left(3'_{2,1}\right)\left(2_{1,2}\right)}{1 - \left(3_{1,2}\right)\left(3'_{2,1}\right)} & \left(1'_{3,2}\right) & \frac{\left(4'_{3,2}\right)\left(2'_{2,1}\right)}{1 - \left(3_{1,2}\right)\left(3'_{2,1}\right)} \\
 \left(3'_{3,2}\right) + \frac{\left(4'_{3,2}\right)\left(3'_{2,1}\right)\left(4_{1,2}\right)}{1 - \left(3_{1,2}\right)\left(3'_{2,1}\right)} & \left(3'_{3,2}\right) & \frac{\left(4'_{3,2}\right)\left(4'_{2,1}\right)}{1 - \left(3_{1,2}\right)\left(3'_{2,1}\right)}
 \end{array}$$

Combining layers  $\frac{1}{2}$  & 3 we obtain the transmission and reflection coefficients, respectively as:

$$t = \frac{\left(4_{0,2}\right)\left(2_{2,3}\right)}{1 - \left(3_{2,3}\right)\left(3'_{3,2}\right)} \quad \text{and} \quad r = \frac{\left(4_{0,2}\right)\left(3_{2,3}\right)\left(2'_{2,2}\right)}{1 - \left(3_{2,3}\right)\left(3'_{3,2}\right)}$$

or in decibels

$$T = 20 \log_{10} |t| \quad dB$$

$$R = 20 \log_{10} |r| \quad dB$$

## 2.3 VALIDATION OF THE THREE DIELECTRIC LAYER MODEL

Figure 2-6, below, depicts a three-layered dielectric structure surrounded by free-space in which the permittivity and thickness of each layer is labelled.

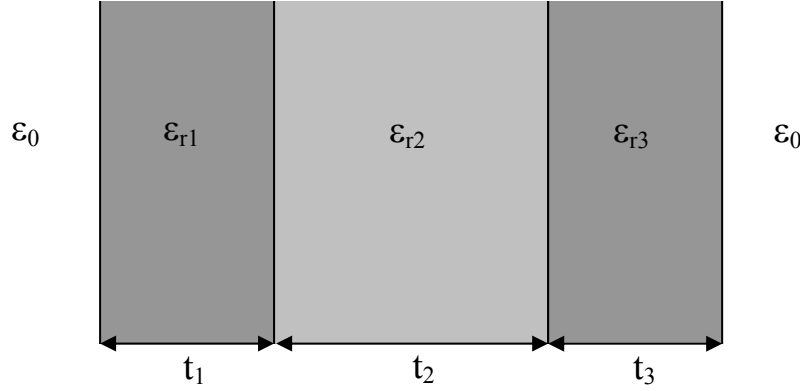


Figure 2-6: Three-Layered Dielectric Structure

Ma and Okamura<sup>[78]</sup> presented equations for the transmission and reflection coefficients of a simplified form of this structure in which the first and third layers formed a container and were of identical thickness and permittivity and the inner second layer was the sample under test. These equations are based on signal flow methods and are reproduced below:

$$t = \frac{(1 - r_1^2)(1 - r_2^2) \exp(-j2k_c t_c) \exp(-jk_s t_s)}{[1 + r_1 r_2 \exp(-j2k_c t_c)]^2 - [r_1 \exp(-j2k_c t_c) + r_2]^2 \exp(-j2k_s t_s)} \quad (2.1)$$

$$r = \frac{[1 + r_1 r_2 \exp(-j2k_c t_c)][r_1 + r_2 \exp(-j2k_c t_c)]}{[1 + r_1 r_2 \exp(-j2k_c t_c)]^2 - [r_2 + r_1 \exp(-j2k_c t_c) + r_2]^2 \exp(-j2k_s t_s)} - \dots \dots$$

$$\dots \dots \frac{[r_2 + r_1 \exp(-j2k_c t_c)][r_1 r_2 + \exp(-j2k_c t_c)] \exp(-j2k_s t_s)}{[1 + r_1 r_2 \exp(-j2k_c t_c)]^2 - [r_2 + r_1 \exp(-j2k_c t_c) + r_2]^2 \exp(-j2k_s t_s)} \quad (2.2)$$

In which:

$r_1$  = reflection coefficient of air/container interface

$r_2$  = reflection coefficient of container/sample interface

$k_c$  = propagation constant in container material (layers 1 and 3)

$k_s$  = propagation constant in sample material (layer 2)

$t_c$  = thickness of container material (layers 1 and 3)

$t_s$  = thickness of sample material (layer 2)

Equations (2.1) and (2.2) have been implemented in the MATLAB program, TR1.m (Appendix C). The data of Ma and Okamura [78] is given as  $\epsilon_{r1} = \epsilon_{r3} (= 2.55 - j0.07)$ ,  $t_1 = t_3 = t_c = 3\text{mm}$ , frequency = 9.4GHz and the sample permittivity  $\epsilon_{r2} = 20 - j1$  and thickness  $t_2 = t_s = 30\text{mm}$ . The solutions obtained from both TR1.m i.e. (2.1) and (2.2) and from D3TR.m i.e. general three layer model, both yield exactly the same results, namely:  $T = -8.5605\text{dB}$  and  $R = -5.1260\text{dB}$ . Wideband solutions using each model (TR1.m and D3TR.m) over a range of frequencies also yield identical results indicating that the two models are numerically equivalent to each other. Ma and Okamura anticipate results of  $T = -8.375\text{dB}$  and  $R = -5.036\text{dB}$  based on a simplifying assumption that multiple reflections can be ignored, which is in close agreement with the modelled data here. No measured data is quoted.

Furthermore, if any two layers are set to zero thickness or for the permittivity of free-space the remaining one layer returns results commensurate with that of a single layer.

In conclusion, the technique of analysing the transmission and reflection coefficients from the generalised model of multiple dielectric layers presented here has been validated using a specific case of a three layered structure. The coincidences between this model and others, previously published, validate the model. Further validation based on experimental measurements is presented in Chapter Five, section 5.5.

## 2.4 CHAPTER SUMMARY

A novel method of determining the transmission and reflection coefficients as functions of frequency arising from a generalised structure of planar dielectric layers has been described. The analytical method assumes that the thickness and permittivity of each layer is known and that it is illuminated by a plane wave at normal incidence. The method is based on signal flow techniques and considers the infinite multiple reflections occurring at dielectric interfaces. This method of analysis employs an algorithm which reduces the signal coefficients of two neighbouring layers into one. Successive applications of the layer reduction technique ultimately reduce the structure to a single layer. The algorithm has been applied to the specific case of three dielectric layers as such a structure has several useful applications. The three-layer model has been validated by replicating precisely previously published results for a simplified three-layer structure. The three-layer model also returns results consistent with those of a single layer when any two layers are reduced to zero thickness or have a permittivity equal to that of free space.

The algorithm described here has a number of advantages over alternative techniques, particularly, in the analysis of thin dielectric layers and/or millimetric wave frequencies. Further extensions of the method would also enable the analysis to be performed for any general angle of incidence, which would permit further applications of the model. To the best of the author's knowledge, the analytical technique to analyse a general structure of planar dielectrics presented here is novel.

This analytical tool is to be employed in the analysis of single and multiple layered dielectric structures considered in the ensuing Chapters of this thesis.

## CHAPTER THREE: THE MEASUREMENT OF PERMITTIVITY IN THE MILLIMETRE WAVE BAND

### 3.1 INTRODUCTION

Chapter One described the aim of measuring the permittivity of human skin in the MMW band and of the potential of dielectric imaging within the MMW band for the detection and location of defects within composite materials. The methods of measuring permittivity which were reviewed in Chapter One are revisited to consider which technique is best suited to both the applications mentioned above. This chapter starts by justifying the choice of a free-space based method. The theoretical background to method is referenced from Chapter Two. The experimental set-up and measurement protocol is then described and the issue of ambiguous solutions is raised. There then follows a description of the method of processing the measured data to find unambiguous solutions for the complex permittivity of the sample under test. The experimental method was developed and validated at J-band and subsequently scaled to the MMW band. Initial results at 60GHz are given in order to further validate the scaled version of the experimental set-up in the MMW band.

### 3.2 SELECTION OF EXPERIMENTAL METHOD

The selection of the experimental method was primarily driven by the aim to measure the permittivity of human skin in the MMW band, particularly up to 100GHz. A wideband technique was sought so that dispersive characteristics, should they exist, could be observed. The measurement need not be made *in vivo* although it should allow the moisture content of the skin sample to be preserved and the temperature to be monitored. For the purposes of these measurements, the skin would be treated as a single, planar dielectric layer. Even though permittivity is a bulk property, it is also acknowledged that it may be important to distinguish between the inner and outer surfaces. It was anticipated that skin would be highly lossy in the MMW band and that its properties would be more than likely to vary, both locally within a sample and on a

sample by sample basis. Local variations could be averaged out if the measurement is performed on a sufficiently large sample, but not so large as to be unfeasible. It was envisaged that skin samples would be available of several tens of square centimetres. Methods using two samples of (assumed) identical properties have to be discounted due to the natural variation between samples. Skin samples are soft, slightly compressible and stretchy. The preparation of accurately dimensioned, small samples would be awkward and could introduce considerable experimental error. Skin, as a dielectric sample, therefore places the following constraints on the experimental method:

- should be wideband,
- must be able to measure very lossy materials,
- moderate sample sizes required,
- minimal sample preparation preferred,
- measurement to be performed on a single sample of constant thickness,

Chapter One reviewed potential methods of permittivity measurement. Section 1.5.7 provides a quick comparison of methods. The leading contenders were considered to be free-space techniques and waveguide techniques. Both techniques are wideband and would be suitable for lossy samples and would require a single sample only. The free-space method would utilise larger samples than the waveguide technique. The termination of a waveguide with the sample appeared attractive as it offers an *in vivo* measurement method but could also call into question whether the result would be influenced by fat, muscle and bone layers beneath the skin. A major concern of waveguide techniques was the preparation and fitting of small skin samples within a waveguide. The attraction of the free-space method is largely in the minimal sample preparation required. The concerns in using free-space techniques were that it required samples of even thickness and that it would not be as accurate as waveguide techniques. Most of the methods to measure permittivity that are conventionally used in the centimetric wave band do not scale conveniently to the millimetre wave band. Free-space techniques are perhaps the exception.

The free-space techniques based on the measurement of the amplitudes of transmission and reflection coefficient at normal incidence was selected for its simplicity and requirements for minimal sample preparation. The method of Ma and Okamura [78] appeared particularly attractive and was therefore selected as the basis for the experimental method. This method would also serve the millimetric wave dielectric imaging of planar composite samples.

### 3.3 THEORY

The theoretical basis is described in Chapter Two and in previously published papers by the author [62][119] which are reproduced in Appendix A. The following is taken from these papers.

A plane wave normally incident on a slab of dielectric sample of thickness  $t_s$  is partially reflected, transmitted and absorbed by the dielectric. The reflected and transmitted signals are comprised of an infinite number of components due to the multiple reflections between the air/dielectric interfaces. Thus the total reflected and transmitted signals are given respectively by:

$$r = \frac{r_1 - r_1 \exp(-2k_s t_s)}{1 - r_1^2 \exp(-2k_s t_s)} \quad (3.1)$$

and

$$t = \frac{(1 - r_1^2) \exp(-k_s t_s)}{1 - r_1^2 \exp(-2k_s t_s)} \quad (3.2)$$

where  $k_s$  is the propagation constant in the sample and  $r_1$  is the reflection coefficient of the sample/air interface. Both are functions of the relative complex permittivity,  $\varepsilon_r$ , of the sample given by:

$$r_1 = -\frac{\sqrt{\varepsilon_r} - \sqrt{\varepsilon_o}}{\sqrt{\varepsilon_r} + \sqrt{\varepsilon_o}} \quad (3.3)$$

and

$$k_s = k_o \sqrt{\epsilon_r} \quad (3.4)$$

where  $k_o$  and  $\epsilon_o$  are the propagation constant and permittivity in free space, respectively.

The measured values of the reflection and transmission coefficients are  $R_m$  and  $T_m$  respectively and relate to  $r$  and  $t$  by the equation pair:

$$R_m = 20 \log_{10} |r| \text{ dB} \quad (3.5)$$

and

$$T_m = 20 \log_{10} |t| \text{ dB} \quad (3.6)$$

Wideband solutions of  $R_m$  and  $T_m$  indicate cyclical variations with frequency due to the multiple reflections between interfaces beating in and out of phase. The frequencies of peaks and troughs occur when the sample thickness is a multiple of a quarter wavelength and may be used to provide an initial estimate of  $\epsilon_r$ .

### 3.4 EXPERIMENTAL SET UP

The experimental set up of Figure 3-1 was used.

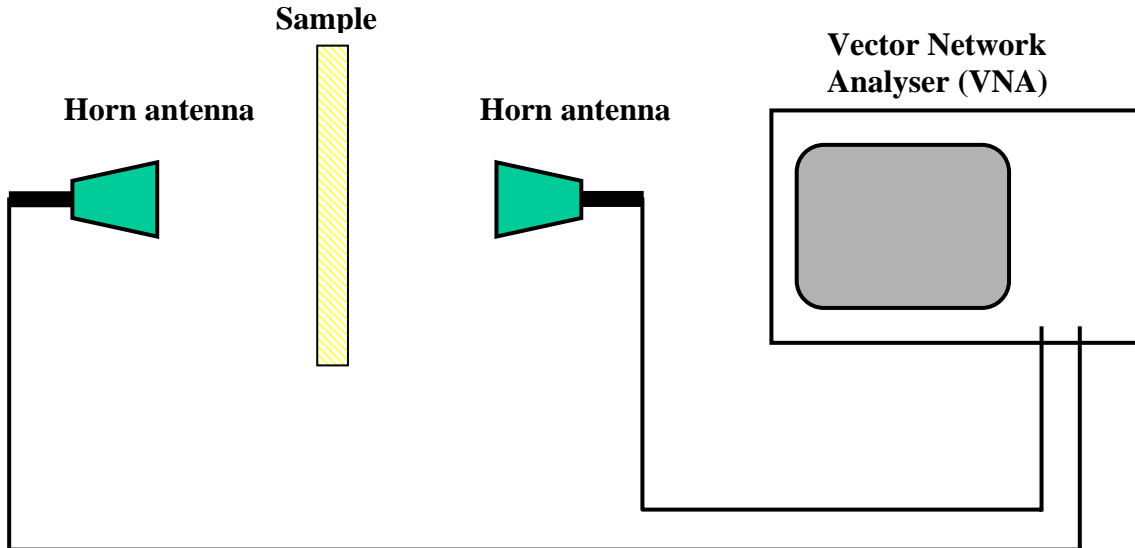


Figure 3-1: Experimental Set Up

Circular samples were clamped on to an annular sample frame placed mid-way between a pair of standard gain waveguide horns connected to a vector network analyser (VNA).  $T_m$  and  $R_m$  were measured via the VNA  $|S_{21}|$  and  $|S_{11}|$  paths, respectively. This method requires that only the amplitudes of the transmission and reflection coefficients need be measured and that there is no need for phase data. The amplitudes only method reduces the requirement to accurately maintain the positional and alignment accuracy of the equipment and to maintain the phase and frequency stability of the VNA source. The horns were aligned for vertical polarisation, parallel with each other and for normal incidence on the sample. Lähteenmäki and Karttaavi [61] have concluded that misalignment errors of up to  $3^0$  have minimal effects on the measured transmission coefficient results. Furthermore, the author's own experience suggests that  $T_m$  and  $R_m$  are relatively insensitive to small alignment errors. The sample was positioned just beyond the far field threshold of each horn ( $= 2D^2/\lambda$ , where D = the horn aperture and  $\lambda$  = the shortest wavelength).

Two experimental rigs were constructed: the first for use at J-band as a means of developing the test method and the second for use in the MMW band. Brief details of the J-band experimentation are given in ‘Free Space Measurement of Permittivity’ [62], Appendix A. The MMW equipment is described below.

The equipment was designed for use at 60GHz, which was the lowest frequency of interest. Measurements at 60GHz required a horn to sample separation of 150mm. The samples were disc shaped of diameter 125mm but with a region exposed to the MMW of 105mm in diameter; the 10mm around the periphery enabling each sample to be clamped to the annular sample frame. The waveguide horn antennas have a -3dB beamwidth of  $20^\circ \pm 2^\circ$  in each plane. The -3dB contour of the beam in the sample plane approximates to a circle of diameter 52.6mm. Samples were therefore sufficiently large to subtend an angle of twice the -3dB beamwidth of the horns; thus they intercepted the entire main beam (at least the first 7 Fresnel zones) and approximate to an infinitely large sample.

Two further pairs of waveguide horns were also used for measurements in the 77GHz band and between 90 and 100GHz. Both pairs of horns also had a -3dB beamwidth of nominally  $20^\circ$  in each plane. The same sample frame was used in these bands, thus samples appeared to be electrically larger at the higher frequencies. Measurements at 90 to 100GHz required a horn to sample separation of 110mm. The -3dB contour of the beam in the sample plane approximates to a circle of diameter 40mm. Samples were therefore sufficiently large to subtend an angle of greater than twice the -3dB beamwidth of the horns and this time they intercepted at least the first 15 Fresnel zones and more closely approximate to an infinitely large sample.

An Agilent HP8510C VNA was used for work between 75 to 100GHz and an Anritsu 37397C VNA was used for work below 65GHz.

The VNA was operated in a time gated mode in order to isolate the first reflection from the sample (reflection measurement) and the main through path between horns (transmission measurement). In this way multiple reflections between the horns and/or

sample are ignored and do not corrupt the reading. The reflection measurement was calibrated with respect to a metal plate fitted in place of the sample. All reflection coefficients were therefore normalised to that of a short circuit in the measurement plane. The transmission measurement was calibrated with respect to the path loss with no sample in place.

Figure 3-2 below shows the equipment set up for work at 60GHz.



Figure 3-2: MMW Equipment (60GHz)

### 3.5 DATA PROCESSING

In the general case, equations (3.1) to (3.6) are solved using an iterative technique to find solution(s) for  $\varepsilon_r$ . Solutions for  $\varepsilon_r$  are sought using an exhaustive search over a user defined search space and resolution which result in computed values of transmission and reflection coefficients ( $T_c$  and  $R_c$ ) which most closely match the

measured values,  $T_m$  and  $R_m$ . However, due to the multiple reflections present in all but very lossy samples, multiple solutions of  $\epsilon_r$  may be found. This ambiguity can easily be overcome based on an initial estimate from the peak and trough frequencies or by fitting data at several nearby frequencies. Both of these techniques have been used. The former was found to be useful in resolving the ambiguities associated with low loss materials since the peaks and troughs were well defined whereas the latter approach proved to be more valuable with lossy samples.

A number of MATLAB programs were written to perform the data processing. Complete listings of the following are reproduced in Appendix C: TR3.m accepts the input of frequency (bandwidth and step size), sample thickness and complex permittivity of a sample and solves (3.1) to (3.6) to compute the transmission and reflection coefficients across the frequency band. P3.m uses the computation of TR3.m to solve the inverse problem at a single frequency i.e. it accepts a user defined frequency and thickness plus the measured transmission and reflection coefficients and searches over a user defined range of  $\epsilon_r'$  and  $\epsilon_r''$  for a solution which results in the closest match between measured and computed transmission and reflection coefficients. Each trial solution for a  $\epsilon_r'$  and  $\epsilon_r''$  pair results in computed values  $T_c$  and  $R_c$  and an error factor is calculated based on the average percentage error between  $T_c$  and  $T_m$  and  $R_c$  and  $R_m$ . The solution is declared for the lowest error factor. Thus it solves to find complex permittivity solution(s) at a single frequency. P5.m performs the function of P3.m over a number of different frequency points. Each trial solution for a  $\epsilon_r'$  and  $\epsilon_r''$  pair results in computed values  $T_c$  and  $R_c$  at each measurement frequency and a error factor (dubbed “score”) is calculated based on the rms percentage error between  $T_c$  and  $T_m$  and between  $R_c$  and  $R_m$  at each frequency; thus three measurement frequencies result in six data points. The solution is declared for the lowest score which is indicative of the quality of the declared solution. No solutions were declared in the cases where the score exceeded 20%. This was an arbitrary threshold beyond which it was deemed that there was too great an inconsistency between measured and computed results. Thus P5.m solves to find complex permittivity solution(s) over a band of frequencies over which the sample is assumed to be non-dispersive.

### 3.6 VALIDATION OF EXPERIMENTAL METHOD

Initial work at J-band on a range of low-loss and lossy materials was conducted. In particular, the method was developed with the aid of a large sheet of PTFE sample whose dielectric properties are well established. Figure 3-3a and Figure 3-3b plot the simulated and measured reflection and transmission coefficients, respectively, over the band 8 to 12GHz. The simulated data shown in blue (computed using the MATLAB program TR3.m) was derived by setting the permittivity of the PTFE to be  $2.08 - j0.00077$ , in keeping with published data at 10GHz<sup>[120]</sup> and the measured sample thickness of  $12.63 \pm 0.4\text{mm}$ . The two dashed lines of simulated data in Figure 3-3a and Figure 3-3b allow for the extremes of the thickness tolerance.

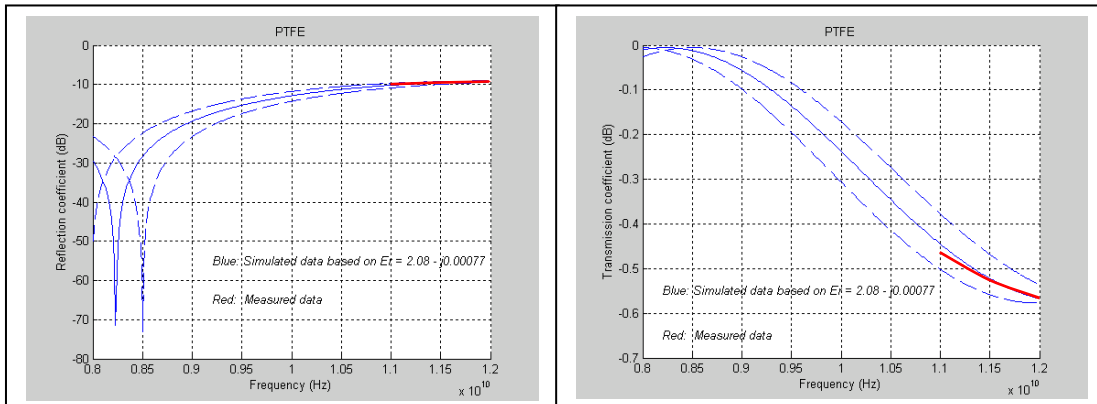


Figure 3-3a:  
Simulated and Measured  
Reflection Coefficients of PTFE

Figure 3-3b:  
Simulated and Measured  
Transmission Coefficient of PTFE

Due to the absence of time gating functions and other limitations of the VNA used for these measurements, an alternative method of calibration was used which was centred on the frequency of 11.4GHz. Hence measured data, shown in red, is only valid over the range 11 to 12GHz, as plotted in Figure 3-3a and Figure 3-3b. The measured data lies within the range of the simulated data allowing for the thickness tolerance. The simulated data of these Figures also illustrates the reflection and transmission coefficient peaks and nulls as multiple reflections beat in and out of phase.

A number of conveniently available materials were measured and the data was processed and yielded the results of Table 3-1<sup>[62]</sup>.

Sample	11.0GHz	12.0GHz	Published result
PTFE	$2.095 - j0.0007$	$2.07 - j0.0012$	$2.08 - j0.00077$ at 10GHz [120]
Polystyrene	$2.47 - j0.014$	$2.49 - j0.006$	$2.48 - j0.003$ at 3GHz [120]
Borosilicate glass (80% SiO <sub>2</sub> )	$4.79 - j0.000$	$4.61 - j0.000$	4.6 at 1MHz (quoted by manufacturers)
MDF board	$2.23 - j0.138$	$2.29 - j0.130$	
Chipboard	$2.34 - j0.197$	$2.38 - j0.178$	

Table 3-1: Permittivity Results at J Band

Subsequently, measurements were made on a number of materials at 60GHz using the Anritsu 37397C VNA. Some of the samples measured were building materials. These materials are of interest for the modelling of the propagation of 60GHz signals in an indoor environment and between nearby buildings. Future wireless local area network (LAN) applications may use 60GHz. These results are presented in Table 3-2<sup>[62]</sup>.

Sample	Measured $\epsilon_r$	Published result
PTFE	$2.04 - j0.0007$	$2.063 - j0.0006$ [115]
Polystyrene (3 samples)	$2.48 - j0.000$	
Fused Quartz (3 samples)	$3.78 - j0.000$	$3.793 - j0.001$ [115]
MDF board	$3.48 - j0.170$	
Chipboard	$3.14 - j0.161$	$2.78/3.15 - j0.136/0.180$ [75] $2.95 - j0.19$ [61]
Plasterboard	$2.95 - j0.035$	$2.60/3.08 - j0.036/0.055$ [75] $2.58 - j0.021$ [61]
Concrete	$6.03 - j0.795$	$6.78 \pm 0.7 - j0.75$ at 51.3GHz [91]

Table 3-2: Permittivity Results at 60GHz

Note<sup>e</sup>: There are no recognised standards for dielectrics in the MMW band<sup>[121]</sup>.

The relatively close agreement between the measured results and previously published data (e.g. for PTFE the difference in  $\epsilon_r'$  is -1.1% and in  $\epsilon_r''$  is +16.7%) confirms that the measurements were valid. These results also illustrate the difficulty that the measurement method has in accurately determining  $\epsilon_r''$  of very low loss materials. This arises due to the very low transmission losses incurred by such samples. For a lossless sample one should observe that  $|S_{11}|^2 + |S_{21}|^2 = 1$ . Any small error in measuring  $|S_{21}|$  such that  $|S_{11}|^2 + |S_{21}|^2 > 1$  results in an impossible situation. The data processing then finds the nearest solution to be  $\epsilon_r'' = 0$ .

---

<sup>e</sup> Confirmed in conversation with R. Clarke, National Physical Laboratory, Teddington, UK who runs the EMMA Club, a dielectrics interest group.

### 3.7 EXPERIMENTAL TOLERANCE

Experimental errors arise for the following reasons:

- noise modulations of VNA readings,
- tolerance on measured sample thickness,
- consistency of sample thickness,
- surface roughness of sample,
- alignment errors,
- accuracy of calibration,
- repeatability of calibration and sample placement,
- sample orientation with respect to plane of polarisation,
- data corruption due to time gating function,
- systematic errors such as the finite size of the samples, assumed plane wave illumination, diffraction and multi-pathing.

The contributions from the fifth, ninth and tenth reasons above are believed to be negligibly small. The effects of the time windowing function should be minimal as it only excludes interfering signals. Future work could be conducted to quantify this by way of simulation. It is proposed here that this could be simulated by performing an inverse FFT on a frequency swept signal (with noise) to convert it to the time domain. Then a time window could be applied to isolate the main response and the time gated data subjected to a FFT to transform it back into the frequency domain. The processed data could be compared for various time gate widths and functions in order to ascertain the effect of the time gating. The effects of surface roughness become appreciable if roughness exceeds a tenth of a wavelength (0.3mm at 100GHz) and is also assumed to be negligibly small. The remaining contributions are specific to the measurements and are quoted in the relevant ‘results’ sections. It is not possible to relate the effects these tolerances have on the solutions for  $\epsilon_r$  due to the iterative search techniques employed. Error analyses and repeated measurements have been quoted in the relevant chapters.

### 3.8 CHAPTER SUMMARY

Chapter Three has considered the candidate techniques to measure the permittivity of skin in the MMW band and has justified the selection of a free-space method based on the measurement of the amplitudes of transmission and reflection coefficients. It is noted that this technique scales conveniently to the MMW band and that it is also suitable for the MMW dielectric imaging of planar composite materials. The theory of the measurement method and the experimental details have been described. It has also been stressed that the processing of the measured data to identify solutions for the complex permittivity of the sample is subject to ambiguity but that these ambiguities are easily resolved. Measured data at J-band and at 60GHz has been presented which validates the method.

THIS PAGE INTENTIONALLY LEFT BLANK

## CHAPTER FOUR: THE PERMITTIVITY OF HUMAN SKIN IN THE MILLIMETRE WAVE BAND

### 4.1 INTRODUCTION

Chapter One reviewed several examples within biomedical engineering where dielectric data of human tissues is required. The increased use of the millimetre wave band naturally raises concerns regarding their safety implications and of the power deposition in tissues, in particular. Prior to this study there has been very little published on the dielectric properties of human tissues in the MMW band. Skin is inevitably considered the highest priority tissue since it is the outermost layer and is expected to absorb most of the incident radiation. In cases where dielectric data of human tissues have been required in the MMW band it has become customary to predict the required values of permittivity and conductivity using standard Debye or Cole-Cole functions. Directly measured data would be useful for the applications mentioned above and would confirm, or otherwise, the validity of current predictions, the models used to generate them and the model parameters. However, as was pointed out in section 1.3.1, the variability of tissue characteristics and the tolerances to which they can be measured permits several models to be admitted.

This Chapter starts with a review of measured data and model parameters concerning the permittivity of water in the MMW band as a precursor to the modelled characteristics of human skin. The chapter then reviews the predicted data for human skin using standard functions based on relaxation phenomena. This includes the author's own attempts to predict the permittivity of human skin between 60 and 100GHz. The next section then reports on the testing protocol conducted on a single sample of human skin fixed in formaldehyde over the bands 57 to 63GHz and 76 to 100GHz. The results are then presented and discussed. This section also includes tests and results on a pig skin sample designed to assess the effects of the fixing process in formaldehyde. Human skin permittivity data is then corrected to values corresponding to 37°C (human arterial blood temperature) and adjusted to account for the formaldehyde fixing process. These values are then compared with the modelled data. A

model and model parameters are then proposed which result in the best fit to the measured data. Some further calculations are presented which determine the power deposition in skin exposed to MMW radiation. Finally, the temperature rises in the surface of human skin exposed to MMW radiation are modelled as a function of exposure time. A summary of the modelled permittivity data and initial measured results, both on human skin, have been published by the IEE Electronics Letters (Sept. 2003). The published paper is reproduced in Appendix A.

## 4.2 PREDICTIONS OF DATA TO THE MMW BAND

### 4.2.1 Introduction

It is generally accepted that the dielectric characteristics of tissues towards the upper microwave region is largely determined by its water content due to the dominance of the relaxation of pure and bound water<sup>[2]</sup>. Skin has a water content of some 60 to 76%<sup>[6]</sup>. The investigation into the MMW characteristics of skin therefore starts with an investigation into the properties of water in this band.

### 4.2.2 Permittivity of Water in the MMW Band

This section aims to predict the permittivity of water based on a single Debye relaxation process described by equation (1.11). One of the main difficulties for the prediction of the permittivity of water in the MMW band is the unknown value of  $\epsilon_{\infty}$ . One means of overcoming this problem is to fit measured data to equation (1.11) in order to solve for  $\epsilon_{\infty}$ . A MATLAB program named FindEi.m (see Appendix C) was written to do this. FindEi.m operates by an iterative approach to search through a range of  $\epsilon_{\infty}$  values to find a solution which results in the lowest rms percentage error between computed values of  $\epsilon_r'$  and  $\epsilon_r''$  at each trial value of  $\epsilon_{\infty}$  and measured data input by the user.

A literature survey was conducted to acquire measured permittivity data for water in the MMW band. The results are summarised in Table 4-1 below.

Permittivity	Freq (GHz)	T (°C)	Notes	Ref. (Date)
12.4 – j19.3	42.25		74% distilled water	[98]
9.0 – j19.5	53.57		films	(2000)
$\epsilon_{\infty} = 4.23, \epsilon_s = 80.4$	$f_c = 17.1$	20	$\sigma_s = 0$ also quoted	
$\epsilon'_r = 19.6 \pm 0.3$ to $28.7 \pm 0.3$	35		$\alpha = 0$	[16]
$\epsilon''_r = 28.7 \pm 0.2$ to $32.7 \pm 0.3$		20		(1988)
$\epsilon_s = 80.1$ to $76.54$		to		and
$\epsilon_{\infty} = 5.7 \pm 0.3$ to $5.5 \pm 0.6$	$f_c = 16.8 \pm 0.3$ to $21.6 \pm 0.2$	37		[102]
$23.1 \pm 1.0 - j 31.2 \pm 0.6$	33.9	25		(1987)
23.1 – j33.5	35	37		[103]
19 – j30.3		20		(1973)
$\epsilon_{\infty} = 4.32$	$f_c = 17.34$	20	$\alpha = 0$	[3]
$9.92_6 \pm 0.07 - j 17.55_9 \pm 0.04$	70	20		(1967)
$10.82 \pm 0.16 - j 19.14 \pm 0.23$		25		[93]
$12.23 \pm 3.12 - j 23.72 \pm 2.54$	44	15		(1977)
$13.97 \pm 2.91 - j 25.73 \pm 2.19$		20		[96]
$16.54 \pm 2.14 - j 26.54 \pm 1.73$		25		(1996)
18.1 – j28.0	37.5	20	Also includes data	[122]
20.6 – j29.0		25	at 30 and 150GHz.	(2001)
23.2 – j30.8		30		
9.1 – j16.0	75	20		
10.0 – j17.5		25		
10.9 – j18.9		30		

Table 4-1: Measured Permittivity data for Water in the MMW band

One further problem is the variety of temperatures at which the measured data of Table 4-1 have been performed. It would be convenient to correct all the data to a common

temperature. Various temperature gradients applicable to the MMW band are also reported in the literature and are summarised in Table 4-2 below, which also includes the calculation of the mean gradients.

Gradient for $\epsilon_r'$	Gradient for $\epsilon_r''$	Freq. (GHz)	Reference
+ 2.24% / $^0\text{C}$	+ 0.76% / $^0\text{C}$	35	[16]
+ 2.45% / $^0\text{C}$	+ 0.59% / $^0\text{C}$	35	[3]
+ 3% / $^0\text{C}$	+ 1.12% / $^0\text{C}$	44	[96]
+ 1.71% / $^0\text{C}$	+ 1.72% / $^0\text{C}$	70	[93]
+ 2.35% / $^0\text{C}$ $(\pm 0.65\% / ^0\text{C})$	+ 1.05% / $^0\text{C}$ $(+0.67/-0.46 \% / ^0\text{C})$	Mean of above (tolerance)	
$\epsilon_s$ : - 0.45% / $^0\text{C}$	$\epsilon_\infty$ : - 0.36% / $^0\text{C}$	$f_c$ : + 2.5% / $^0\text{C}$	[16]

Table 4-2: Temperature gradients

Amalgamating the data of Table 4-1 and Table 4-2 and making the necessary temperature corrections results in the values given in Table 4-3 below.

Parameter	$20^0\text{C}$ $\epsilon_r'$	$20^0\text{C}$ $\epsilon_r''$	$37^0\text{C}$ $\epsilon_r'$	$37^0\text{C}$ $\epsilon_r''$
$f = 35\text{GHz}$	$19.3 \pm 0.6$	$28.9 \pm 0.4$	$28.7 \pm 0.3$	$33.0 \pm 0.6$
$f = 44\text{GHz}$	$14.0 \pm 3.0$	$25.7 \pm 2.2$	$19.6 \pm 5.5$	$30.3 \pm 5.0$
$f = 70\text{GHz}$	$9.93 \pm 0.07$	$17.56 \pm 0.04$	$13.9 \pm 1.2$	$20.7 \pm 1.8$
$\epsilon_s$	80.2			74.0
$\epsilon_\infty$	4.3			4.0
$f_c$	$17.1 \pm 0.2 \text{ GHz}$			$24.4 \pm 0.3 \text{ GHz}$
$\sigma_s$	0			0

Table 4-3: Model Input Parameters for Water

Deionised water should have zero static conductivity and is the value assumed above.

The data of Table 4-3 was input into the single relaxation Debye formula (Debye1.m), in order to predict the permittivity of water at three key frequencies within the MMW band; 60, 77 and 94GHz at both  $20^0\text{C}$  (nominally room temperature) and  $37^0\text{C}$  (human arterial blood temperature). The results are summarised in Table 4-4 below.

T $^0\text{C}$	Freq. GHz	Permittivity				
		Mean value	Max $\epsilon_r'$	Min $\epsilon_r'$	Max $\epsilon_r''$	Min $\epsilon_r''$
20	60	$10.0 - \text{j}20.0$	$11.7 - \text{j}19.8$	$9.78 - \text{j}19.8$	$10.1 - \text{j}20.3$	$11.5 - \text{j}19.3$
	77	$7.87 - \text{j}16.1$	$9.58 - \text{j}15.9$	$7.69 - \text{j}15.9$	$7.86 - \text{j}16.3$	$9.41 - \text{j}15.5$
	94	$6.73 - \text{j}13.4$	$8.44 - \text{j}13.2$	$6.58 - \text{j}13.2$	$6.70 - \text{j}13.6$	$8.32 - \text{j}12.9$
37	60	$13.9 - \text{j}24.4$	$15.9 - \text{j}23.9$	$13.7 - \text{j}24.2$	$14.1 - \text{j}24.6$	$15.5 - \text{j}23.5$
	77	$10.4 - \text{j}20.2$	$12.3 - \text{j}19.8$	$10.3 - \text{j}20.0$	$10.5 - \text{j}20.4$	$12.1 - \text{j}19.4$
	94	$8.42 - \text{j}17.0$	$10.4 - \text{j}16.7$	$8.32 - \text{j}16.8$	$8.52 - \text{j}17.2$	$10.2 - \text{j}16.4$

Table 4-4: Modelled Results for Water  
( $f = 60, 77, 94$  GHz and  $T = 20^0\text{C}, 37^0\text{C}$ )

The value of  $\epsilon_r''$  is only weakly dependent on  $\sigma_s$ . Values of  $\sigma_s = 1.0 \text{ Sm}^{-1}$  result in a change of  $\epsilon_r''$  by only 1.4%.

#### 4.2.3 Modelling the Dielectric Properties of Human Skin

Whilst the commonly accepted wisdom is that the properties of biological tissue in the MMW band will be determined by its free water content, that is not to say that the properties of human skin will be identical to those of water. The following sub-sections consider various attempts to model the dielectric properties of human skin in the MMW band.

#### 4.2.3.1 Predicted Data From 4-Term Cole-Cole Function of Gabriel

Gabriel [43] has published a comprehensive review of measured data of human tissue up to a frequency of 20GHz. Appendix C of reference [43] also includes a four term Cole – Cole expression for the prediction of data on up to 44 tissue types. The paper is available on-line at:

<http://www.brooks.af.mil/AFRL/HED/hedr/reports/dielectric/home.html>

and an automated means of running the prediction calculations is also accessible via:

<http://niremf.iroe.fi.cnr.it/tissprop/>

Walters et al [42] have used this model to predict the permittivity of dry skin to be 5.8 – j7.5 at 94GHz.

Gabriel's model is based on the following four term Cole – Cole expression (retaining the nomenclature already established):

$$\epsilon_r = \epsilon_\infty + \sum_{m=1}^4 \frac{\Delta\epsilon_m}{1+(j\omega\tau_m)^{1-\alpha_m}} + \frac{\sigma_s}{j\omega\epsilon_o} \quad (4.2)$$

Expanding (4.2) gives:

$$\epsilon_r = \epsilon_\infty + \frac{\Delta\epsilon_1}{1+(j\omega\tau_1)^{\alpha_1}} + \frac{\Delta\epsilon_2}{1+(j\omega\tau_2)^{\alpha_2}} + \frac{\Delta\epsilon_3}{1+(j\omega\tau_3)^{\alpha_3}} + \frac{\Delta\epsilon_4}{1+(j\omega\tau_4)^{\alpha_4}} + \frac{\sigma_s}{j\omega\epsilon_o} \quad (4.3)$$

The model parameters given for dry and wet skin are given in Table 4-5, below:

	$\sigma_s$	$\epsilon_\infty$	$\Delta\epsilon_1$	$\tau_1$ (ps)	$\alpha_1$	$\Delta\epsilon_2$	$\tau_2$ (ps)	$\alpha_2$
Dry	0.0	4.0	32.0	7.234	0.0	1100	32.481	0.2
Wet	0.0	4.0	39.0	7.958	0.1	280	79.577	0.0

	$\Delta\epsilon_3$	$\tau_3$ ( $\mu$ s)	$\alpha_3$	$\Delta\epsilon_4$	$\tau_4$ (ms)	$\alpha_4$
Dry	0.0	159.155	0.2	0.0	15.915	0.2
Wet	3e4	1.592	0.16	3e4	1.592	0.2

Table 4-5: Model Parameters <sup>[43]</sup>

Since  $f_{cm} = \frac{1}{2\pi\tau_m}$  the relaxation frequencies may be calculated as in Table 4-6:

	m = 1	m = 2	m = 3	m = 4
Dry	22.0 GHz	4.9 GHz	1 kHz	10 Hz
Wet	20.0 GHz	2.0 GHz	100 kHz	100 Hz

Table 4-6: Modelled Relaxation Frequencies <sup>[43]</sup>

From Table 4-5 and Table 4-6 the following is noted:

- Terms for which  $\alpha_m = 0$  are frequency independent. These are the first term for dry skin and the second term for wet skin.
- Terms for which  $\Delta\epsilon_m = 0$  contribute nothing. These are the third and forth term for dry skin.
- The moisture content of *dry* and *wet* skin is not defined.
- The relaxation frequencies are considerably different from the author's own predictions, indeed the first terms appear to be closer to those of pure water, rather than concentrated suspensions assumed by Pethig <sup>[6]</sup>.

The results for the permittivity of dry and wet human skin using the model of Gabriel [43] are reproduced in Table 4-7 and Table 4-8, below and Figure 4-1 and Figure 4-2.

Tissue name	Frequency [GHz]	Conductivity [S/m]	Relative permittivity	Loss tangent
Skin, Dry	60	36.397	7.9753	1.3673
Skin, Dry	77	38.179	6.5649	1.3577
Skin, Dry	94	39.181	5.7894	1.2942

Table 4-7: Modelled Dielectric Data of dry skin from Gabriel [43]

Tissue name	Frequency [GHz]	Conductivity [S/m]	Relative permittivity	Loss tangent
Skin, Wet	60	39.519	10.216	1.1589
Skin, Wet	77	42.969	8.5368	1.175
Skin, Wet	94	45.41	7.5137	1.1557

Table 4-8: Modelled Dielectric Data of wet skin from Gabriel [43]

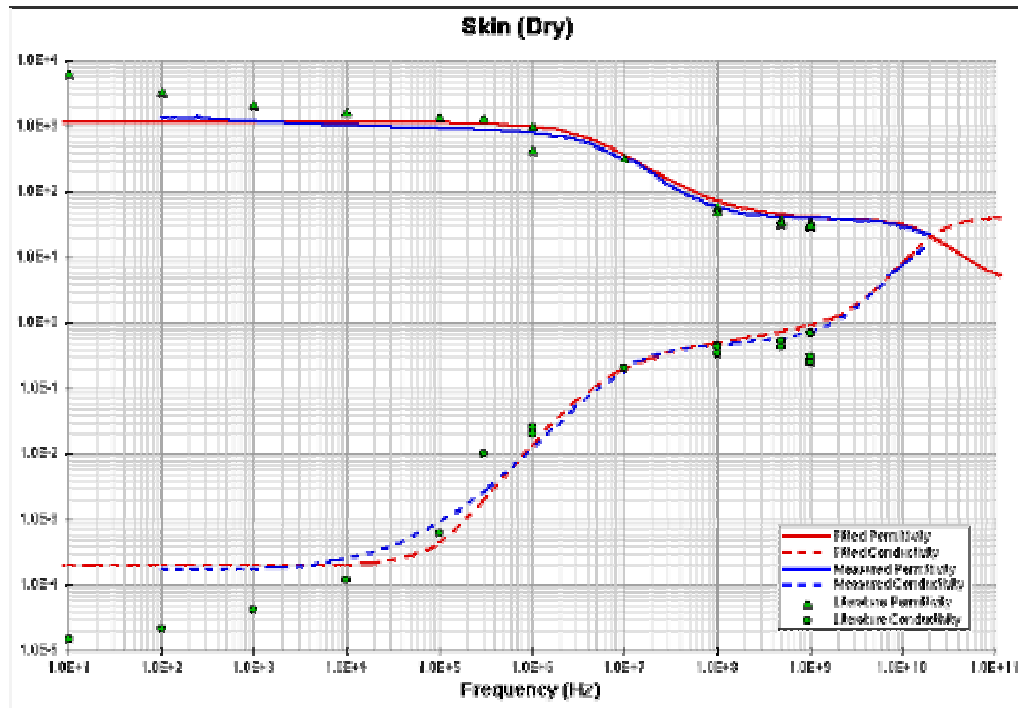


Figure 4-1: Modelled Dielectric Data of dry skin from Gabriel [43]

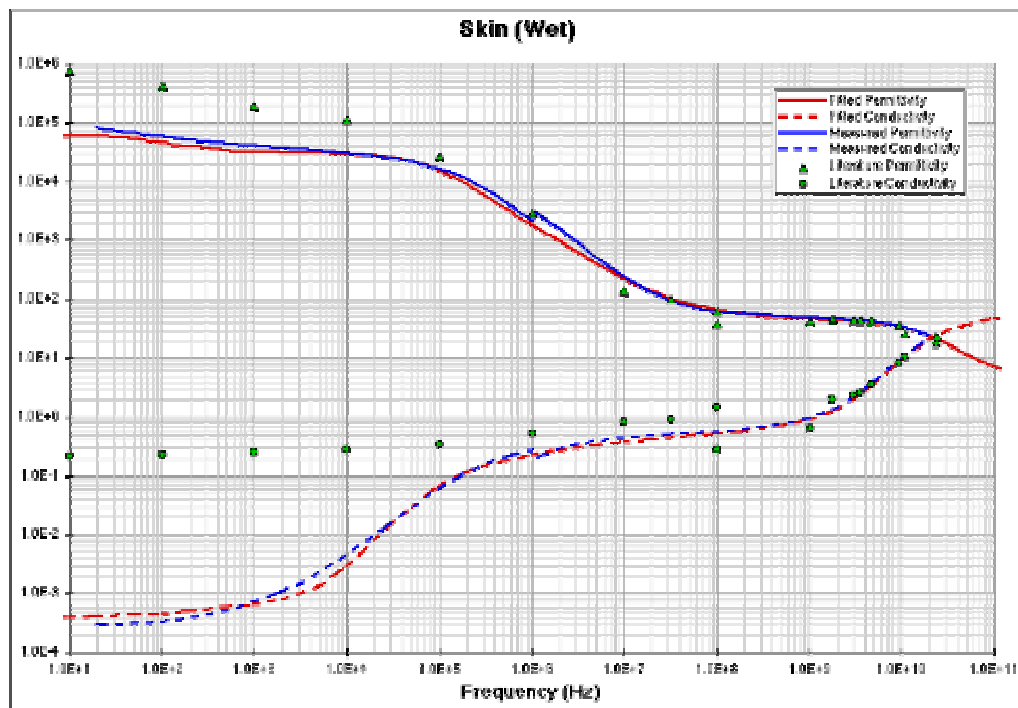


Figure 4-2: Modelled Dielectric Data of wet skin from Gabriel [43]

#### 4.2.3.2 Single and Double Term Debye Predictions of Kuznetsov

Kuznetsov [123] includes in his text book “Biophysics of Electromagnetic Effects” (in Russian) tabulated data for the permittivity of human skin in the MMW band. This data is based on predictions from measured data at lower frequencies supplied in earlier papers. One set of data is based on the two-term Debye function of Mashimo et al [18] (1987). The two-term Debye model is expressed as:

$$\Re\{\epsilon^*\} = \epsilon_\infty + \frac{\Delta\epsilon_l}{1+(\omega\tau_l)^2} + \frac{\Delta\epsilon_h}{1+(\omega\tau_h)^2} \quad (4.4)$$

where  $\Delta\epsilon_l = 17.9$  i.e. the low frequency relaxation term ( $= \epsilon_s - \epsilon_\infty$ )

$\Delta\epsilon_h = 15.0$  i.e. the high frequency relaxation term ( $= \epsilon_s - \epsilon_\infty$ )

$\epsilon_\infty = 3.97$

$\tau_l = 1.18\text{ ns}$  (which gives a low relaxation frequency of 134.87MHz)

and  $\tau_h = 7.1\text{ ps}$  (which gives a high relaxation frequency of 22.416GHz)

These model parameters are chosen as a best fit to measured data of tissue and biological materials in the band 10MHz to 10GHz. Clearly, the third term on the right hand side of (4.4) is associated with the relaxation of free water and is the dominant term in the MMW band.

The second set of data is based on the measurements of England [124] (1950) and Cook [23] (1951). England used waveguide methods to measure the permittivity of human skin from the breast and leg (plus other tissues) at 3.0, 9.4 and 23.6GHz, all at 37°C. England’s results are:

$\epsilon_r = 43.5 - j16.5$ ,  $35.5 - j13.0$  and  $23.0 - j13.0$  at 3.0, 9.4 and 23.6GHz, respectively. Cook used the dielectric fill of a coaxial line terminated in a short circuit method (i.e. that of Roberts and Von Hippel [117]) to measure the permittivity of freshly excised human skin samples (plus other tissues) recovered from three sites at frequencies

between 1.76GHz and 4.68GHz and at a temperature of 37°C. Cook proposed a single term Debye function to fit the measured data having the following parameters:

$$\varepsilon_s = 42, (51), \quad \varepsilon_\infty = 4.0, \quad \tau = 6.9 \text{ ps}, (8.5 \text{ ps}), \quad \sigma_s = 0.014 \Omega / \text{cm}$$

The bracketed numbers refer to skin from near the faecal fistula whereas the non-bracketed numbers refer to skin from the breast and instep. The relaxation times ( $\tau$ ) quoted relate to relaxation frequencies of 23.06GHz (18.7GHz). Cook's work supports the idea that the complex permittivity of tissues in the microwave band can be described by a single time constant Debye equation with additional losses for ionic conductivity.

The predicted results from both the above models tabulated by Kuznetsov [123] are summarised in Table 4-1 below.

Frequency (GHz)	Single term Debye Refs [124][23]	Two term Debye Ref [18]
60	$8.7 - j14.6$	$5.8 - j5.0$
75	$7.27 - j11.0$	$5.2 - j4.1$
100	$5.9 - j8.6$	$4.7 - j3.2$

Table 4-9: Predicted Permittivity of Skin, Kuznetsov [123]

#### 4.2.3.3 Predicted Data From Single Debye Relaxation

The author's attempt to predict the permittivity of human skin in the MMW band is based on a single Debye relaxation in which the following model parameters have been used.

*Relaxation frequency,  $f_c$ .* Pethig [6] states that skin is 60 to 76% water by weight and that the relaxation frequency of pure water at 37°C is 25GHz, but in (eye) lens nucleus (65% water) it is around 9GHz (some 36% of the pure water value). It may therefore be

reasonable to assume a similar reduction in the relaxation frequency in skin. The relaxation frequency of pure water at  $37^0\text{C}$  is  $f_c = 24.4\text{GHz}$  and at  $20^0\text{C}$  is  $f_c = 17.1\text{GHz}$  (Table 4-3) and the temperature gradient of  $f_c$  is  $+ 2.5\% / {}^0\text{C}$  [16] (Table 4-2). One may therefore estimate the free water relaxation frequency in skin at  $37^0\text{C}$  to be 36% of  $24.4\text{GHz}$ , which is  $8.784\text{GHz}$ . Similarly at  $20^0\text{C}$  one may estimate 36% of  $17.1\text{GHz}$ , which is  $6.156\text{GHz}$ . Alternatively, one may apply the temperature correction to the value at  $37^0\text{C}$  ( $= 8.784\text{GHz}$ ) to estimate the frequency at  $20^0\text{C}$  to be  $6.164\text{GHz}$ . The two estimates for skin at  $20^0\text{C}$  are in very close agreement with each other and may be rounded to  $6.16\text{GHz}$ .

The relaxation frequency is therefore set at  $8.78\text{GHz}$  at  $37^0\text{C}$  and  $6.16\text{GHz}$  at  $20^0\text{C}$ .

$\varepsilon_\infty$ . The previously used values for pure water are  $\varepsilon_\infty = 4.0$  ( $37^0\text{C}$ ) and  $\varepsilon_\infty = 4.3$  ( $20^0\text{C}$ ) are very close to the value used by Gabriel [43] and shall be used here.

$\varepsilon_s$ . This should correspond to the value of  $\varepsilon_r$  well below the relaxation frequency. Taking the value of  $\varepsilon_r$  at one tenth the relaxation frequency should be an appropriate approximation. According to the data from Gabriel [43], we obtain:

$$\varepsilon_r = 39.6 \text{ for dry skin at } 0.878\text{GHz at } 37^0\text{C} \text{ and}$$

$$\varepsilon_r = 48.2 \text{ for wet skin at } 0.878\text{GHz at } 37^0\text{C}$$

These may be corrected to (based on a gradient of  $-0.45\% / {}^0\text{C}$ ):

$$\varepsilon_r = 36.8 \text{ for dry skin at } 20^0\text{C} \text{ and}$$

$$\varepsilon_r = 44.8 \text{ for wet skin at } 20^0\text{C}$$

These values are in fairly close agreement with the values of  $\varepsilon_s = 36$  (dry) and 43 (wet) from the Gabriel model (deduced from the quoted values for  $\Delta\varepsilon_1$  and  $\varepsilon_\infty$  in Table 4-5).

$\sigma_s$ . This is set to zero.

The modelled results at the three frequencies of interest are presented in Table 4-10 below:

Frequency (GHz)	Dry skin $37^0\text{C}$	Dry skin $20^0\text{C}$	Wet skin $37^0\text{C}$	Wet skin $20^0\text{C}$
60	$4.75 - \text{j}5.10$	$4.64 - \text{j}3.30$	$4.93 - \text{j}6.33$	$4.72 - \text{j}4.11$
77	$4.46 - \text{j}4.01$	$4.51 - \text{j}2.58$	$4.57 - \text{j}4.98$	$4.55 - \text{j}3.22$
94	$4.31 - \text{j}3.30$	$4.44 - \text{j}2.12$	$4.38 - \text{j}4.09$	$4.47 - \text{j}2.64$

Table 4-10: Modelled Permittivity of Skin Based on Single Debye Relaxation

More complete results are presented in Figure 4-3 to 4-6, inclusive.

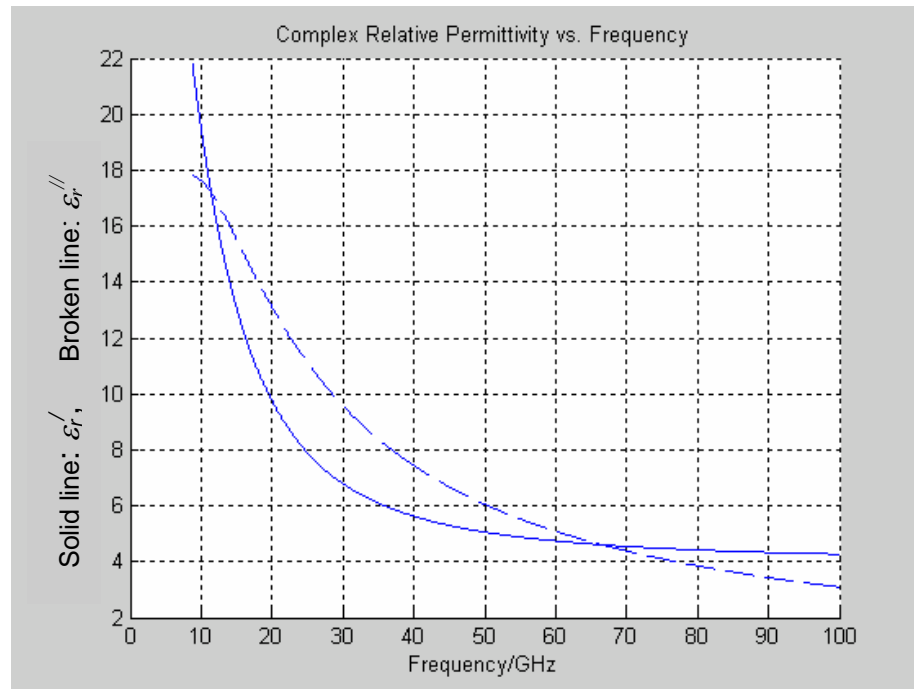


Figure 4-3: Single Debye Relaxation (Dry skin,  $37^0\text{C}$ )

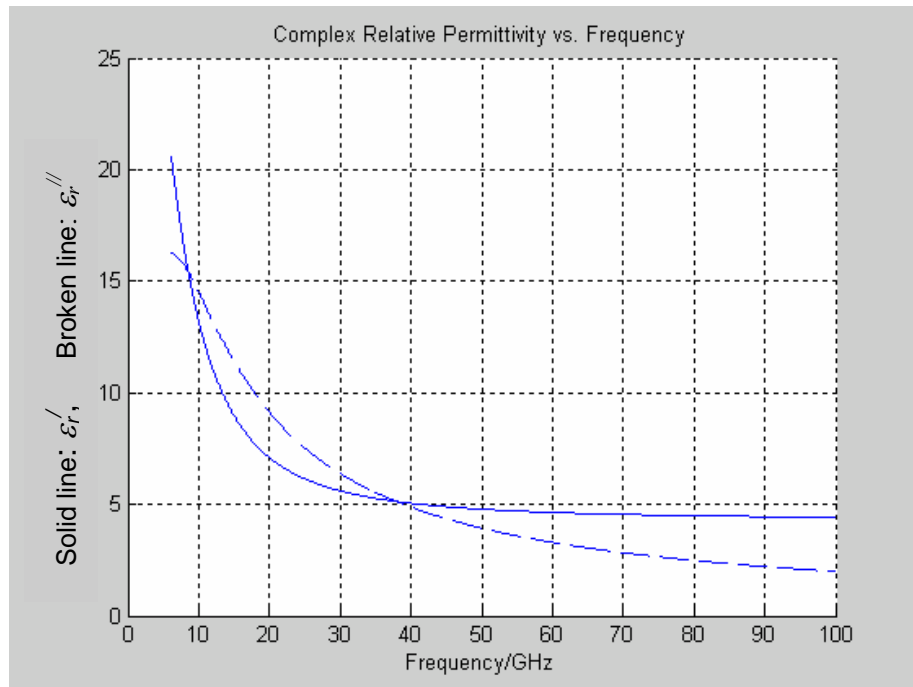


Figure 4-4: Single Debye Relaxation (Dry skin, 20°C)

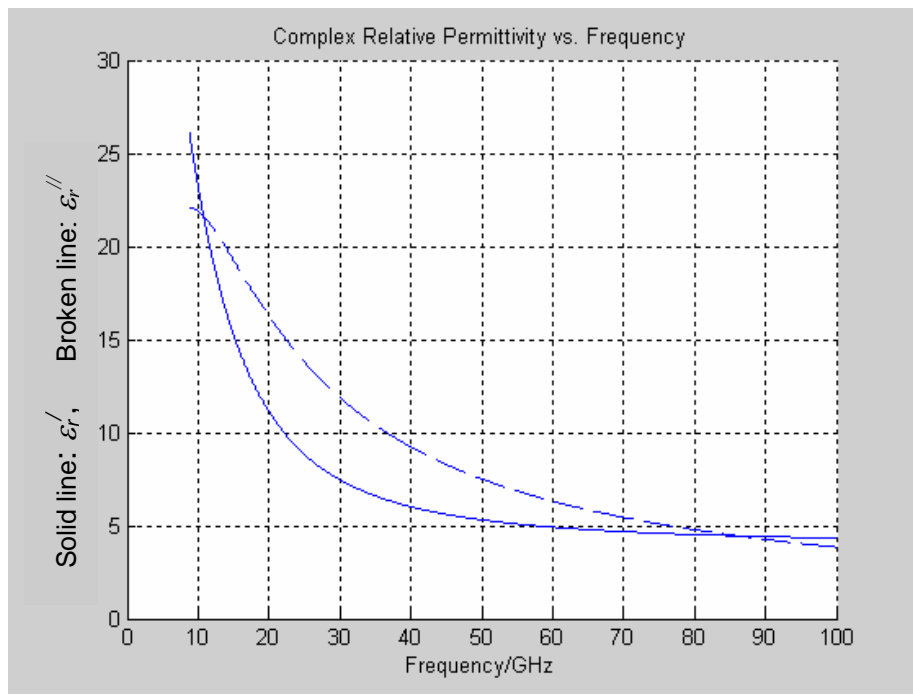


Figure 4-5: Single Debye Relaxation (Wet skin, 37°C)

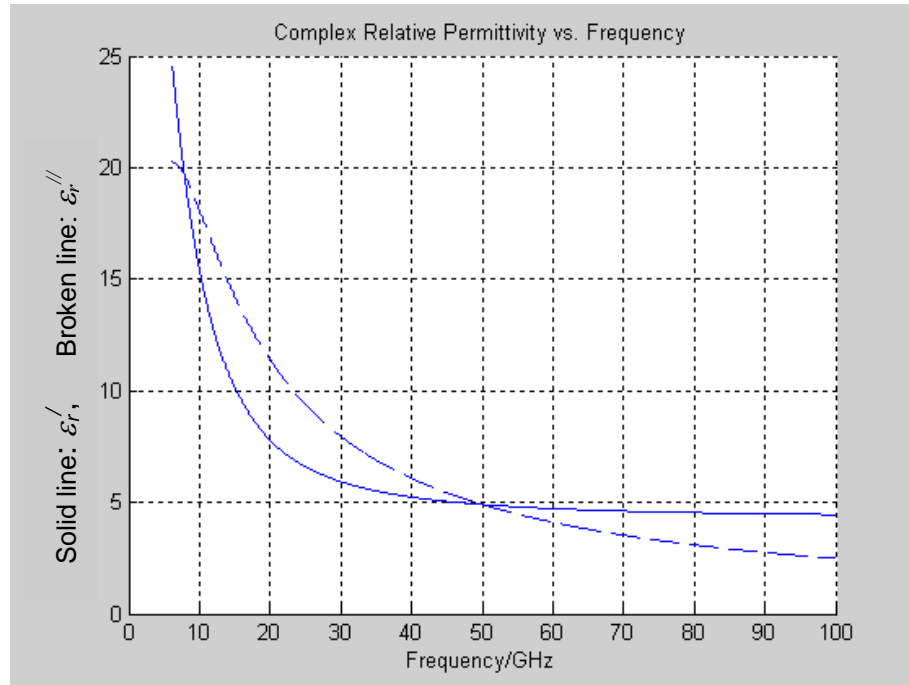


Figure 4-6: Single Debye Relaxation (Wet skin, 20°C)

#### 4.2.3.4 Single Debye Relaxation Parameters of Ghodgaonkar and Daud

Ghodgaonkar and Daud [125] comment that the microwave and MMW dielectric properties of tissues are determined by their water content which at these frequencies is characterised by a single Debye relaxation. They have sought to fit the low frequency parameters,  $\epsilon_s$  and  $\tau$ , to the measured complex permittivity of human skin *in vivo* in the band 16 to 25GHz and assumed values of  $\epsilon_\infty = 1.5$  and  $\sigma = 0.92$  S/m (see also section 1.3.3 and ref [21]). The skin measurements were performed on the palm of the hand (20 subjects) and the sole of the foot (5 subjects) since skin is both thick and smooth at these locations. The measured complex permittivity data is averaged across all subjects and the parameters  $\epsilon_s$  and  $\tau$  solved at 1GHz intervals. Their results are summarised below:

The permittivity of skin on the palm varied from  $9.9 - j17.2$  at 16GHz to  $5.3 - j14.3$  at 25GHz and that for the sole varied from  $6.2 - j11.1$  at 16GHz to  $4.4 - j6.9$  at 25GHz.

These permittivity values resulted in the following model parameters:

Palm:  $\epsilon_S = 41.01$  (16GHz) to  $54.24$  (25GHz)  
 $\tau = 19.14\text{ps}$  (16GHz) to  $22.85\text{ps}$  (25GHz)

Sole:  $\epsilon_S = 27.76$  (16GHz) to  $17.82$  (25GHz)  
 $\tau = 21.31\text{ps}$  (16GHz) to  $13.69\text{ps}$  (25GHz)

This data raises several issues. Firstly, one would expect that the low frequency parameters  $\epsilon_S$  and  $\tau$  to be constant, irrespective of the frequency of measurement whereas their data has a clearly defined frequency gradient in each case. Furthermore, the frequency gradients are of the opposite sign for each location. Secondly, since the parameters are so heavily frequency dependent it is not possible to apply them to predict the permittivity at higher frequencies. Thirdly, it has already been noted in section 1.3.3 that the permittivity of skin of the palm (and, possibly, the sole) is lower than that of skin elsewhere on the human body due to its thick, horny nature. Finally, this data perhaps confirms that a single Debye relaxation model with fixed parameters does not fit measured data and that human skin requires a more complex model.

#### 4.2.3.5 Comparison Between Data of the Various Models

Table 4-11 summarises the various predicted data for dry human skin at 37°C in the MMW band.

Freq. (GHz)	Single term Debye [123][124][23]	Two term Debye [123][18]	Four term Cole- Cole [43]	Single term Debye (author's own)
60	8.7 – j14.6	5.8 – j5.0	7.98 – j10.90	4.75 – j5.10
75	7.27 – j11.0	5.2 – j4.1	6.69 – j9.11	
77			6.56 – j8.91	4.46 – j4.01
94			5.79 – j7.49	4.31 – j3.30
100	5.9 – j8.6	4.7 – j3.2	5.60 – j7.09	

Table 4-11: Summary of Predicted Permittivity  
(Human skin, dry, 37°C)

There is considerable variation in the data; up to a factor of 1.8 in  $\epsilon'_r$  and a factor of 2.9 in  $\epsilon''_r$ . The single term Debye consistently yields values having the highest  $\epsilon'_r$  and  $\epsilon''_r$ , whereas the author's own predictions, also based on a single term Debye function consistently have the lowest  $\epsilon'_r$  (and very nearly the lowest  $\epsilon''_r$ ). The closest agreement between any two is that of the author's own work and the two term Debye function. Gabriel's data [43] for wet skin yield results which are only marginally lower than the estimates for pure water, however, the percentage margins are not consistent. The author's estimations for dry skin (37°C) based on a single frequency Debye relaxation are approximately a half the magnitude of Gabriel's values. The mis-match between data could very well be due to the rather indeterminate descriptions of *dry* and *wet* skin as no moisture content has been defined in either case. It may well be that a true indication of the properties of wet skin can be estimated by combining the properties of pure water and those of perfectly dry skin using mixture equations. One simple mixture equation would be to combine that data of the two constituents in accordance with their volumetric proportions.

## 4.3 PERMITTIVITY MEASUREMENTS ON HUMAN SKIN IN THE MMW BAND

### 4.3.1 Introduction

This section describes the measurements and results of tests on a single human skin sample at frequencies in the band 57 to 100GHz. The measurements were made using the free-space method described in Chapter Three and measured data was processed using the MATLAB programs P3.m (at a single spot frequency) and P5.m (over a range of frequencies) in order to yield the sample permittivity. Measurements made in the 57 to 63GHz band were made using the Anritsu 37397C VNA and those made in the band 76 to 100GHz used the Agilent (HP)8510C VNA. Initial results were published in the papers ‘Permittivity of Human Skin in the Millimetre Wave Band’,<sup>[119]</sup> and ‘Free Space Measurement of Permittivity’,<sup>[62]</sup> which are reproduced in full in Appendix A.

### 4.3.2 Initial Tests on Bovine Pericardium and Porcine Skin (57 to 63 GHz)

Samples of bovine pericardium and porcine skin were used for initial tests of biological tissues in the band 57 to 63 GHz<sup>[62]</sup>. Both tissue samples were excised from a freshly butchered animal, stitched onto a metal supporting frame and chemically fixed in a 10% formaldehyde solution. Prior to measurement they were rinsed in water, dried with tissue paper and allowed to stand for several minutes to further dry. The pericardium sample was measured whilst still damp but without any film of surface moisture whereas the skin sample was only slightly damp at the time of measurement. The samples were then secured to the sample frame; the outer surface being exposed to the illuminating horn. The transmission and reflection coefficients of the tissue samples were measured three times for random sample orientations at the frequencies of 57, 60 and 63 GHz. Very little variability in the readings was observed and so the mean reading was processed at each frequency. Sample thickness was measured by averaging micrometer readings taken at ten locations (pericardium) or seven locations (skin) on the periphery of the sample.

### 4.3.3 Human Skin Sample Preparation

A sample of human skin was obtained from National Disease Research Interchange (NDRI), Philadelphia. The skin sample was fresh and obtained from a recently deceased white, 50 year old female. The site from which the skin sample was removed is not known. However, it is most likely to originate from the thigh or torso and not the palm or sole, given its area and uniformity. The sample was fixed in 10% formaldehyde prior to shipment and has continued to have been stored in a 10% formaldehyde solution. It has not been frozen at any stage. A circular section of diameter = 135mm was prepared by scraping the fat from it and rinsing it clean in distilled water. The sample was lightly stretched over an annular stainless steel frame and stitched into position. Thus the stainless steel frame, with skin sample attached, can be clamped to the sample frame (Figure 3-2) so as to present a circular skin sample of diameter = 105mm to the MMW measurement, with the outer surface of the skin in the measurement/calibration plane facing towards the illuminating horn. The exposed sample has no visible defect or abnormality. Fortunately, the sample has two distinctive marks on its periphery which have been used to ensure a consistent orientation of the sample.

Prior to each measurement the sample was removed from the formaldehyde, rinsed in tap water and dabbed dry with tissue paper. It was then left to stand in the open laboratory at a nominal temperature of 20°C for four hours in order to dry. During the drying time it was not exposed to any draughts, sources of heat or direct sunlight. A four hour drying time was deemed sufficient to dry the sample to the point where it had no surface film of water, appeared (and felt) dry and yet was soft and pliable; much like the texture of skin *in vivo*. Slight differences in sample drying may have arisen from variations in the ambient temperature and humidity. This drying protocol has been used consistently for all tests.

#### 4.3.4 Measurements on Human Skin (76 to 100 GHz)

Two sets of measurements were made: one set on ‘wet’ skin (not subjected to the four hour drying time described in section 4.3.3) and the other set on ‘dry’ skin (dried as described in section 4.3.3).

For the dry skin, five measurements of the reflection and transmission coefficient were made and recorded over the band 76 to 100GHz. VNA data was downloaded to a disc but since the traces were smooth curves and had no rapid variations with frequency it was sufficient to use the VNA marker to record the data at 76GHz, 77GHz, 78GHz and thereafter at 2GHz intervals up to 100GHz. The mean of the five measurements was taken as the reading to be processed and the experimental repeatability was taken as  $\pm$  the standard deviation ( $\sigma_n$ ). Earlier work on porcine skin and bovine pericardium samples (ref [62], Appendix A) indicated that any variation in the measured data due to variations in sample orientation with respect to the plane of polarisation was within experimental repeatability. Nevertheless, a constant sample orientation was maintained for all measurements. The skin thickness was measured using a micrometer at six points around the edge of the sample. Finally, the ambient room temperature was noted from a digital thermometer using a thermocouple probe. The wet skin measurements were identical to those of the dry skin except that they were made every 1GHz over the band 90 to 100GHz.

#### 4.3.5 Measurements on Human Skin (57 to 63 GHz)

Initial measurements were made on the (dry) skin sample at 57, 60 and 63 GHz using the same drying and measurement protocols described earlier (sections 4.3.3 and 4.3.4). Two sets of data were acquired each based on five measurements of the transmission and reflection coefficients. The mean values were processed using the MATLAB program P5.m in order to obtain a permittivity solution across the measurement bandwidth.

Subsequently, thirty repeated measurements were made; one measurement per day, with the sample being dried on each occasion, as described in section 4.3.3, and stored in formaldehyde between measurements. This was conducted in order to ascertain the repeatability of the experimental method. On these occasions, single readings of transmission and reflection coefficients using the VNA 8 trace averaging function were recorded at 57, 60 and 63GHz. The sample thickness was re-measured for each test and was based on the mean of eighteen micrometer measurement points around its edge. The ambient temperature was also noted from a digital thermometer using a thermocouple probe.

#### 4.3.6 Effects of Formaldehyde Fixing

Fixing a tissue in formaldehyde is a diffusion process in which some of the tissue water is replaced by formaldehyde. The rate of fixing is a function of tissue type and volume to surface area ratio. It is anticipated that the fixing process dries the sample and alters its dielectric characteristics. In order to assess this, a second sample of porcine skin sample was obtained from a freshly butchered animal and prepared as previously described. This was measured over the band 57 to 63GHz in the same way as the repeated tests described in section 4.3.5 above, both before and after fixing in a 10% formaldehyde solution for ten days. Three repeat readings were made on each occasion and a constant sample orientation was maintained.

### 4.3.7 Results & Discussion

#### 4.3.7.1 Initial Results on Animal Tissues

The results of the initial tests on the porcine skin and bovine pericardium are given in Table 4-12 below. These results were unambiguous solutions obtained by processing the results at the three test frequencies of 57, 60 and 63 GHz.

Sample	Temp. (°C)	Thickness (mm)	Measured $\epsilon_r$ 57 to 63 GHz (P5.m)
Bovine Pericardium	$19.8 \pm 0.2$	$0.28 \pm 0.06$	$5.43 - j14.33$
Porcine Skin	$21.0 \pm 0.2$	$2.33 \pm 0.17$	$5.79 - j6.36$

Table 4-12: Initial Results of Animal Tissues

The similarity in the results for the real part of the permittivity of the two tissue samples is perhaps unsurprising since both are composed predominantly of collagen. The variation in their imaginary parts is probably due to their differing moisture contents.

#### 4.3.7.2 Human Skin (76 to 100GHz)

The raw measured data on the human skin sample at frequencies between 76 and 100GHz is given in Table 4-13, below. The mean values and standard deviations of the measured coefficients based on five repeated measurements are quoted. This data has subsequently been processed using MATLAB programs P3.m and P5.m to identify the solutions for its permittivity. The processed permittivity results are given in Table 4-14.

Frequency (GHz)	Wet Skin				Dry Skin			
	Reflection Coeff (dB)		Transmission Coeff. (dB)		Reflection Coeff. (dB)		Transmission Coeff. (dB)	
	Mean	$\sigma_n$	Mean	$\sigma_n$	Mean	$\sigma_n$	Mean	$\sigma_n$
76					-5.186	0.136	-12.16	0.63
77					-5.154	0.128	-12.54	0.62
78					-5.244	0.131	-13.24	0.73
80					-5.582	0.148	-14.52	0.98
82					-5.218	0.138	-14.94	0.87
84					-5.198	0.124	-14.56	0.80
86					-5.386	0.135	-14.54	0.86
88					-5.428	0.165	-14.52	0.87
90	-4.546	0.156	-21.52	0.72	-5.870	0.219	-14.34	0.87
91	-4.680	0.144	-21.66	0.71				
92	-4.876	0.143	-21.86	0.71	-5.778	0.200	-14.24	0.87
93	-5.002	0.135	-22.04	0.69				
94	-5.036	0.138	-22.20	0.70	-5.946	0.210	-14.52	0.84
95	-5.030	0.181	-22.38	0.75				
96	-4.952	0.240	-22.46	0.70	-5.750	0.331	-15.06	0.91
97	-4.736	0.254	-22.60	0.70				
98	-4.506	0.240	-22.80	0.70	-5.490	0.352	-15.42	0.95
99	-4.356	0.235	-23.08	0.71				
100	-4.290	0.255	-23.46	0.71	-5.292	0.296	-15.92	0.99
Thickness (mm)	$1.52_5 \pm 0.12$				$1.37 \pm 0.11$			
Temp. (°C)	30				30			

Table 4-13: Measured Data on Human Skin at 30°C (76 to 100GHz)

Frequency (GHz)	Wet Skin		Dry Skin	
	P3.m	P5.m (score)	P3.m	P5.m (score)
76			$10.6 - j3.2$	
77			$10.4 - j3.2$	$10.4 - j3.3$
78			$10.1 - j3.4$	(2.4)
80			$9.2 - j3.7$	
82			$9.7 - j3.7$	
84			$9.5 - j3.5$	
86			$9.0 - j3.4$	
88			$8.8 - j3.3$	
90	$13.2 - j5.3$		$7.9 - j3.0$	
91	$12.5 - j5.2$			
92	$11.7 - j5.1$		$7.9 - j2.9$	
93	$11.1 - j5.0$			
94	$10.9 - j5.0$		$7.5 - j2.9$	
95	$10.9 - j4.9$	$12.3 - j5.2$		$7.9 - j3.0$
96	$11.1 - j5.0$	(4.1)	$7.8 - j3.0$	(3.6)
97	$12.1 - j5.1$			
98	$14.2 - 5.4$		$8.3 - j3.1$	
99	$15.5 - j5.6$			
100	$15.9 - 5.7$		$8.5 - j3.2$	

Table 4-14: Permittivity Results for Human Skin at 30°C (76 to 100GHz)

It is evident that the four hour drying period at an ambient room temperature of 30°C has reduced the skin thickness, transmission losses and consequently, the  $\epsilon_r^{\parallel}$  solution over the corresponding values for the wet skin. The results of Table 4-14 are quoted to the first decimal place since this was the resolution of the permittivity solutions sought.

#### 4.3.7.3 Error Analysis on Human Skin Data (76 to 100GHz)

The following experimental tolerances apply to the measurements in the 76 to 100GHz band:

- Tolerance on sample thickness. The skin sample thickness was measured at six points. The mean value with a tolerance of  $\pm \sigma_{n-1}$  is quoted in Table 4-13.
- Accuracy of reflection coefficient calibration. The reflection coefficient is measured with respect to a short circuit provided by a metal plate fitted in the sample frame. Repeated fittings of the plate together with short term drift indicate variations of  $\pm 0.06$ dB. Long term drift of  $< 0.01$ dB was observed.
- Accuracy of reflection measurement. VNA trace-to-trace noise modulations result in variations of around  $\pm 0.1$ dB.
- Accuracy of transmission coefficient calibration. The transmission coefficient is measured with respect to no sample fitted in the frame. Repeated checks together with short term drift indicate variations of  $\pm 0.015$ dB. Long term drift of  $< 0.01$ dB was observed.
- Accuracy of transmission coefficient measurement. VNA trace-to-trace noise modulations result in variations of around  $\pm 0.3$ dB.
- Repeatability of sample placement. This is evaluated through the five repeated measurements. Initial work on the porcine skin and bovine pericardium suggested no additional variation due to sample orientation. The human skin sample was mounted in a consistent orientation for all measurements.

The above sources of error indicate that any individual measurement is subject to total errors of  $\pm 0.16$ dB (reflection coefficient) and  $\pm 0.315$ dB (transmission coefficient). The total reflection coefficient tolerance of  $\pm 0.16$ dB is on a par with the typical  $\sigma_n$  of the repeated readings whereas the total transmission coefficient tolerance of  $\pm 0.315$ dB is somewhat less than the typical  $\sigma_n$  of the repeated readings. The variability of repeated measurements includes these errors and so is a fair representation of the total experimental tolerance. Table 4-13 quotes the  $\sigma_n$  of the five repeated measurements and

a total tolerance of  $\pm \sigma_n$  is taken (an allowance of  $\pm 2\sigma_n$  yields results outside the measured range). Similarly, a thickness tolerance of  $\pm \sigma_{n-1}$  is taken.

Two further corrections to the measured coefficients which ought to be considered are described below:

- Dynamic range limitations. The measured reflection coefficient when no sample is fitted to the frame is below -35dB. This has the effect of elevating a nominal reading of -5dB by 0.004dB and, strictly, all readings should be offset more negatively by this correction. Similarly, the measured transmission coefficient when the short circuiting plate is in place is below -45dB for the dry skin tests (76 to 100GHz) and -52dB for the wet skin tests (90 to 100GHz). This low level signal results from a diffracted sidelobe to sidelobe route or multi-pathing between the antennas and so by-passes the sample. This has the effect of elevating the nominal readings by 0.004dB and again the measured data should be offset more negatively by these correction factors. However, both are negligibly small and have not been included.
- Dielectric focussing. The presence of a dielectric slab provides a small degree of focussing of the energy from the illuminating horn into the receiving horn. A small correction should therefore be made to  $T_m$  in accordance with Shimabukuro et al<sup>[82]</sup>. This correction requires an estimate of the permittivity of the sample which can be calculated from processing the uncorrected  $T_m$  data. The correction is negligibly small ( $\sim 0.01$ dB for the skin data presented here) and has not been included.

It is not possible to relate the experimental tolerance to the permittivity solutions due to the search technique used. However, it is possible to process the measured data with errors included in order to ascertain what new permittivity solutions are identified. The various errors may combine in several permutations but only those resulting in maximum and minimum values of  $\epsilon_r'$  and  $\epsilon_r''$  are of interest. A sample of the dry skin data has been processed to ascertain these limits. Some solutions differ by as little as 1.3% whilst others differ by up to 42% from their nominal values. On average, the combinations of all the maximum tolerances result in permittivity solutions differing by  $\pm 18.6\%$  from their nominal values. It has to be stressed that such errors result from the

combinations of all maximum tolerances and that the typical errors will be significantly lower. A more reliable means of ascertaining the actual errors is through repeated measurements which has been carried out in the band 57 to 63GHz.

#### 4.3.7.4 Human Skin (57 to 63GHz)

The (P5.m) permittivity results of the two initial measurements on the human skin over the band 57 to 63GHz are given below:

$$\text{Test One} \quad \epsilon_r = 13.2 - j8.7 \quad T = 22^{\circ}\text{C} \quad (57 \text{ to } 63\text{GHz})$$

$$\text{Test Two} \quad \epsilon_r = 9.9 - j9.1 \quad T = 23^{\circ}\text{C} \quad (57 \text{ to } 63\text{GHz})$$

These two tests result in a large disparity between their solutions.

The statistics pertaining to the thirty repeated measurements in the band 57 to 63GHz (including the above two) are summarised in Table 4-15 and Table 4-16 below. Table 4-15 summarises the measured data and Table 4-16 the processed permittivity results. The data of Table 4-15 was recorded at the three spot frequencies only, since the measured coefficients were simple monotonic functions of frequency.

Frequency (GHz)		57 (dB)	60 (dB)	63 (dB)			
Reflection Coefficient (dB)	Max	-4.25	-4.24	-4.10	Mean Thickness (mm)	Max	1.569
	Min	-4.90	-4.96	-4.77		Min	1.477
	Mean	-4.55	-4.51	-4.33		Mean	1.515
	$\sigma_n$	0.161	0.158	0.143		$\sigma_n$	0.025
Transmission Coefficient (dB)	Max	-18.5	-19.8	-20.5	Temperature $^{\circ}\text{C}$	Max	24.5
	Min	-25.4	-25.4	-26.1		Min	18.5
	Mean	-20.63	-21.83	-22.67		Mean	22.06
	$\sigma_n$	1.380	1.240	1.285		$\sigma_n$	1.480

Table 4-15: Statistical Summary of Measured Data on Human Skin (57 to 63GHz)

Permittivity solutions have been found at each measurement frequency (57, 60 and 63GHz) at which data was recorded using the MATLAB program P3.m and also using the data across all three measurement frequencies using the MATLAB program P5.m. Both sets of results are recorded in Table 4-16 below.

Frequency (GHz)	Real part of Permittivity $\epsilon_r'$				Imaginary part of Permittivity $\epsilon_r''$			
	Max	Min	Mean	$\sigma_n$	Max	Min	Mean	$\sigma_n$
57	14.02	9.24	12.02	1.320	9.46	7.28	7.93	0.523
60	13.76	9.17	11.82	1.083	9.03	7.22	8.01	0.437
63	14.48	10.09	12.73	1.021	8.87	7.38	8.16	0.441
57 to 63 (P5.m)	13.76	9.83	12.23	0.970	9.12	7.33	8.04	0.444

Table 4-16: Statistical Summary of Permittivity Results on Human Skin  
(57 to 63GHz)

Note: Solutions having maximum, minimum or mean values of  $\epsilon_r'$  do not generally coincide with the maximum, minimum or mean values of  $\epsilon_r''$ . The data of Table 4-16 is quoted to the second decimal place since this was the resolution of the permittivity solutions sought.

The nominal mean P5.m result is  $12.23 - j8.04$  and values lie typically in the range of  $\pm 2\sigma_n$ . All P3.m and P5.m permittivity solutions were unambiguous; unique solutions being found in the search space of  $\epsilon_r' = 9$  to 15 and  $\epsilon_r'' = 7$  to 10. The 57 to 63GHz (P5.m) results tend to be the average of the results at individual frequencies (P3.m). The error factors calculated by P3.m at each frequency were all less than 0.1 (typically 0.01 to 0.03). The scores calculated by P5.m were all less than 3.8 (mean = 1.55,  $\sigma_n = 0.641$ ). These low error factors and scores indicate that the solutions found were of a high quality since the calculated transmission and reflection coefficients based on these solutions result in very close matches to the measured values.

#### 4.3.7.5 Error Analysis on Human Skin Data (57 to 63GHz)

Experimental tolerances differ from the earlier errors relating to the 76 to 100GHz band due to the different equipment used. The following experimental tolerances apply to the measurements in the 57 to 63GHz band.

- Tolerance on sample thickness. The skin sample thickness was measured at eighteen points. These points typically varied between 1.3 and 1.7mm and the mean of the eighteen (typically close to 1.5mm) was taken for each measurement and a total tolerance of  $\pm 0.2\text{mm}$  applies. The sampled standard deviation of the eighteen points,  $\sigma_{n-1} = 0.09\text{mm}$ , typically. The statistics of the thirty repeated mean measurements are given in Table 4-15.
- Accuracy of reflection coefficient calibration. Repeated fittings of the short circuit reference plate together with short term drift indicate variations of  $\pm 0.02\text{dB}$  (typically) and  $\pm 0.05\text{dB}$  (maximum).
- Accuracy of reflection measurement. VNA trace-to-trace noise modulations result in variations of around  $\pm 0.01\text{dB}$  (typically) and  $\pm 0.033\text{dB}$  (maximum).
- Dynamic range of reflection coefficient measurement. The match with no sample in-situ varies between -23 to -27dB and requires a correction of between 0.06 and 0.02dB. Corrected values of reflection coefficient are given in Table 4-15. This correction is larger than the corresponding value at higher frequencies and cannot be ignored. This is because the sample frame appears electrically smaller at the longer wavelengths and so couples more strongly to the measurement.
- Accuracy of transmission coefficient calibration. Repeated checks of the “through” calibration path together with short term drift indicate variations of  $\pm 0.01\text{dB}$  (typically) and  $\pm 0.03\text{dB}$  (maximum).
- Accuracy of transmission coefficient measurement. VNA trace-to-trace noise modulations result in variations of around  $\pm 0.30\text{dB}$  (typically) and  $\pm 0.44\text{dB}$  (maximum).

- Dynamic range of transmission coefficient measurement. The isolation of the short circuit reference plate in the transmission path is better than -48dB. This results in a correction of 0.01dB which is negligibly small.
- Focussing effect of dielectric. The correction calculated using the method of Shimabukuro et al<sup>[82]</sup> is around 0.01dB and is negligibly small.
- Repeatability of sample placement. This is evaluated through the thirty repeated measurements. The human skin sample was mounted in a consistent orientation for all measurements.
- Anisotropy of sample. A trial was conducted in which the reflection and transmission coefficients were measured when the skin sample was mounted at 45° increments. The variation in the measured coefficients was within the spread of results observed at the fixed orientation and so it was concluded that the skin sample behaves isotropically in the MMW band.

The above sources of error indicate that any individual measurement is subject to maximum total errors of  $\pm 0.083\text{dB}$  (reflection coefficient) and  $\pm 0.47\text{dB}$  (transmission coefficient). The total reflection coefficient tolerance of  $\pm 0.083\text{dB}$  is approximately half the typical  $\sigma_n$  ( $= 0.154\text{dB}$ ) of the repeated readings and the total transmission coefficient tolerance of  $\pm 0.47\text{dB}$  is approximately a third the typical  $\sigma_n$  ( $= 1.302\text{dB}$ ) of the repeated readings. A maximum thickness tolerance of  $\pm 0.2\text{mm}$  on each measurement is taken. The repeated measurements reflect the variations due to the repeatability of sample placement, the accuracy of the VNA measurements, calibration and the processing to find permittivity solutions and inconsistencies in the drying of the sample. Thus all sources of error contribute to the statistical variations in the permittivity solutions of Table 4-16. Experimental errors/repeatability can best be judged by the maximum, minimum and standard deviation values of Table 4-16.

#### 4.3.7.6 Projecting Results to 37<sup>0</sup>C, Unfixed

The measured permittivity of the human skin may be adjusted so as to project the results to a temperature of 37<sup>0</sup>C (= arterial blood temperature) by applying the average temperature gradients for water identified by Table 4-2

i.e.  $\epsilon_r'$ : +2.35%/<sup>0</sup>C and  $\epsilon_r''$ : +1.05%/<sup>0</sup>C.

It has to be stressed, however, that the wide range of temperature gradients reported in the literature is a source of potential error.

#### 4.3.7.7 The Effects of Fixing in Formaldehyde

The permittivity results of the repeated tests on the porcine skin sample fresh and fixed are summarised in Table 4-17 below. Three repeated tests were made after 4:00hrs, 4:25hrs and 4:45hrs drying times, respectively.

Frequency (GHz)	Permittivity FRESH	Permittivity FIXED
57 – 63	3.89 – j3.36 4.34 – j3.08 4.74 – j2.47	4.06 – j2.04 4.80 – j1.76 4.74 – j1.40
Mean (max/min) Percentage Change in $\epsilon_r'$	+ 4.6 (+9.6/0.0)	
Mean (max/min Percentage Change in $\epsilon_r''$ )	- 72.0 (-76.4/-64.7)	

Table 4-17: Changes in Porcine Skin Due to Formaldehyde Fixing

Thus the “fresh” skin value of  $\epsilon_r'$  is 0.954 times that of the “fixed” skin value,

And the “fresh” skin value of  $\epsilon_r''$  is 1.72 times that of the “fixed” skin value.

Note that these values differ slightly from the initial results reported in Table 4-12 due to the increased drying time allowed here. The low value of permittivity of porcine skin with respect to human skin is probably due to its tougher, more horny, nature. It is also worth noting that Hwang et al [26] observed a reduction in permittivity and relaxation

frequency in a sample of pork muscle following treatment in ethanol, which displaces some of the water in the tissue, as does formaldehyde. This observation supports the effects of formaldehyde fixing noted here. Permittivity and relaxation frequency were subsequently increased when the sample was re-hydrated following immersion in a saline solution. Formaldehyde fixing, however, is an irreversible process.

#### **4.3.7.8 Summary of Results on Human Skin**

Table 4-18 summarises the measured permittivity solutions on the fixed sample of dry human skin at individual frequencies of interest and averaged over some relevant bands. These results are quoted at their measured temperatures in the middle column. Corrected values pertaining to fresh (i.e. unfixed by formaldehyde) skin at 37°C are given in the right hand column. This assumes that the percentage changes seen in the results on porcine skin in the range 57 to 60GHz may be applied to human skin over the band 57 to 100GHz.

Data on the fixed skin at the ambient temperature is quoted with a tolerance of  $\pm 2\sigma_n$  (57 to 63GHz, see sections 4.3.7.4 and 4.3.7.5) and with a tolerance of  $\pm 18.6\%$  (76 to 100 GHz, see section 4.3.7.3). Data on the skin corrected for unfixed values at 37°C is subject to two further sources of error. The formaldehyde fixing correction for  $\epsilon_r'$  varies by +5.0% to -4.6% and for  $\epsilon_r''$  the variation is +7.3% to -4.4% from the mean values applied here. The temperature gradient correction for  $\epsilon_r'$  also varies by  $\pm 0.65\text{ }^{\circ}\text{C}$  and for  $\epsilon_r''$  the variation is +0.67/-0.46  $\text{ }^{\circ}\text{C}$  from the mean gradients applied here. This results in total errors of approximately  $\pm 18\%$  for the fixed skin at ambient temperatures and approximately  $\pm 24\%$  for the corrected fresh skin at 37°C across the whole measurement band.

Frequency (GHz)	Permittivity (fixed, ambient Temp.)	Permittivity (fresh, 37°C)
57	12.0 ( $\pm 2.6$ ) – j7.9 ( $\pm 1.0$ )	15.5 (+5.6/-4.8) – j15.8 (+3.9/-3.4)
60	11.8 ( $\pm 2.2$ ) – j8.0 ( $\pm 0.9$ )	15.2 (+5.1/-4.3) – j15.9 (+3.8/-3.2)
63	12.7 ( $\pm 2.0$ ) – j8.2 ( $\pm 0.9$ )	16.4 (+4.9/-4.3) – j16.2 (+4.0/-3.1)
57 – 63	12.2 ( $\pm 2.0$ ) – j8.0 ( $\pm 0.9$ )	15.8 (+4.8/-4.2) – j16.0 (+3.7/-3.3)
76	10.6 ( $\pm 2.0$ ) – j3.2 ( $\pm 0.6$ )	11.8 (+3.4/-3.1) – j5.9 (+1.6/-1.4)
77	10.4 ( $\pm 1.9$ ) – j3.2 ( $\pm 0.6$ )	11.6 (+3.3/-3.0) – j5.9 (+1.6/-1.4)
78	10.1 ( $\pm 1.9$ ) – j3.4 ( $\pm 0.6$ )	11.2 (+3.3/-2.9) – j6.3 (+1.6/-1.5)
76 - 78	10.4 ( $\pm 1.9$ ) – j3.3 ( $\pm 0.6$ )	11.6 (+3.3/-3.0) – j6.1 (+1.6/-1.5)
80	9.2 ( $\pm 1.7$ ) – j3.7 ( $\pm 0.7$ )	10.2 (+3.0/-2.6) – j6.8 (+1.9/-1.7)
82	9.7 ( $\pm 1.8$ ) – j3.7 ( $\pm 0.7$ )	10.8 (+3.1/-2.8) – j6.8 (+1.9/-1.7)
84	9.5 ( $\pm 1.8$ ) – j3.5 ( $\pm 0.7$ )	10.6 (+3.1/-2.8) – j6.5 (+1.8/-1.7)
86	9.0 ( $\pm 1.7$ ) – j3.4 ( $\pm 0.6$ )	10.0 (+2.9/-2.6) – j6.3 (+1.6/-1.5)
88	8.8 ( $\pm 1.6$ ) – j3.3 ( $\pm 0.6$ )	9.8 (+2.8/-2.5) – j6.1 (+1.6/-1.5)
90	7.9 ( $\pm 1.5$ ) – j3.0 ( $\pm 0.6$ )	8.8 (+2.6/-2.3) – j5.5 (+1.6/-1.4)
92	7.9 ( $\pm 1.5$ ) – j2.9 ( $\pm 0.5$ )	8.8 (+2.6/-2.3) – j5.4 ( $\pm 1.3$ )
94	7.5 ( $\pm 1.4$ ) – j2.9 ( $\pm 0.5$ )	8.3 (+2.5/-2.1) – j5.4 ( $\pm 1.3$ )
96	7.8 ( $\pm 1.5$ ) – j3.0 ( $\pm 0.6$ )	8.7 (+2.6/-2.3) – j5.5 (+1.6/-1.4)
98	8.3 ( $\pm 1.5$ ) – j3.1 ( $\pm 0.6$ )	9.2 (+2.7/-2.3) – j5.7 (+1.6/-1.4)
100	8.5 ( $\pm 1.6$ ) – j3.2 ( $\pm 0.6$ )	9.4 (+2.8/-2.4) – j5.9 (+1.6/-1.4)
90 - 100	7.9 ( $\pm 1.5$ ) – j3.0 ( $\pm 0.6$ )	8.8 (+2.6/-2.3) – j5.5 (+1.6/-1.4)

Table 4-18: Summary of Permittivity Results on Dry Human Skin

#### 4.3.8 Comparison Between Predicted and Measured Results

There is little consensus between the measured results of Table 4-18 and the modelled results of Table 4-11. This discrepancy is not altogether surprising as it affirms the comment by Ghodgaonkar, Gandhi and Iskander [21] that both the real and imaginary parts of the complex permittivity of skin *in vivo* are expected to be significantly lower than for excised skin. They conjecture that this is due to the variations in water content, blood content and epidermal thickness. The measured permittivity does exhibit a gradual reduction with increasing frequency, as expected, but does not exhibit an increase in conductivity with increasing frequency, as would be expected.

Differences also exist between this data and that previously reported in the literature, which in itself is rather inconsistent. Ghodgaonkar et al [21] report the permittivity of skin on the palm to be around  $\epsilon_r = 4 - j7$  at 57GHz, whereas Hwang et al [26] report it to be  $\epsilon_r = 6.0 - j2.5$  and Boric-Lubecke et al [24][25] report it to be  $\epsilon_r = (11.3 \text{ to } 13.0) - j(3.5 \text{ to } 5.5)$  at 40GHz. Here, values of  $\epsilon_r = 15.49 - j15.78$  (fresh,  $37^0\text{C}$ ) or  $\epsilon_r = 12.02 - j7.93$  (fixed,  $22^0\text{C}$ ) at 57GHz are presented in Table 4-18. Boric-Lubecke et al also quote results for skin on the elbow and back of the hand at 40GHz at  $\epsilon_r = (16.0 \text{ to } 17.0) - j(10.5 \text{ to } 12.0)$  which is in much closer agreement with the measured data presented here. This agreement would appear to affirm the comment of Boric-Lubecke et al [24] (also supported by the results of Hwang et al) that palm skin has a lower permittivity due to its thick and horny nature.

#### 4.4 PROPOSED MODEL FOR HUMAN SKIN

A MATLAB program called CCfit.m (Appendix C) was written to search for parameter values of the Cole-Cole function of equation (1.14) which result in the closest fit to the measured data. Two sets of “target” permittivity values were trialled which correspond to the measured data for the fixed skin at ambient temperature and the fresh skin at 37<sup>0</sup>C, as defined in Table 4-19 below:

	$\epsilon_r$ at 60GHz	$\epsilon_r$ at 77GHz	$\epsilon_r$ at 94GHz
Fixed, ambient temp.	12.23 – j8.04	10.4 – j3.3	7.9 – j3.0
Fresh, 37 <sup>0</sup> C	15.76 – j16.00	11.55 – j6.09	8.78 – j5.54

Table 4-19: Target Data for Cole-Cole Fit

Program CCfit.m searches for parameter values ( $\epsilon_s$ ,  $\epsilon_\infty$ ,  $f_c$ ,  $\sigma_s$  and  $\alpha$ ) which result in the lowest rms percentage error between the target values of complex permittivity and the values computed at each trial combination of parameters. The best fit sets of parameters are tabulated below (Table 4-20).

	$\epsilon_s$	$\epsilon_\infty$	$f_c$ (GHz)	$\sigma_s$	$\alpha$	$\epsilon_r$ at 60GHz (best fit)	$\epsilon_r$ at 77GHz (best fit)	$\epsilon_r$ at 94GHz (best fit)
Fixed, Ambient Temp.	31.3	8.9	13.6	0	0	9.99-j4.83	9.58-j3.84	9.36-j3.17
Fresh, 37 <sup>0</sup> C	36.0	8.9	21.8	0	0	12.06-j8.70	10.91-j7.10	10.28-j5.96

Table 4-20: Best Fit Cole-Cole Parameters

The best fit Cole-Cole parameters result in an rms percentage error between the target and computed values of permittivity (real and imaginary parts at three frequencies, i.e. six data points) of 20.9 for the fixed skin and 23.4 for the fresh skin values. These are quite significant errors, as can be seen from a comparison between the target and best fit values of permittivity. In both cases, the best fit  $\alpha$  parameter is found to be zero and so the Cole-Cole function simplifies to the single relaxation Debye equation (1.11). The most significant difference between the two parameter sets is the very much reduced relaxation frequency associated with the fixed skin, which is consistent with the reduced water content of tissue fixed in formaldehyde. The higher relaxation frequency associated with the corrected characteristics of fresh skin at  $37^0\text{C}$  is only marginally lower than that expected for free water at this temperature. Table 4-21 below compares the model parameters identified here with those relating to the other single relaxation frequency Debye models reported in section 4.2.3.

	$\epsilon_s$	$\epsilon_\infty$	$f_c$ (GHz)	$\sigma_s$
Present study (fresh skin, $37^0\text{C}$ )	36.0	8.9	21.8	0
Author's own model (section 4.2.3.3)	39.6	4.0	8.784	0
Cook <sup>[23]</sup> breast and instep (section 4.2.3.2)	42	4.0	23.06	$0.014 \Omega/\text{cm}$
Ghodgaonkar and Daud <sup>[25]</sup> Palm (section 4.2.3.4) 25GHz	54.2	1.5	6.96	0.92 S/m
Sole	17.82	1.5	11.63	0.92 S/m

Table 4-21: Comparison of Model Parameters For Single Term Debye Function  
(*Human skin,  $37^0\text{C}$* )

The data of Table 4-21 serves to illustrate the wide variation in model parameters attributed to human skin in the MMW band. The parameters proposed in the present work fall within the ranges previously published (with the exception of  $\epsilon_\infty$ ) and accord with expectations.

#### 4.5 POWER DEPOSITION IN HUMAN SKIN

In this section the power deposition and heating of human skin exposed to MMW radiation is evaluated. The evaluation is based on the corrected permittivity of human skin of Table 4-18, namely:

$\epsilon_r = 15.76 - j16.00$  (60GHz),  $\epsilon_r = 11.55 - j6.09$  (77GHz) and  $\epsilon_r = 8.78 - j5.54$  (94GHz) and also on an incident power density of  $10\text{mW/cm}^2$ , which is the NRPB basic restriction in the 10 to 300GHz band<sup>[38]</sup>. Part of the incident radiation is reflected at the air/skin interface and a factor of  $1 - |r_1|^2$  is transmitted into the skin surface, where  $|r_1|$  is the magnitude of the air/skin reflection coefficient and is given by equation (3.3). On propagating into the skin its power is absorbed exponentially with depth into the skin and heat is generated as a result. The skin depth is defined as being the depth at which the field strength has decayed by a factor of  $1/e$  ( $\sim 1/2.7183$ ) of its surface value (or power decayed to  $1/e^2$ ), therefore 86.5% of the power is deposited into a surface layer of one skin depth<sup>f</sup>. The skin depth,  $\delta = 1/\alpha$ , where  $\alpha$  is the real part of the propagation constant and is given by equation (1.6). Values of the coefficient of surface transmission, skin depth and power deposition in a volume having a surface area of 1cm x 1cm and a thickness of one skin depth (assuming a power density of  $10\text{mW/cm}^2$  incident on the air/skin interface) at the three frequencies of interest are tabulated in Table 4-22 below.

Frequency (GHz)	Coefficient of Surface Transmission, T	Skin Depth, $\delta$ (mm)	Power Deposited / skin depth (mW) / (cm <sup>3</sup> )	
60	0.543	0.435	4.70	$43.5 \times 10^{-3}$
77	0.666	0.714	5.76	$71.4 \times 10^{-3}$
94	0.705	0.567	6.10	$56.7 \times 10^{-3}$

Table 4-22: Power Deposition in Skin

---

<sup>f</sup> NOTE: do not confuse “skin depth” with the thickness of the human skin sample; this is an unfortunate coincidence of terms.

The rise in skin surface temperature is solved using the method of Walters et al [42]. A one-dimensional thermal model, based on a solution of the heat conduction equation is used in which it is assumed that a plane surface of skin is illuminated by a plane wave and that heat diffusion along the surface of the skin and cooling due to blood perfusion and surface heat losses to the air above are negligibly small. The model equation is therefore a simplified version of the bioheat transfer equation (BHTE), formulated by H. H. Pennes in 1948 [126].

$$k\nabla^2T(x,t) + Q(x,t) = \rho C \frac{\partial T(x,t)}{\partial t} \quad (4.5)$$

where  $T(x,t)$  is the temperature at depth,  $x$  and time,  $t$

$C$  is the specific heat (of skin)

$k$  is the thermal conductivity (of skin)

$Q(x,t)$  is the rate of energy deposition at depth,  $x$  and time,  $t$

and  $Q(x,t) = \frac{I_0 T}{\delta} e^{-x/\delta}$  (4.6)

where  $I_0$  is the incident power density

$\delta$  is the skin depth

$T$  is the coefficient of surface transmission  $= 1 - |r_1|^2$

Assuming insulated boundary conditions (i.e. no heat loss from the skin into the space around it), the solution to the thermal model (4.5) at the surface ( $x = 0$ ) gives:

$$T_{sur} = T_0 \left[ 2 \sqrt{\frac{t}{\pi\tau}} + e^{\sqrt{\tau}} \operatorname{erfc}\left(\sqrt{\frac{t}{\tau}}\right) - 1 \right] \quad (4.7)$$

In which  $T_0 = \frac{I_0 \delta T}{k}$  and  $\tau = \frac{\delta^2 \rho C}{k}$

Where  $\operatorname{erfc}(x)$  is the complimentary error function,  $\tau$  is the thermal time constant i.e. the time for the thermal energy to diffuse a distance equal to the energy penetration depth ( $= \delta$ ) and  $T_{sur}$  is the surface temperature rise.

For exposure times  $> \tau$  the complementary error function term becomes very small.

Re-arranging (4.7) gives:

$$T_{sur} = C_1 \sqrt{t} - C_2 \left( 1 - e^{\frac{t}{\tau}} \operatorname{erfc} \left( \sqrt{\frac{t}{\tau}} \right) \right) \quad (4.8)$$

where  $C_1 = \frac{2I_0 T}{\sqrt{\pi k \rho C}}$  and  $C_2 = \frac{I_0 T \delta}{k}$

Walters et al [42] quote values of  $\rho k C = 1.7 \times 10^6 \text{ W}^2 \text{ s/m}^4 {}^\circ\text{C}^2$  (thermal inertia of skin) and  $k = 0.3 \text{ Wm}^{-1} {}^\circ\text{K}^{-1}$  (thermal conductivity of skin). Assuming also an incident power density,  $I_0 = 100 \text{ W/m}^2$  ( $= 10 \text{ mW/cm}^2$ ) and values of  $T$  and  $\delta$  given in Table 4-22, corresponding values of  $C_1$ ,  $C_2$  and  $\tau$  at each frequency of interest may be calculated and are presented in Table 4-23, below.

Frequency (GHz)	Model Parameters		
	$C_1$ ( ${}^\circ\text{C s}^{-0.5}$ )	$C_2$ ( ${}^\circ\text{C}$ )	$\tau$ (s)
60	$46.99 \times 10^{-3}$	$78.74 \times 10^{-3}$	3.574
77	$57.64 \times 10^{-3}$	$158.51 \times 10^{-3}$	9.629
94	$61.01 \times 10^{-3}$	$133.35 \times 10^{-3}$	6.073

Table 4-23: Surface Temperature Model Parameters

This contrasts with the data of Walters et al based on  $\epsilon_r = 5.8 - j7.5$  at 94GHz (taken from predictions using the 4 term Cole-Cole function of Gabriel [43]) which results in  $T = 0.69$ ,  $\delta = 0.19\text{mm}$ ,  $C_1 = 59.7 \times 10^{-3} {}^\circ\text{C.s}^{-0.5}$ ,  $C_2 = 43.7 \times 10^{-3} {}^\circ\text{C}$  and  $\tau = 0.682 \text{ s}$ . (Their calculation of  $\delta$  uses an unfamiliar equation which returns a result approximately half that obtained from the equation  $\delta = I/\alpha$  and is believed to be a major source of disparity between the two sets of results.)

A MATLAB program called Trise.m (Appendix C) has been written to solve equation (4.8) to determine the rise in skin surface temperature as a function of time. The program was validated through a confirmation of the temperature rises calculated by

Walters et al<sup>[42]</sup>. Trise.m was used to predict skin surface temperature rises at the three frequencies of interest and is plotted in Figure 4-7.

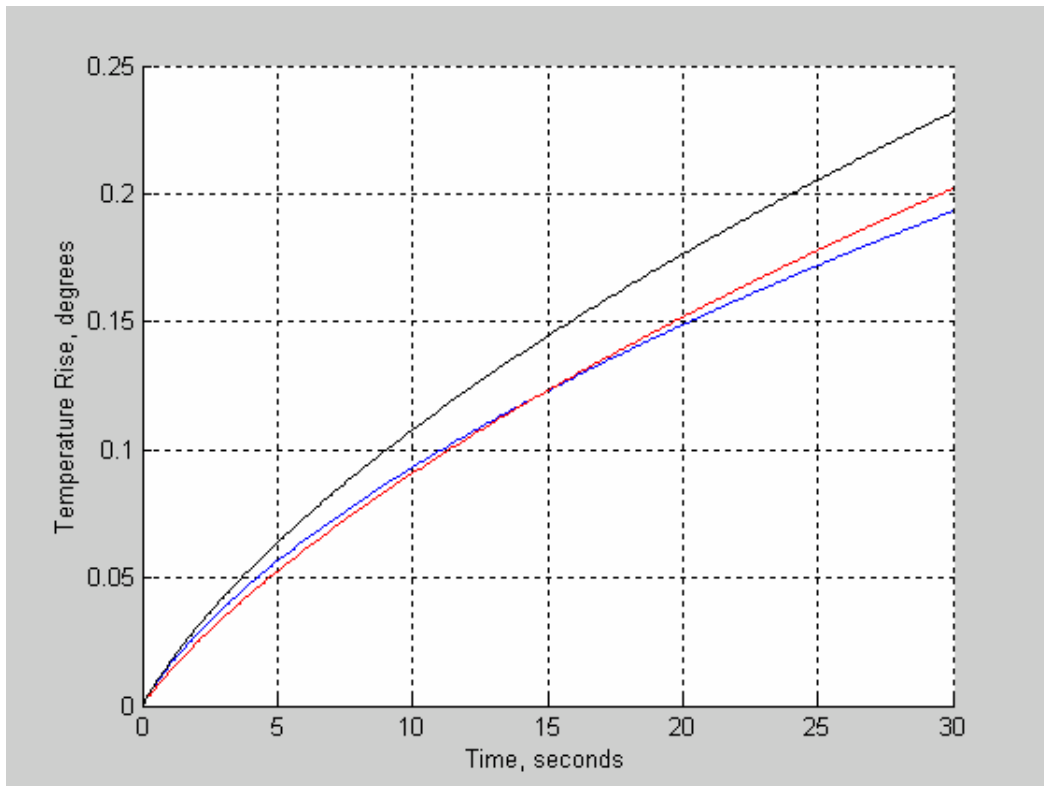


Figure 4-7: Skin Surface Temperature Rises  
(Black = 94GHz, Red = 77GHz, Blue = 60GHz)

Figure 4-7 indicates modest temperature rises. Since also they are based on assumptions of negligible heat losses, actual temperature rises are likely to be even lower. The rise of  $0.2^{\circ}\text{C}$  in skin surface temperature arising from a thirty second exposure will be barely noticed by the body's thermo-regulatory system. Whilst the temperatures continue to rise with prolonged exposure, the thermo-regulatory system will start to take effect after about 30 seconds. The threshold for human pain is approximately  $43^{\circ}\text{C}$ , above which burn damage is incurred. Cell kill rate due to elevated temperature may be quantified using the Arrhenius equation. Walters et al<sup>[42]</sup> consider power densities some 100 times greater than here and predict rises of around  $7^{\circ}\text{C}$  in three seconds which they find is on

the threshold for pricking pain sensation in human subjects. Therefore, the current basic restrictions of the NRPB are sufficient to avoid skin surface burns.

Lebedev and Permyakov [127] have considered the influence of skin roughness on the absorbed power distribution under a MMW horn antenna. They concluded that skin wrinkles of height greater than the skin depth result in a five to ten fold increase in absorbed power at the tip of a wrinkle compared with a plane skin layer. Depressions result in reduced radiation. They concluded that the perturbation in the absorbed power distribution is negligibly small for wrinkles of height less than a half the skin depth. The typical wrinkle height observed in this study was  $\pm 0.09\text{mm}$  (i.e.  $\pm \sigma_{n-1}$  of thickness measurements) which is always less than half the skin depths calculated here. Furthermore, most of the wrinkles on the skin sample used in this work were on the inner surface; the outer, illuminated surface being much the flatter.

#### 4.6 CHAPTER SUMMARY

This Chapter started by reviewing the measured and modelled data on water through the MMW. This sought to predict the permittivity of water at 60, 77 and 94GHz at room temperature ( $20^{\circ}\text{C}$ ) and human body temperature ( $37^{\circ}\text{C}$ ). This also established some of the model parameters applicable to water and wet dielectrics which are applied in the various models based on the relaxation phenomena of water.

There then followed a review of the models used to describe the permittivity of human skin into the MMW band. This included the author's own attempts to predict the permittivity of human skin based on a single relaxation Debye equation. A great variety of models and model parameters have been published and applied and, consequently, they result in a wide range of predictions for the complex permittivity of human skin in the MMW band in the technical literature.

The method and testing protocol on a single sample of excised human skin previously fixed in formaldehyde was described and the results presented. This included thirty

repeated tests at 60GHz, plus additional data between 76 to 100GHz. The experimental errors and repeatability were discussed in each case. The effects of the fixing process in formaldehyde were ascertained from tests on a fresh and fixed porcine skin sample. These indicated a significant reduction in the imaginary part of the permittivity for the fixed tissue and were in keeping with the notion that the formaldehyde displaces water from the tissue. The permittivity results for the human skin were then corrected to unfixed values at body temperature. This corrected data was in reasonable agreement with previously published data for skin on the elbow and back of the hand at 40GHz. The total experimental errors are approximately  $\pm 18\%$  for the fixed skin at ambient temperatures and approximately  $\pm 24\%$  for the corrected fresh skin at  $37^{\circ}\text{C}$  across the whole measurement band.

The dielectric relaxation models were then re-visited and model parameters were sought to fit the measured data. The model parameterisation settled on a single relaxation Debye function, even though it was at liberty to parameterise a more complex Cole-Cole function. The model parameters identified for the unfixed, body temperature permittivity values of human skin were typically within the ranges of previously published model parameters for human skin *in vivo*.

Finally, the permittivity results of the skin (unfixed at body temperature) were used to calculate the heat deposition and model the surface temperature rise in skin exposed MMW signals at frequencies of 60, 77 and 94GHz at a power density of  $100\text{W/m}^2$ , the NRPB basic restriction. This found that there was at most a  $0.2^{\circ}\text{C}$  rise after a thirty second exposure and so concluded that the current restrictions were adequate to avoid heat pain and skin burns.

## CHAPTER FIVE: DETECTION AND LOCATION OF DEFECTS IN COMPOSITES

### 5.1 INTRODUCTION

Radio frequency (RF) measurements offer the potential to determine the structural integrity of composite materials in a non-destructive, non-contacting manner. Defects such as delaminations, voids, matrix cracks and improper cure result in changes in the dielectric properties of the composite [71][70]. The presence of such defects may be determined via a measurement of dielectric properties, such as permittivity, or by the absorption, scattering and reflections of an electromagnetic (EM) signal, propagating in the medium, which is incident on a discontinuity resulting from the defect. Ideally, one would desire a diagnostic tool which is non-contacting and capable of achieving a spatial resolution in the order of the likely defect dimensions. The non-contacting requirement dictates a free-space RF based measurement and the requirement for fine resolution dictates the use of millimetre wave (MMW) frequencies (30GHz to 300GHz) because of the fine spatial resolution they afford.

This Chapter describes some experimental work to determine the feasibility of the free-space measurement of permittivity in the 90GHz to 100GHz band to detect and locate a variety of defects in planar fibreglass composite samples. The work described in this chapter is summarised in the author's paper "Damage and Defect Detection in Composites Using Millimetre Wave Permittivity Measurement", which is reproduced in Appendix A.

Several composite samples were manufactured; some being kept as control samples having no defects and others having damage induced within them. The defect categories were: low-level impact damage, incomplete curing and vacuum release during the curing cycle. Additionally, a large sheet of composite sample was manufactured and the spatial variation in its permittivity was mapped. This sample was subsequently subjected to low-level impact damage and then re-examined using the MMW technique in order to judge the spatial resolution to which the defect can be resolved. The

structural integrity of all composite samples has been determined using a Physical Acoustics UltraPAC II ultra-sound imaging C-scan with a 5 MHz probe to enable a comparison between the MMW measurements and the severity and extent of defects. Additionally, a three layered structure comprising of two composite layers with an air gap between them was modelled and tested. This structure was designed to represent a solid composite containing a large void defect between delaminated layers. The modelled and measured results were compared with each other and with a single solid composite with no air void to determine the ability of the MMW measurement technique to detect the large void.

This Chapter contains sections which describe the sample preparation, defects and ultra-sound testing. The results of the MMW permittivity measurements and ultra-sound images are then presented and discussed. The Chapter concludes that there are resolvable differences in the permittivity between nominally ideal and defective samples.

## 5.2 SAMPLE PREPARATION

Twelve fibreglass composite samples were manufactured from Fibredux 916G, a woven pre-preg tape (10 layers, all aligned). All but sample 12 were manufactured as a disc of diameter 125mm, sample 12 was a sheet of dimensions 500mm x 250mm. A further six samples of fibreglass composite samples were manufactured from Fibredux 913G, a unidirectional pre-preg tape (10 layers, cross-ply). These six were also manufactured as discs of diameter 125mm. Table 5-1 summarises the details of the samples. Three samples of each control and defect category (except impact damaged samples) were manufactured in order to judge the statistical spread of results.

All the samples were cut from the same sheet and all were processed in the same way prior to curing. The curing process was carried out under a vacuum of 200mbar. The Fibredux 916G samples were cured by temperature ramping at a rate of 1.5°C per minute to a final temperature of 130°C followed by a dwell at this temperature for 30 minutes. The Fibredux 913G samples were cured by temperature ramping at 1.5°C per minute to a temperature of 100 °C followed by a dwell at this temperature for 1 hour then a further temperature ramp at 1.5°C per minute to 120°C followed by a dwell at this temperature for 1 hour. The samples were cooled down by opening the door after switching the oven off. The vacuum was released and the samples removed from the oven. The vacuum was released at 80°C for the samples that had the vacuum released early, otherwise the cure cycle continued as per normal. The incompletely cured samples were removed from the oven once it had reached its final temperature i.e. zero dwell time.

Sample #	Defect	Composition
1, 2, 3	None – used as control	Fibredux 916G Woven 10 layers 125mm discs
4	3 Joule impact in centre	
5	2 Joule impact in centre	
6, 7, 8	Incompletely cured	
9, 10, 11	Vacuum released during cure	
12	Initially none then 2 Joule impact	500 x 250mm sheet
13, 14, 15	None – used as control	Fibredux 913G Unidirectional 10 layers 125mm discs
16, 17, 18	Vacuum released during cure	

Table 5-1: Sample details

### 5.3 ULTRA-SOUND TESTING

The quality of every sample was assessed using a 5MHz ultra-sound imaging C-scanner. The samples were supported in water above the bottom of the water tank and the transducer acquired an image of the sample in a raster scanning fashion. The ultra-sound equipment was operated in a time gated mode to capture the two-way transmission path of the signal (through the sample, reflected from the tank base and back through the sample). Undamaged composite material transmits the signal through it with little attenuation, whereas the presence of defects scatters and absorbs the signal

resulting in a highly attenuated transmission path. In the ultra-sound images, the attenuation of the transmission path is colour coded: green being minimal attenuation, red being slightly greater attenuation and blue being highly attenuated and indicative of a defect. The ultra-sound images are given in Figure 5-1 and Figure 5-2.

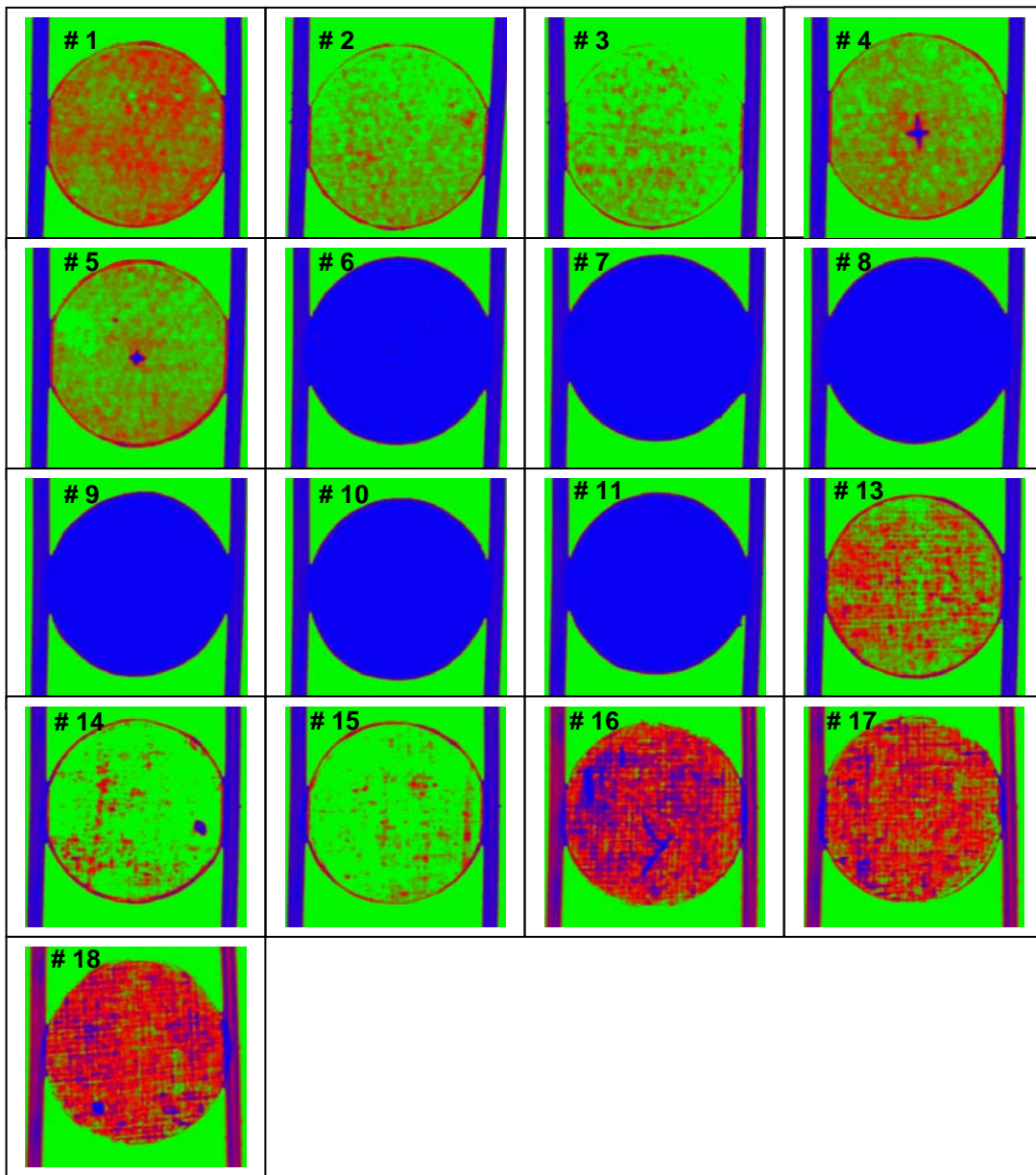


Figure 5-1: Samples 1 to 11 & 13 to 18 Ultra-Sound Images  
(Green/red: no defect, blue: defect)

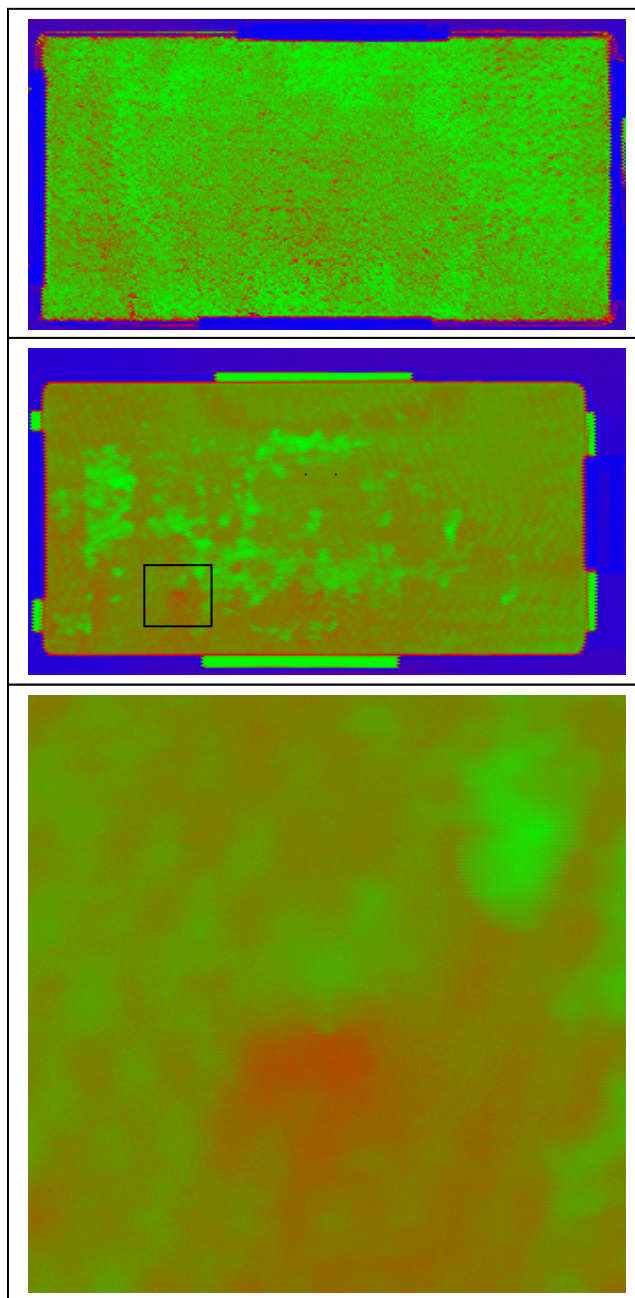


Figure 5-2: Sample #12 Ultra-Sound Images

Upper: before impact damage, centre: after impact damage, lower: close up of impact damage (inset area of centre image).  
(Green/red: no defect, blue: defect )

## 5.4 EXPERIMENTAL TESTS

The permittivity of samples 1 to 11 was measured at a consistent sample orientation. The impact site (samples 4 and 5) was nominally in the centre of each sample which in turn was opposite the phase centres of the waveguide horns. Additionally, the measurement on sample 1 was repeated several times at random sample orientations in order to judge the effects of fibre orientation with respect to the plane of polarisation and also to ascertain the experimental repeatability.

Sample 12 was secured to the frame so as to expose the measurement of permittivity at 14 sites evenly distributed across its surface plus additional sites centred at 10mm, 20mm and 40mm left and right of the designated impact site, see Figure 5-3. A 2 Joule impact was then inflicted on the site and the permittivity measurements and ultra-sound tests repeated. The impact created a star shaped delamination with the peak extents of the delamination in the reinforcing fibre orientations and the composite surface was smoothed back into shape by hand so as to minimise the physical distortion of the sample.

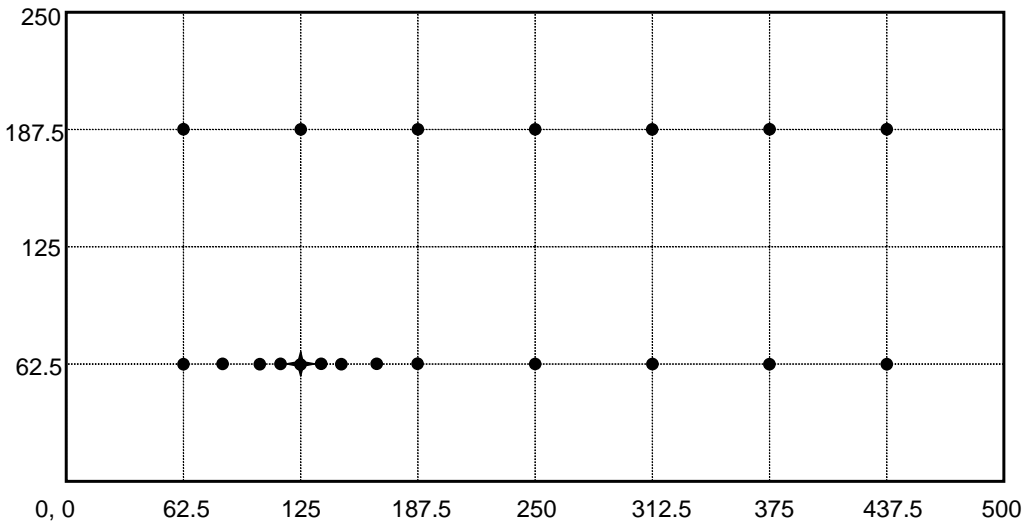


Figure 5-3: Sample #12 Map  
 (● = measurement centre, + = impact centre. All coordinates in mm.)

A three layer structure was made from composite samples #1 and #2 with an air gap of nominally 1.6mm between them, as defined by the thickness of some steel spacers. The structure was clamped in place onto the sample frame; the steel spacers being around the periphery and so not visible to the measurement. The thickness of each layer (composite, air, composite) was measured and the transmission and reflection coefficients across the band 90 to 100GHz was also measured and recorded. In addition to this, the structure was modelled using the MATLAB program, D3TR.m (based on the general theory of planar dielectric layers described in Chapter 2), with the following input parameters:

#### Layer 1 (composite sample #1)

- Thickness,  $t_1 = 1.254 \pm 0.01$  mm
- Permittivity,  $\epsilon_{r1} = 3.78 - j0.086$  (see Results section 5.5.1, Table 5-2)

#### Layer 2 (air)

- Thickness,  $t_2 = 1.60 \pm 0.06$  mm  
(repeated runs were made for  $t_2 = 1.60, 1.54, 1.66$  and  $1.56$  mm)
- Permittivity,  $\epsilon_{r2} = 1 - j0$

#### Layer 3 (composite sample #2)

- Thickness,  $t_3 = 1.264 \pm 0.01$  mm
- Permittivity,  $\epsilon_{r3} = 3.78 - j0.093$  (see Results section 5.5.1, Table 5-2)

In order to judge the effect of the air layer (void) a single dielectric layer was modelled over the same band using the MATLAB program TR3.m with the following input parameters:

- Thickness = 4.118 mm ( $= t_1 + t_2 + t_3$ )
- Permittivity =  $3.78 - 0.09$  (the mean of  $\epsilon_{r1}$  and  $\epsilon_{r3}$ )

The results are given in section 5.5.

## 5.5 RESULTS / DISCUSSION

### 5.5.1 Composite Samples #1 to #18

A summary of the permittivity results for samples 1 to 11 and 13 to 18 is given in Table 5-2. The permittivity results for sample 12 both before and after the impact is given in Table 5-3.

Sample #	Thickness	Permittivity
1	$1.28 \pm 0.02$ mm	$3.78 - j0.086$
2	$1.28 \pm 0.02$ mm	$3.78 - j0.093$
3	$1.28 \pm 0.02$ mm	$3.76 - j0.099$
4	$1.275 \pm 0.02$ mm	No solution
5	$1.27 \pm 0.02$ mm	No solution
6	$1.51 \pm 0.05$ mm	$3.61 - j0.074$
7	$1.51 \pm 0.04$ mm	$3.57 - j0.130$
8	$1.50 \pm 0.01$ mm	$3.37 - j0.109$
9	$1.65 \pm 0.02$ mm	$3.20 - j0.047$
10	$1.63 \pm 0.05$ mm	$3.21 - j0.065$
11	$1.60 \pm 0.03$ mm	$3.27 - j0.053$
13	$1.36 \pm 0.01$ mm	$4.49 - j0.151$
14	$1.35 \pm 0.02$ mm	$4.06 - j0.138$
15	$1.37 \pm 0.02$ mm	$4.23 - j0.085$
16	$1.575 \pm 0.03$ mm	$4.21 - j0.073$
17	$1.55 \pm 0.02$ mm	$4.21 - j0.123$
18	$1.54 \pm 0.02$ mm	$4.22 - j0.073$

Table 5-2: Samples 1 to 11 & 13 to 18 Permittivity Results

Location (x,y in mm)	Permittivity (before damage)	Permittivity (after damage)
62.5, 62.5	$3.80 - j0.115$	$3.90 - j0.131$
85, 62.5 40mm left of impact	$3.85 - j0.103$	$3.89 - j0.138$
105, 62.5 20mm left of impact	$3.85 - j0.100$	$3.95 - j0.127$
115, 62.5 10mm left of impact	No reading	$3.89 - j0.138$
125, 62.5 impact site	$3.84 - j0.084$	No solution
135, 62.5 10mm right of impact	No reading	$3.86 - j0.127$
145, 62.5 20mm right of impact	$3.81 - j0.088$	$3.86 - j0.134$
165, 62.5 40mm right of impact	$3.73 - j0.078$	$3.83 - j0.104$
187.5, 62.5	$3.70 - j0.120$	$3.73 - j0.144$
250, 62.5	$3.75 - j0.088$	No Measurements Necessary (too remote from impact site)
312.5, 62.5	$3.82 - j0.091$	
375, 62.5	$3.74 - j0.103$	
437.5, 62.5	$3.77 - 0.097$	
62.5, 187.5	$3.76 - j0.102$	
125, 187.5	$3.77 - j0.103$	
187.5, 187.5	$3.76 - j0.096$	
250, 187.5	$3.77 - j0.104$	
312.5, 187.5	$3.72 - j0.112$	
375, 187.5	$3.73 - j0.103$	
437.5, 187.5	$3.69 - j0.096$	

Table 5-3: Sample 12 Permittivity Results

The control samples (1, 2 and 3) of the Fibredex 916G exhibit a range in  $\epsilon_r'$  of 3.76 to 3.78 and in  $\epsilon_r''$  of 0.086 to 0.099. Sample 12, also Fibredex 916G, has a spatial variation in  $\epsilon_r'$  of 3.69 to 3.85 and in  $\epsilon_r''$  of 0.078 to 0.120. This composite material has reasonably consistent dielectric properties both on a sample by sample basis and within any given sample. The 3 and 2 Joule impact damages of samples 4 and 5 respectively have resulted in considerable shape distortion around the impact site and this is clearly visible on the ultra-sound images of Figure 5-1. This distortion has scattered the MMW signals in such a way as to yield transmission and reflection coefficients across the measurement band which cannot be related to any value of permittivity. Clearly, the absence of a solution is resolvable from the defect-free samples. The incompletely cured samples (6, 7 and 8) differ visually in colour and feel tacky and pliable to the touch. Their ultra-sound images indicate that they are ridden with defects and are typical of materials with a large void content. These samples have a variation in  $\epsilon_r'$  of 3.37 to 3.61 and in  $\epsilon_r''$  of 0.074 to 0.130. The spread in  $\epsilon_r'$  is outside the range of that for the nominally ideal samples (1, 2, 3 and 12) and therefore resolvable from them. The spread in  $\epsilon_r''$  is not resolvable from the nominally ideal samples. Those samples for which the vacuum was released early (9, 10 and 11) are slightly thicker than the nominally ideal samples due to their large void content, but otherwise appear similar. Their ultra-sound images indicate that they are also ridden with defects. These samples have a variation in  $\epsilon_r'$  of 3.20 to 3.27 and in  $\epsilon_r''$  of 0.047 to 0.065; the reduction in both  $\epsilon_r'$  and  $\epsilon_r''$  being consistent with a large material void content. The ranges of both  $\epsilon_r'$  and  $\epsilon_r''$  are outside the spread in values for the nominally ideal samples and therefore are resolvable from them. Furthermore, these results are also outside the ranges for the incompletely cured samples and so are resolvable from these, too.

The ultra-sound image of sample 12, Figure 5-2, indicated that it had no defects. Even after the impact damage was inflicted the impact site was barely visible on the ultra-sound image. From a visual inspection of sample 12 a star shaped delamination was easily seen to extend 5mm left and right of the impact centre. The damage suffered by sample 12 appears to be considerably less than that of sample 5 for the same impact on the same material; indeed there is noticeably less shape distortion. No permittivity

solution was found when the MMW measurement was aligned with the centre of the impact site. One may conjecture that the MMW energy is scattered from the fracture even though no foreign material is present, in the same way that light is scattered from crazed glass. However, perfectly reasonable results were obtained, which were consistent with the undamaged material, when the measurement was displaced by as little as 10mm either side of the impact centre. One might reasonably expect that the -3dB contour of the beam footprint on the sample (circle diameter 40mm) would set the limit of spatial resolution but that large defects marginally outside this range may still be visible to the measurement whilst minor defects within this range may not. The latter situation would appear to be the case here.

A useful indication of the ability to resolve the differing fault categories of samples #1 to #11 can be gained from the grouping of their permittivity results in the complex permittivity plane, as in Figure 5-4, below.

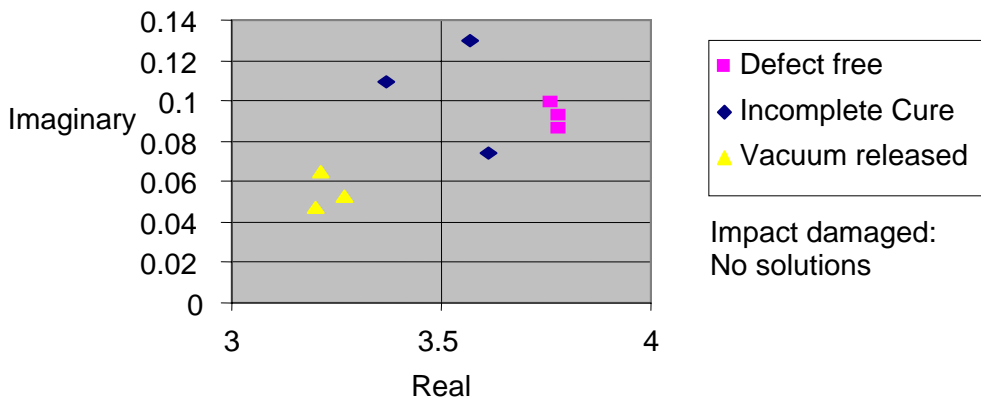


Figure 5-4: Summary of Permittivities of Samples #1 to #11

The ranges of the real and imaginary parts of the permittivities of cross-ply samples #13 to #18 overlap and so the samples in which the vacuum was released early during the cure cycle are not resolvable from the nominally defect free samples. An examination of the ultra-sound images of these samples indicates that samples #16 to #18 (early vacuum release) have not incurred the level of defects that this treatment inflicted on the woven samples #9 to #11. Relatively few defects, coloured blue in Figure 5-1, are

present in samples #16 to #18 and, consequently, their permittivity is little changed from the defect free samples.

### 5.5.2 Experimental Tolerances and Repeatability (Samples #1 to #18)

Errors arise due to the accuracy with which the calibration is maintained, variations in sample orientation, experimental repeatability, noise modulations of the VNA results and the consistency of the sample thickness together with the accuracy to which it can be measured. However, it is not possible to anticipate what effects these error sources have on the solutions for sample permittivity due to the iterative search technique employed. The tolerance on the transmission coefficient can be significant for low-loss materials. This method is best suited to the measurement of lossy samples and has difficulty in accurately determining  $\varepsilon_r^{\parallel}$  of low loss materials. Repeated processing of the data for extremes of all error sources suggest a maximum variation of around  $\pm 4\%$  in  $\varepsilon_r'$  and  $\pm 25\%$  in  $\varepsilon_r^{\parallel}$  for the composite samples. The repeated measurements on sample 12 suggest average variations in  $\varepsilon_r'$  of  $\pm 1.0\%$  and in  $\varepsilon_r^{\parallel}$  of  $\pm 13\%$ .

The fibres in the samples run in two orthogonal axes (the warp and weft of the woven samples and the perpendicular layer orientation of successive layers in the cross-ply samples). All the results quoted here were based on measurements conducted for the same sample orientation i.e. such that the fibres ran parallel and perpendicular to the plane of polarisation. The variability in solutions due to other random sample orientations was  $< \pm 0.3\%$  in  $\varepsilon_r'$  and  $\sim \pm 12\%$  in  $\varepsilon_r^{\parallel}$ .

### 5.5.3 Three-Layered Structure

The simulation has been run for values of  $t_2 = 1.60, 1.54, 1.66$  and  $1.56$  mm and the transmission and reflection coefficients have been plotted in Figure 5-5 . The plots in Figure 5-5 also have the measured data superimposed on them plotted in the red '+' symbols. It is evident from Figure 5-5 that the multiple reflections beat in and out of phase and result in a series of transmission and reflection peaks and troughs. It can be seen from the plots how the peak and trough frequencies are a function of the width of the air gap ( $= t_2$ ). Shifting these peak and trough frequencies can have a significant effect on the values of transmission and reflection coefficients at any frequency. The (a) lines relates to the nominal value of  $t_2$  whereas lines (b) and (c) allow for the tolerance on  $t_2$ . Line (d) relates to a value of  $t_2 = 1.56$ mm, which gives the closest match to the measured data.

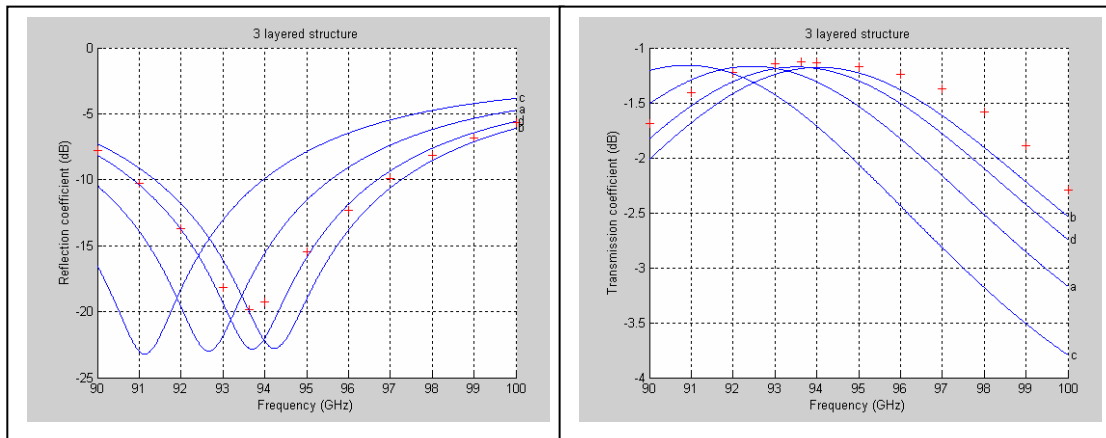


Figure 5-5: Measured (+) and Simulated Transmission and Reflection Coefficients (solid lines) of Three Layered Structure  
(a):  $t_2 = 1.60$ mm, (b):  $t_2 = 1.54$ mm, (c):  $t_2 = 1.66$ mm and (d):  $t_2 = 1.56$ mm

It may be noticed from Figure 5-5 that the measured transmission peak and reflection trough are slightly broader than the simulated profiles. This is attributed to the fact that the structure was slightly domed i.e. the thickness of the air gap,  $t_2$ , reduced slightly with distance from the centre (but within the tolerances quoted here).

### 5.5.4 Error Analysis (Three Layered Structure)

The tolerance on the thickness of the composite layers  $t_1$  and  $t_3$  is  $\pm 0.01\text{mm}$  and that of the air gap  $t_2$  is  $\pm 0.06\text{mm}$ . The experimental tolerance in determining the complex permittivities of the composite layers is that  $\varepsilon_{r1}$  varies from  $3.90 - j0.073$  to  $3.65 - j0.092$  and  $\varepsilon_{r3}$  varies from  $3.90 - j0.079$  to  $3.65 - j0.099$ . The most significant variation in the transmission and reflection coefficients is caused by the shift in the frequencies of the transmission coefficient peak and reflection coefficient trough encountered at extremes of these tolerances. The minimum peak/trough frequency is obtained for maximum thicknesses of all layers and maximum real parts of the permittivities and the maximum peak/trough frequency is obtained for the opposite extremes. There is a less significant effect on the general uplifting or depression of the coefficients at extremes of tolerances. Figure 5-6 shows plots of the simulated data for nominal thicknesses and permittivities and also for the combinations giving rise to maximum and minimum peak and trough frequencies. The transmission coefficient is measured to a tolerance of  $\pm 0.05\text{dB}$  and the reflection coefficient to a tolerance of  $\pm 0.36\text{dB}$ . The measured data together with upper and lower limits corresponding to these tolerances is also plotted (+) in Figure 5-6 and are seen to lie within the range of the modelled data when the experimental tolerances are applied.

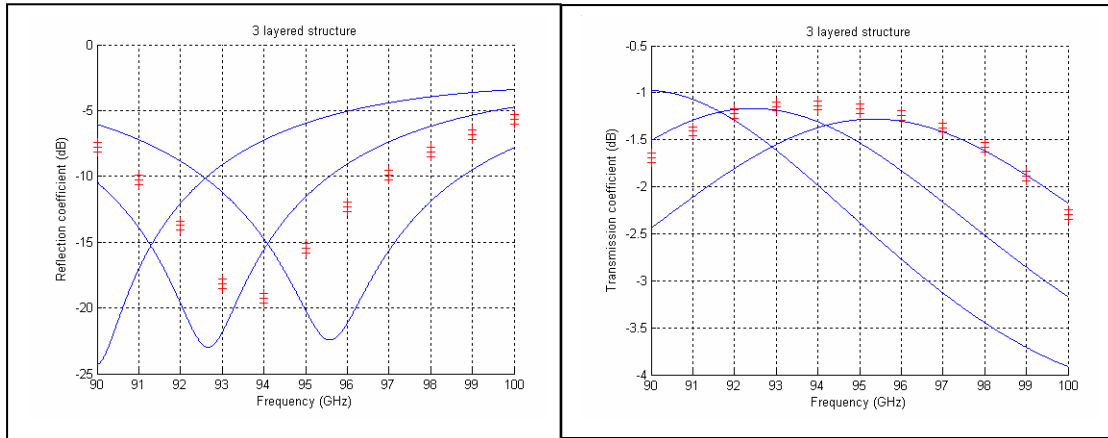


Figure 5-6: Measured (red +) and Simulated Data (blue solid lines) for Nominal Values and Extremes of Tolerances for the Three Layered Structure

### 5.5.5 Sensitivity Analysis of Three Layered Structure

The sensitivity of the simulated data to variations in the input parameters can best be illustrated by the change in frequency of the peaks and troughs and also by the change in levels at the peak and trough frequencies i.e. where the gradient is zero. The effects on these parameters as a result of perturbing the input variables used in the three layered model validation are summarised in Table 5-4, below.

Change in input parameter	Changes in output data			
	Transmission Peak		Reflection Trough	
	Frequency (%)	Level (% of dB)	Frequency (%)	Level (% of dB)
$t_2 \pm 3.75\%$	-1.69/+1.74	-0.77/+0.86	-1.64/+1.71	+1.04/-0.91
$t_2 \pm 7.5\%$	-3.31/+3.54	-1.54/+1.71	-3.24/+3.45	+2.17/-1.70
$t_1, t_3 \pm 0.8\%$	$\pm 0.42$	$\pm 0.17$	$\pm 0.43$	$\pm 0.86$
$t_1, t_3 \pm 1.6\%$	$\pm 0.86$	$+0.39/-0.26$	$\pm 0.88$	$+1.78/-1.65$
$\epsilon_{r1} = 3.78 (\pm 3.2\%) - j0.086 (\pm 38\%)$	+0.45/-0.39	+15.8/-17.1	+0.51/-0.45	+13.9/-7.7
$\epsilon_{r1} = \epsilon_{r3} = 3.78 (\pm 3.2\%) - j0.086 (\pm 38\%)$	+0.92/-0.79	+32.5/-35.7	+0.97/-0.86	+15.8/-9.6

Table 5-4: Sensitivity Analysis of Modelled Results on Three Layered Structure

The data of Table 5-4 indicates small percentage changes resulting from perturbations in the layer thicknesses. This amounts to small changes in the absolute values of the levels, due to their modest levels when expressed in dB, but very significant shifts in the peak/trough frequencies due to the use of high millimetric wave frequencies. This would become significantly lower at lower frequency bands. The large tolerance on the imaginary part of the permittivity of layers one and three has resulted in

correspondingly large variations in the peak/trough levels, especially that of the transmission coefficient peak. Applying the same tolerance to two dielectric layers has approximately doubled the variations in peak/trough frequency and transmission peak level, however, the reflection trough level is largely unchanged.

### 5.5.6 Modelled Three Layer vs. Modelled Single Layer

The modelled results of the three layered structure using nominal parameter values and the modelled results of a single layer of solid dielectric are presented in Figure 5-7.

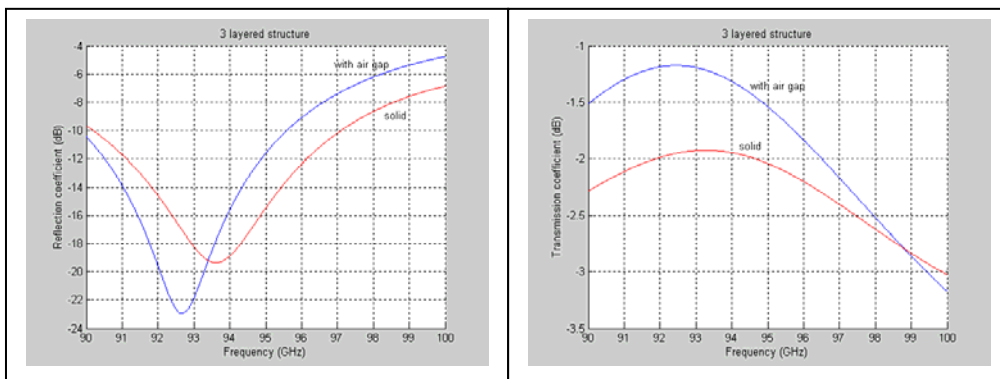


Figure 5-7: Modelled Reflection (Left) and Transmission (Right) Coefficients of Dielectric Structures

*(Blue = with air gap. Red = without air gap)*

The presence of the air gap has resulted in only slight differences in the transmission and reflection coefficients. Both the reflection troughs and transmission peaks have a higher Q-factor in the case of the structure with the air gap, which is to be expected since the air dielectric is less lossy than the composite. The solid composite sample has a reflection trough level some 3.6dB (17.7%) above that of the “with air gap” structure and a reflection trough frequency 0.9GHz (0.97%) higher than the “with air gap” structure. The solid composite also has a transmission peak level some 0.7dB (58.3%) below that of the “with air gap” structure and a transmission peak frequency 0.8GHz (0.86%) higher than the “with air gap” structure. From the sensitivity analysis of section 5.5.5 it can be seen that the changes in the peak and trough frequencies could result

from small variations in layer thicknesses of the three layered structure which are within the measured tolerances. The differences in peak and trough levels are outside the range of measured tolerances. Again, from the sensitivity analysis (section 5.5.5) it can be seen that the changes in the reflection trough level could result from the measured tolerance in the layer permittivities. However, the change in the transmission peak level of 0.7dB is outside the range resulting from experimental errors, but nevertheless is a small level change. In conclusion, the transmission and reflection coefficients of the solid dielectric and that including the air gap differ by such small amounts as to be within the experimental tolerances of the three layered “with air gap” structure. The transmission peak level is an exception to this and there is a small but resolvable difference which may be the basis of differentiating the two structures. It is anticipated that a middle layer having a greater dielectric contrast with the outer layers would accentuate the difference and be more readily resolved. One is forced to accept that whilst composite samples having a large void content may be resolved from nominally defect free material the presence of a substantial air gap is barely discernible using this method.

The above analysis shows that the measured transmission and reflection coefficients of a three layered structure are remarkably insensitive to the permittivity of the middle layer, assuming all three layers have comparable thicknesses. If this problem is reversed one may measure the transmission and reflection coefficient of a three layered structure (e.g. a sample within a container) to find the permittivity of the middle layer, assuming all thicknesses and the permittivity of the outer layers are all known. This was the basis of the experimental work of Ma and Okamura <sup>[78]</sup>. However, small errors in the measured transmission and reflection coefficients result in large errors in the permittivity of the middle layer. This may be mitigated somewhat by ensuring that the middle layer is much thicker than the two outer layers.

## 5.6 CHAPTER SUMMARY

This chapter has considered the feasibility of the free space measurement of permittivity in the band 90 to 100GHz to detect and locate defects within two types of fibreglass based composites. A number of Fibredux 916G woven samples were manufactured; some being nominally defect free and others having defects arising from incomplete cure, early vacuum release and low level impacts. The extent of defects was determined by ultra-sound testing. Those incompletely cured and those having the early vacuum release incurred large void content whereas the impact damaged samples suffered a star shaped delamination with the peak extents of the delamination in the reinforcing fibre orientations. The permittivity of samples in each fault category was resolvable from the others. A single large sample of Fibredux 916G was manufactured and its permittivity was mapped. This indicated a consistent permittivity across its surface. A low-level impact inflicted on this sample was barely discernible from the ultra-sound test but was easily resolvable from undamaged material using the permittivity test with a spatial resolution of < 10mm.

Similar test have been conducted on samples of Fibredux 913G cross-ply samples. One set of samples was subjected to the early vacuum release but the ultra-sound tests indicated the presence of minor defects only. The permittivity of these samples was not resolvable from the nominally defect free samples.

The three layered dielectric model was then used to model a composite with a large air gap within it. There was good agreement between measured and modelled results. However, the modelled results of the structure with the air gap do not differ appreciably from modelled results of an equivalent structure without the air gap and it is marginal as to whether it would be possible to resolve these two cases in practice due to measurement tolerances.

The free space method to measure the permittivity of a sample within a container is briefly considered. Accurate determination of the sample permittivity requires highly accurate transmission and reflection data.

THIS PAGE INTENTIONALLY LEFT BLANK

## CHAPTER SIX: CONCLUSIONS

This Chapter summarises the conclusions arising from the earlier Chapters. It also includes a section on the future possibilities arising from this work.

### 6.1 CONCLUSIONS ARISING FROM CHAPTER ONE

The reviews of Chapter One highlighted several key issues and problems which have become the themes addressed by this thesis. The first of these concerns the very sparse dielectric data on human tissues in the MMW band. Common wisdom suggests that the dielectric behaviour of tissues in this region is determined by their water content. The MMW band is above the frequencies of the relaxation frequencies of polar materials and below the frequencies of the absorption spectra. As a result the dielectric properties are expected to exhibit a gradual reduction of  $\epsilon'$  and an increase in  $\sigma$  with increasing frequency, in keeping with the Kramers-Kronig relations. The MMW band is of growing importance due to the increased communications and sensor applications exploiting it. The lack of data on tissues is largely due to the difficulties with their measurement. Several medical, safety, sensor and communications applications are currently driving the demand for dielectric data on tissues, particularly, human skin, in the MMW band. Recently, some permittivity data in the MMW band on human tissues, particularly skin, has been published. Often this data has been inconsistent. It has also revealed how the permittivity of thick, horny skin (e.g. from the palm or sole) is lower than that of other sites. The accuracy of previously published data on human skin in the MMW band is questioned since:

- (a) coaxial probe methods were used which are notoriously difficult to calibrate in the MMW band,
- (b) the skin at certain measurement sites is not representative of skin elsewhere on the human body,

- (c) the tissue depth (hence type and moisture content) which couples to the measurement varies with frequency and
- (d) the measured data is often inconsistent with the trends expected from relaxation phenomena.

The second issue concerning biological tissues is that differences may exist between tissues *in vivo* and *ex vivo*. Such differences may be expected due to the differing water (and blood) content of tissues when excised. Cellular changes after tissue excision will affect the dielectric properties below the microwave band but the retention of tissue water content should preserve the correct MMW dielectric characteristics.

Thirdly, the spread of relaxation processes applicable to tissues in the microwave and MMW bands is not entirely clear. The highest relaxation frequency expected is that of the tissue bulk ‘free’ water which is centred at about 25GHz. At frequencies well above this i.e. the MMW band, one would expect tissue characteristics to be described by a single Debye term. Yet in spite of this, several models have been advanced, some of which are not founded on, or limited to, the physical processes known to exist. Many of these functions are Debye-like and are often parameterised to fit measured data, usually made at lower frequencies. In the past, measured data has failed to resolve the issue since it is corrupted by tolerances and permits several models to be accommodated. Furthermore, tissues exhibit a high degree of natural variation. Whilst no specification on the measurement tolerance of the permittivity of human tissues in the MMW band appears to have been defined, it is suggested here that a tolerance of  $\pm 10\%$  should be considered desirable but that a tolerance of  $\pm 20\%$  would be of value.

The fourth key issue concerns the measurement of complex permittivity of lossy planar materials, e.g. skin, in the MMW band. Various candidate techniques were considered. Techniques commonly used to measure the permittivity in the microwave band do not scale conveniently to the MMW band. Some are not suitable for the measurement of tissue, either because of its physical characteristics or its high losses. Waveguide and free-space techniques were considered to be the two most viable methods.

Finally, there is growing interest in the feasibility of RF signals, particularly in the MMW band, to detect defects and monitor the cure state of composites. This is brought about by the concern that lightweight composite materials may contain defects which would undermine their strength. The free-space method of permittivity measurement in the MMW band appears attractive since it offers a non-contacting, non-invasive method of defect detection whilst achieving reasonable spatial resolution.

One of the main challenges identified from the problems associated with both human tissues and defect detection in composites is the ability to measure the permittivity of a planar material well into the MMW band. The primary motivation of this thesis is the acquisition of dielectric data on human tissues in the MMW band and subsequently the determination of power deposition in the human body (or at least its skin) exposed to MMW energy. The defect detection in composites is a useful spin-off of the experimental method developed for the tissue characterisation.

## 6.2 CONCLUSIONS ARISING FROM CHAPTER TWO

An algorithm for modelling the transmission and reflection coefficients of a generalised structure of planar dielectrics has been presented. The model assumes that the dielectric structure is illuminated by a plane wave at normal incidence. This model is based on signal flow techniques and computes the transmission and reflection coefficients as functions of frequency, layer thicknesses and layer permittivities and considers the infinite multiple reflections occurring at dielectric interfaces. This method of analysis employs an algorithm which reduces the signal coefficients of two neighbouring layers into those of an equivalent single layer. Successive applications of the layer reduction technique ultimately reduce the structure to a single layer. Whilst alternative models to perform this function have been published, the author is not aware of any previous models based on signal flow methods. The model presented here is therefore, to the best of the author's knowledge, original. Signal flow methods are useful tools supporting ray tracing methods of propagation and are also more closely associated with the optical techniques used in the MMW band. The algorithm could also be extended to consider

any general angle of incidence which, in turn, paves the way for further applications of the analytical method. The model described in Chapter Two therefore has several important advantages over the alternative methods.

The general model has been coded to solve the specific case of three dielectric layers. This, in turn, has been verified against previously published data by replicating precisely the previously published results for a simplified three-layer structure. It has also been shown that the three layer case is consistent with the single dielectric layer case as any two layers become infinitely thin or their permittivities approach that of free-space. This model has been developed to support the work on defect detection in composites but has a number of other potential applications.

### 6.3 CONCLUSIONS ARISING FROM CHAPTER THREE

Waveguide and free-space techniques were considered to be the most suitable methods of permittivity measurement in the MMW band over wide bandwidths on lossy planar materials. A free-space method based on the measurement of the amplitudes of reflection and transmission coefficient was selected for the present work. This technique was preferred for the following reasons:

- Free-space methods are non-contacting, which is desirable for the application of defect detection in composites.
- Free-space methods scale conveniently to the MMW band. The experiment can easily be accommodated on an optical bench just under a metre in length. Whilst waveguide techniques would also be compact, waveguide dimensions and hence sample sizes reduce to very small proportions.
- Waveguide methods pose problems associated with the preparation of small samples sizes and their fit within a waveguide (or terminating a waveguide), whereas free-space techniques pose problems associated with diffraction around finite sized samples. Of these two sets of problems, those associated with free-space techniques were thought to be the easiest to overcome. This requires large

samples sizes and could limit the lowest frequency at which free-space methods would be feasible.

- The requirement for large sample sizes (diameter = 105mm at 60GHz) results in a loss of spatial resolution, which is undesirable for the detection and location of defects in composites but is desirable for tissues due to the spatial averaging it affords.
- The ‘amplitudes only’ measurement is acknowledged as being less accurate than alternative methods requiring the measurement of amplitude and phase. Nevertheless, its relative simplicity was appealing and the necessity for high accuracy was questionable since samples were expected to exhibit a high degree of natural variation. The accurate determination of phase requires the MMW frequency source to be phase stable over the duration of the calibration and measurement and also demands that samples be mounted with a high degree of mechanical precision. The relaxation of these requirements may actually minimise experimental tolerances.

The experimental set-up of a VNA connected to a pair of standard gain waveguide horns either side of a sample frame has been described. The sample frame must be placed just beyond the far field threshold of each horn. The sample frame has been designed to accommodate a sample sufficiently large as to intercept twice the -3dB beamwidth from each horn at the lowest measurement frequency; this accommodates the first seven Fresnel zones at 60GHz. The same frame has been used at higher frequencies and therefore appears to be electrically larger. The horns and sample frame have been accurately aligned, although in practice the measured coefficients are not very sensitive to small alignment errors. The VNA must be operated in a time gated mode so as to exclude multiple reflections between the horns and/or sample.

The transmitted and reflected signals from the sample are comprised of an infinite series of components arising from multiple reflections between the sample/air interfaces. The signal flow methods from Chapter Two have been used to relate these coefficients to the sample permittivity. Measured data is processed to identify permittivity solutions which result in a best fit of computed data to measured data. This processing stage performs an

exhaustive trial for complex permittivity values over a user defined search space and resolution. In some cases, more than one complex permittivity solution may be identified. This ambiguity may be resolved from an initial estimate based on the transmission and reflection peak/trough frequencies or by fitting data at several frequency points. Experience has shown that eliminating ambiguities by one or other of these methods is relatively simple. The experimental and data processing methods have been verified at J-band against standard materials. It was also noted that this method cannot identify the imaginary part of the permittivity of very low-loss dielectrics reliably. This arises due to the limited accuracy with which very low transmission coefficients may be measured. However, the method was able to give reliable results on moderately lossy materials which were in close agreement with previously published data.

Previously published papers describing work based on this measurement technique have been limited to highly lossy materials in which the analysis is simplified to omit the multiple reflections between the sample/air interfaces. This simplification also significantly reduces the problem of ambiguous solutions. However, the present study has indicated that such simplifying assumptions are not necessary and that the technique has a wider range of application (i.e. to moderately lossy samples). It is therefore concluded that the experimental and processing methods selected and developed here are suitable for the measurement of the permittivity of skin tissue and composite materials in the MMW band.

A number of potential error sources were identified but their effects on the permittivity solutions declared by the searching technique used is impossible to anticipate.

During the course of this work, it has also come to the author's attention that no standard dielectric materials are defined in the MMW band. A range of stable and highly repeatable low, medium and high loss dielectrics of both solid and liquid form should be defined at least to 100GHz to support the growing interest in the MMW band.

#### 6.4 CONCLUSIONS ARISING FROM CHAPTER FOUR

Several applications have previously been identified which require knowledge of the permittivity of human skin in the MMW band. Due to the lack of measured data, the permittivity of skin at MMW frequencies has often been predicted from models based on the relaxation phenomena of water and wet dielectrics. Measured data is required to establish the correct model and model parameters and to support work of the applications identified in Chapter One, section 1.4.

It is widely acknowledged that the dielectric behaviour of skin in the MMW band is determined by its water content. This is characterised by a single relaxation Debye model. A review of measured and modelled data for water through the MMW band has been conducted and has established appropriate model parameters and temperature gradients. This has been applied to predict the permittivity of water at 60, 77 and 94GHz at room temperature ( $20^{\circ}\text{C}$ ) and human body temperature ( $37^{\circ}\text{C}$ ). However, the predicted data is subject to considerable tolerances due to the wide variety of data reported in the literature.

A great variety of models and model parameters have been published and applied in the modelling of the permittivity of human skin in the MMW band. These include single and double relaxation frequency Debye models and four term Cole-Cole functions. The single relaxation frequency Debye model has the appeal that it is based on the relaxation frequency of water, whereas some of the other models have been concocted to fit measured data and do not attempt to model the physical processes involved. An attempt has been made to predict the permittivity of human skin based on a single relaxation Debye equation using parameters gleaned from the earlier study on water and other models published in the literature. The modelled data is compared with that of the other models previously published. No two models provide consistent data; even single relaxation frequency Debye models differing in model parameters yield a wide variation in data. The data of some models differs by a factor of between 1.8 and 2.9 from the data of others. There is even some evidence to suggest that a single relaxation frequency Debye model cannot be applied to human skin. This lack of agreement is due to the fact

that skin exhibits a high degree of natural variation. Skin from the palm of the hand (and, possibly the sole of the foot) has a significantly lower permittivity than skin from other sites. Palm skin lacks hair cells and is thicker and hornier than skin from other sites and, dielectrically, behaves as if it is drier. Whilst very little experimental data has been published, much of what has pertains to the palm and is not representative of skin at other sites. It is clear that the dielectric properties of human skin in the MMW band are functions of epidermal thickness and water content. The accuracy of previously published data on human skin in the MMW band has already been questioned in section 6.1.

The permittivity of a single sample of human skin has been measured at frequencies from 57 to 100GHz using the free-space method described in Chapter Three. The preparation and testing protocol on the skin sample, previously fixed in formaldehyde, has been described and the results presented. This included thirty repeated tests in the 57- 60GHz band, plus additional data between 76 to 100GHz. The experimental errors and repeatability have been discussed and quantified in each case. The measured results indicate general trends of a gradual reduction in  $\epsilon'_r$  and  $\epsilon''_r$  with increasing frequency (as is to be expected) but fail to show a consistent increase in  $\sigma$  with increasing frequency. This may be due to tissue variations, particularly the drying, on the day of the measurements since the measurements made at 76 to 100GHz were conducted in a hot lab during the summer whereas the tests at 57 to 63GHz were made in cooler conditions during the winter. The consistency of the 57 to 63GHz data over the thirty repeated tests engenders a high degree of confidence in these results. It is worth noting that previously published data for human skin also shows inconsistencies with the trends expected from relaxation phenomena.

The effects of the fixing process in formaldehyde were ascertained from tests on a fresh and fixed porcine skin sample at 60GHz. These indicated that the “fresh” skin value of  $\epsilon'_r$  is 0.954 times that of the “fixed” skin value, whereas the “fresh” skin value of  $\epsilon''_r$  is 1.72 times that of the “fixed” skin value. The reduction in the imaginary part of the permittivity for the fixed tissue is consistent with the notion that the formaldehyde displaces water from the tissue. The changes in fresh/fixed porcine skin permittivity

observed at 60GHz have been applied to the permittivity results for the human skin at all frequencies of measurement. The measured human skin permittivity results have been corrected to unfixed values at body temperature ( $37^0\text{C}$ ) using the same temperature gradients previously identified for water in the MMW band. This corrected data is in reasonable agreement with previously published data for skin on the elbow and back of the hand at 40GHz. It is believed that the results corrected to unfixed skin at  $37^0\text{C}$  are fairly representative of fresh skin and differ from skin *in vivo* only in marginal variations in water content. The total experimental errors are approximately  $\pm 18\%$  for the fixed skin at ambient temperatures and approximately  $\pm 24\%$  for the corrected fresh skin at  $37^0\text{C}$  across the whole measurement band. These tolerances are close to the value of  $\pm 20\%$  identified in section 1.4.1 as being of value to the scientific community. The measured results presented in Chapter Four and their corrections to fresh skin values at  $37^0\text{C}$  represent a significant extension to the database on the dielectric properties of human tissues in the MMW band.

The measured skin permittivity data has been used to determine the parameters a Cole-Cole function. The model parameterisation settled on a single relaxation frequency Debye function, even though it was at liberty to parameterise a more complex Cole-Cole function. The best fit model parameters have resulted in a model in which the rms percentage error between modelled and measured permittivity is approximately 21%. The model parameters identified for the unfixed, body temperature permittivity values of human skin were typically within the ranges of previously published model parameters for human skin *in vivo*. It is concluded that whilst a single relaxation frequency Debye function does not provide a perfect fit to measured data, nevertheless, it does provide the best fit. It is conjectured that the rather poor fit of experimental results to the Debye function (both in this study and previously published data in the literature) arises from differing dielectric properties of the three discrete layers of skin; the epidermis, dermis and subcutaneous layers. The work of Chapter Five concludes that the transmission and reflection coefficients from three dielectric layers are very insensitive to the dielectric contrast between the permittivity of the middle layer and that of the outer layers. Therefore, the measured coefficients vary only slightly (perhaps within experimental errors) for considerable variations in the permittivity of the middle

layer. Such variations may account for the discrepancies from a single Debye function and yet may not yield resolvable differences in the measured transmission and reflection coefficients. It may yet be possible to describe each layer of human skin with its own unique Debye function if each layer could be measured in isolation of the others, however, the fit of all three layers, in combination, to one Debye function remains a poor one.

Finally, the permittivity results of the skin (unfixed at body temperature) were used to calculate the heat deposition and model the surface temperature rise in skin exposed MMW signals at frequencies of 60, 77 and 94GHz at a power density of  $100\text{W/m}^2$ , the NRPB basic restriction. This found that there was at most a  $0.2\text{ }^\circ\text{C}$  rise after a thirty second exposure and so it is concluded that the current restrictions are sufficient to avoid heat pain and skin burns.

## 6.5 CONCLUSIONS ARISING FROM CHAPTER FIVE

Chapter Five addressed the problem of the detection and location of defects within composite materials in a non-contacting, non-destructive manner. It considered the feasibility of the method of permittivity measurement by the free-space technique, supported by the modelling of multi-layered dielectrics, to solve this problem. Practical tests on composite samples and modelled responses carried out over the frequency band 90 to 100 GHz were used. The key issues that this work sought to explore were:

- Do defective samples have permittivity values which are resolvable from nominally defect free materials?
- If so, can the free space technique reliably identify them?
- Are some defects more easily resolvable from others?
- What spatial resolution of defect detection can be achieved in this band?
- Can the transmission and reflection properties of planar layered composite structures be simulated by the multi-layered dielectrics model?

These questions are answered by the following conclusions.

The complex permittivity of various composite samples has been determined in the 90 to 100GHz band using the free space measurement of the amplitudes of transmission and reflection coefficient. It has then been applied to map the permittivity variation of a 500mm by 250mm sheet of 10 layer woven Fibredux 916G composite material. The variation in permittivity across the sheet was found to be  $\epsilon_r' = 3.77 \pm 2.1\%$  and  $\epsilon_r'' = 0.099 \pm 21\%$ . This composite material has reasonably consistent dielectric properties both on a sample by sample basis and within any given sample. There are resolvable differences in the permittivity between samples of the Fibredux 916G which are nominally ideal compared with those damaged by impact, incompletely cured samples and those for which the vacuum was released during cure; each category being resolvable from the others. The measurement of the permittivity of this material can therefore be used not only as a means of detecting defects but also of determining the nature of the defect. The measurement of permittivity can find no solution for the impact damaged samples which clearly differentiates them from nominally ideal samples. The inability to find a solution is thought to arise from the shape distortion of the impact and the presence of a fracture within the material. The measurement method was successful in identifying the impact damage in sample #12, where shape distortion was minimal, even though the defect was barely visible on an ultra-sound image. The MMW technique described here is therefore more sensitive to this form of damage than the ultra-sound imaging technique. The resolution between the nominally ideal samples and those incompletely cured is based on small differences in the real part of their permittivity only. The differences are on the resolvable limit when experimental repeatability is taken into consideration. Nevertheless, an accurate measurement of permittivity has the potential to monitor the state of cure of a composite material. There are, however, clear differences in both real and imaginary parts of the permittivity between those samples in which the vacuum was released during cure and all other samples. The lower values of both real and imaginary parts of their permittivity are consistent with the large void content of these samples.

The spatial resolution of the measurement technique is dependent on the severity of the fault. The spatial resolution of the MMW beam on the sample was 20mm in this experiment (i.e. a circle of diameter = 40mm) and this should dictate the resolution of the measurement. However, the impact damaged area of sample #12 could not be resolved from the undamaged material until the equipment was aligned to within 10mm of the impact centre, suggesting a resolution of less than 10mm.

The results of cross-ply composite samples #13 to #18 are inconclusive. The influence of the small areas of defect in samples #16 to #18 is too insignificant to be resolved from the natural material variations and experimental tolerances. The early vacuum release has failed to incur the large void content that this treatment inflicted on the woven samples. As a result, the permittivity of these samples is not resolvable from the nominally ideal ones.

A model based on signal flow methods for simulating the transmission and reflection coefficients from a general structure of any number of planar dielectric layers of arbitrary thicknesses has been applied in the analysis of a three layered structure of dielectrics. A structure comprising two outer layers of composite material with an air gap in between has been modelled and measured. This structure mimics a large void defect within an otherwise solid composite. An error analysis and sensitivity analysis of the model has been carried out using values of the tolerances applicable to the experimental work. This confirms that the modelled and simulated data agree with each other to within the limits of experimental tolerances. It has been observed that the transmission and reflection coefficients undergo a cyclical variation with frequency characterised by peaks and troughs. The most significant factor in determining the transmission and reflection coefficients is the manner in which the peak and trough frequencies are sensitive to the thicknesses of each dielectric layer. Low-loss materials result in low transmission coefficients which may only be measured with a large percentage error.

Additionally, the modelled results of the three layered composite structure containing an air gap have been compared with modelled results from an equivalent solid composite

having no air gap. This has shown that the transmission and reflection coefficients of the two structures differ only marginally from each other. The sensitivity analysis of the three layer model suggests that most of the experimental tolerances associated with the measurement of the three layered structure fall within the range of the results expected from the single dielectric layer. One measurement parameter (the transmission peak level) may just be capable of providing the resolution between the two dielectric structures. However, whilst composite samples having a large void content may be resolved from nominally defect free material, one is forced to conclude that the presence of a substantial air gap is barely discernible using this method.

The transmission and reflection coefficients of a three layered structure such as a sample material between two container layers is insensitive to the permittivity of the middle (sample) layer. When the problem is inverted, it provides a means of deducing the permittivity of the middle sample layer from measurement of the transmission and reflection coefficients and layer thicknesses together with knowledge of the permittivity of the outer container layers. Small errors in the transmission and reflection coefficients result in large errors in the permittivity solutions for the sample, especially when there is low dielectric contrast between the container and sample materials.

With regard to the questions forming the key issues:

- Yes, the permittivity of defective composites does differ from that of defect free material.
- Yes, the free space method can identify most of these defects reliably, as shown by the consistency of results on three samples in each fault category.
- Yes, some defects can more readily be resolved from others. The scattering of signals from impact damaged areas make these easy to detect and locate. The differing permittivity of defective samples enables the faults to be detected and resolved from each other. Large air voids are not easily detected using this method.
- A spatial resolution of 20mm or lower (circle of radius = 20mm) is achievable. 10mm resolution of low level impact damage has been demonstrated. This

damage was barely visible from conventional ultra-sound based non-destructive testing techniques.

- Yes, the transmission and reflection properties of planar layered composite structures can be simulated by the multi-layered dielectrics model. Measured data is within the experimental tolerance of simulated data.

The two most significant conclusions from this work are that (i) the method described here is very capable of detecting minor impact damage with fine spatial resolution and (ii) its ability to detect and resolve defects is limited by the tolerance of the measurement. It is in these areas that the most significant contributions towards novel work reside.

## 6.6 FUTURE POSSIBILITIES

The work described in this thesis has enormous potential for further research. Future research possibilities may be exploited in all aspects of the work described in this thesis i.e. the experimental methods developed here, the continuation of the investigation of the dielectric properties of tissues and the detection of defects in composites. During the course of conducting this work, the author has gained experience in making measurements of permittivity by three different methods: the free-space method, a coaxial probe and the perturbation of a resonant cavity. Each method is best suited to particular types of dielectrics and frequency ranges and the author feels that he has acquired a large repertoire of measurement and analytical capabilities.

The author is currently exploring further research opportunities in the following areas:

**Water contamination of aviation fuels.** Work has been proposed in collaboration with colleagues at Cranfield University, Shrivenham to investigate whether it is feasible to determine the concentration of water contaminating aviation fuel using a dielectric spectroscopy method. Currently, the measurement of water contamination is only feasible in samples taken to a specialist laboratory and does not use an RF method. It is

proposed to use the coaxial probe method to measure the permittivity of a fuel sample across a bandwidth encompassing the relaxation frequency of water. The aviation industry eagerly seeks a method that could be easily used on the aircraft.

**Defect detection in composites.** A continuation of the work described in Chapter Five has been proposed in collaboration with colleagues at Cranfield University, Shrivenham and UMIST. Future work would seek to establish the feasibility of the present method in other composite materials and further refine the characterisation of defects. It is further proposed to use these measurement techniques to monitor the curing of composite materials.

The two areas of future research proposed above have recently enabled Cranfield University to secure funding to upgrade their VNA facilities (currently limited to 65GHz) to cover the band up to 110GHz. Once upgraded, it will enable repeated measurements on the human skin sample to 110GHz. Future work in this area would seek to refine the measurement accuracy and enable more accurate models/model parameters to be established (see section 4.4). Similarly, other tissues may be characterised. The author also hopes to develop a method of making the measurements on tissues *in vivo*, probably using a waveguide technique.

Other future possibilities resulting from the work of this thesis include:

- The use of the theory on multi-layered dielectrics to optimise the design of wide band stealthy coatings, particularly in the MMW band.
- The use of the theory on multi-layered dielectrics for the design of MMW band frequency selective surfaces.
- The use of dielectric measurements in the MMW band to verify food processing and control. The author has been contacted by Prof. Meriakri, of the Institute of Radio Engineering and Electronics Russian Academy of Sciences (IRE RAS), Moscow, concerning possible future work in this area.
- Applying the dielectric measurements to the monitoring of the drying of materials<sup>[128][129]</sup> e.g. timber and paper.

- The validation of equipment designed to measure the dielectric characteristics of soil for remote sensing and surveying purposes. This is currently under consideration with a colleague whose interests are in remote sensing.
- The author would like to address his own conclusion (section 6.3) to establish a range of standard dielectric reference materials for use in the MMW band.

It is clear that the current work is capable of spawning several future research opportunities.

**REFERENCES**

- 1 WILLIAMS, G and THOMAS, D. K.: 'Phenomenological and molecular theories of dielectric and electrical relaxation, Novocontrol Application Note Dielectrics NR3, ©Novocontrol GmbH, 1998
- 2 FOSTER, K. R. and SCHWAN, H. P.: 'Dielectric properties of tissues and biological materials: A critical review', Critical Reviews in Bioengineering, 1989, 17, 1, pp 25 - 104
- 3 GRANT, E.H. and SHACK, R.: 'Complex permittivity measurements at 8.6 mm wavelength over the temperature range 1-60°C', Brit. J. Appl. Phys., 1967, 18, pp. 1807-1814
- 4 RAICU, V, KITUGAWA, N and IRIMAJIRI, A.: 'A quantitative approach to the dielectric properties of skin', Physics in medicine and biology, 2000, 45, 2, pp. L1 - L4
- 5 PETHIG, R.: 'Dielectric properties of body tissues', Clinical physics and physiological measurements, 1987, 8, supplement A, pp. 5 – 12
- 6 PETHIG, R.: 'Dielectric properties of biological materials: biophysical and medical applications', IEEE trans. Electrical Insulation, Oct 1984, E1-19, 5, pp 453 – 474
- 7 STUCHLY, M. A. and STUCHLY, S. S.: Ch. 5: 'Electrical properties of biological substances', 'Biological effects and medical applications of electromagnetic energy' (Editor: O. P. Gandhi), Pub. Prentice-Hall, 1990, pp 75 - 112.
- 8 MARTIN, J, BROQUETAS, A. and JOFRE, L.: 'Dynamic active microwave thermography applied to hyperthermia monitoring', J. Photographic Science, 1991, 39, pp 146 – 148
- 9 PAULSEN, K. D, MOSKOWITZ, M. J. and RYAN, T. P.: 'Temperature field estimation using electrical impedance profiling methods. I. Reconstruction algorithm and simulated results', Int. J. hyperthermia, 1994, 10, 2, pp 209 – 228
- 10 PAKHOMOV, A. G, AKYEL, Y, PAKHAMOVA, O. N, STUCK, B. E. and MURPHY, M. R.: 'Current state and implications of research on biological effects of millimetre waves. A review of the literature', Bioelectromagnetics, 1998, 19, 7, pp 393 – 413
- 11 PAKHOMOV, A. G. and MURPHY, M. R.: 'Low intensity millimeter waves as a novel therapeutic modality', IEEE Trans. Plasma Science, Feb 2000, 28, 1, pp 34 – 39
- 12 GANDHI, O. P.: 'Some basic properties of biological tissues for potential biomedical applications of millimeter waves', J. Microwave Power, 1983, 18, 3, pp 295 – 304

- 13 EDRICH, J. and HARDEE, P. C.: 'Complex permittivity and penetration depth of muscle and fat tissues between 40 and 90GHz', IEEE Trans. MTT, May 1976, MTT-24, pp 273 – 5
- 14 HAGMANN, M. J. and GANDHI, O. P.; 'Substitution method for swept frequency measurements of dielectric properties at microwave frequencies', IEEE Trans. MTT, Jan 1982, MTT-30, 1, pp103 – 106
- 15 GANDHI, O. P, HAGMANN, M. J, HILL, D. W, PARTLOW, L. M. and BUSH, L.: 'Millimeter wave absorption spectra of biological samples', Bioelectromagnetics, 1980, 1, 3, pp285 – 298
- 16 STEEL, M. C, and SHEPPARD, R. J.: 'The dielectric properties of rabbit tissue, pure water and various liquids suitable for tissue phantoms at 35GHz', Phys. Med. Biol, 1988, 33, 4, pp 467 – 472
- 17 TOFIGHI, M. R. and DARYOUSH, A. S.: 'Characterisation of biological tissues up to millimeter wave: test fixture design', IEEE MTT-S Digest 2000, pp1041 - 4
- 18 MASHIMO, S, KUWABARA, S, YAGIHARA, S. and HIGASI, K.: 'Dielectric relaxation time and structure of bound water in biological materials', J. Phys. Chem., 1987, 91, 6337 - 8
- 19 GHODGAONKAR, D. K, ISKANDER, M. F. and GANDHI, O. P.: 'Complex permittivity measurement of biological tissues and human skin in vivo at millimetre wavelengths', Bioelectromagnetics Society 7<sup>th</sup> annual meeting
- 20 ISKANDER, M. F, SMITH, S, GANDHI, O. P. and GHODGAONKAR, D. K.: 'Dielectric properties measurements at millimetre waves using a free space method', Bioelectromagnetics Society 7<sup>th</sup> annual meeting
- 21 GHODGAONKAR, D. K. and GANDHI, O. P, and ISKANDER, M. F.: 'Complex permittivity of human skin in vivo in the frequency band 26.5 – 60GHz', Int. Symp. Antennas and Propagation Society, IEEE July 2000, 2, pp 1100 – 1103
- 22 HEY-SHINTON, G. L, MATTHEWS, P. A. and MESTAY, J.: 'The complex permittivity of human tissue at microwave frequencies', Phys. Med. Biol., 1982, 27, pp 1067 – 1071
- 23 COOK, H. F.: 'The dielectric behaviour of some types of human tissues at microwave frequencies', British J. Appl. Physics, 1951, pp 295 – 300
- 24 BORIC-LUBECKE, O, NIKAWA, Y, SNYDER, W, LIN, J. and MIZUNO, K.: 'Novel microwave and millimeter-wave biomedical applications', IEEE 4<sup>th</sup> Int. Conf. Telecommunications in Modern Satellite, Cable and Broadcasting Systems 1999 *TELSIKS'99*, 1, pp 186 - 193
- 25 BORIC-LUBECKE, O, NIKAWA, Y, SNYDER, W, LIN, J. and MIZUNO, K.: 'Skin properties at millimeter waves', Proc. Asia Pacific Microwave Conference 1998 *APMC'98*, 2, pp 877 – 880

- 26 HWANG, H, YIM, J, CHO, J-W. and CHEON, C.: '110GHz broadband measurement of permittivity on human epidermis using 1 mm coaxial probe', Proc. IEEE MTT-S Int. Microwave Symp. Digest, June 2003, Philadelphia, PA, USA, 1, pp 399 - 402
- 27 ALISON, J. M. and SHEPPARD, R. J.: 'Dielectric properties of human blood at microwave frequencies', J. Phys. Med. Biol., 1993, 38, pp 971 – 978
- 28 STUCHLY, M. A.: 'Applications of time-varying magnetic fields in medicine', Critical reviews in biomedical engineering, 1990, 18, 2, pp 89 – 124
- 29 STUCHLY, M. A.: 'Electromagnetics in biology and medicine [Foreword]', Radio science, Jan/Feb1995, 30, 1, pp 149 - 150
- 30 MYERSON, R. J. and EMAMI, B.: 'Normal tissue effects of hyperthermia in conjunction with radiotherapy', Advances in radiation biology, 1992, 15, pp 195 - 215
- 31 LAGENDIJK, J. J. W.: 'Hyperthermia treatment planning', Physics in medicine and biology, 2000, 45, 5, pp R61 - R76
- 32 CHOU, C. K, BASSEN, H, OSEPCHEUK, J, BALZANO, Q, PETERSEN, R, MELTZ, R, CLEVELAND, R, LIN, J. C. and HEYNICK, L.: 'Radio frequency electromagnetic exposure: tutorial review on experimental dosimetry', Bioelectromagnetics, 1996, 17, 3, pp 195 - 208
- 33 KATO, H. and ISHIDA, T.: 'Present and future status of noninvasive selective deep heating using RF in hyperthermia', Medical and biological engineering and computing, July 1993, 31, 55, pp S2 - S11
- 34 KATO, H, KOYAMA, T, NIKAWA, Y. and SAITO, M.: 'Research and development of hyperthermia machines for present and future clinical needs', Int. J. of Hyperthermia, 1998, 14, 1, pp 1 - 11
- 35 SAMULSKI, T. V.: 'Superficial hyperthermia with microwaves', book 'Radiation research: A twentieth Century Perspective', (Ed. W.C. Dewey), New York: Academic, 1992, pp 895 - 900
- 36 HAND, J. W.: 'Heat delivery and thermometry in clinical hyperthermia', Recent results in cancer research, 1987, 104, pp 1 - 23
- 37 CHAKRABORTY, D. P. and BREZOVICH, I.A.: 'Error sources effecting thermocouple thermometry in RF electromagnetic fields', Journal of microwave power, 1982, 17, 1, pp 17 – 28
- 38 'Basic restrictions for time varying Electric and magnetic fields up to 300 GHz'  
[http://www.who.int/docstore/peh-emf/EMFStandards/who-0102/Europe/United\\_Kingdom\\_files/table\\_uk.htm](http://www.who.int/docstore/peh-emf/EMFStandards/who-0102/Europe/United_Kingdom_files/table_uk.htm)

- 39 '1998 ICNIRP Guidelines for limiting exposure to time-varying electric, magnetic and electromagnetic fields (up to 300GHz): NRPB advice on aspects of implementation in the UK'  
[http://www.nrpb.org/publications/documents\\_of\\_nrpb/abstracts/absd10-2.htm](http://www.nrpb.org/publications/documents_of_nrpb/abstracts/absd10-2.htm)
- 40 KIRUCHI, M, AMEMIYA, Y, EGAWA, S, ONOYAMA, Y, KATO, H, KANAI, H, SAITO, Y, TSUKIYAMA, I, HIRAOKA, M, MIZUSHINA, S, YAMASHITA, T, NIKAWA, Y, MATSUDA, J. and MIYAKAWA, M.: 'Guide to the use of hyperthermia equipment. 2. Microwave heating', Int. J. of Hyperthermia, 1992, 9, 3, pp 341 - 360
- 41 KHIZHNYAK, E. P. and ZISKIN, M. C.: 'Heating patterns in biological phantoms caused by millimeter wave electromagnetic induction', IEEE Trans. Biomedical Engineering, Sept 1994, 41, 9, pp 865 – 873
- 42 WALTERS, T. J, BLICK, D. W, JOHNSON, L. R, ADAIR, E. R. and FOSTER, K.R.: 'Heating and pain sensation produced in human skin by millimeter waves: comparison to a simple thermal model', Health Physics, March 2000, 78, 3, pp 259 – 267
- 43 GABRIEL, C. and GABRIEL, S.: 'Compilation of the dielectric properties of body tissue at RF and microwave frequencies', Final report for AFOSR/NL Bolling AFB DC 20332-0001, June 1996.
- 44 <http://ourworld.cs.com/soundweapon/millivision.htm>
- 45 'Passive Millimeter –Wave Imaging',  
[www.uxocoe.btrc.com/TechnicalReps/SD47.pdf](http://www.uxocoe.btrc.com/TechnicalReps/SD47.pdf)
- 46 MARTIN, C, LOVBERG, J, CLARK, S. and GALLIANO, J.: 'Real time passive millimeter-wave imaging from a helicopter platform', Proc. 19<sup>th</sup> Digital Avionics Systems Conference, Philadelphia, PA, USA, Oct. 2000, 1, pp 2B1/1 - 8
- 47 APPLEBY, R, ANDERTON, R. N, PRICE, S, SALMON, N. A, SINCLAIR, G.N, COWARD, P.R, BARNES, A. R, MUNDAY, P. D, MOORE, M, LETTINGTON, A. H. and ROBERTSON, D. A.: 'Mechanically scanned real-time passive millimeter wave imaging at 94GHz', Proc. SPIE – Int. Soc. Opt. Eng. Passive Millimeter-Wave Imaging Technology VI and Radar Sensor Technology VII, Orlando, FL, USA, April 2003, 5077, pp 1 - 6
- 48 MARTIN, C. A, CLARK, S. E, LOVBERG, J. A. and KOLINKO, V. G.: 'Passive millimeter-Wave imaging technology for phased-array systems', Proc. SPIE – Int. Soc. Opt. Eng. Passive Millimeter-Wave Imaging Technology VI and Radar Sensor Technology VII, Orlando, FL, USA, April 2003, 5077, pp 33 - 41
- 49 LOVBERG, J. A, GALLIANO, J. A. and CLARK, S. E.: 'Passive millimeter-wave imaging for concealed article detection', SPIE Proc. Command, Control, Communications, and Intelligence Systems fro Law Enforcement, Boston, MA, USA, Nov. 1996, 2938, ISBN 0-8194-2340-8, pp 120 - 130

- 50 ‘Sensor fusion for detection of concealed weapons’, Jane’s IDR, 1<sup>st</sup> Feb 2004
- 51 HUGUENIN, G. R.: ‘Millimeter-wave concealed weapons detection and through-the-wall imaging systems’, SPIE Proc. Command, Control, Communications, and Intelligence Systems for Law Enforcement, Boston, MA, USA, Nov. 1996, 2938, ISBN 0-8194-2340-8, pp 152 – 159
- 52 GRESHAM, I, JAIN, N, BUDKA, T, ALEXANIAN, A, KINAYMAN, N, ZIEGNER, B, BROWN, S. and STAECCKER, P.: ‘A 76-77GHz pulsed Doppler radar module for autonomous cruise control applications’, IEEE MTT-S Int. Symp. Digest, June 2000, 3, pp 1551 - 1554
- 53 METZ, C, GRUBERT, J, HEYEN, J, JACOB, A. F, JANOT, S, LISSEL, E, OBERSCHMIDT, G. and STANGE, L. C.: ‘Fully integrated automotive radar sensor with versatile resolution’, IEEE Trans. MTT, Dec. 2001, 49, 2, pp 2560 - 2566
- 54 CAMIADE, M, DOMNESQUE, D, OUARCH, Z. and SION, A.: ‘Fully MMIC-based front end for FMCW automotive radar at 77GHz’, IEEE MTT-S Int. Symp. Digest, June 1999, 4, pp 1489 - 1492
- 55 GROLL, H. P. and DETLEFSEN, J.: ‘History of automotive anticollision radars and final experimental results of a MM-wave car radar developed by the Technical University of Munich’, IEEE Trans. Aerospace and Electronic Systems Magazine, 1997, 12, 8, pp 15 – 19
- 56 IHARA, T. and FUJIMURA, K.: ‘Research and development trends of millimeter-wave short-range application systems’, IEICE Trans. Communications, Dec 1996, E79-B, 12, pp 1741 - 1753
- 57 ROUGERON, G, GAUDAIRE, F, GABILLET, Y. and BOUATOUCH, K.: ‘Simulation of the indoor propagation of a 60GHz electromagnetic wave with a time-dependent radiosity algorithm’, Computers and Graphics-UK, 2002, 26, 1, pp 125 - 141
- 58 LOYEZ, C, ROLLAND, N, ROLLAND, P. A. and LAFOND, O.: ‘Indoor 60GHz radio channel sounding and related T/R module considerations for high data rate communications’, Electronics Letters, 2001, 37, 10, pp 654 - 655
- 59 GEORGE, J, SMULDERS, P. F. M. and HERBEN, M. H. A. J.: ‘Application of fan-beam antennas for 60GHz indoor wireless communication’, Electronics Letters, 2001, 37, 2, pp 73 - 74
- 60 WU, G, HASE, Y. and INOUE, M.: ‘An ATM-based indoor millimeter-wave wireless LAN for multimedia transmissions’, IEICE Trans. Communications, 2000, E83B, 8, pp 1740 – 1752
- 61 LÄHTEENMÄKI, J and KARTTAAVI, T.: ‘Measurement of dielectric parameters of wall materials at 60GHz band’, Electronics Letters, 1996, 32, pp. 1442-4

- 62 ALABASTER, C.M., and DAHELE, J.S.: 'Free space measurement of permittivity', Proc. Int. Conf. on Antennas and Propagation, April 2003, Exeter, Vol. 2, pp. 538-541
- 63 STARNER, T.: "The challenges of wearable computing: Part 1" IEEE Micro, July/August 2001, 21, 4, pp 44 – 52
- 64 STARNER, T.: "The challenges of wearable computing: Part 2", IEEE Micro, July/August 2001, 21, 4, pp 54 – 67
- 65 HALL, P. S, RICCI, M. and HEE, T. M.: "Measurement of on-body propagation characteristics", IEEE Antennas and Propagation Society International Symposium, June 2002, 2, pp 310 – 313
- 66 WEI, J. B, SHIDAKER, T. and HAWLEY, M. C.: 'Recent progress in microwave processing of polymers and composites', Trends in Polymer Science, 1996, 4, 1, pp18 – 24
- 67 THOSTENSON, E. T. and CHOU, T. W.: 'Microwave Processing: fundamentals and applications', Composites Part A: Applied Science and Manufacturing, 1999, 30, pp 1055 - 1071
- 68 MIJOVIC, J. and WIJAYA, J.: 'Review of cure of polymers and composites by microwave energy', Polymer Composites, June 1990, 11, 3, pp 184 - 191
- 69 ZOUGHI, R. and BAKHTIARI, S.: 'Microwave nondestructive detection and evaluation of disbonding and delamination in layered dielectric slabs', IEEE Trans. Inst. & Measurement, Dec. 1990, 39, 6, pp 1059 - 1063
- 70 GOPALSAMI, N., BAKHTIARI, S., DIECKMAN, S.L., RAPTIS, A.C. and LEPPER, M.J.: 'Millimeter-Wave Imaging For Nondestructive Evaluation of Materials', Materials Evaluation, 1994, 54, 3, pp 412 – 415
- 71 BRAMATI, M. and SALERNO, E.: 'Experiments on some particular permittivity sensors in non destructive testing of dielectric materials', J. Microwave Power and Electromagnetic Energy, 1992, 27, 4, pp 209 – 216
- 72 SEMENOV, V. S.: 'Radio detection of local flaws in dielectrics', Russian J. Nondestructive Testing, 2002, 38, 9, pp 700 - 703
- 73 BAKHTIARI, S., GOPALSAMI, N. and RAPTIS, A.C.: 'Characterisation of Delamination and Disbonding in Stratified Dielectric Composites by Millimeter Wave Imaging', Materials Evaluation, 1995, 53, 4, pp 468 – 471
- 74 BIRCH, J. R, SIMONIS, G. J, AFSAR, M. N, CLARKE, R. N, DUTTA, J. M, FROST, H. M, GERBAUX, X, HADNI, A, HALL, W. F, HEIDINGER, R, HO, W. W, JONES, C. R, KÖNIGER, F, MOORE, R. L, MATSUP, H, NAKANO, T, RICHTER, W, SAKAI, K, STEAD, M. R, STUMPER, U, VIGIL, R. S, and WELLS, T. B.: 'An intercomparison of Measurement techniques for the determination of the dielectric properties of solids at near millimetre wavelengths', IEEE Trans MTT, June 1994, 42, 6, pp956 - 963

- 75 CORREIA, L.: 'Material characterisation' ch. 8.2 in COST 231 Final report ed. Damosso E and Correia L: Digital mobile radio towards future generation systems, European Commission, Directorate General XIII, Belgium, 1999, pp 418-425
- 76 JAIN, R. C. and VOSS, W. A. G.: 'Dielectric measurement methods for industrial scientific and medical applications in the microwave frequency range', IETE Technical Review, Sept & Dec 1994, 11, 5 & 6, pp 297 - 311
- 77 GHODGAONKAR, M. F, VARADAN, V. V. and VARADAN, V. K.: 'A free-space method for measurement of dielectric constants and loss tangents at microwave frequencies', IEEE Trans. Instr. and measurement, June 1989, 37, 3, pp 789 - 793
- 78 MA, Z. and OKAMURA, S.: 'Permittivity determination using amplitudes of transmission and reflection coefficients at microwave frequency', IEEE Trans. MTT, 1999, 47, pp. 546-550
- 79 KADABA, P. K.: 'Simultaneous measurement of complex permittivity and permeability in the millimeter region by a frequency domain technique', IEEE Trans. Instr. and measurement, Dec 1984, IM-33, 4, pp 336 - 340
- 80 CULLEN, A. L.: 'A new free-wave method for ferrite measurement at millimeter wavelengths', Radio Science, Dec 1987, 22, 7, pp 1168 - 1170
- 81 LYNCH, A. C, GRIFFIYHS, H. D, APPLETON, S, CULLEN, A. L, KHOSROWBEYGI, A. and BENJAMIN, R.: 'Free wave measurement of permeability and permittivity of ferrites at millimeter-wave frequencies', IEE Proc. Science and Measurement Technology, March 1995, 142, 2, pp169 - 175
- 82 SHIMABUKURO, F, LAZAR, S, CHERNICK, M and DYSON, H.: 'A quasi-optical method for measuring the complex permittivity of materials', IEEE Trans. MTT, 1984, MTT-32, pp 659-665
- 83 ZHENG, L, and ZIQIANG, Y.: 'Measurement of complex permittivity and permeability of materials by quasi-optical method', Int. J. IR & MMW, 1989, 10, 5, pp 557 - 563
- 84 FRIEDSAM, G. L. and BIEBL, E. M.: 'A broadband free-space dielectric properties measurement system at millimeter wavelengths', IEEE Trans. Instr. and measurement, Apr 1997, 42, 2, pp515 - 518
- 85 IIJIMA, Y, TANAKA, T, KIMURA, M. and SATO, R.: 'Measurement of complex permittivity and permeability at millimeter wavelength using a free space method', Int. Symp. Electromagnetic Compatibility, May 1999, pp 412 – 415
- 86 KOH, G.: 'Dielectric properties of ice at millimeter wavelengths', Geophysical research letters, 1997, 24, 18, pp2311 - 2313

- 87 LYASHCHENKO, A. K. and ZASETSKY, A. Y.: 'Complex dielectric permittivity and relaxation parameters of concentrated aqueous electrolyte solutions in millimeter and centimetre wavelength ranges', *J. Molecular Liquids*, 1998, 77, pp61 - 75
- 88 JOSE, K. A, VARADAN, V. K. and VARADAN, V. V.: 'Wideband and non contact characterisation of the complex permittivity of liquids', *Microwave and Optical Technology Letters*, July 2001, 30, 2, pp 75 - 79
- 89 OTSUKA, K, HASHIMOTO, O. and ISHIDA, T.: 'Measurement of complex permittivity of low-loss dielectric material at 94GHz frequency band using free-space method', *Microwave and Optical Technology Letters*, Sept 1999, 22, 5, pp 291 - 292
- 90 AFSAR, M. N, TKACHOV, I. I. and KOCHARYAN, K. N.: 'A novel W-band spectrometer for dielectric measurements', *IEEE trans. MTT*, Dec 2000, 48, 12, pp 2637 - 2643
- 91 POLIVKA, J.: 'Measuring the permittivity of concrete at millimeter waves', *Int. J. IR & MMW*, 1996, 17, 10, pp1673 - 1683
- 92 GVOZDEV, V. I, KRIVORUCHKO, V. I. and TIMOFEEV, L. P.: 'Measurement of the parameters of a dielectric in the millimeter wave band', *Measurement Techniques*, 2000, 43, 4, pp 374 - 376
- 93 SZWARNOWSKI, S and SHEPPARD, R. J.: 'Precision waveguide cells for the measurement of permittivity of lossy liquids at 70GHz', *J. Physics E: Scientific Instruments*, 1977, 10, pp1163 - 7
- 94 DUDECK, K. E. and BUCKLEY, L. J.: 'Dielectric material measurement of thin samples at millimeter wavelengths', *IEEE Trans. Instr. and measurement*, Oct 1992, 41, 5, pp 723 – 725
- 95 ABDULNOUR, J, AKYEL, C. and WU, K.: 'A generic approach for permittivity measurement of dielectric materials using a discontinuity in a rectangular waveguide or microstrip line', *IEEE Trans. MTT*, May 1995, 43, 5, pp 1060 - 1066
- 96 GLIBITSKIY, G. M.: 'Measurement of permittivity of aqueous solutions at 44GHz by FM receiver', *Int. J. IR & MMW*, 1996, 17, 12, pp 2207 - 2214
- 97 SPHICOPoulos, T, TEODORIDIS, V. and GARDIOL, F.: 'Simple non destructive method for the measurement of material permittivity', *J. Microwave Power and Electromagnetic Energy*, 1985, 20, 3, pp 165 - 172
- 98 ALEKSEEV, S. I. and ZISKIN, M. C.: 'Reflection and absorption of millimeter waves by thin absorbing films', *Bioelectromagnetics*, 2000, 21, pp264 - 271
- 99 GANDHI, O. P, WAHID, P. F. and ISKANDER, M. F.: 'A modified "infinite" sample method for precision measurements of the complex permittivities of biological tissues', *Bioelectromagnetics Soc. LA 28/6 to 2/7 1982*

- 100 ABBAS, Z, POLLARD, R. D. and KELSALL, R. W.: 'A rectangular dielectric waveguide technique for determination of permittivity of materials at W-band', IEEE Trans. MTT, Dec 1998, 46, 2, pp 2011 – 2015
- 101 VAN LOON, R. and FINSY, R.: 'Measurement of complex permittivity of liquids at frequencies from 60 to 150GHz', Reviews Sci. Instrum., Apr. 1974, 45, 4, pp 523 - 525
- 102 STEEL, M. C, SHEPPARD, R. J. and COLLINS, R.: 'Precision waveguide cells for the measurement of complex permittivity of lossy liquids and biological tissues at 35GHz', J. Physics E: Scientific Instruments, 1987, 20, pp872 - 877
- 103 VAN LOON, R. and FINSY, R.: 'Measurement of complex permittivity of liquids at frequencies from 5 to 40GHz', Reviews Sci. Instrum., Sept. 1973, 44, 9, pp 1204 - 1208
- 104 HOSHI, N, NIKAWA, Y, KAWAI, K. and EBISU, S.: 'Application of microwaves and millimeter waves for the characterisation of teeth for dental diagnosis and treatment', IEEE Trans. MTT, June 1998, 46, 6, pp 834 - 838
- 105 STAEBELL, K. F. and MISRA, D.: 'An experimental technique for in vivo permittivity measurement of materials at microwave frequencies', IEEE Trans. MTT, March 1990, 38, 3, pp 337 - 339
- 106 MISRA, D. K. and EUNG DAM RONG, D.: 'Coaxial aperture sensor and its applications – a tutorial overview', IEEE Int, symposium on circuits and systems, Sydney, NSW, Australia, May 2001
- 107 MISRA, D, CHABBRA, M, EPSTEIN, B. R, MIROTZNIK, M. and FOSTER, K. R.: 'Noninvasive electrical characterisation of materials at microwave frequencies using an open-ended coaxial line: test of an improved calibration technique', IEEE Trans. MTT, Jan 1990, 38, 1, pp 8 - 14
- 108 RZEPECKA, M. A.: 'A cavity perturbation method for routine permittivity measurement', Journal of microwave power, 1973, 8, pp 3 - 11
- 109 CAMPBELL, A. M.: 'Measurement and analysis of the microwave dielectric properties of tissues', PhD thesis, University of Glasgow, 1990
- 110 CAMPBELL, A. M. and LAND, D. V.: 'Dielectric properties of female human breast tissue measured in vitro at 3.2GHz', Phys. Med. Biol. 1992, 37, 1, 193 - 210
- 111 DRESSEL, M, KLEIN, O, DONOVAN, S. and GRÜNER, G.: 'Microwave cavity perturbation technique: Part III: applications', Int. J. IR & MMW, 1993, 14, 12, pp2489 - 2517
- 112 VERTIY, A. A, GAVRILOV, S. P. and ÖZEL, M. E.: 'Millimeter wave investigation of dielectric cylinders absorption cross-section by resonant method', Int. J. IR & MMW, 1996, 17, 7, pp 1285 - 1299

- 113 VERTIY, A. A, GAVRILOV, S. P, TRETYAKOV, O, A. and ÖZEL, M. E.: 'Determination of electrodynamical parameters of dielectric pipe-shaped materials using millimeter wave cavity', Int. J. IR & MMW, 1996, 17, 9, pp 1541 - 1556
- 114 AFSAR, M, DING, H and TOURSHAN, K.: 'A new 60GHz open-resonator technique for precision permittivity and loss-tangent measurement', IEEE Trans. Inst. & Meas., Apr. 1999, 48, 2, pp 626 - 630
- 115 AFSAR, M and DING, H.: 'A novel open-resonator system for precise measurement of permittivity and loss-tangent', IEEE Trans. Inst. & Meas., 2001, 50, pp 402 - 405
- 116 GABRIEL, C, SHEPPARD, R. J. and GRANT, E. H.: 'Dielectric properties of ocular tissues at 37<sup>0</sup>C', Phys. Med. Biol., 1983, 28, 1, pp 43 – 49
- 117 ROBERTS, S. and VON HIPPEL, A.: 'A new method for measuring dielectric constant and loss in the range of centimetre waves', J. Appl. Physics, 1946, 17, 7, pp 610 - 616
- 118 RAMO, S., WHINNERY, J. R. and VAN DUZER, T.: 'Fields and Waves in Communication Electronics', John Wiley & Sons Inc, 2nd Ed. 1984, ISBN 0-471-81103-3
- 119 ALABASTER, C.M.: 'Permittivity of Human Skin in the Millimetre Wave Band' IEE Electronics Letters, 16<sup>th</sup> October 2003, Vol. 39, No. 21, pp1521-1522
- 120 VON HIPPEL, A. (Ed): 'Dielectric materials and applications' Artech House ISBN 0-89006-805-4
- 121 GUDKOV, O. I, POTAPOV, A. A, KASHCHENKO, M. V. and VTORUSHIN, B. A.: 'Reference materials for permittivity', Measurement Techniques, 1981, 24, 2, pp 142 - 4
- 122 MERIAKRI, V. V, CHIGRAI, E. E, PANGONIS, L. I. and PARKHOMENKO, M. P.: 'Millimeter waves for water content monitoring in materials and media' 4<sup>th</sup> Int. Kharkov Symp. Physics and Engineering of Millimeter and Sub-Millimeter Waves, June 2001, 2, pp 814 - 816
- 123 KUZNETSOV, A.N.: 'Biophysics of electromagnetic effects' [in Russian], Energoatomizdat, Moscow, 1994
- 124 ENGLAND, T. S.: 'Dielectric properties of the human body for wavelengths in the 1-10cm range', Nature, Sept. 1950, 166, pp 480 – 481
- 125 GHODGAONKAR, D. K. and DAUD, A. B.: 'Calculation of Debye parameters of single Debye relaxation equation for human skin in vivo', IEEE Conf. Proc. 4<sup>th</sup> Nat. Conf. Telecomms Technology, Shah Alam, Malaysia, 2003, pp 71 – 74
- 126 PENNES, H. H.: 'Analysis of tissue and arterial blood temperatures in the resting human forearm', Journal of applied physiology, 1948, 1, 2, pp 93 – 122

- 127 LEBEDEV, A. M. and PERMYAKOV, V. A.: 'Influence of skin roughness on the absorbed-power distribution under a millimeter-wave horn antenna', Radio and Communications Technology, 1998, 3, 11, pp38 – 42
- 128 HILL, J. M. and MARCHANT, T. R.: 'Modelling microwave heating', Applied Mathematical Modelling, June 1996, 20, pp 3 - 15
- 129 JONES, P. L and ROWLEY, A. T.: 'Dielectric drying', Drying Technology, 1996, 14, 5, pp 1063 – 1098

THIS PAGE INTENTIONALLY LEFT BLANK

**APPENDIX A: PUBLISHED PAPERS**

The following papers have been published as a result of work described in this thesis. These papers are reproduced in full on the ensuing pages.

ALABASTER, C.M., and DAHELE, J.S.: 'Free space measurement of permittivity', Proc. Int. Conf. on Antennas and Propagation, April 2003, Exeter, Vol. 2, pp. 538-541

ALABASTER, C.M.: 'Permittivity of Human Skin in the Millimetre Wave Band' IEE Electronics Letters, 16<sup>th</sup> October 2003, Vol. 39, No. 21, pp1521-1522

The following paper has been submitted for publication and is reproduced in full.

ALABASTER, C.M., DAHELE, J.S., and BADCOCK, R.A.: 'Damage and Defect Detection in Composites Using Millimetre Wave Permittivity Measurement', Journal of Nondestructive Evaluation. Submitted 31.10.03.

During the course of the work on this thesis, the author has also published the papers listed below. These are not related to the work of this thesis and are not reproduced here but are mentioned as evidence of the author's ability to conduct research.

ALABASTER, C.M., HUGHES, E.J. and MATTHEW, J.H.: 'Medium PRF Radar PRF Selection Using Evolutionary Algorithms', IEEE Trans. Aerospace and Electronic Systems, July 2003, Vol. 39, Iss. 3, pp 990 - 1001

ALABASTER, C.M., and HUGHES, E.J.: 'Medium PRF Radar PRF Optimisation Using Evolutionary Algorithms', Proc. IEEE Radar 2003 Conference, May 2003, Huntsville, AL, pp 192 - 202

HUGHES, E.J. and ALABASTER, C.M.: 'Novel PRF Schedules for Medium PRF Radar', Proc. IEEE Radar 2003 Conference, September 2003, Adelaide, S.A., pp 678 - 683

THIS PAGE INTENTIONALLY LEFT BLANK

## FREE SPACE MEASUREMENT OF PERMITTIVITY

C M Alabaster & J S Dahle

Cranfield University, UK

### ABSTRACT

This paper presents a free space technique for the measurement of the complex permittivity of a slice of dielectric sample. The experimental set up is described and the technique validated by measurements on well characterised dielectrics at J band whereupon it is concluded that the method would be suitable for use in the millimetre wave band. Measured data on a variety of plastics, glass, building materials and biological tissues samples at 60GHz is then given and includes new data for the permittivity of skin at this frequency.

### INTRODUCTION

This paper presents a free space technique of measuring the complex permittivity of dielectrics which has been developed in the J band and subsequently employed at 60GHz to characterise a variety of materials.

There is a growing interest in the characteristics of dielectric materials in the millimetre wave (MMW) band as an ever increasing number of radar and communications systems seek to exploit these frequencies. Different materials are relevant for different applications and yet there is a paucity of permittivity data available in the published literature. Many of the measurement methods in use at centimetric wave frequencies do not scale well to the MMW band. Those methods which have been applied successfully are either based on measurements of the transmission and/or reflection coefficients arising from samples inserted within waveguide (or terminating a waveguide) Alekseev and Ziskin (1), or made in free space, Kadaba (2), or by the perturbation of the resonant frequency (or electrical length) and quality factor of an open resonator, Afsar and Ding (3). A free space method was preferred for this study since it is deemed the most suitable for wideband measurements on lossy dielectrics and requires minimal sample preparation. Furthermore, the method used here is similar to that of Ma and Okamura (4) and is based on a measurement of only the amplitudes of transmission and reflection coefficients, and not their phases, and so relaxes the requirement for mechanical precision implicit in other techniques.

The next section of this paper describes the theory of the technique. Further sections then describe the

experimental set up and calibration of both the J band and 60GHz systems. The results are then presented and discussed; these include permittivity data for plastics, glass, building materials and biological tissues at 60GHz. There follows a brief section outlining further work planned in this area, then finally the conclusions are summarised.

### THEORY

A plane wave normally incident on a slab of dielectric sample of thickness  $t_s$  is partially reflected, transmitted and absorbed by the dielectric. The reflected and transmitted signals are comprised of an infinite number of components due to the multiple reflections between the air/dielectric interfaces. Thus the total reflected and transmitted signals are given respectively by:

$$r = \frac{r_1 - r_1 \exp(-2k_s t_s)}{1 - r_1^2 \exp(-2k_s t_s)} \quad (1)$$

and

$$t = \frac{(1 - r_1^2) \exp(-k_s t_s)}{1 - r_1^2 \exp(-2k_s t_s)} \quad (2)$$

where  $k_s$  is the propagation constant in the sample and  $r_1$  is the reflection coefficient of the sample/air interface. Both are functions of the relative complex permittivity,  $\epsilon_r$ , of the sample given by.

$$r_1 = -\frac{\sqrt{\epsilon_r} - \sqrt{\epsilon_0}}{\sqrt{\epsilon_r} + \sqrt{\epsilon_0}} \quad (3)$$

and

$$k_s = k_0 \sqrt{\epsilon_r} \quad (4)$$

where  $k_0$  and  $\epsilon_r$  are the propagation constant and permittivity in free space, respectively.

The measured values of the reflection and transmission coefficients are  $R_m$  and  $T_m$  respectively and relate to  $r$  and  $t$  by the equation pair:

$$R_m = 20 \log_{10} |r| \text{ dB} \quad (5a)$$

and

$$T_m = 20 \log_{10} |t| \text{ dB} \quad (5b)$$

Wideband solutions of  $R_m$  and  $T_m$  indicate cyclical variations with frequency due to the multiple reflections between interfaces beating in and out of phase. The frequencies of peaks and troughs occur when the sample thickness is a multiple of a quarter wavelength and may be used to provide an initial estimate of  $\epsilon_r$ . For very lossy samples, equations (1) and (2) simplify to:

$$r = r_1 \quad (6)$$

and

$$t = (1 - r_1^2) \exp(-k_s t_s) \quad (7)$$

## EXPERIMENTAL SET UP

A slice of sample was held in place on a rigid frame placed mid-way between a pair of standard gain horns connected to a vector network analyser (VNA).  $T_m$  and  $R_m$  were measured via the VNA  $|S_{21}|$  and  $|S_{11}|$  paths respectively. The horns were aligned for vertical polarisation, parallel with each other and for normal incidence on the sample. Lähteenmäki and Karttaavi (5) conclude that misalignment errors of up to  $3^\circ$  have minimal effects on the results. Furthermore, the authors own experience suggests that  $T_m$  and  $R_m$  are relatively insensitive to small alignment errors. The sample was positioned just beyond the far field threshold of each horn ( $= 2D^2/\lambda$ , where D = the horn aperture and  $\lambda$  = the longest wavelength) to ensure plane wave incidence. The sample was sufficiently large to subtend an angle of twice the 3dB beamwidth of the horns; thus it intercepted the entire main beam and approximates to an infinitely large sample.

In the general case, equations (1) to (5) are solved using an iterative technique to find solution(s) for  $\epsilon_r$ . Solutions for  $\epsilon_r$  are sought over a user defined search space and resolution which result in computed values of transmission and reflection coefficients ( $T_c$  and  $R_c$  respectively) which most closely match the measured values  $T_m$  and  $R_m$ . However, due to the multiple reflections present in all but very lossy samples, multiple solutions of  $\epsilon_r$  may be found. This ambiguity can easily be overcome based on an initial estimate from the peak and trough frequencies or by fitting data at several nearby frequencies. (4) applied this technique to lossy samples within a container at 9.4GHz and ignored the multiple reflections in order to minimise the ambiguities.

The presence of the dielectric provides a degree of focusing of the signals onto the receiver of the transmitted path. A small correction must therefore be made to  $T_m$  in accordance with Shimabukuro et al (6). This correction requires an estimate of the permittivity of the sample which can be calculated from processing the uncorrected  $T_m$  data. The correction is typically very small and so the initial estimate is valid.

Initial measurements were made at J band with the intention of assessing the suitability of this technique for use in the MMW band. The calibration procedure resulted in valid data over the band 11 to 12GHz. This necessitated a sample size of 500mm x 500mm, which was large enough to intercept the first five Fresnel zones and a distance between the horn apertures of just over 1 metre. Clearly, this is becoming unfeasibly large at centimetric wavelengths.

The measurements at  $60 \pm 3$ GHz required a distance between horns of 305mm and a sample of 105mm diameter. This intercepts the first 7 Fresnel zones and was large enough to avoid total internal reflection (and multiple modes within the sample) at all points across its surface for samples whose  $\epsilon_r < 9.2$ . Solutions for  $\epsilon_r$  were computed for which the rms percentage error between computed and measured transmission and reflection coefficients at 57, 60 and 63GHz was a minimum.

## Calibration

The transmission measurement was calibrated by normalising the VNA  $|S_{21}|$  measurement with the sample in place to one in which no sample was present. Multiple reflections between the horns and sample gave rise to ripple on the measurement. This was overcome using the trace smoothing function at J band and by using the time gating feature to isolate the main through path in the 60GHz measurements. The latter is the preferable technique but was not available on the VNA used at J band.

The  $|S_{11}|$  measurement was calibrated in free space in the plane of the forward surface of the sample. This was accomplished via a one port reflection calibration of the VNA; the short circuit being provided by an inflexible metal plate fitted on the sample frame, an open circuit being provided by the same metal plate displaced  $\lambda/4$  back from its short position using metal shims and a matched load being provided by free space. Multiple reflections between sample and horn were overcome using the trace smoothing or time gating as with the  $|S_{21}|$  measurements. This method of  $|S_{11}|$  calibration restricts the band of measurements to  $\pm 5\%$  of the centre frequency as defined by the  $\lambda/4$  shims. The bandwidth could be extended by offsetting several calibrations using shims of the appropriate thickness up to the limitation of the horn bandwidth.

## Preparation of Biological Samples

Both tissue samples were excised from a freshly butchered animal, stitched onto a metal supporting frame and chemically fixed in formaldehyde. Prior to

measurement they were rinsed in water, dried with tissue paper and allowed to stand for several minutes to further dry. The pericardium sample was measured whilst still damp but without any film of surface moisture whereas the skin sample was only slightly damp at the time of measurement. The samples were then secured to the sample frame; the outer surface being exposed to the illuminating horn. Sample thickness was measured by averaging micrometer readings taken at 10 locations (pericardium) or 7 locations (skin) on the periphery of the sample.

## Applications

Measurements were made on a number of building materials since this is of interest in the modelling of indoor propagation of wireless local area network (LAN) signals at 60GHz. There is very little data published for biological tissues in the MMW band. Data on skin is required in order to assess the health and safety implications of exposure to MMW signals. As far as the authors are aware, these measurements of permittivity are the first on skin in the MMW band.

## RESULTS & DISCUSSION

### J Band

Table 1 presents results over 11 to 12 GHz. These coincide quite closely with previously published data also listed in Table 1. Multiple solutions were obtained for the chipboard and medium density fibre (MDF) board but were readily resolved by fitting the data across the measurement band.

**Sources of error.** For the low-loss materials the values of  $T_m$  are less than 1dB and so great accuracy is required in its measurement. Repeated readings of the reflection and transmission coefficients suggest an experimental repeatability of  $\pm 0.11\text{dB}$  in  $R_m$  and  $\pm 0.18\text{dB}$  in  $T_m$ . This renders the determination of the imaginary part of  $\epsilon_r$  subject to large percentage errors for the low loss materials. Similar problems were experienced with the 60GHz data. A significant source of error is the variation of sample thickness and the unaccounted roughness of the surface. It is not possible to predict the consequence of the tolerances of the measured data on the result for  $\epsilon_r$  due to the iterative search technique employed. However, for the PTFE sample the measured values of  $T_m$  and  $R_m$  were within the ranges of values computed from equations (1) to (5) based on the published permittivity data and the measured thickness of  $12.6\text{mm} \pm 0.4\text{mm}$  over the band 11 to 12GHz. Furthermore, the peak in  $T_m$  at 8.2GHz affords an initial estimate of  $\epsilon_r \sim 2.1$ .

TABLE 1 – Permittivity Results at J Band

Sample	11.0GHz	12.0GHz	Published result
PTFE	$2.095 - j0.0007$	$2.07 - j0.0012$	$2.08 - j0.00077$ at 10GHz (7)
Polystyrene	$2.47 - j0.014$	$2.49 - j0.006$	$2.48 - j0.003$ at 3GHz (7)
Borosilicate glass (80% SiO <sub>2</sub> )	$4.79 - j0$	$4.61 - j0$	4.6 at 1MHz (as quoted by manufacturers)
MDF board	$2.23 - j0.138$	$2.29 - j0.130$	
Chipboard	$2.34 - j0.197$	$2.38 - j0.178$	

### 60GHz

Table 2 presents data for the best fit solution across the measurement band of 57 to 63GHz, together with previously published data where available. The measured data coincides quite closely with previously published values. As at J band multiple solutions of  $\epsilon_r$  were obtained for the building materials which are all moderately lossy. Solutions for the very lossy biological tissues were unique.

TABLE 2 – Permittivity Results at 60GHz

Sample	Measured $\epsilon_r$	Published result
PTFE	$2.04 - j0.0007$	$2.063 - j0.0006$ (3)
Polystyrene (3 samples)	$2.48 - j0$	
Fused Quartz (3 samples)	$3.78 - j0$	$3.793 - j0.001$ (3)
MDF board	$3.48 - j0.170$	
Chipboard	$3.14 - j0.161$	$2.78/3.15 - j0.136/0.180$ (8) $2.95 - j0.19$ (5)
Plasterboard	$2.95 - j0.035$	$2.60/3.08 - j0.036/0.055$ (8) $2.58 - j0.021$ (5)
Concrete	$6.03 - j0.795$	$6.78 \pm 0.7 - j0.75$ at 51.3GHz (9)
Bovine Pericardium	$5.43 - j14.33$	
Porcine skin	$5.79 - j6.36$	

**Tissue characteristics.** The similarity in the results for the real part of the permittivity of the two tissue samples is perhaps unsurprising since both are composed predominantly of collagen. The variation in their imaginary parts is probably due to their differing moisture contents. The transmission and reflection coefficients of the tissue samples were measured three times for random sample orientations. Very little variability in the readings was observed and so the results tabulated above were based on averaged readings.

## FUTURE WORK

Future work aims to extend the characterisation of tissues to include human skin and measurements in the 77 and 94GHz bands. It is also planned to characterise road materials at 77GHz since this band is used by automobile radar.

A significant application of the techniques described in this paper is to use a measurement of the permittivity of laminated composite materials to non-invasively detect and locate faults arising during the curing of these materials. Such faults would seriously undermine the strength of the materials and could go undetected until they fail. In this application the superior spatial resolution of high frequency MMW (94GHz) is desirable.

## CONCLUSIONS

The free space measurement of the amplitudes of reflection and transmission coefficients is a reliable and accurate means of determining the complex permittivity over a 10% bandwidth. This bandwidth could be extended by offsetting the frequencies of several calibrations. The technique developed at J band scales successfully to MMW frequencies and is indeed conveniently applied at 60GHz and would be suitable for use at yet higher frequencies. It has been used successfully to measure a variety of dielectric materials which can be prepared in slices of known thickness. However, it is not best suited to the accurate determination of the imaginary part of permittivity of very low loss materials. The complex permittivity of a variety of building materials has been measured and is in close agreement with previously published data. The method has also provided new data on the complex permittivity of porcine skin and bovine pericardium tissues at 60GHz.

Multiple solutions arise in low and medium lossy dielectrics. Resolution of the ambiguities may be

accomplished by fitting measured and computed data over the measurement bandwidth and/or by making initial estimates based on frequencies of peaks or troughs.

## ACKNOWLEDGEMENTS

The authors would like to thank Anritsu Limited for the loan of the VNA used for the 60GHz measurements and Peter Ziopoulos and his staff, also of Cranfield University, for the preparation of the biological samples.

## REFERENCES

1. Alekseev S and Ziskin M, 2000, "Reflection and absorption of millimetre waves by thin absorbing films", *Bioelectromagnetics*, 21, 264-271
2. Kadaba P, 1984, "Simultaneous measurement of complex permittivity and permeability in the millimetre region by a frequency-domain technique", *IEEE Trans. Inst. & Meas.*, IM-33, 336-340
3. Afsar M and Ding H, 2001, "A novel open-resonator system for precise measurement of permittivity and loss-tangent", *IEEE Trans. Inst. & Meas.*, 50, 402-405
4. Ma Z and Okamura S, 1999, "Permittivity determination using amplitudes of transmission and reflection coefficients at microwave frequency", *IEEE Trans. MTT*, 47, 546-550
5. Lähteenmäki J and Karttaavi T, 1996, "Measurement of dielectric parameters of wall materials at 60GHz band", *Electronics Letters*, 32, 1442-4
6. Shimabukuro F, Lazar S, Chernick M and Dyson H, 1984, "A quasi-optical method for measuring the complex permittivity of materials", *IEEE Trans. MTT*, MTT-32, 659-665
7. Von Hippel A, 1995, "Dielectric materials and applications" Artech House ISBN 0-89006-805-4
8. Correia L, 1999, "Material characterisation" ch. 8.2 in COST 231 Final report ed. Damosso E and Correia L: Digital mobile radio towards future generation systems, European Commission, Directorate General XIII, Belgium, 418-425
9. Polívka J, 1996, "Measuring the permittivity of concrete at millimetre waves", *Int. J. IR & MMW*, 17, 1673-1683

**Results:** Fig. 2 shows CW current, voltage, output power ( $L-I-V$ ) and spectral characteristics (inset) of the fabricated VCSELs. The VCSEL exhibits a low threshold current of 1.5 mA with threshold voltage of 1.7 V and slope efficiencies  $\sim 0.35$  W/A. The laser emits near 3.8 mW peak power at a 12.3 mA drive current. The spectral response and the near-field pattern (inset in Fig. 2) operating at 10 mA and 5 mA, respectively, confirm that only the fundamental mode is present over the full operation range. More than 90% series resistance of the VCSELs is within  $60\text{--}65\ \Omega$ , indicating a good regrowth interface and the advantages of low resistance of larger aperture VCSELs. Additionally, the rollover current is around 12 mA, which is also larger than for small size aperture VCSELs, which should lead to better reliability [2]. To measure the high-speed VCSEL under large signal modulation, microwave and lightwave probes was used in conjunction with a 10 Gbit/s pattern generator and a 12 GHz photoreceiver. The eye diagrams were taken for back-to-back (BTB) transmission on our VCSELs. The measurements on our VCSELs were conducted on an SMA sub-mount operating at 10 Gbit/s with 5 mA bias current and 6 dB extinction ratio (Fig. 3a). The wide open eye pattern indicates good performance of the single-mode VCSEL. The rise time ( $T_r$ ) and fall time ( $T_f$ ) are estimated to be 28 ps and 38 ps, respectively, with jitter (peak-peak) = 14 ps. For comparison, the conventional oxide multiple-mode VCSEL with 8  $\mu\text{m}$  aperture diameter operating at 10 Gbit/s with 5 mA bias current shows more noisy eye pattern with jitter = 17 ps (see Fig. 3b).

**Conclusions:** A high-power ( $>3.8$  mW) and high-speed performance (10 Gbit/s operation) large-area single mode VCSEL is reported, with low threshold, employing oxygen implantation, MOCVD regrowth and selective oxidation. The concept should be applicable to long wavelength VCSELs.

© IEE 2003

2 July 2003

Electronics Letters Online No: 20030982

DOI: 10.1049/el:20030982

T.-H. Hsueh, H.-C. Kuo, F.-I. Lai, L.-H. Laih and S.C. Wang (*Institute of Electro-Optical Engineering, National Chiao Tung University, 1001 Ta Hsueh Road, Hsinchu, Taiwan 30050, Republic of China*)  
E-mail: taohung.eo90g@nctu.edu.tw

## References

- 1 CHOQUETTE, K.D., and GEIB, K.M.: 'Fabrication and performance of vertical cavity surface-emitting lasers' in WILMSEN, C., TEMKIN, H., and COLDREN, L. (Eds.): 'Vertical-cavity surface-emitting lasers' (Cambridge University Press, 1999), Chap. 5
- 2 JUNG, C., JAGER, R., GRABHERR, M., SCHNITZER, P., MICHALZIK, R., WEIGL, B., MULLER, S., and EBELING, K.J.: '4.8 mW singlemode oxide confined top-surface emitting vertical-cavity laser diodes', *Electron. Lett.*, 1997, **33**, pp. 1790–1791
- 3 HAWKINS, B.M., HAWTHORNE, R.A., III, GUENTER, J.K., TATUM, J.A., and BIARD, J.R.: 'Reliability of various size oxide aperture VCSELs'. ECTC 2002, San Diego, CA, USA
- 4 GRABHERR, M., JAGER, R., MICHALZIK, R., WEIGL, B., REINER, G., and EBELING, K.J.: 'Efficient single-mode oxide-confined GaAs VCSELs emitting in the 850 nm wavelength regime', *Electron. Lett.*, 1997, **9**, pp. 1304–1306
- 5 MARTINSSON, H., VUKUSIC, J.A., GRABHERR, M., MICHALZIK, R., JAGER, R., EBELING, K.J., and LARSSON, A.: 'Transverse mode selection in large-area oxide-confined vertical-cavity surface-emitting lasers using a shallow surface relief', *IEEE Photonics Technol. Lett.*, 1999, **11**, pp. 1536–1538
- 6 WIEDENMANN, D., KING, R., JUNG, C., JÄGER, R., SCHNITZER, P., MICHALZIK, R., and EBELING, K.J.: 'Design and analysis of single-mode oxidized VCSEL's for high-speed optical interconnects', *IEEE J. Quantum Electron.*, 1999, **5**, pp. 503–511
- 7 UNOLD, H.J., MAHMOUD, S.W.Z., JÄGER, R., KICHERER, M., RIEDL, M.C., and EBELING, K.J.: 'Improving single-mode VCSEL performance by introducing a long monolithic cavity', *IEEE Photonics Technol. Lett.*, 2000, **12**, pp. 939–941
- 8 YOUNG, E.W., CHOQUETTE, K.D., CHUANG, S.L., GEIB, K.M., FISCHER, A.J., and ALLERMAN, A.A.: 'Single-transverse-mode vertical-cavity lasers under continuous and pulsed operation', *IEEE Photonics Technol. Lett.*, 2001, **13**, pp. 927–929

## Permittivity of human skin in millimetre wave band

C.M. Alabaster

The complex permittivity of a human skin sample is measured over the band 60 to 100 GHz using a quasi-optical method. The results are presented and compared with predictions from standard models. There is a wide range of modelled results; each model providing a partial fit with the measured data.

**Introduction:** Currently, very little measured data is available for the permittivity of biological tissues in the millimetre wave (MMW) band. This Letter presents the first measured permittivity data for human skin in the MMW band. Hitherto, the permittivity of biological tissues in the MMW band has been extrapolated from models of permittivity as functions of frequency such as Debye and Cole-Cole type equations. Model parameters have been based on measured data at lower, centimetric, frequencies. With the increasing use made of the MMW band for communications, radar and other passive sensor applications it becomes important to have measured data available. Since it is anticipated that human skin will be very lossy within the MMW band it may be assumed that MMW radiation incident on the human body will be almost entirely absorbed (or reflected) by the skin layer. Consequently, it is particularly important to have reliable data on the characteristics of human skin. Such data can verify or adjust the standard models and be used as a basis for determining the heat deposition and propagation of MMW signals in the body. This Letter describes the quasi-optical experimental method and theory used and presents the measured results for a single, *ex-vivo* sample of human skin fixed in formaldehyde together with a comparison of data from standard permittivity extrapolation models.

**Theory:** A plane wave normally incident on a slab of dielectric sample of thickness  $t_s$  is partially reflected, transmitted and absorbed by the dielectric. The reflected and transmitted signals are comprised of an infinite number of components due to the multiple reflections between the air/dielectric interfaces. Thus the total reflected ( $r$ ) and transmitted ( $t$ ) signals are given respectively by:

$$r = \frac{r_1 - r_1 \exp(-2k_s t_s)}{1 - r_1^2 \exp(-2k_s t_s)} \quad (1)$$

and

$$t = \frac{(1 - r_1^2) \exp(-2k_s t_s)}{1 - r_1^2 \exp(-2k_s t_s)} \quad (2)$$

where  $k_s$  is the propagation constant in the sample and  $r_1$  is the reflection coefficient of the sample/air interface. Both are functions of the relative complex permittivity,  $\epsilon_r$ , of the sample given by:

$$r_1 = -\frac{\sqrt{\epsilon_r} - \sqrt{\epsilon_0}}{\sqrt{\epsilon_r} + \sqrt{\epsilon_0}} \quad (3)$$

and

$$k_s = k_0 \sqrt{\epsilon_r} \quad (4)$$

where  $k_0$  and  $\epsilon_0$  are the propagation constant and permittivity in free space, respectively.

**Experimental method:** A slice of sample was held in place on a rigid circular frame placed between and just beyond the far-field threshold of a pair of standard gain horns connected to a vector network analyser (VNA), similar to the method of [1]. The amplitudes of the transmission and reflection coefficients were measured via the VNA  $|S_{21}|$  and  $|S_{11}|$  paths, respectively. The horns were aligned for vertical polarisation, parallel with each other and for normal incidence on the sample. The sample was sufficiently large to subtend an angle of twice the 3 dB beamwidth (at least the first seven Fresnel zones) of the horns; thus it intercepted the entire main beam and approximates to an infinitely large sample. The VNA was used in a time gated mode to isolate the reflection from the sample or the main through signal for the reflection and transmission measurements, respectively. The

reflection measurement was calibrated with respect to a metal short circuiting plate placed in the sample frame whereas the transmission measurement was calibrated with respect to the path loss with no sample in place.

Equations (1) to (4) are solved using an iterative technique to find solution(s) for  $\epsilon_r$ . Solutions for  $\epsilon_r$  are sought over a user defined search space and resolution which result in computed values of transmission and reflection coefficients which most closely match the measured values. However, due to the multiple reflections present in all but very lossy samples, multiple solutions of  $\epsilon_r$  may be found. This ambiguity can easily be overcome based on an initial estimate from the peak and trough frequencies caused by the multiple reflections beating in and out of phase or by fitting data at several nearby frequencies [2].

The skin sample was obtained from a white, 50 year old, female donor. Its fat was removed and it was scrapped to a near uniform thickness ( $\sim 1.5$  mm) and fixed in 10% formalin soon after excision. The skin was lightly stretched over an annular stainless steel frame and stitched into location around the frame periphery. Prior to measurement, the sample was rinsed in water and allowed to dry for 4 h. A 105 mm diameter of the sample was exposed to the measurement.

A PTFE sample, the properties of which are well established, was measured in the same way in order to verify the method.

**Results and discussion:** The permittivity of the PTFE sample was determined to be:  $\epsilon_r = 2.04 - j0.0007$  and  $2.00 - j0.0023$  at 60 and 94 GHz, respectively, which are in close agreement with previously published data. The results for the skin sample are given in Table 1. Table 1 quotes the permittivity values which represent the best solutions over given bands and at certain spot frequencies of interest. The results are quoted at both the measurement temperature and extrapolated to 37°C. The following temperature gradients have been applied as they represent the mean of those reported in the literature based on data for water in the MMW band: real part of  $\epsilon_r$ : +2.35%/°C, imaginary part of  $\epsilon_r$ : +1.05%/°C [3–6].

**Table 1:** Measured permittivity data for human skin

Frequency (GHz)	Measured permittivity, $T$ (°C)	Permittivity (extrapolated to 37°C)
57–63	23	9.9–j9.1
60	23	13.2–j10.4
76–78	30	9.9–j9.0
77	30	10.4–j3.3
84	30	10.4–j3.2
90–100	30	12.1–j3.5
90	30	11.1–j3.4
94	30	7.5–j2.9
		8.7–j3.1

Table 2 quotes the values for dry human skin at 37°C predicted from standard models used to extrapolate the permittivity of biological material.

**Table 2:** Predicted permittivity data for human skin (37°C)

Frequency (GHz)	Reference [7] single term Debye	Reference [7] two term Debye	Reference [8] four term Cole-Cole
60	8.7–j14.6	5.8–j5.0	7.98–j10.90
75	7.27–j11.0	5.2–j4.1	6.69–j9.11
77			6.56–j8.91
94	5.9–j8.6	4.7–j3.2	5.79–j7.49
100			5.60–j7.09

The results of Table 1 indicate that both real and imaginary parts of the permittivity show a reduction with increasing frequency, as is to be expected from relaxation phenomena. The sample was slightly moist at the time of measurement. An increase in the permittivity was observed when measured wet and is in line with expectations. Indeed, significant variation in the permittivity of skin is also anticipated on a sample by sample basis. The effects of the formaldehyde fixing were undetermined. The effects of measurement error are not possible to quantify due to the iterative search technique used. Repeated measurements indicate possible errors of up to  $\pm 15\%$ . It is also worth noting that extrapolations of the permittivity data to new temperatures may be

unreliable as there is a wide variety in the temperature gradients reported in the literature.

The measured values show a consistently higher real part of permittivity than the predicted values, whereas the imaginary parts are in reasonable agreement. No one model provides the most consistent fit to the measured data. The likely reasons for the discrepancies in the two sets of data include: (i) the unknown moisture content of the sample used here and also those used in measurements to set the model parameters, (ii) the effects of fixing in formaldehyde and (iii) natural tissue variations.

**Acknowledgments:** The author wishes to thank J. Dahele of Cranfield University, PhD supervisor, for help and advice; P. Ziopoulos and V. Wise of Cranfield University for the preparation of the skin sample; the National Disease Research Interchange, Philadelphia, for the provision of the human skin sample, and the Anritsu Corporation and Birmingham University for the use of their VNAs.

© IEE 2003  
*Electronics Letters Online No: 20030967*  
*DOI: 10.1049/el:20030967*

28 August 2003

C.M. Alabaster (*Department of Aerospace, Power and Sensors, Cranfield University, Shrivenham, Nr Swindon, Wiltshire SN11 8SQ, United Kingdom*)  
E-mail: c.m.alabaster@rmcs.cranfield.ac.uk

## References

- MA, Z., and OKAMURA, S.: 'Permittivity determination using amplitudes of transmission and reflection coefficients at microwave frequency', *IEEE Trans. Microw. Theory Tech.*, 1999, **47**, (5), pp. 546–550
- ALABASTER, C.A., and DAHELE, J.S.: 'Free space measurement of permittivity'. Proc. Int. Conf. on Antennas and Propagation, Exeter, UK, 2003, Vol. 2, pp. 538–541
- STEEL, M.C., and SHEPPARD, R.J.: 'The dielectric properties of rabbit tissue, pure water and various liquids suitable for tissue phantoms at 35 GHz', *Phys. Med. Biol.*, 1998, **33**, (4), pp. 467–472
- GRANT, E.H., and SHACK, R.: 'Complex permittivity measurements at 8.6 mm wavelength over the temperature range 1–60°C', *Brit. J. Appl. Phys.*, 1967, **18**, pp. 1807–1814
- GLIBITSKIY, G.M.: 'Measurement of permittivity of aqueous solutions at 44 GHz by FM receiver', *Int. J. Infrared Millim. Waves*, 1996, **17**, (12), pp. 2207–2214
- SZWARNOWSKI, S., and SHEPPARD, R.J.: 'Precision waveguide cells for the measurement of permittivity of lossy liquids at 70 GHz', *J. Phys. E. Sci. Instrum.*, 1977, **10**, (11), pp. 1163–1167
- KUZNETSOV, A.N.: 'Biophysics of electromagnetic effects' (Energoatomizdat, Moscow, 1994) [in Russian]
- GABRIEL, C., and GABRIEL, S.: 'Compilation of the dielectric properties of body tissue at RF and microwave frequencies'. Final report for AFOSR/NL Bolling AFB DC 20332-0001, June 1996. (Full text of this reference is available at: <http://www.brooks.af.mil/AFRL/HED/hebt/reports/dielectric/home.html>; Automated calculations based on this model also available at: <http://niremf.iroe.fi.cnri.tissprop/>)

## Lee-metric decoding of BCH and Reed-Solomon codes

X.-W. Wu, M. Kuijper and P. Udaya

A Lee-metric list-decoding algorithm for Reed-Solomon (RS) codes over  $GF(p)$  is presented. The algorithm is obtained by generalising the Guruswami–Sudan (Hamming metric) list-decoding algorithm for RS codes. The algorithm can be used to decode the Lee-metric BCH codes, and outperforms the known Lee-metric decoding algorithm for BCH codes.

**Introduction:** For block codes over  $GF(p)$ , where  $p$  is an odd prime, it has been found [1–3] that for certain channels the Lee metric is a more appropriate metric than the Hamming metric. For  $\alpha \in GF(p)$ , denote by  $\tilde{\alpha}$  the smallest non-negative integer such that  $\alpha = \tilde{\alpha} \cdot 1$ , where 1 is the multiplicative unity of  $GF(p)$ . The Lee value  $|\alpha|$  of  $\alpha$  is

# Damage and Defect Detection in Composites Using Millimetre Wave Permittivity Measurement

C. M. Alabaster, J. S. Dahele and R. A. Badcock, Cranfield University.

E-mail: [c.m.alabaster@rmcs.cranfield.ac.uk](mailto:c.m.alabaster@rmcs.cranfield.ac.uk)

## Abstract.

A free space measurement of permittivity within the millimetre wave band is employed to detect and locate defects within fibreglass composite samples. This technique offers a non-contacting and non-destructive method of locating a variety of defects. The millimetric wave experimental technique is described and its theoretical basis is supplied. Experiments have been conducted on twelve samples of composite materials some of which were nominally ideal control samples; others had damage induced within them deliberately. The defect categories were: low-level impact damage, incomplete cure and vacuum release during cure. Ultrasound C-scan imaging was used to confirm the presence/absence of defects in each sample. The permittivity of a large planar sample was mapped and found to be reasonably consistent. The measured permittivity data is then studied to determine the feasibility of identifying the defects. The results demonstrate the ability to resolve defects from nominally ideal material and to identify the nature of the defect. The experimental method can also detect low-level impact damage with a superior sensitivity to that of the ultra-sound imaging technique. The spatial resolution of the millimetric technique is around 40mm or better.

Keywords: composites, permittivity, millimetre wave, defect detection, damage detection.

## I INTRODUCTION

Radio frequency (RF) measurements offer the potential to determine the structural integrity of composite materials in a non-destructive, non-contacting manner. Defects such as delaminations, voids, matrix cracks and improper cure result in changes in the dielectric properties of the composite [1]. The presence of such defects may be determined via a measurement of dielectric properties, such as permittivity, or by the absorption, scattering and reflections of an electromagnetic (EM) signal, propagating in the medium, which is incident on a discontinuity resulting from the defect. Ideally, one would desire a diagnostic tool which is non-contacting and capable of achieving a spatial resolution in the order of the likely defect dimensions. The non-contacting requirement dictates a free-space RF based measurement and the requirement for fine resolution dictates the use of millimetre wave (MMW) frequencies (30GHz to 300GHz). The use of MMW in this role was discussed by Gopalsami, Bakhtiari et al [1] [2] in which a 75 to 110GHz imaging system was developed and employed to detect sub-surface voids and disbonds in Kevlar/epoxy composite samples. Millimetric measurements also offer a high contrast between defective and nominally ideal material.

This paper describes some experimental work to determine the feasibility of a free-space measurement of permittivity in the 90GHz to 100GHz band to detect and locate a variety of defects in planar fibreglass composite samples. Several composite samples were manufactured; some being kept as control samples having no defects and others having damage induced within them. The defect categories were: low-level impact damage, incomplete curing and vacuum release during the curing cycle. Additionally, a large sheet of composite sample was manufactured and the spatial variation in its permittivity was mapped. This sample was subsequently subjected to a low-level impact damage and then re-examined using the MMW technique in order to judge the spatial resolution to which the defect can be resolved. The structural integrity of all composite samples has been determined using a Physical Acoustics UltraPAC II ultra-sound imaging C-scan with a 5 MHz probe to enable a comparison between the MMW measurements and the severity and extent of defects.

Section (II) describes the theory which underpins the measurement method. In section (III) the experimental set up and calibration method are described and details are given of the method of processing the measured data in order to determine the sample permittivity. This section also describes the sample preparation, defects and ultra-sound testing. The results of the MMW permittivity measurements and ultra-sound images are given in section (IV). Finally, section (V) draws some conclusions, chief amongst which are that there are resolvable differences in the permittivity between nominally ideal and defective samples.

## II THEORY [3][4]

A plane wave normally incident on a slab of dielectric sample of thickness  $t_s$  is partially reflected, transmitted and absorbed by the dielectric. The reflected and transmitted signals are comprised of an infinite number of components due to the multiple reflections between the air/dielectric interfaces. Thus the total reflected and transmitted signals are given respectively by:

$$r = \frac{r_1 - r_1 \exp(-2k_s t_s)}{1 - r_1^2 \exp(-2k_s t_s)} \quad (1)$$

and

$$t = \frac{(1 - r_1^2) \exp(-k_s t_s)}{1 - r_1^2 \exp(-2k_s t_s)} \quad (2)$$

where  $k_s$  is the propagation constant in the sample and  $r_1$  is the reflection coefficient of the sample/air interface. Both are functions of the relative complex permittivity,  $\varepsilon_r$ , of the sample given by:

$$r_1 = -\frac{\sqrt{\varepsilon_r} - \sqrt{\varepsilon_o}}{\sqrt{\varepsilon_r} + \sqrt{\varepsilon_o}} \quad (3)$$

and

$$k_s = k_0 \sqrt{\epsilon_r} \quad (4)$$

where  $k_0$  and  $\epsilon_0$  are the propagation constant and permittivity in free space, respectively.

The measured values of the reflection and transmission coefficients are  $R_m$  and  $T_m$  respectively and relate to  $r$  and  $t$  by the equation pair:

$$R_m = 20 \log_{10} |r| \text{ dB} \quad (5a)$$

and

$$T_m = 20 \log_{10} |t| \text{ dB} \quad (5b)$$

Wideband solutions of  $R_m$  and  $T_m$  indicate cyclical variations with frequency due to the multiple reflections between interfaces beating in and out of phase. The frequencies of peaks and troughs occur when the sample thickness is a multiple of a quarter wavelength and may be used to provide an initial estimate of  $\epsilon_r$ . Note that permittivity (and hence relative permittivity) is a complex quantity i.e.  $\epsilon_r = \epsilon_r' - j\epsilon_r''$ , where  $\epsilon_r'$  is the relative dielectric constant and  $\epsilon_r''$  is the relative loss factor.

### III EXPERIMENTAL Work

#### A Experimental Set Up

A method similar to that of Ma and Okamura [5] was employed and has also been described in previous publications [3] [4]. Circular samples were clamped on to an annular sample frame placed mid-way between a pair of standard gain waveguide horns connected to a vector network analyser (VNA).  $T_m$  and  $R_m$  were measured via the VNA  $|S_{21}|$  and  $|S_{11}|$  paths,

respectively, over the frequency band 90 to 100GHz. This method requires that only the amplitudes of the transmission and reflection coefficients need be measured and that there is no need for phase data. The amplitudes only method reduces the requirement to accurately maintain the positional and alignment accuracy of the equipment and to maintain the phase and frequency stability of the VNA source. The chosen frequency band represents a compromise between spatial resolution, which improves as frequency increases, and the availability of test equipment and components which accompanies technological developments to exploit the atmospheric window at 94GHz. Furthermore, the band is restricted to 10GHz since it is assumed in the processing of measured data that the samples exhibit a negligible degree of dispersion.

The horns were aligned for vertical polarisation, parallel with each other and for normal incidence on the sample. Lähteenmäki and Karttaavi<sup>[6]</sup> have concluded that misalignment errors of up to 3° have minimal effects on the results. Furthermore, the authors own experience suggests that  $T_m$  and  $R_m$  are relatively insensitive to small alignment errors. The sample was positioned just beyond the far field threshold of each horn ( $=2D^2/\lambda$ , where D = the horn aperture and  $\lambda$  = the longest wavelength) to ensure plane wave incidence. Measurements at 90 to 100GHz required a horn to sample separation of 110mm. The samples were disc shaped of diameter 125mm but with a region exposed to the MMW of 105mm in diameter; the 10mm around the periphery enabling each sample to be clamped to the annular sample frame. The -3dB contour of the beam in the sample plane approximates to a circle of diameter 40mm. Samples were therefore sufficiently large to subtend an angle of greater than twice the -3dB beamwidth of the horns; thus they intercepted the entire main beam (at least the first 15 Fresnel zones) and approximate to an infinitely large sample.

## B Calibration

The VNA was operated in a time gated mode in order to isolate the first reflection from the sample (reflection measurement) and the main through path between horns (transmission

measurement). In this way multiple reflections between the horns and/or sample are ignored and do not corrupt the reading. The reflection measurement was calibrated with respect to a metal plate fitted in place of the sample. All reflection coefficients were therefore normalised to that of a short circuit in the measurement plane. The transmission measurement was calibrated with respect to the path loss with no sample in place.

### C Data Processing

In the general case, equations (1) to (5) are solved using an iterative technique to find solution(s) for  $\varepsilon_r$ . Solutions for  $\varepsilon_r$  are sought over a user defined search space and resolution which result in computed values of transmission and reflection coefficients which most closely match the measured values  $T_m$  and  $R_m$ . However, due to the multiple reflections present in all but very lossy samples, multiple solutions of  $\varepsilon_r$  may be found. This ambiguity can easily be overcome based on an initial estimate from the peak and trough frequencies or by fitting data at several nearby frequencies.  $T_m$  and  $R_m$  were recorded every 2GHz over the band 90 to 100GHz and solutions for  $\varepsilon_r$  were computed for which the rms percentage error between computed and measured transmission and reflection coefficients at all six frequencies was a minimum. No solutions were declared in the cases where the rms percentage error exceeded 20%. This was an arbitrary threshold beyond which it was deemed that there was too great an inconsistency between measured and computed results.

### D Samples

Twelve Fibreglass composite samples were manufactured from Fibredux 916G, a woven pre-preg tape (10 layers, all aligned). All but sample 12 were manufactured as a disc of diameter 125mm, sample 12 was a sheet of dimensions 500mm x 250mm. Table (i) summarises the details of the twelve samples. Three samples of each control and defect category (except impact damaged samples) were manufactured in order to judge the statistical spread of results.

All the samples were cut from the same sheet and all were processed in the same way prior to curing. The curing process was carried out under a vacuum of 200mbar. The woven pre-preg tape Fibredux 916G were cured by temperature ramping at a rate of 1.5°C per minute to a final temperature of 130°C followed by a dwell at this temperature for 30 minutes. The samples were cooled down by opening the door after switching the oven off. The vacuum was released and the samples removed from the oven. The vacuum was released at 80°C for the samples that had the vacuum released early, otherwise the cure cycle continued as per normal. The incompletely cured samples were removed from the oven once it had reached its final temperature i.e. zero dwell time.

The quality of every sample was assessed using a 5MHz ultra-sound imaging C-scanner. The samples were supported in water above the bottom of the water tank and the transducer acquired an image of the sample in a raster scanning fashion. The ultra-sound equipment was operated in a time gated mode to capture the two-way transmission path of the signal (through the sample, reflected from the tank base and back through the sample). Undamaged composite material transmits the signal through it with little attenuation, whereas the presence of defects scatters and absorbs the signal resulting in a highly attenuated transmission path. A representative sample of the ultra-sound images is given in figure 1.

## E Experimental Tests

Initial measurements were made on a sample of PTFE in order to validate the method since the permittivity of PTFE in the band 90 to 100GHz is reasonably well established.

The permittivity of samples 1 to 11 was measured at a consistent sample orientation. The impact site (samples 4 and 5) was nominally in the centre of each sample which in turn was opposite the phase centres of the waveguide horns. Additionally, the measurement on sample 1 was repeated several times at random sample orientations in order to judge the effects of fibre

orientation with respect to the plane of polarisation and also to ascertain the experimental repeatability.

Sample 12 was secured to the frame so as to expose the measurement of permittivity at 14 sites evenly distributed across its surface plus additional sites centred at 10mm, 20mm and 40mm left and right of the designated impact site, see figure 2. A 2 Joule impact was then inflicted on the site and the permittivity measurements and ultra-sound tests repeated. The impact created a star shaped delamination with the peak extents of the delamination in the reinforcing fibre orientations and the composite surface was smoothed back into shape by hand so as to minimise the physical distortion of the sample.

#### IV RESULTS / DISCUSSION

##### A Results

The permittivity of the PTFE sample was determined to be:  $\epsilon_r = 2.00 - j0.0023$  at 94GHz, which is in close agreement with previously published data [7][8].

A summary of the ultra-sound tests and permittivity results for samples 1 to 11 is given in Table (ii). The permittivity results for sample 12 both before and after the impact is given in Table (iii). A representative sample of the ultra-sound images is given in figure 1. These are plotted on a grey-scale; pure white represents 100% transmittance whereas black indicates 0% transmittance.

##### B Discussion

The control samples (1, 2 and 3) of the Fibredux 916G exhibit a range in  $\epsilon_r'$  of 3.76 to 3.78 and in  $\epsilon_r''$  of 0.086 to 0.099. Sample 12, also Fibredux 916G, has a spatial variation in  $\epsilon_r'$  of 3.69 to

3.85 and in  $\varepsilon_r^{\parallel}$  of 0.078 to 0.120. This composite material has reasonably consistent dielectric properties both on a sample by sample basis and within any given sample. The 3 and 2 Joule impact damages of samples 4 and 5 respectively have resulted in considerable shape distortion around the impact site and this is clearly visible on the ultra-sound images of figure 1b and 1c. This distortion has scattered the MMW signals in such a way as to yield transmission and reflection coefficients across the measurement band which cannot be related to any value of permittivity. Clearly, the absence of a solution is resolvable from the defect-free samples. The incompletely cured samples (6, 7 and 8) differ visually in colour and feel tacky and pliable to the touch. Their ultra-sound images (figure 1d) indicate that they are ridden with defects. These samples have a variation in  $\varepsilon_r'$  of 3.37 to 3.61 and in  $\varepsilon_r^{\parallel}$  of 0.074 to 0.130. The spread in  $\varepsilon_r'$  is outside the range of that for the nominally ideal samples (1, 2, 3 and 12) and therefore resolvable from them. The spread in  $\varepsilon_r^{\parallel}$  is not resolvable from the nominally ideal samples. Those samples for which the vacuum was released early (9, 10 and 11) are slightly thicker than the nominally ideal samples due to the presence of large voids within them, but otherwise appear similar. Their ultra-sound images (figure 1d) indicate that they are also ridden with defects. These samples have a variation in  $\varepsilon_r'$  of 3.20 to 3.27 and in  $\varepsilon_r^{\parallel}$  of 0.047 to 0.065; the reduction in both  $\varepsilon_r'$  and  $\varepsilon_r^{\parallel}$  being consistent with a large material void content. The ranges of both  $\varepsilon_r'$  and  $\varepsilon_r^{\parallel}$  are outside the spread in values for the nominally ideal samples and therefore are resolvable from them. Furthermore, these results are also outside the ranges for the incompletely cured samples and so are resolvable from these, too.

The ultra-sound image of sample 12, figure 1e, indicated that it had no defects. Even after the impact damage was inflicted the impact site was barely visible on the ultra-sound image, figure 1f. From a visual inspection of sample 12 a star shaped delamination was easily seen to extend 5mm left and right of the impact centre. The damage suffered by sample 12 appears to be considerably less than that of sample 5 for the same impact on the same material; indeed there is noticeably less shape distortion. No permittivity solution was found when the MMW measurement was aligned with the centre of the impact site. One may conjecture that the MMW

energy is scattered from the fracture even though no foreign material is present, in the same way that light is scattered from crazed glass. However, perfectly reasonable results were obtained, which were consistent with the undamaged material, when the measurement was displaced by as little as 10mm either side of the impact centre. One might reasonably expect that the -3dB contour of the beam footprint on the sample (circle diameter 40mm) would set the limit of spatial resolution but that large defects outside this range may still be visible to the measurement whilst minor defects within this range may not. The latter situation would appear to be the case here.

### C Experimental Tolerances and Repeatability

Errors arise due to the accuracy with which the calibration is maintained, variations in sample orientation, experimental repeatability, noise modulations of the VNA results and the consistency of the sample thickness together with the accuracy to which it can be measured. However, it is not possible to anticipate what effects these error sources have on the solutions for sample permittivity due to the iterative search technique employed. The tolerance on the transmission coefficient can be significant for low-loss materials. This method is best suited to the measurement of lossy samples and has difficulty in accurately determining  $\varepsilon_r^{||}$  of low loss materials. Repeated processing of the data for extremes of all errors sources suggest a maximum variation of around  $\pm 4\%$  in  $\varepsilon_r^{'}$  and  $\pm 25\%$  in  $\varepsilon_r^{||}$  for the composite samples. The repeated measurements on sample 12 suggest average variations in  $\varepsilon_r^{'}$  of  $\pm 1.0\%$  and in  $\varepsilon_r^{||}$  of  $\pm 13\%$ .

The fibres in the samples run in two orthogonal axes (the warp and weft of the woven samples). All the results quoted here were based on measurements conducted for the same sample orientation i.e. such that the fibres ran parallel and perpendicular to the plane of polarisation. The variability in solutions due to other random sample orientations was  $< \pm 0.3\%$  in  $\varepsilon_r^{'}$  and  $\sim \pm 12\%$  in  $\varepsilon_r^{||}$ .

## V CONCLUSIONS

The complex permittivity of PTFE and various composite samples has been determined in the 90 to 100GHz band using the free space measurement of the amplitudes of transmission and reflection coefficient. It has then been applied to map the permittivity variation of a 500mm by 250mm sheet of 10 layer woven Fibredux 916G composite material. The variation in permittivity across the sheet was found to be  $\varepsilon_r' = 3.77 \pm 2.1\%$  and  $\varepsilon_r'' = 0.099 \pm 21\%$ . This composite material has reasonably consistent dielectric properties both on a sample by sample basis and within any given sample. There are resolvable differences in the permittivity between samples of the Fibredux 916G which are nominally ideal compared with those damaged by impact, incompletely cured samples and those for which the vacuum was released during cure; each category being resolvable from the others. The measurement of the permittivity of this material can therefore be used not only as a means of detecting defects but also of determining the nature of the defect. The measurement of permittivity can find no solution for the impact damaged samples which clearly differentiates them from nominally ideal samples. The inability to find a solution is thought to arise from the shape distortion of the impact and the presence of a fracture within the material. The measurement method was successful in identifying the impact damage in sample 12, where shape distortion was minimal, even though the defect was barely visible on an ultra-sound image. The MMW technique described here is therefore more sensitive to this form of damage than the ultra-sound imaging technique. The resolution between the nominally ideal samples and those incompletely cured is based on small differences in the real part of their permittivity only. The differences are on the resolvable limit when experimental repeatability is taken into consideration. Nevertheless, an accurate measurement of permittivity has the potential to monitor the state of cure of a composite material. There are, however, clear differences in both real and imaginary parts of the permittivity between those samples in which the vacuum was released during cure and all other samples.

The spatial resolution of the measurement technique is dependent on the severity of the fault. The spatial resolution of the MMW beam on the sample was 40mm in this experiment and this should dictate the resolution of the measurement. However, the impact damaged area of sample 12 could not be resolved from the undamaged material until the equipment was aligned to within 10mm of the impact centre, suggesting a resolution of less than 10mm.

#### ACKNOWLEDGEMENTS

Ms Viv Wise, Cranfield University, for the manufacture of the samples.

Birmingham University, for the use of their MMW VNA facility

#### REFERENCES

- 1 GOPALSAMI, N., BAKHTIARI, S., DIECKMAN, S.L., RAPTIS, A.C. and LEPPER, M.J.: 'Millimeter-Wave Imaging For Nondestructive Evaluation of Materials', *Materials Evaluation*, 1994, 54, 3, pp.412-415
- 2 BAKHTIARI, S., GOPALSAMI, N. and RAPTIS, A.C.: 'Characterisation of Delamination and Disbonding in Stratified Dielectric Composites by Millimeter Wave Imaging', *Materials Evaluation*, 1995, 53, 4, pp.468-471
- 3 ALABASTER, C.M., and DAHELE, J.S.: 'Free space measurement of permittivity', Proc. Int. Conf. on Antennas and Propagation, April 2003, Exeter, Vol. 2, pp. 538-541
- 4 ALABASTER, C.M.: 'Permittivity of Human Skin in the Millimetre Wave Band' IEE Electronics Letters (accepted)
- 5 MA, Z. and OKAMURA, S.: 'Permittivity determination using amplitudes of transmission and reflection coefficients at microwave frequency', *IEEE Trans. MTT*, 1999, 47, pp. 546-550
- 6 LÄHTEENMÄKI, J and KARTTAAVI, T.: 'Measurement of dielectric parameters of wall materials at 60GHz band', *Electronics Letters*, 1996, 32, pp. 1442-4
- 7 AFSAR, M.N., TKACHOV, I.I. and KOCHARYAN, K.N.: 'A Novel W-Band Spectrometer for Dielectric Measurements', *IEEE trans. MTT*, 2000, 48, 12, pp.2637-2643
- 8 SHIMABUKURO, F.I., LAZAR, S., CHERNICK, M.R. and DYSON, H.B.: 'A Quasi-Optical Method for Measuring the Complex Permittivity of Materials', *IEEE trans. MTT*, 1984, MTT-32, 7, pp.659-665

## Table and Figure captions

Table (i) Sample details

Table (ii) Samples 1 to 11 Ultra-Sound Tests & Permittivity Results

Table (iii) Sample 12 Permittivity Results

Figure 1 Ultra-Sound C-scan Images

(a) *Nominally ideal (samples 1 – 3)*, (b) *3 Joule Impact (sample 4)*, (c) *2 Joule Impact (sample 5)*, (d) *Improperly cured and early vacuum release (samples 6 – 11)*, (e) *Large sheet (sample 12)* and (f) *Close up of impact zone, sample 12*

*White = 100% transmittance (defect-free), Black = 0% transmittance (defect)*

Figure 2 Sample 12 ( $\bullet$  = measurement centre,  $\star$  = impact centre. All coordinates in mm.)

Table (i)

Sample #	Defect	Composition
1, 2, 3	None – used as control	Fibredux 916G Woven 10 layers 125mm discs
4	3 Joule impact in centre	
5	2 Joule impact in centre	
6, 7, 8	Incompletely cured	
9, 10, 11	Vacuum released during cure	500 x 250mm sheet
12	Initially none then 2 Joule impact	

Table (ii)

Sample #	Ultra-sound	Permittivity
1	No defects	$3.78 - j0.086$
2	No defects	$3.78 - j0.093$
3	No defects	$3.76 - j0.099$
4	Small star shaped delamination in centre	No solution
5	Large star shaped delamination in centre	No solution
6	Defect over entire surface	$3.61 - j0.074$
7	Defect over entire surface	$3.57 - j0.130$
8	Defect over entire surface	$3.37 - j0.109$
9	Defect over entire surface	$3.20 - j0.047$
10	Defect over entire surface	$3.21 - j0.065$
11	Defect over entire surface	$3.27 - j0.053$

Table (iii)

Location (x,y in mm)	Permittivity (before damage)	Permittivity (after damage)
62.5, 62.5	$3.80 - j0.115$	$3.90 - j0.131$
85, 62.5 40mm left of impact	$3.85 - j0.103$	$3.89 - j0.138$
105, 62.5 20mm left of impact	$3.85 - j0.100$	$3.95 - j0.127$
115, 62.5 10mm left of impact	No reading	$3.89 - j0.138$
125, 62.5 impact site	$3.84 - j0.084$	No solution
135, 62.5 10mm right of impact	No reading	$3.86 - j0.127$
145, 62.5 20mm right of impact	$3.81 - j0.088$	$3.86 - j0.134$
165, 62.5 40mm right of impact	$3.73 - j0.078$	$3.83 - j0.104$
187.5, 62.5	$3.70 - j0.120$	$3.73 - j0.144$
250, 62.5	$3.75 - j0.088$	No Measurements Necessary (too remote from impact site)
312.5, 62.5	$3.82 - j0.091$	
375, 62.5	$3.74 - j0.103$	
437.5, 62.5	$3.77 - 0.097$	
62.5, 187.5	$3.76 - j0.102$	
125, 187.5	$3.77 - j0.103$	
187.5, 187.5	$3.76 - j0.096$	
250, 187.5	$3.77 - j0.104$	
312.5, 187.5	$3.72 - j0.112$	
375, 187.5	$3.73 - j0.103$	
437.5, 187.5	$3.69 - j0.096$	

Figure 1

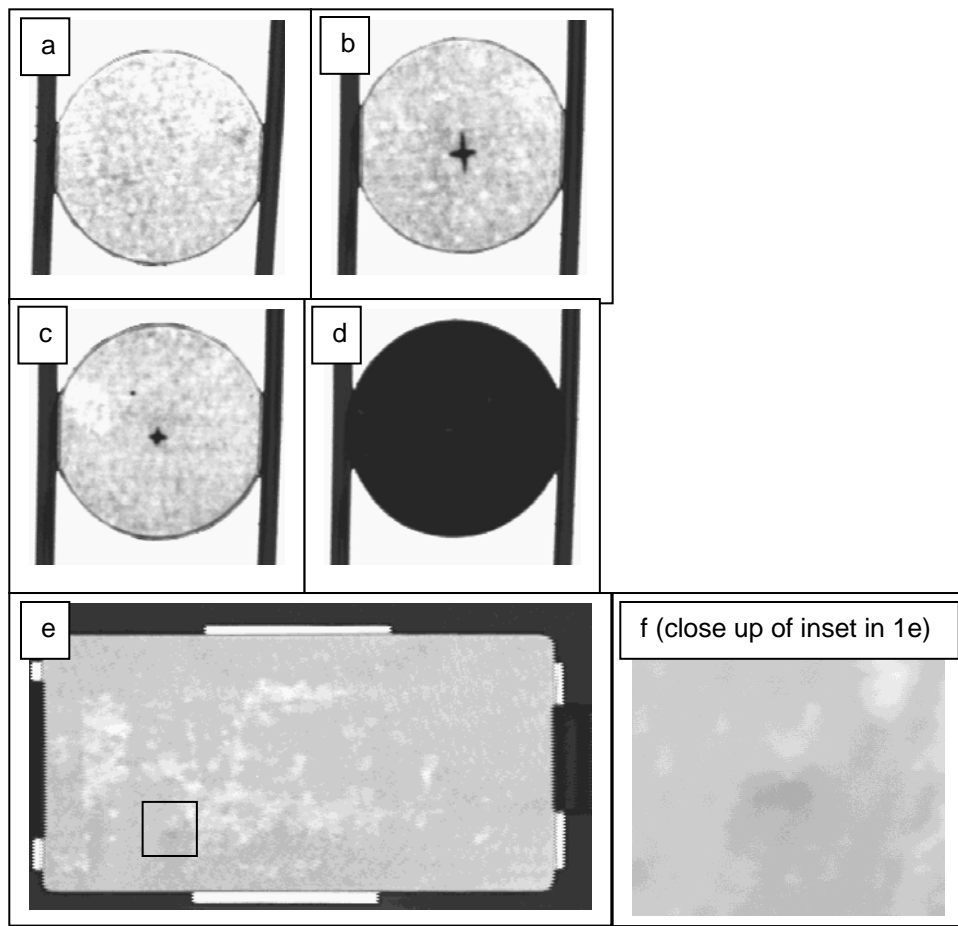
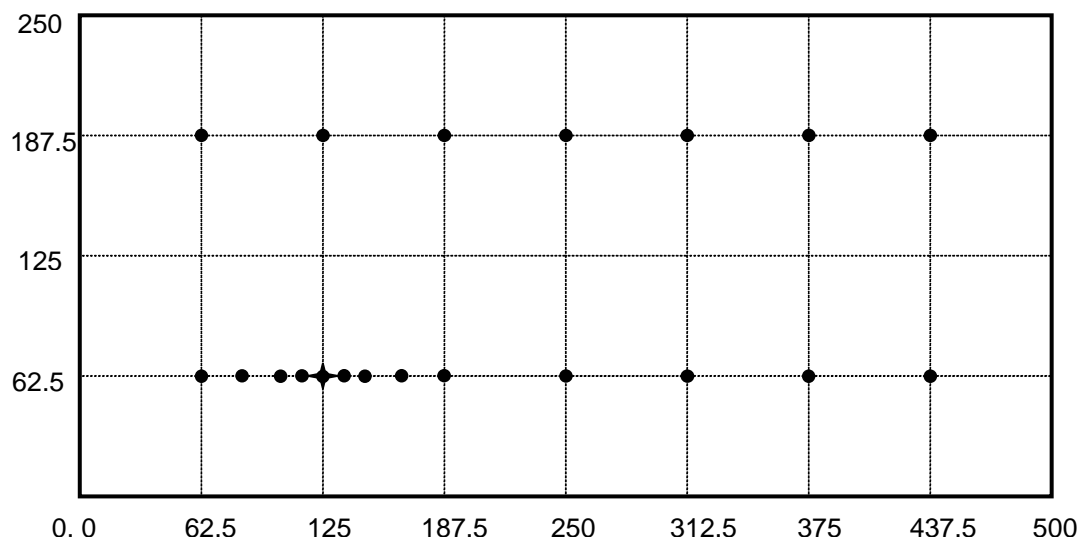


Figure 2



**APPENDIX B: UNPUBLISHED REPORTS**

The following reports have been written and are reproduced here:

ALABASTER, C.M.: 'Final Report on Permittivity Measurements of Soil at Hurn and Barnsfield Heath Test Sites' Final report to DSTL under contract ZAA002E

ALABASTER, C.M.: 'Further work since M.Phil to PhD Transfer' Cranfield University internal distribution. Extracts from.

THIS PAGE INTENTIONALLY LEFT BLANK



**FINAL REPORT ON PERMITTIVITY MEASUREMENTS  
OF SOIL AT HURN AND BARNSFIELD HEATH TEST  
SITES.**

By:

**Clive Alabaster**

Department of Aerospace, Power & Sensors  
Cranfield University  
RMCS Shrivenham

**Abstract**

This is the final report on measurements made on the permittivity of soil in situ at two trials sites in support of de-mining including ground penetrating radar equipment over two one week periods. The measurements were made in the top soil of pre-prepared tracks using the coaxial probe technique over the band 100MHz to 5GHz. The measurement method, data processing and validation techniques are briefly described and indicate that the method is accurate and reliable. The lists of permittivity results show large variations associated with varying weather conditions and smaller variations associated with position, spatial averaging and depth.

**Contents**

SECTION	PAGE
1 Introduction	1
2 Requirements	1 – 2
3 Measurement theory and technique	3 – 4
4 Validation	4 – 6
5 Results	6 – 17
6 Conclusions	18
Acknowledgments	19
References	19

## 1 Introduction

This report provides a brief description of the measurements of the permittivity of the soil in-situ at two QinetiQ trials sites and summarises the results. The measurements were made at Hurn and Barnsfield Heath over two one week periods to coincide with trials of de-mining equipment, including ground penetrating radar (GPR). This work was conducted as part of a contract with DSTL to enable them to judge the performance of the GPR.

The complex relative permittivity of the soil was measured using the coaxial probe technique over the band 100MHz to 5GHz. This technique was validated through a comparison of sample results obtained by the perturbation of a resonant cavity technique and by measurement of de-ionised water, whose permittivity is well known.

The second section of this report summarises the requirement from DSTL. Section three briefly describes the coaxial probe measurement theory and technique. The forth section gives details of the validation technique and of the experimental accuracy obtained. Section five summarises the results and finally there are the conclusions.

## 2 Requirements

The requirement is to provide the following data on the soil at various locations along pre-prepared tracks at Hurn (H) and Barnsfield Heath (B):

- Permittivity ( $\epsilon$ ),
- Loss tangent ( $\tan\delta$ ),
- Conductivity ( $\sigma$ ),
- Permeability ( $\mu$ ).

This data is required over the frequency band 100MHz to 5GHz and should ideally be made in-situ. It was agreed with DSTL personnel prior to the trials to provide data at the spot frequencies of 100MHz, 500MHz, 1GHz, 3GHz and 5GHz.

As a result of the geophysical survey conducted out by the National Soil Research Institute (NSRI), Cranfield University, Silsoe, over the 16<sup>th</sup> and 17<sup>th</sup> April 2002 it was found that there was a negligibly small amount of magnetic material in the soil. It was therefore concluded that the relative permeability of the soil would be close to one ( $\mu_r = 1$ ) and no measurements of it were made.

### 3 Measurement Theory & Technique

The permittivity of a dielectric,  $\epsilon$ , is often referenced to that of free space,  $\epsilon_0$ , by:

$$\epsilon = \epsilon_0 \epsilon_r \quad (1)$$

where  $\epsilon_0 \sim 8.85 \times 10^{-12}$  F/m and  $\epsilon_r$  is the relative permittivity of the dielectric.

(Relative) permittivity is a complex quantity whereby:

$$\epsilon_r = \epsilon'_r + j\epsilon''_r \quad (2)$$

where  $\epsilon'_r$  is the real part of the relative permittivity and is greater than one,

and  $\epsilon''_r$  is the imaginary part of the permittivity and is less than zero.

The loss tangent is defined as:

$$\tan \delta = \frac{\epsilon''_r}{\epsilon'_r} \quad (3)$$

The conductivity of a lossy dielectric is given by:

$$\sigma = \omega \epsilon_0 \epsilon''_r \quad (4)$$

where  $\omega$  is the angular frequency ( $= 2\pi f$ ) and  $f$  is frequency.

A measurement of the complex relative permittivity at a known frequency therefore yields all the data required.

The impedance,  $Z$ , or its inverse, admittance  $Y$  ( $= 1/Z$ ), at the open end of a coaxial probe terminated in a dielectric medium is a function of its permittivity. For a semi-infinite half space of the medium with an infinite ground plane extending from the coaxial cable, as depicted in figure 1, and assuming the presence of only the principal mode fields at the opening, the aperture admittance is given by<sup>[1]</sup>:

$$Y = \frac{2jk^2}{\omega\mu_0 \left[ \ln\left(\frac{b}{a}\right) \right]^2} \int_a^b \int_a^b \int_0^\pi \cos(\phi') \frac{\exp(-jkr)}{r} d\phi' d\rho' d\rho \quad (5)$$

where  $k = \omega\sqrt{\mu_0\epsilon_0\epsilon_r'(1 - j\tan\delta)}$  and is the propagation constant of the medium,

$$r = \sqrt{\rho^2 + \rho'^2 - 2\rho\rho' \cos(\phi')}$$

$a$  is the radius of the inner conductor of the coaxial probe,

$b$  is the inner radius of the outer conductor of the coaxial probe

$\mu_0$  is the permeability of free space ( $= 4\pi \times 10^{-7}$  H/m)

$r$ ,  $\varphi$  and  $z$  are cylindrical coordinates with the primed coordinates representing the source point and the unprimed coordinates representing field points. In practice the absence of the ground plane (and the embedding of the open probe tip into the medium) has negligible effect on the admittance<sup>[1]</sup>.

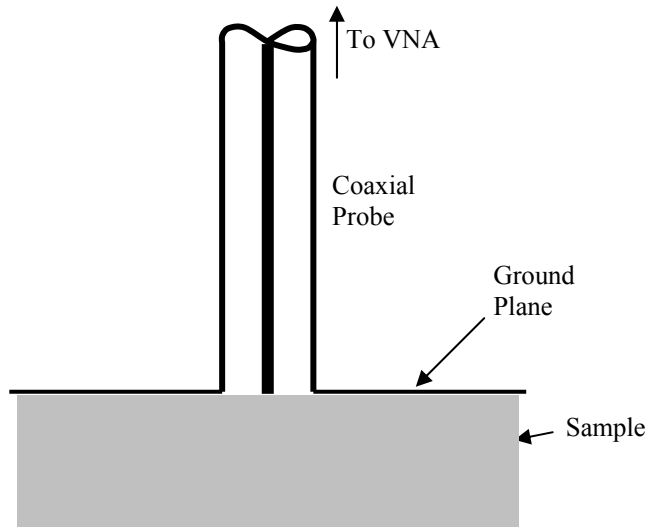


Figure 1: Probe Configuration

The probe was manufactured from 141 semi-rigid microwave coaxial cable having a length of 30cm, a characteristic impedance of  $50\Omega$ ,  $a = 0.4572\text{mm}$  and  $b = 1.4478\text{mm}$ . No extended ground plane was used to facilitate the insertion of the probe into the soil. The impedance at the tip was determined by a measurement of the reflection coefficient using a HP8719C vector network analyzer (VNA). The measurements were calibrated at the probe tip with respect to a short circuit provided by soldering a thin copper sheet across the aperture. The calibration accuracy was checked after each set of measurements by replacing the short circuit and ensuring that the magnitude and phase of the reflection coefficient had been maintained. The measured impedance data was then processed off-line using a MATLAB program to solve equation (5) so as to yield the complex relative permittivity of the soil medium. The processing approximated the volume integration of (5) with a discrete summation process and utilized a two stage optimization process to find the correct permittivity. The first stage was based on a simple genetic algorithm operating over 10 generations. This then passed its best solution to a gradient optimizer to refine the solution which was output as the result.

#### **4 Validation**

The sources of measurement error are listed below:

- Sweep to sweep fluctuations in the VNA readings,
- Maintenance of the calibration accuracy,
- Systematic errors in the processing of the measured data.

The sweep to sweep variations were minimized by setting the VNA display to take 32 video averages. Nevertheless some variation in the measured impedance was still observed; the greatest variation being at high values of Z, which occurred at the lower frequencies. Repeated readings on one set of soil data indicated a variation in the real part of Z ranging from  $\pm 8.3\%$  at 100MHz to  $\pm 2.6\%$  at 5GHz and a variation in the imaginary part of Z from  $\pm 3.7\%$  at 100MHz to  $\pm 1.5\%$  at 5GHz.

Calibration inaccuracies arise from the VNA drift and bending/distortion of the cables and probe. The checking procedure after each set of measurements indicated maximum typical errors in the magnitude of the reflection coefficient ranging from 0dB at 100MHz to 0.015dB at 5GHz. Similarly, maximum typical errors in the phase of the

reflection coefficient ranged from  $0.01^0$  at 100MHz to around  $1^0$  or less at 5GHz. This results in additional errors at 5GHz of  $\pm 2.1\%$  in the real part of Z and  $\pm 1.8\%$  in the imaginary part of Z.

The total variation in Z yields the following uncertainty in computing the relative permittivity:

$$\varepsilon_r' : \pm 3.7\% \text{ at 100MHz to } \pm 3.2\% \text{ at 5GHz}$$

$$\varepsilon_r'' : \pm 2.1\% \text{ at 100MHz to } \pm 0.2\% \text{ at 5GHz}$$

Systematic errors in the processing arise from the approximation of the integration using the summation process and from the fact that repeated runs of the optimization yield subtly different solutions. The probe technique and data processing was validated through a measurement on de-ionised water, whose permittivity at 3GHz is quoted variously between  $76.7 - j12.04$  and  $77 - j11.55$ . Repeated processing of the data from the water measurement at 3GHz found solutions which differed by less than 0.1% in both  $\varepsilon_r'$  and  $\varepsilon_r''$ . This is negligibly small. Readings made on water at 3GHz yielded the results  $\varepsilon_r = 77.7 - j11.47$  and  $77.6 - j10.92$ . Due to the near coincidence of these readings with the published results it was concluded that the method was reliable and repeatable and that the most significant sources of error remain those due to the variation in measured impedance and are quantified above.

In addition to the above, a sample of the top soil sand from between tracks 1 and 2 at Barnsfield Heath was recovered on the 17<sup>th</sup> April 2002 for lab analysis. A single measurement of its relative permittivity was made using the perturbation of a resonant cavity method and found to be:

$$\varepsilon_r' : 7.88 \text{ (6.60 to 9.26)}$$

$$\varepsilon_r'' : 0.43 \text{ (0.36 to 0.50)}$$

The figures in brackets indicate the range of experimental uncertainty in the result. This data is in close agreement with that of test 30 (see results section), which was made at the same site in July in similarly dry conditions. It should be appreciated that differences are expected due to the varying moisture percentage in the samples of the

two measurements (which is unknown) and the differing compaction of an extracted sample from the soil in-situ.

## 5 Results

The permittivity results from the two trials weeks are summarized on the following pages. Some notes of explanation are given below.

Location code: B = Barnsfield Heath, H = Hurn. The number which follows indicates the track number. Most measurements were taken in the gaps between tracks, thus for example H1-H2 means in the gap between tracks 1 and 2 at the Hurn site. In certain cases repeated measurements were made in order to establish the repeatability of the data, its spatial variation over a localized area or to obtain a depth profile of changes.

Depth: This was limited to around 3cm at Hurn due to the nature of the flint gravel track and to around 15cm at Barnsfield Heath due to the hardness of the compacted sand. All measurements are therefore limited to the top soil layer.

**FIRST TRIAL WEEK May-02**

<b>TEST</b>	1	4	7
DATE	20.5.02	21.5.02	23.5.02
TIME	am	am	pm
LOCATION	H1-H2	H2-H3	B1-B2
DEPTH	3cm	3cm	5cm
NOTES	Trial only.	As for test 3, very damp locally.	First in series of measurements to determine depth profile.
<b>FREQ</b>	<b>Relative Permittivity</b>	<b>Relative Permittivity</b>	<b>Relative Permittivity</b>
100MHz	15.99 - j1.82	19.96 - j3.44	11.12 - j1.16
500MHz	13.52 - j1.56	19.44 - j1.85	12.17 - j1.00
1GHz	13.53 - j1.43	19.67 - j1.88	12.66 - j1.20
3GHz	12.63 - j1.61	18.29 - j2.58	11.50 - j1.51
5GHz	9.04 - j1.22	13.49 - j2.15	8.18 - j1.05
<b>TEST</b>	2	5	8
DATE	20.5.02	22.5.02	23.5.02
TIME	pm	am	pm
LOCATION	B1-B2	B1-B2	B1-B2
DEPTH	15cm	15cm	10cm
NOTES	Trial only.	More overnight rain, drier locally.	Second in series of measurements to determine depth profile.
<b>FREQ</b>	<b>Relative Permittivity</b>	<b>Relative Permittivity</b>	<b>Relative Permittivity</b>
100MHz	13.22 - j2.54	27.61 - j3.52	10.14 - j1.12
500MHz	15.93 - j1.08	26.20 - j1.80	11.27 - j0.99
1GHz	16.47 - j1.03	26.22 - j2.11	11.91 - 1.14
3GHz	15.59 - j1.74	24.29 - j3.33	10.83 - j1.32
5GHz	12.04 - j1.42	18.28 - j3.02	7.66 - j0.83
<b>TEST</b>	3	6	9
DATE	21.5.02	22.5.02	23.5.02
TIME	am	Immediately after test 5. B1-B2 a few cm from test 5.	pm
LOCATION	H1-H2		B1-B2
DEPTH	3cm	15cm	15cm
NOTES	Overnight rain and damp.	Repetition of test 5 for repeatability check.	Third in series of measurements to determine depth profile.
<b>FREQ</b>	<b>Relative Permittivity</b>	<b>Relative Permittivity</b>	<b>Relative Permittivity</b>
100MHz	22.53 - j7.40	23.44 - j3.26	9.55 - j0.88
500MHz	21.07 - j2.94	22.71 - j1.64	10.54 - j1.01
1GHz	20.96 - j2.48	22.77 - j1.81	11.23 - j1.11
3GHz	19.35 - j3.01	21.16 - j2.88	10.17 - j1.25
5GHz	14.29 - j2.57	15.95 - j2.58	7.13 - j0.73

**FIRST TRIAL WEEK May-02**

<b>TEST</b>	10	13
DATE	23.5.02	24.5.02
TIME	pm	am
LOCATION	B1-B2	Hurn test track
DEPTH	18cm (max. depth possible.) Forth in series of measurements to determine depth profile.	3cm
NOTES		Repeat of above a few cm offset.
<b>FREQ</b>	<b>Relative Permittivity</b>	<b>Relative Permittivity</b>
100MHz	8.10 - j1.22	21.08 - j3.04
500MHz	9.48 - j1.02	21.29 - j1.66
1GHz	10.26 - j1.10	21.90 - j1.90
3GHz	9.16 - j1.21	19.98 - j3.09
5GHz	6.32 - j0.69	14.96 - j2.79
<b>TEST</b>	11	14
DATE	23.5.02	24.5.02
TIME	am	pm
LOCATION	B1-B2	H1-H2
DEPTH	15cm	3cm
NOTES	More overnight rain, very wet.	
<b>FREQ</b>	<b>Relative Permittivity</b>	<b>Relative Permittivity</b>
100MHz	24.42 - j2.37	14.24 - j2.09
500MHz	24.75 - j1.60	14.29 - j1.35
1GHz	25.10 - j2.06	14.83 - j1.45
3GHz	23.05 - j3.52	13.33 - j1.80
5GHz	17.39 - j3.38	9.46 - j1.32
<b>TEST</b>	12	15
DATE	24.5.02	24.5.02
TIME	am	pm
LOCATION	Hurn test track	H2-H3
DEPTH	3cm	3cm
NOTES	More overnight rain, very wet ground but drying quickly. Sample recovered.	Very wet locally
<b>FREQ</b>	<b>Relative Permittivity</b>	<b>Relative Permittivity</b>
100MHz	12.56 - j1.61	17.15 - j2.75
500MHz	13.60 - j1.25	17.26 - j1.62
1GHz	14.32 - j1.38	17.81 - j1.81
3GHz	13.05 - j1.98	16.24 - j2.48
5GHz	9.30 - j1.61	11.86 - j2.11

**SECOND TRIAL WEEK July-02**

<b>TEST</b>	16	19
DATE	8.7.02	9.7.02
TIME	11:45	11:15
LOCATION	H6-H7	B5-B6
DEPTH	3cm	15cm
NOTES	Damp, heavy recent rain, light rain during test.	Very wet, recent heavy rain, lots of standing water nearby. First in series of measurements to determine depth profile.
<b>FREQ</b>	<b>Relative Permittivity</b>	<b>Relative Permittivity</b>
100MHz	44.36 - j4.10	28.26 - j5.34
500MHz	42.21 - j2.49	25.67 - j2.40
1GHz	42.23 - j2.78	26.01 - j2.18
3GHz	38.32 - j5.16	23.61 - j3.27
5GHz	31.11 - j5.33	19.38 - j3.33
<b>TEST</b>	17	20
DATE	8.7.02	9.7.02
TIME	16:45	11:15
LOCATION	H1-H2	B5-B6
DEPTH	3cm	5cm
NOTES	Very wet, raining.	Very wet, recent heavy rain, lots of standing water nearby. Second in series of measurements to determine depth profile.
<b>FREQ</b>	<b>Relative Permittivity</b>	<b>Relative Permittivity</b>
100MHz	36.97 - j7.10	33.20 - j4.00
500MHz	33.69 - j3.19	30.79 - j2.23
1GHz	33.67 - j2.88	31.08 - j2.34
3GHz	30.56 - j4.08	28.18 - j3.93
5GHz	24.87 - j4.26	23.09 - j4.12
<b>TEST</b>	18	21
DATE	8.7.02	9.7.02
TIME	17:40	12:00
LOCATION	H2-H3	B6-B7
DEPTH	3cm	15cm
NOTES	Very wet, slight rain.	Very wet
<b>FREQ</b>	<b>Relative Permittivity</b>	<b>Relative Permittivity</b>
100MHz	32.52 - j5.03	30.38 - j3.22
500MHz	29.52 - j2.45	28.53 - j1.84
1GHz	29.74 - j2.42	29.02 - j2.07
3GHz	26.94 - j3.52	26.53 - j3.51
5GHz	22.05 - j3.57	22.05 - j3.69

**SECOND TRIAL WEEK July-02**

<b>TEST</b>	22	25
DATE	9.7.02	11.7.02
TIME	15:05	10:15
LOCATION	B1-B2	H6-H7
DEPTH	15cm	1cm
NOTES	Very wet on surface, beginning to dry. First of three measurements in close proximity (10cm).	Dry. First of three measurements in close proximity (10cm).
<b>FREQ</b>	<b>Relative Permittivity</b>	<b>Relative Permittivity</b>
100MHz	24.68 - j1.89	30.89 - j6.05
500MHz	23.45 - j1.72	26.11 - j2.59
1GHz	23.95 - j1.68	25.72 - j2.23
3GHz	21.89 - j2.66	23.86 - j2.99
5GHz	18.03 - j2.61	19.58 - j3.11
<b>TEST</b>	23	26
DATE	9.7.02	11.7.02
TIME	15:10	11:20
LOCATION	B1-B2	H6-H7
DEPTH	15cm	1cm
NOTES	Very wet on surface, beginning to dry. Second of three measurements in close proximity.	Dry. Second of three measurements in close proximity (10cm).
<b>FREQ</b>	<b>Relative Permittivity</b>	<b>Relative Permittivity</b>
100MHz	26.86 - j1.73	24.55 - j4.71
500MHz	25.77 - j1.78	20.12 - j2.13
1GHz	26.46 - j1.85	19.87 - j1.73
3GHz	24.23 - j3.03	18.72 - j2.34
5GHz	20.25 - j3.14	15.37 - j2.24
<b>TEST</b>	24	27
DATE	9.7.02	11.7.02
TIME	15:15	11:25
LOCATION	B1-B2	H6-H7
DEPTH	15cm	1cm
NOTES	Very wet on surface, beginning to dry. Third of three measurements in close proximity.	Dry. Third of three measurements in close proximity (10cm).
<b>FREQ</b>	<b>Relative Permittivity</b>	<b>Relative Permittivity</b>
100MHz	24.49 - j1.42	23.80 - j3.79
500MHz	22.25 - j1.54	19.38 - j1.87
1GHz	22.31 - j1.50	19.13 - j1.58
3GHz	20.39 - j2.22	18.00 - j2.23
5GHz	17.10 - j2.22	14.88 - j2.10

**SECOND TRIAL WEEK July-02**

<b>TEST</b>	28	31
DATE	11.7.02	12.7.02
TIME	13:20	11:10
LOCATION	H1-H2	B5-B6
DEPTH	2cm	12cm
NOTES	Dry.	Dry ground but light rain just started.
<b>FREQ</b>	<b>Relative Permittivity</b>	<b>Relative Permittivity</b>
100MHz	30.63 - j10.52	35.60 - j14.23
500MHz	23.99 - j4.21	32.40 - j4.53
1GHz	23.28 - j3.04	31.69 - j3.60
3GHz	21.96 - j2.98	29.41 - j4.31
5GHz	18.19 - j2.76	23.76 - j4.02
<b>TEST</b>	29	32
DATE	11.7.02	12.7.02
TIME	15:00	11:30
LOCATION	H2-H3	B6-B7
DEPTH	2cm	10cm
NOTES	Dry.	Dry ground with light rain.
<b>FREQ</b>	<b>Relative Permittivity</b>	<b>Relative Permittivity</b>
100MHz	17.71 - j2.59	12.06 - j2.84
500MHz	13.97 - j1.71	11.37 - j1.16
1GHz	13.98 - j1.38	11.10 - j1.10
3GHz	13.34 - j1.44	10.94 - j1.10
5GHz	11.28 - 1.26	9.26 - j0.80
<b>TEST</b>	30	33
DATE	12.7.02	12.7.02
TIME	10:10	12:00
LOCATION	B1-B2	B6-B7
DEPTH	15cm	10cm
NOTES	Dry.	Dry ground with light rain. Repeat of previous results offset a few cm away.
<b>FREQ</b>	<b>Relative Permittivity</b>	<b>Relative Permittivity</b>
100MHz	11.36 - j3.94	16.21 - j3.69
500MHz	7.95 - 1.37	15.19 - j1.56
1GHz	8.19 - 1.05	14.77 - j1.41
3GHz	8.20 - j0.76	14.29 - j1.66
5GHz	6.73 - j0.39	11.93 - j1.43

## 6 Conclusions

The following observations can be made from a comparison of the tests:

(i) Effects of rain water.

The wet conditions have caused a significant increase in the permittivity of the top soil. Comparisons between tests 1 and 3 and tests 2 and 5 indicate the effect of overnight rain. The very wet conditions early in the second trial week have given rise to permittivity readings about twice those of corresponding readings taken in drier conditions.

(ii) Variations between tracks.

On the whole the permittivity of the flint gravel of the Hurn track soil is slightly higher than that of the sandy Barnsfield Heath tracks.

(iii) Local variations.

Comparisons between tests 22 to 24 and tests 25 to 27 indicate the variations within a 10cm diameter at the Barnsfield Heath and Hurn sites respectively. The Barnsfield Heath tracks are marginally more homogenous than those at Hurn.

(iv) Depth profile.

Tests 7 to 10 give a profile of changes over depths of 5 to 18cm at Barnsfield Heath. This data indicates a steady reduction in permittivity with increasing depth, probably due to the reducing moisture content at depth.

## Acknowledgements

My thanks go to my colleague, Dr Evan Hughes, for his invaluable assistance with the programs used to process the results. I am also indebted to Prof. J. Dahele for his help and advice.

**References**

- 1 Devendra\_MK, Eungdamrong\_D "Coaxial aperture electrical sensor and its application – a tutorial overview" The 2001 IEEE International symposium on circuits and systems 6-9 May 2001 Sydney, NSW Australia, Vol. 2 p 449-452.

**FURTHER WORK SINCE M.PHIL. TO PH.D. TRANSFER**  
**(EXTRACTS FROM)**

*C.M. Alabaster, Dept. Aerospace, Power & Sensors, Cranfield University,  
RMCS Shrivenham.*

### Introduction

Work has continued with the measurement of the permittivity of dielectrics using the perturbation of a resonant cavity technique described within the transfer report. The aim of this work has been to:

- improve the experimental accuracy and
- correctly measure the permittivity of a liquid sample accommodated within a tube or capillary made from a second dielectric whose influence cannot be ignored.

This progress report provides a technical update of the work in the two areas described above together with test results from the experimental work.

### Improved Accuracy

The experimental accuracy has been improved through a combination of the use of an alternative network analyser (the HP8752C) and a more accurate determination of the sample volumes. In the measurements reported within the transfer report an experimental accuracy of between 5% and 14% at 3GHz was achieved. The major contribution to the error was identified as being the tolerance on the perturbed frequency,  $\delta f$ . This was quoted as  $\pm 100\text{kHz}$  which was set by the frequency resolution of the HP8719C vector network analyser used. The HP8752C network analyser has a much finer frequency resolution of  $(\text{span})/10000$  or 500Hz for a span of 5MHz. However, it is limited in that its upper frequency of operation is only 3GHz. In reality this does not pose difficulties for the present work, since the highest frequency cavity used is resonant at just under 3GHz. It is unlikely that higher frequency cavities will be used since they become too small to be feasible. The use of the HP8752C now means that the accuracy of the measurement of  $\delta f$  is determined by the response width and not the analyser. Recall that for rectangular cavities operating in the  $\text{TE}_{101}$  mode which are perturbed by a sample of dielectric in the centre of the cavity:

$$\varepsilon'_r = 1 + \frac{\delta f \cdot V_{cav}}{2f_0 V_{sam}} \quad (1)$$

where  $\delta f$  is the perturbation in the resonant frequency of the cavity

$V_{cav}$  is the cavity volume

$V_{sam}$  is the sample volume

and  $f_0$  is the unperturbed resonant frequency of the cavity.

Initial measurements of permittivity were accurate to 6 to 8% but this has been subsequently refined to between 1.5 and 3.5% typically. The subsequent improvements have been brought about by more accurate measurements of the sample dimensions and

hence their volumes,  $V_{sam}$ . A more thorough indication of the experimental tolerances is included within the results section of this report.

Since the lack of frequency resolution was identified as being the limitation preventing the measurement of the loss factor,  $\epsilon_r''$ , it should now be possible to proceed with these measurements. Recall also that:

$$\epsilon_r'' = \frac{V_{cav}}{4V_{sam}} \left( \frac{1}{Q_{0m}} - \frac{1}{Q_{0c}} \right) \quad (2)$$

where  $Q_{0m}$  is the unloaded Q-factor of the perturbed cavity  
and  $Q_{0c}$  is the unloaded Q-factor of the unperturbed cavity.

As can be seen from (2), the measurement of  $\epsilon_r''$  entails the measurement of the unloaded Q-factor of the unperturbed and perturbed cavity. This could not be achieved with any meaningful accuracy due to the lack of frequency resolution of the HP8719C. The unloaded Q-factor of cavity #3, whose unperturbed resonant frequency is nominally 2996MHz, has been measured at 4439 using the HP8752C network analyser. This compares well with the calculation of 4770 provided within the transfer report. Although no measurements of  $\epsilon_r''$  have yet been made, such measurements are now feasible with an experimental tolerance estimated to be less than 10%.

### Measurements of samples in tubes

During work conducted and reported on in the transfer report, there were significant difficulties in achieving accurate results on liquid (often de-ionised water) samples. The difficulty arose since the liquid must be contained in some tube or capillary, whose volume was not insignificant compared with the volume of liquid. These measurements were based on the calculation of  $\epsilon_r'$  which assumed that the sample volume,  $V_{sam}$  equalled that of the liquid and not of the liquid plus container. Furthermore, it was assumed that the perturbation in the resonant frequency of the cavity was due entirely to the liquid sample (and not influenced by the container). However, experience showed that the effects of the container could not be ignored.

Initially, attempts were made to minimise the effects of the container by containing the liquid in PTFE and polyethylene capillaries since the relative permittivities of these materials (2.06 and 2.25 respectively) are somewhat lower than that of the glass (nominally 4) used previously. This was unsuccessful. There were several practical difficulties in performing the measurements as it was very awkward to introduce water into these capillaries and then to glue them to the sample plug. Water is not drawn into a PTFE or polyethylene capillary in the same way as it is with glass ones. In spite of this, the results indicated that large errors were apparent and that the capillary could not be neglected.

Measurements on de-ionised water samples which partially filled a polyethylene capillary returned results for  $\epsilon_r'$  which could be above, below or in very close agreement with, the published value of 76.7, depending on the extent to which the capillary was filled.

The measurement of the permittivity of a liquid sample in a capillary returns a result which is the effective permittivity of two or more dielectrics i.e. the sample liquid, the capillary material and, possibly, the air filling the capillary above the liquid surface in a partially filled capillary. The solution to the problem entailed resolving the permittivity of the sample from the measurement of the effective value of the two (or more) dielectrics and knowledge of the other dielectrics. From some initial results it was noticed that the effective permittivity appeared to be close to the weighted volumetric average of the various dielectrics, where:

$$\text{Weighted volumetric average permittivity} = \left( \frac{V_1}{V_T} \epsilon_1 \right) + \left( \frac{V_2}{V_T} \epsilon_2 \right) + \dots \quad (3)$$

where  $\epsilon_1$  and  $\epsilon_2$  are the permittivities of dielectrics 1 and 2 respectively, and  $V_1$  and  $V_2$  are the volumes of dielectrics 1 and 2 respectively and  $V_T$  is the total volume of all dielectrics.

The geometry of the problem is illustrated in figure 1.

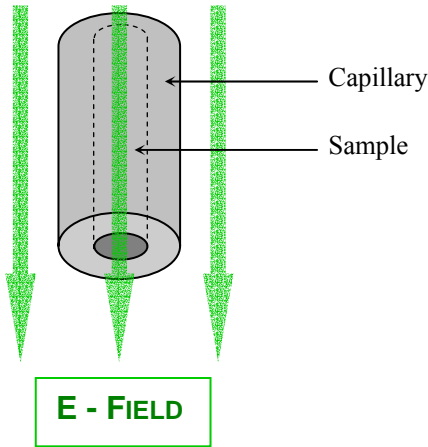


Figure 1

Previous attempts to measure the permittivity of liquid samples using the perturbation of a resonant cavity technique such as Rzepecka, 1973 [1] have neglected the effects of two coaxial teflon tubes surrounding the sample and still quote only a 2% error in  $\epsilon_r'$  and a 5% error in  $\epsilon_r''$  at 2450MHz! Other measurements of permittivity reported in the literature [2, 3] neglect the effects of a plug of dielectric material used to contain the sample but acknowledge that it is the source of experimental errors.

From an analysis of the problem it has been determined that the effective permittivity of a solid cylinder of dielectric surrounded by an annulus of a second dielectric of the same length when exposed to a uniform E field which is perpendicular to the axis of the samples is given by:

$$\epsilon_{eff} = \left( \frac{r_1}{r_2} \right)^2 (\epsilon_1 - \epsilon_2) + \epsilon_2 \quad (4)$$

where  $\epsilon_{eff}$  is the effective permittivity of the two media  
 $\epsilon_1$  is the permittivity of the inner dielectric  
 $\epsilon_2$  is the permittivity of the outer dielectric  
 $r_1$  is the radius of the inner dielectric (or the inner radius of outer dielectric)  
and  $r_2$  is the outer radius of the outer dielectric.

The annex at the end of this report derive this equation and indicates how the effective permittivity for other dielectric structures, E-field orientations and numbers of dielectrics may be determined. (4) is a specific form of Weiner's mixed dielectric equations (Weiner, 1912<sup>[4]</sup>), which are also described in the Annex, in the form used by Campbell and Land<sup>[5]</sup>. Equation (4) does in fact amount to the weighted volumetric average of the two dielectrics.

Equation (4) neglects the following:

- fringing effects,
- the sine wave variation in E-field strength across the  $a$  and  $d$  dimensions of the cavity, i.e. it assumes a constant E-field. This is a valid approximation if  $r_2$  is very much less than the  $a$  and  $d$  dimensions of the cavity.

Conversely, equation (4) may be re-arranged to solve the permittivity of an unknown sample ( $\epsilon_1$ ) in terms of the known tube or capillary material ( $\epsilon_2$ ) and its inner and outer radii ( $r_1$  and  $r_2$ ) thus:

$$\epsilon_1 = \left( \frac{r_2}{r_1} \right)^2 (\epsilon_{eff} - \epsilon_2) - \epsilon_2 \quad (5)$$

Work has been on-going to provide experimental data to confirm the validity of equations 4 and 5. Measurements have been performed to measure the effective permittivity of de-ionised water samples contained in fused quartz and borosilicate glass capillaries at 2996MHz. Similarly, measurements have been made of the effective permittivity of air filled capillaries. Measurements have also been made on borosilicate glass samples contained in a sleeve of PTFE at the same frequency. The experimentally determined values of  $\epsilon_r'$  from equation (1) have been compared with the predictions from (4). The results are summarised in table 1.

It may also be worth noting that in (1) if  $V_{sam}$  = volume of outer dielectric, then the result for  $\epsilon_r'$  refers to the outer dielectric only whereas if  $V_{sam}$  = total volume of capillary and sample, then the result for  $\epsilon_r'$  refers to the effective permittivity of the sample and capillary.

## Results

Table 1 below summarises the most recent results having the best experimental tolerance.

Dielectric structure (see note 1)	Experimentally determined permittivity ± tol		Predicted effective permittivity from equation 4 ± tol		Percentage discrepancy
FQ only	3.82	3.46 %	3.78 (see note 2)		+ 1.06 %
BG only	4.49, 4.48, 4.47, 4.46 4.515	2.34 % 2.34 % 1.18 %	(see note 2)		
PTFE only	2.05	1.3 %	2.06 (see note 2)		- 0.5 %
FQ capillary air filled.	3.188	2.53 %	3.158	1.48 %	+ 0.95 %
FQ capillary water filled.	19.40 19.74 (see note 3)	3.1 % 2.5 %	20.107	1.48 %	- 3.52 % - 1.84 %
PTFE sleeve with air inner.	1.94	1.23 %	1.95	1.53 %	- 0.5 %
PTFE sleeve with BG inner.	2.294	1.42 %	2.316	2.64 %	- 0.95 %

### Notes

- 1 FQ = Fused Quartz.  
BG = Borosilicate Glass.  
PE = Polyethylene.

- 1  $\epsilon_r'$  for fused quartz at 3GHz is given as 3.78 in data tables.  
 $\epsilon_r'$  for PTFE at 3GHz is given as 2.06 in data tables.  
 $\epsilon_r'$  for borosilicate glass at 3GHz is given as 4.05 in data tables, however,  
 $\epsilon_r'$  for soda borosilicate glass at 3GHz is given as 4.82 in data tables.  
 Clearly there are various grades of borosilicate glass and the exact grade of the samples used was not known.
- 2 These results have been used in equation (5) to provide estimates of the permittivity of the water sample. These results are:  $73.54 \pm 4.4\%$  and  $75.06 \pm 3.8\%$  respectively for the two readings and are some 4.1 % and 2.1 % respectively below the published value of 76.7.

### **Discussion/Conclusions**

- 1 Experimental tolerances of less than  $\pm 3.5\%$  can routinely be achieved and in many cases an accuracy of less than  $\pm 1.5\%$  is achieved. Factors limiting the accuracy of the measurement are now the Q-factor of the cavity and uncertainty in  $V_{\text{sam}}$ , together with the unaccounted effects listed in paragraph 5 below.
- 2 The measurement of the permittivity of a single solid dielectric is within approximately 1% of the published value in data tables.
- 3 The experimentally determined effective permittivity of two dielectrics differs from the value predicted from equation (4) by 3.52 % (worst case) and 1 % (typically).
- 4 The measurement of the effective permittivity of a water sample within a capillary has been used to determine the permittivity of just the water to an accuracy of around 4 %.
- 5 The remaining inaccuracy in results is thought to be due to:
  - the small volume of glue used to secure the samples to the sample plug,
  - slight misalignment of the sample such that the boundary between dielectrics runs parallel to the E-field and
  - the assumptions made in the formulation of equation 4 (i.e. neglect of fringing fields and non-uniformity of the E-field strength across the sample radius).

No assessment of these errors has been made. However, it may be noted that since all results are within the known experimental tolerance of previously published data that the unaccounted for errors may be assumed to be very small.

### Annex: The effective permittivity of layered dielectrics.

The permittivity of a dielectric is defined in terms of the capacitance of a capacitor in which the volume between its plates is filled with the dielectric in question. The effective permittivity of layered dielectrics immersed within an electric field can be derived by considering the dielectrics to be between the plates of a capacitor whose plates generate the an electric field in the desired orientation with respect to the dielectric boundaries. It is useful to note that any surface which runs perpendicular to the electric field can be considered as a conducting surface. This helps in establishing the geometry of the capacitor plates necessary to generate an electric field of the correct orientation.

The simplest case is of two plane layers in which the E-field is orientated at right angles to the boundary layer.

#### Case 1: Two plane layered dielectrics with orthogonal E-field

This case is illustrated in figure 2, below.

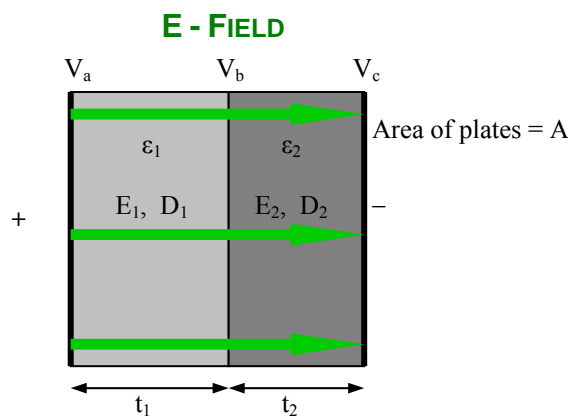


Figure 2

The lines of electric displacement are normal to the boundary and so from the boundary condition that the normal component of electric displacement is continuous across a boundary of dielectrics, we have:  $D_1 = D_2 = D$ .

In dielectric 1 (lhs)  $D = \epsilon_1 E_1$  and this must also equal  $\epsilon_2 E_2$  of dielectric 2 (rhs).

$$\text{Since } E_1 = \frac{V_a - V_b}{t_1} \text{ and } E_2 = \frac{V_b - V_c}{t_2}$$

and the potential difference between the plates,  $V = V_a - V_c$

it follows that

$$V = t_1 E_1 + t_2 E_2$$

$$= D[t_1/\epsilon_1 + t_2/\epsilon_2]$$

Since in general  $E = \frac{\sigma}{\epsilon}$

where  $\sigma$  is the surface charge density on the capacitor plates and  $D = \epsilon E$   
we have  $D = \sigma$ .

The total charge on the plates  $Q = A\sigma = AD$

$$\text{The capacitance of the capacitor is } C = \frac{Q}{V} = \frac{A}{\frac{t_1}{\epsilon_1} + \frac{t_2}{\epsilon_2}} \quad (6)$$

Since in general

$$C = \frac{\epsilon_{eff} A}{t} \quad (7)$$

where  $\epsilon_{eff}$  is the effective permittivity of the dielectric(s) between the plates  
and  $t$  is the separation between the plates i.e.  $t = t_1 + t_2$

Equating (6) and (7) gives:

$$\frac{\epsilon_{eff} A}{t_1 + t_2} = \frac{A}{\frac{t_1}{\epsilon_1} + \frac{t_2}{\epsilon_2}}$$

Therefore:

$$\epsilon_{eff} = \frac{t_1 \epsilon_1 \epsilon_2 + t_2 \epsilon_1 \epsilon_2}{t_1 \epsilon_2 + t_2 \epsilon_1} \quad (8)$$

If  $\epsilon_2 = 1$  (air) then (8) becomes:

$$\epsilon_{eff} = \frac{\epsilon_1 (t_1 + t_2)}{t_1 + \epsilon_1 t_2} \quad (9)$$

Equation (9) is consistent with the work of Lee, Ho and Dahele [6] which uses an expression for the effective permittivity of microstrip with a substrate formed from layers of dielectric material and air.

From (6) we can see that this capacitance is the series combination of a capacitor having plates of area,  $A$ , dielectric,  $\epsilon_1$ , and plate separation,  $t_1$ , with a capacitor having plates of area,  $A$ , dielectric,  $\epsilon_2$ , and plate separation,  $t_2$ , as illustrated in figure 3 below.

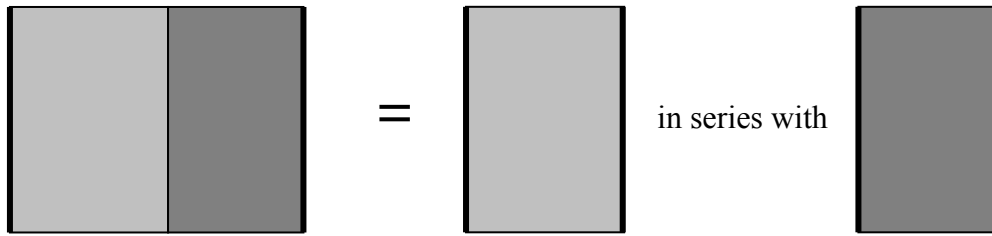


Figure 3

These concepts can now be extended to replicate the geometry of the dielectrics representing a sample inside a capillary.

### **Case 2: Two coaxially mounted cylindrical dielectric layers with radial E-field**

The case of the radial E-field is conveniently chosen since it corresponds to the field pattern generated by a coaxial capacitor *and* ensures that the E-field is normal to the boundary layer between the dielectrics. The dielectric geometry replicates that of a sample within a tube or capillary and is illustrated in figure 4 below.

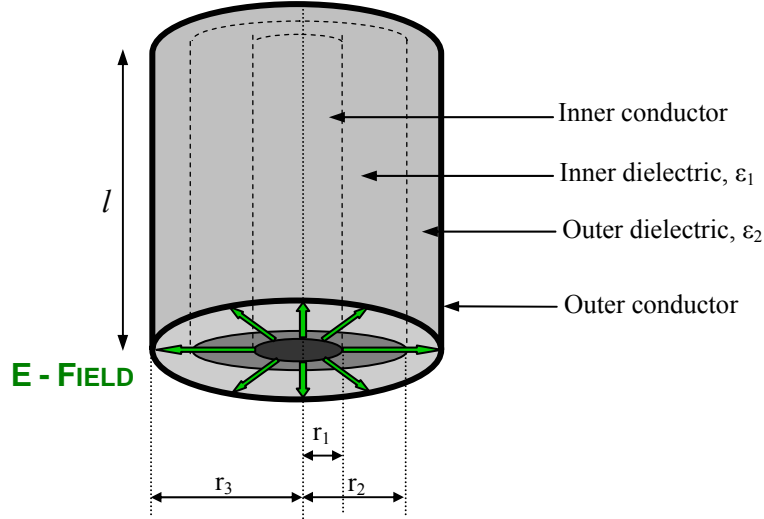


Figure 4

The general formula for the capacitance of a coaxial capacitor is given by:

$$C = \frac{2\pi\epsilon_{eff}l}{\log_e\left(\frac{r_3}{r_1}\right)} \quad (10)$$

Where  $r_1$  is the radius of the inner conductor and  $r_3$  is the radius of the outer conductor.

As before, since the E-field is perpendicular to the boundary between dielectrics, this capacitor can be thought of as being the series combination of a coaxial capacitor of inner conductor radius  $r_1$  and outer conductor of radius  $r_2$  with a second coaxial capacitor of inner conductor radius  $r_2$  and outer conductor of radius  $r_3$ .

Therefore 
$$C = \left( \frac{1}{C_1} + \frac{1}{C_2} \right)^{-1}$$

where 
$$C_1 = \frac{2\pi\epsilon_1 l}{\log_e\left(\frac{r_2}{r_1}\right)}$$
 and 
$$C_2 = \frac{2\pi\epsilon_2 l}{\log_e\left(\frac{r_3}{r_2}\right)}$$

This gives

$$C = \frac{2\pi\epsilon_1\epsilon_2}{\epsilon_2 \log_e\left(\frac{r_2}{r_1}\right) + \epsilon_1 \log_e\left(\frac{r_3}{r_2}\right)} \quad (11)$$

Equating (10) with (11) gives:

$$\epsilon_{eff} = \frac{\epsilon_1\epsilon_2 \log_e\left(\frac{r_3}{r_1}\right)}{\epsilon_2 \log_e\left(\frac{r_2}{r_1}\right) + \epsilon_1 \log_e\left(\frac{r_3}{r_2}\right)} \quad (12)$$

Whilst this case illustrates the correct geometry of the dielectrics, the E-field does not run radially when these samples are within the cavity. For the TE<sub>101</sub> mode the E-field runs parallel with the longitudinal axis of the samples, i.e. parallel to the boundaries.

### **Case 3: Two coaxially mounted cylindrical dielectric layers with longitudinal E-field**

A longitudinal E-field can exist only if the capacitor plates are mounted at the upper and lower circular surfaces of the dielectrics, and not coaxially. The condition that the E-field is perpendicular to the boundaries no longer exists. This case approximates the conditions inside the resonant cavity. The approximation is based on the assumption that there is negligible variation in the E-field across the radius  $r_2$ . The geometry of this case is illustrated in figure 5.

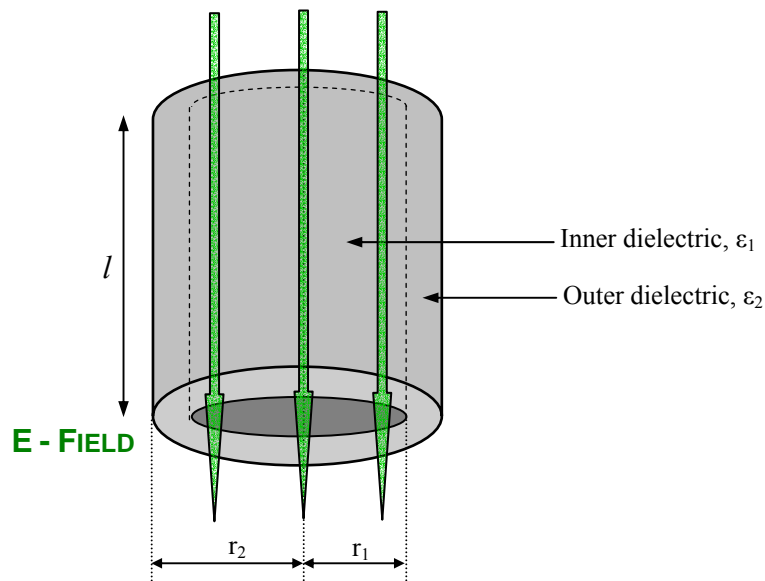


Figure 5

However, such a capacitor can be regarded as the *parallel* combination of a parallel plate capacitor having annular shaped plates of inner radius  $r_1$  and outer radius  $r_2$  with a parallel plate capacitor having circular plates of radius  $r_1$ , as illustrated in figure 6.

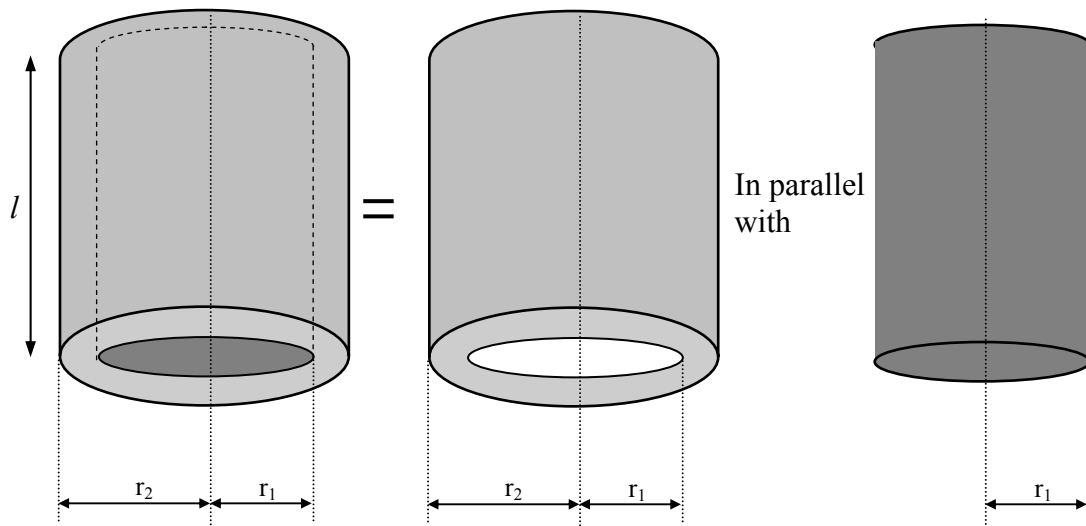


Figure 6

In general the capacitance of the parallel plate capacitor with circular plates of radius  $r_2$  is given by

$$C = \frac{\epsilon_{eff} \pi r_2^2}{l} \quad (13)$$

In this case

$$C = C_1 + C_2$$

where  $C_1 = \frac{\epsilon_2 \pi (r_2^2 - r_1^2)}{l}$  and  $C_2 = \frac{\epsilon_1 \pi r_1^2}{l}$

Therefore

$$C = \frac{\pi r_2^2}{l} \left[ \left( \frac{r_1}{r_2} \right)^2 (\epsilon_1 - \epsilon_2) + \epsilon_2 \right] \quad (14)$$

Equating (13) and (14) gives:

$$\epsilon_{eff} = \left( \frac{r_1}{r_2} \right)^2 (\epsilon_1 - \epsilon_2) + \epsilon_2 \quad \text{which is equation (4)}$$

Note that this ignores fringing effects and assumes that the dielectrics are parallel to the E-field and that there is no variation in E-field strength across  $r_2$ .

Equation (4) is also well behaved since it is trivial to show that as:

$r_1 \rightarrow 0$  (the inner dielectric is lost),  $\epsilon_{eff} \rightarrow \epsilon_2$  and as  
 $r_2 \rightarrow r_1$  (the outer dielectric is lost),  $\epsilon_{eff} \rightarrow \epsilon_1$ .

### General theories of mixed dielectrics

The effective static permittivity of two dielectrics was first derived by Weiner <sup>[4]</sup>. This work is briefly described by Campbell and Land <sup>[5]</sup> who note that the description was based on simple capacitor theory whereby a capacitor is filled with fibres of the two dielectrics stretching either from plate to plate or parallel to the plates. They quote the following pair of equations for the case of dielectric boundaries (a) parallel to the plates and (b) normal to the plates (using the notation already established in this report):

$$\frac{1}{\epsilon_{eff}} = \frac{\phi}{\epsilon_1} + \frac{(1-\phi)}{\epsilon_2} \quad \text{parallel} \quad (15a)$$

$$\epsilon_{eff} = \phi \epsilon_1 + (1-\phi) \epsilon_2 \quad \text{normal} \quad (15b)$$

where  $\phi$  is the volume fraction of dielectric 1  
and  $(1 - \phi)$  is the volume fraction of dielectric 2.

Campbell and Land go on to outline that various other mixture equations have been derived. These are equally valid for the formulation of the effective conductivity of a

dielectric mixture, however, they cannot be employed in the description of tissues as they are very much more complex than simple two phase mixtures. Furthermore, it is noted that any formula valid for static relative permittivity may easily be transposed to the case of complex relative permittivity.

(15a) is equivalent to (8) and (15b) is equivalent to (3) and hence (4), as is shown below.

### The equivalence of (3), (4) and (15b)

From an inspection of (3) and (15b) it is obvious that the two equations are equivalent to each other. With reference to figures 5 and 6:

The total volume of both dielectrics  $V_T = \pi r_2^2 l$

and the volume of the outer dielectric  $V_2 = \pi(r_2^2 - r_1^2)l$

and the volume of the inner dielectric  $V_1 = \pi r_1^2 l$

Recall (3) Weighted volumetric average =  $\left( \frac{V_1}{V_T} \varepsilon_1 \right) + \left( \frac{V_2}{V_T} \varepsilon_2 \right)$

Therefore  $\varepsilon_{eff} = \frac{\pi r_1^2 l}{\pi r_2^2 l} \varepsilon_1 + \frac{\pi(r_2^2 - r_1^2)l}{\pi r_2^2 l} \varepsilon_2$

which after cancellation and rearrangement reduces to (4).

### Extensions of the analysis

This analysis can be extended to consider more complex structures of dielectrics by considering the overall capacitance of more complex networks of capacitors. The orientation of the capacitor plates must be perpendicular to the E-field and the capacitive networks must be constructed based on the orientation of the E-field with respect to the dielectric boundaries. It is perhaps worth pointing out that the consideration of capacitors is a useful model for deriving effective permittivities of mixed dielectrics as it stems directly from the definition of permittivity. The capacitor plates do not necessarily correspond to the location of conducting surfaces in the real life application.

C. M. Alabaster  
6<sup>th</sup> April 2001

**References**

- 1 M.A. Rzepecka "A cavity perturbation method for routine permittivity measurement" Journal of microwave power vol. 8, p3-11, 1973.
- 2 M.C. Steel and R.J. Sheppard "The dielectric properties of rabbit tissue, pure water and various liquids suitable for tissue phantoms at 35GHz" Physics in medicine and biology vol. 23, No. 4, p467-472, 1998.
- 3 M.C. Steel, R.J. Sheppard and R. Collins "Precision waveguide cells for the measurement of complex permittivity of lossy liquids and biological tissue at 35GHz" J. Physics E: Scientific Instruments vol. 20, p872-877, 1987.
- 4 O. Wiener "Herkunft und Stellung der Aufgabe" Abh. Sachs. Akad. Wiss. Math-Phys. K1 vol 32, p509-604, 1912.
- 5 A.M. Campbell and D.V. Land "Dielectric properties of female human breast tissue in vitro at 3.2GHz" Physics in medicine and biology vol. 37, No. 1, p193-210, 1992.
- 6 K.F. Lee, K.Y. Ho and J.S. Dahele "Circular-Disk Microstrip Antenna with an air gap" IEEE transactions on Antennas and Propagation vol. AP-32, p880-884, 1984.

**APPENDIX C: PROGRAM LISTINGS**

The following MATLAB® programs have been written and used in the course of this work, full listings of which are reproduced here.

Debye1.m

TR3.m

P3.m

P5.m

D3TR.m

TR1.m

FindEi.m

CCfit.m

Trise.m

THIS PAGE INTENTIONALLY LEFT BLANK

**Debye1.m**

```

% A program to plot the locus of real and imaginary parts of complex
% permittivity in the vicinity of a relaxation frequency based on a
% single time constant Debye relaxation process.
%
clear all
tic
%
% INPUT VARIABLES
%
fc = 1e9;
f = 10e6:10e6:100e9;
conds = 5e-4;
Ez = 20;
Ei = 2;
%
% SET A FEW CONSTANTS
%
Eo = 8.8542e-12;
Ez = abs(Ez)
Ei = abs(Ei)
%
% A FEW INITIAL CALCULATIONS
%
tau = (2*pi*fc)^-1;
w = 2*pi.*f;
%
% MAIN CALCULATION
%
E = Ei + ((Ez-Ei)./(1+(j.*w.*tau))) - (j*conds./(w.*Eo));
%
% PLOT RESULTS
%
x1 = log10(f./fc);
x2 = real(E);
x3 = -1*imag(E);
y1 = (real(E)-Ei)./(Ez-Ei);
y2 = -1*imag(E)./(Ez-Ei);
y3 = conds./(w.*Eo);
y4 = -1*imag(E)-(conds./(w.*Eo));
y5 = f./1e9;
figure(1)
hold on
grid on
plot(x1,y1,'b-')
xlabel('Log. Normalised Frequency')
ylabel('real part of E')

```

```

title(")
figure(2)
hold on
grid on
plot(x1,y3,'g-')
plot(x1,y2,'b-')
xlabel('Log. Normalised Frequency')
ylabel('Blue = Imag part of E, Green = Conductivity')
figure(3)
hold on
grid on
plot(x2,y4,'b-')
xlabel('Real part of Permittivity')
ylabel('Imaginary part of Permittivity')
title('Locus of real and imaginary parts of E with frequency')
figure(4)
hold on
grid on
plot(y5,x2,'b-')
plot(y5,x3,'b--')
xlabel('Frequency/GHz')
ylabel('Solid line: real (Er), Broken line: Imag (Er)')
title('Complex Relative Permittivity vs. Frequency')
%
% SOME SPECIFIC RESULTS
%
for f = [fc 60e9 77e9 94e9];
    w = 2*pi.*f;
    E = Ei + ((Ez-Ei)./(1+(j.*w.*tau))) - (j*conds./(w.*Eo));
    f,E
end
toc

```

**TR3.m**

```

% To automate the calculation of transmission and reflection coefficients similar
% to ref [32] equations (1) and (2) but assumes there is no sample container.
% This program takes into account the multiple reflections between sample/air %
% interfaces.
% This program also plots the transmission and reflection coefficients as the test
% frequency is swept.
% It can also allow for dispersive materials.
%
% Sample is COMPOSITE
%
clear all
tic

```

```

%
% ENTER VARIABLES
%
for n = -1:1;
ts = 4.118e-3+(n*0.0e-3);
f = 90e9:10e6:100e9;
w = 2*pi.*f;
lambda = 3e8./f;
Ers = 3.78-(j*0.090);
%
% SET A FEW CONSTANTS
%
Ero = 1;
Eo = 8.854191e-12;
Uo = 4*pi*1e-7;
Ao = 0;
%
% CALCULATIONS
%
Es = Eo*Ers;
Bo = 2*pi./lambda;
As = w.*sqrt(((Uo*real(Es))/2)*(sqrt(1+((imag(Ers)/real(Ers))^2))-1)));
Bs = w.*sqrt(((Uo*real(Es))/2)*(sqrt(1+((imag(Ers)/real(Ers))^2))+1)));
Ko = (Ao+(j*Bo));
Ks = (As+(j*Bs));
r1 = ((sqrt(Ers)-1)^-1)/(sqrt(Ers)+1);
t = (((1-r1.^2).*exp(-1.*Ks.*ts))./(1-(r1.^2.*exp(-2.*Ks.*ts))));
r = ((r1-(r1.*exp(-2.*Ks.*ts)))./(1-(r1.^2.*exp(-2.*Ks.*ts))));
T = 20*log10(abs(t));
R = 20*log10(abs(r));
%
% PLOT RESULTS
figure(1)
hold on
grid on
plot(f/1e9,T,'r-')
xlabel('Frequency (GHz)')
ylabel('Transmission coefficient (dB)')
title('')
figure(2)
hold on
grid on
plot(f/1e9,R,'r-')
xlabel('Frequency (Hz)')
ylabel('Reflection coefficient (dB)')
title('')
end
%
toc

```

**P3.m**

```

% To calculate the complex permittivity of a sample from measurements of
% transmission and reflection coefficients assuming there is no sample container.
% This program takes into account the multiple reflections between sample/air
% interfaces.
%
% SAMPLE = Composite #25
%
clear all
tic
%
% ENTER VARIABLES
%
f = 100e9;
Rm = -4.43;
Tm = -2.65;
ts = 1.25375e-3;
%
% SET SOME CONSTANTS
%
Ero = 1;
Eo = 8.854191e-12;
Uo = 4*pi*1e-7;
Ao = 0;
%
% SOME INITIAL CALCULATIONS
%
Test_Frequency = {f/1e9 'GHz'}
w = 2*pi*f;
lambda = 3e8/f;
Bo = 2*pi/lambda;
Ko = Ao+(Bo*j);
MaxEF = 20;
%
% SET SEARCH SPACE AND RESOLUTION
%
x = [3.0:0.01:4.0];
y = [0:0.001:0.25];
z = zeros(length(x),length(y));
%
% MAIN CALCULATION
%
for n = 1:length(x);
    for m = 1:length(y);
        Ersa = x(n);
        Ersb = y(m);

```

```

Ers = Ersa -j*Ersb;
Ks = sqrt(Ers)*Ko;

r1 = ((sqrt(Ers)-1)*-1)/(sqrt(Ers)+1);
tc = (((1-r1^2)*exp(-ts*Ks))/(1-(r1^2*exp(-2*ts*Ks)))); 
rc = ((r1-(r1*exp(-2*ts*Ks)))/(1-(r1^2*exp(-2*ts*Ks)))); 
Tc = 20*log10(abs(tc)+eps);
Rc = 20*log10(abs(rc)+eps);

Error_Factor=(((abs(abs(Tc)-abs(Tm))/(2*abs(Tm)))+((abs(abs(Rc)-
abs(Rm))/(2*abs(Rm))))*100;
%
% Meshed plot of solutions
%
z(n,m) = 1/Error_Factor;
%mesh(y,x,z);
%
% Updates best solution
%
if Error_Factor < MaxEF
    MaxEF = Error_Factor;
    Best_Ers=Ers;
    Best_Error_Factor=Error_Factor;
    Best_Tc=Tc;
    Best_Rc=Rc;
    Best_Ks=Ks;
else
end

end
end
%
% DISPLAYS RESULTS OF BEST SOLUTION
%
disp RESULTS
Best_Ers
Best_Error_Factor
Best_Tc;
Best_Rc;
Best_Ks;
Toc

```

**P5.m**

```
% To calculate the complex permittivity of a sample from measurements
% of transmission and reflection coefficients assuming there is no
% sample container. This program finds the complex permittivity
% which results in the best fit to the measured transmission and
% reflection coefficients at a number of discrete frequencies.
% This program takes into account the multiple reflections between sample/air
% interfaces.
%
% SAMPLE = Composite #16
%
clear all
tic
%
% ENTER VARIABLES
%
format short
f=[90e9:2e9:100e9];
ts = 1.36e-3
Rm = [-6.2 -6.7 -8.0 -9.6 -11.6 -14.8];
Tm = [-2.13 -1.87 -1.62 -1.45 -1.36 -1.34];
tstol = 0.02e-3;
Rmtol = 0.36;
Tmtol = 0.14;
%
% SET A FEW CONSTANTS
%
Ero = 1;
Eo = 8.854191e-12;
Uo = 4*pi*1e-7;
Max_score = 20;
%
% A FEW INITIAL CALCULATIONS
%
lambda = 3e8./f;
Ao = 0;
Bo = 2*pi./lambda;
Ko = Ao+(Bo.*j);
%
% MAIN CALCULATION
%
% Sets range of search space and resolution
%
x = [4.0:0.01:5.0];
y = [0:0.001:0.25];
%
% Calculates trial Ers and Ks and increments successive trial values
```

```

%
for n = 1:length(x);
for m = 1:length(y);

Ersa = x(n);
Ersb = y(m);
Ers = Ersa -j*Ersb;
Ks = sqrt(Ers).*Ko;
%
% Main calculation
%
r1 = ((sqrt(Ers)-1)/(sqrt(Ers)+1));
tc = (((1-r1.^2).*exp(-ts.*Ks))./(1-(r1.^2.*exp(-2*ts.*Ks)))); 
rc = ((r1-(r1.*exp(-2*ts.*Ks)))./(1-(r1.^2.*exp(-2*ts.*Ks)))); 
Tc = 20.*log10(abs(tc)+eps);
Rc = 20.*log10(abs(rc)+eps);
%
% Calculates rms percentage error over all T and R data points
%
delta_T = (Tc-Tm).*100./Tm;
delta_R = (Rc-Rm).*100./Rm;
score = sqrt((sum(delta_T.^2)+sum(delta_R.^2))/(length(Tm)+length(Rm)));
%
% Keeps the lowest score and best solution
%
if score < Max_score
    Max_score = score;
    Best_score = score;
    Best_Ers=Ers;
    Best_Tc=Tc;
    Best_Rc=Rc;
    Best_Ks=Ks;
else
end

end
end
%
% RESULTS OUTPUT
%
disp RESULTS
Best_Ers
Best_score
Best_Tc;
Best_Rc;
Best_Ks;
%

```

```

% Follow on program from TR3.m to plot transmission and reflection
% coefficients from best solution and overlay measured data.
%
for n = -1:1;
tss = ts+(n*tstol);
fs = 90e9:10e6:100e9;
w = 2*pi.*fs;
Ers = Best_Ers;
Es = Eo*Ers;
As = w.*((sqrt(((Uo*real(Es))/2)*(sqrt(1+((imag(Ers)/real(Ers))^2))-1))));
Bs = w.*((sqrt(((Uo*real(Es))/2)*(sqrt(1+((imag(Ers)/real(Ers))^2))+1))));
Ko = (Ao+(j*Bo));
Ks = (As+(j*Bs));
r1 = ((sqrt(Ers)-1)*-1)./(sqrt(Ers)+1);
t = (((1-r1.^2).*exp(-1.*Ks.*tss))./(1-(r1.^2.*exp(-2.*Ks.*tss)))); %Transmission coefficient
r = ((r1-(r1.*exp(-2.*Ks.*tss)))./(1-(r1.^2.*exp(-2.*Ks.*tss)))); %Reflection coefficient
T = 20*log10(abs(t));
R = 20*log10(abs(r));
figure(1)
hold on
grid on
plot(fs,T,'b-')
plot(f,Tm,'r+')
plot(f,Tm+Tmtol,'r+')
plot(f,Tm-Tmtol,'r+')
xlabel('Frequency (Hz)')
ylabel('Transmission coefficient (dB)')
title('sample #16')
figure(2)
hold on
grid on
plot(fs,R,'g-')
plot(f,Rm,'r+')
plot(f,Rm+Rmtol,'r+')
plot(f,Rm-Rmtol,'r+')
xlabel('Frequency (Hz)')
ylabel('Reflection coefficient (dB)')
title('sample #16')
end
%
toc

```

**D3TR.m**

```

% General 3-layered dielectric structure.
%
% To predict transmission and reflection coefficients.
%
% INPUT DATA
%
f = 90e9:0.01e9:100e9;
t1 = 1.254e-3;
t2 = 1.60e-3;
t3 = 1.264e-3;
Er1 = 3.78 - (j*0.086);
Er2 = 1 - (j*0);
Er3 = 3.78 - (j*0.093);
%
% SET A FEW CONSTANTS
%
E0 = 8.854191e-12;
Er0 = 1;
Er4 = 1;
U0 = 4*pi*1e-7;
%
% SOME PRELIMINARY CALCULATIONS
%
w = 2.*pi.*f;
lambda = 3e8./f;
%
E1 = E0*Er1;
E2 = E0*Er2;
E3 = E0*Er3;
%
A0 = 0;
B0 = 2*pi./lambda;
K0 = (A0+(j.*B0));
%
A1 = w.*(sqrt(((U0*real(E1))/2).*(sqrt(1+((imag(Er1)/real(Er1))^2))-1)));
B1 = w.*(sqrt(((U0*real(E1))/2).*(sqrt(1+((imag(Er1)/real(Er1))^2))+1)));
K1 = (A1+(j.*B1));
%
A2 = w.*(sqrt(((U0*real(E2))/2).*(sqrt(1+((imag(Er2)/real(Er2))^2))-1)));
B2 = w.*(sqrt(((U0*real(E2))/2).*(sqrt(1+((imag(Er2)/real(Er2))^2))+1)));
K2 = (A2+(j.*B2));
%
A3 = w.*(sqrt(((U0*real(E3))/2).*(sqrt(1+((imag(Er3)/real(Er3))^2))-1)));
B3 = w.*(sqrt(((U0*real(E3))/2).*(sqrt(1+((imag(Er3)/real(Er3))^2))+1)));
K3 = (A3+(j.*B3));
%
```

```

% CALCULATE THE REFLECTION COEFFICIENTS AT INTERFACES
%
r01 = ((sqrt(Er1)-sqrt(Er0)).*-1)./(sqrt(Er1)+sqrt(Er0));
r12 = ((sqrt(Er2)-sqrt(Er1)).*-1)./(sqrt(Er2)+sqrt(Er1));
r23 = ((sqrt(Er3)-sqrt(Er2)).*-1)./(sqrt(Er3)+sqrt(Er2));
r34 = ((sqrt(Er4)-sqrt(Er3)).*-1)./(sqrt(Er4)+sqrt(Er3));
%
r10 = -1.*r01;
r21 = -1.*r12;
r32 = -1.*r23;
r43 = -1.*r34;
%
% CALACULATION OF COEFFICIENTS FOR EACH LAYER
%
% first layer
%
one0_1 = (r01+(r12.*exp(-2.*K1.*t1)))./(1+(r01.*r12.*exp(-2.*K1.*t1)));
two0_1 = ((1+r12).*(1+r01).*exp(-K1.*t1))./(1+(r01.*r12.*exp(-2.*K1.*t1)));
three0_1 = (r12.*(1+r01).*exp(-2.*K1.*t1))./(1+(r01.*r12.*exp(-2.*K1.*t1)));
four0_1 = ((1+r01).*exp(-K1.*t1))./(1+(r01.*r12.*exp(-2.*K1.*t1)));
%
oned2_1 = (r21+(r10.*exp(-2.*K1.*t1)))./(1+(r10.*r21.*exp(-2.*K1.*t1)));
twod2_1 = ((1+r10).*(1+r21).*exp(-K1.*t1))./(1+(r10.*r21.*exp(-2.*K1.*t1)));
threed2_1 = (r10.*(1+r21).*exp(-2.*K1.*t1))./(1+(r10.*r21.*exp(-2.*K1.*t1)));
fourd2_1 = ((1+r21).*exp(-K1.*t1))./(1+(r10.*r21.*exp(-2.*K1.*t1)));
%
% second layer
%
one1_2 = (r12+(r23.*exp(-2.*K2.*t2)))./(1+(r12.*r23.*exp(-2.*K2.*t2)));
two1_2 = ((1+r23).*(1+r12).*exp(-K2.*t2))./(1+(r12.*r23.*exp(-2.*K2.*t2)));
three1_2 = (r23.*(1+r12).*exp(-2.*K2.*t2))./(1+(r12.*r23.*exp(-2.*K2.*t2)));
four1_2 = ((1+r12).*exp(-K2.*t2))./(1+(r12.*r23.*exp(-2.*K2.*t2)));
%
oned3_2 = (r32+(r21.*exp(-2.*K2.*t2)))./(1+(r32.*r21.*exp(-2.*K2.*t2)));
twod3_2 = ((1+r21).*(1+r32).*exp(-K2.*t2))./(1+(r32.*r21.*exp(-2.*K2.*t2)));
threed3_2 = (r21.*(1+r32).*exp(-2.*K2.*t2))./(1+(r32.*r21.*exp(-2.*K2.*t2)));
fourd3_2 = ((1+r32).*exp(-K2.*t2))./(1+(r32.*r21.*exp(-2.*K2.*t2)));
%
% third layer
%
one2_3 = (r23+(r34.*exp(-2.*K3.*t3)))./(1+(r23.*r34.*exp(-2.*K3.*t3)));
two2_3 = ((1+r34).*(1+r23).*exp(-K3.*t3))./(1+(r23.*r34.*exp(-2.*K3.*t3)));
three2_3 = (r34.*(1+r23).*exp(-2.*K3.*t3))./(1+(r23.*r34.*exp(-2.*K3.*t3)));
four2_3 = ((1+r23).*exp(-K3.*t3))./(1+(r23.*r34.*exp(-2.*K3.*t3)));
%
oned4_3 = (r43+(r32.*exp(-2.*K3.*t3)))./(1+(r43.*r32.*exp(-2.*K3.*t3)));
twod4_3 = ((1+r32).*(1+r43).*exp(-K3.*t3))./(1+(r43.*r32.*exp(-2.*K3.*t3)));
threed4_3 = (r32.*(1+r43).*exp(-2.*K3.*t3))./(1+(r43.*r32.*exp(-2.*K3.*t3)));

```

```

fourd4_3 = ((1+r43).*exp(-K3.*t3))./(1+(r43.*r32.*exp(-2.*K3.*t3)));
%
% COMBINING LAYERS 1 & 2
%
one0_12 = one0_1 + ((four0_1.*three1_2.*twod2_1)./(1-(threed2_1.*three1_2)));
two0_12 = (four0_1.*two1_2)./(1-(threed2_1.*three1_2));
three0_12 = three0_1 + ((four0_1.*three1_2.*fourd2_1)./(1-(threed2_1.*three1_2)));
four0_12 = (four0_1.*four1_2)./(1-(threed2_1.*three1_2));
%
oned3_12 = oned3_2 + ((fourd3_2.*threed2_1.*two1_2)./(1-(threed2_1.*three1_2)));
twod3_12 = (fourd3_2.*twod2_1)./(1-(threed2_1.*three1_2));
threed3_12 = threed3_2 + ((fourd3_2.*threed2_1.*four1_2)./(1-(threed2_1.*three1_2)));
fourd3_12 = (fourd3_2.*fourd2_1)./(1-(threed2_1.*three1_2));
%
% COMBINING LAYERS 12 & 3
%
t = (four0_12.*two2_3)./(1-(three2_3.*threed3_12));
r = one0_12 + ((four0_12.*three2_3.*twod3_12)./(1-(three2_3.*threed3_12)));
%
% OUTPUTTING RESULTS IN dB
%
T = 20.*log10(abs(t));
R = 20.*log10(abs(r));
%
% Measured Data
% for n = -1:1;
% Ttol = 0.05;
% Rtol = 0.36;
% T = [-1.69 -1.41 -1.225 -1.145 -1.135 -1.17 -1.24 -1.37 -1.58 -1.89 -2.295]...
% -n*Ttol*ones(1,11);
% R = [-7.77 -10.24 -13.74 -18.145 -19.24 -15.445 -12.33 -9.90 -8.145 -6.815 -5.645]...
% -n*Rtol*ones(1,11);
%
% PLOT FIGURES
%
figure(1)
hold on
grid on
plot(f/1e9,T,'b-')
xlabel('Frequency (GHz)')
ylabel('Transmission coefficient (dB)')
title('3 layered structure')
figure(2)
hold on
grid on
plot(f/1e9,R,'b-')
xlabel('Frequency (GHz)')

```

```

ylabel('Reflection coefficient (dB)')
title('3 layered structure')
end

```

**TR1.m**

```

% To automate the calculation of transmission and reflection coefficients from ref
% [32] equations (1) and (2). This takes into account the effects of a sample
% container and of multiple reflections between interfaces.
% This program also plots the transmission and reflection coefficients as the test
% frequency is swept. It can also allow for dispersive materials.
%
clear all
tic
%
% ENTER VARIABLES
%
%for n = -1:1;
%for m = -1:1;
f = 9e9:10e6:10e9;
Erc = 2.55 - (j*0.07);
Ers = 20 - (j*1);
tc = 3e-3;%+(m*0.01e-3);
ts = 30e-3;%+(n*0.05e-3);
%
% SET A FEW CONSTANTS
%
Ero = 1;
Eo = 8.854191e-12;

Uo = 4*pi*1e-7;
%
% CALCULATIONS
%
w = 2*pi.*f;
lambda = 3e8./f;
Ec = Eo*Erc;
Es = Eo*Ers;
Ao = 0;
Bo = 2*pi./lambda;
Ac = w.*((sqrt(((Uo.*real(Ec))/2).*((sqrt(1+((imag(Erc)./real(Erc)).^2))-1))))));
Bc = w.*((sqrt(((Uo.*real(Ec))/2).*((sqrt(1+((imag(Erc)./real(Erc)).^2))+1))))));
As = w.*((sqrt(((Uo.*real(Es))/2).*((sqrt(1+((imag(Ers)./real(Ers)).^2))-1))))));
Bs = w.*((sqrt(((Uo.*real(Es))/2).*((sqrt(1+((imag(Ers)./real(Ers)).^2))+1))))));
Ko = (Ao+(j*Bo));
Kc = (Ac+(j*Bc));
Ks = (As+(j*Bs));

```

```

r1 = ((sqrt(Erc)-sqrt(Ero)).*-1)./(sqrt(Erc)+sqrt(Ero));
r2 = ((sqrt(Ers)-sqrt(Erc)).*-1)./(sqrt(Ers)+sqrt(Erc));
t = abs(((1-(r1).^2).*((1-(r2).^2).*exp(-2.*Kc.*tc).*exp(-1.*Ks.*ts)))./(((1+(r1.*r2.*exp(-2.*Kc.*tc))).^2)...
    -(((r1.*exp(-2.*Kc.*tc)+r2).^2).*exp(-2.*Ks.*ts))));;
r = abs((((1+(r1.*r2.*exp(-2.*Kc.*tc))).*(r1+(r2.*exp(-2.*Kc.*tc))))-...
    ((r2+(r1.*exp(-2.*Kc.*tc))).*((r1.*r2)+exp(-2.*Kc.*tc).*exp(-2.*Ks.*ts)))./...
    (((1+(r1.*r2.*exp(-2.*Kc.*tc))).^2)-...
    (((r2+(r1.*exp(-2.*Kc.*tc))).^2).*exp(-2.*Ks.*ts))));;
T = 20.*log10(t);
R = 20.*log10(r);
%
% PLOTS RESULTS
%
figure(1)
hold on
grid on
plot(f,T,'b-')
xlabel('Frequency (Hz)')
ylabel('Transmission coefficient (dB)')
title('Container plus sample, incl. MR')
figure(2)
hold on
grid on
plot(f,R,'g-')
xlabel('Frequency (Hz)')
ylabel('Reflection coefficient (dB)')
title('Container plus sample, incl. MR')
%end
%end
toc

```

### FindEi.m

```

% A program to find the value of permittivity at some frequency
% infinitely higher than the relaxation frequency, by fitting
% trial values to measured data.
%
clear all
tic
%
% INPUT DATA
%
f = [25e9 60e9 77e9 94e9];
Em = [43.7972-j*36.7261 17.9368-j*26.0777 14.0756-j*21.5739 11.9234-j*18.2447];
fc = 25e9;
Ez = 78-j*20;

```

```

conds = 0;
%
% SET A FEW CONSTANTS
%
Eo = 8.85e-12;
Ez = abs(Ez);
Max_score = 1000;
%
% A FEW PRELIMINARY CALCULATIONS
%
tau = (2*pi*fc)^-1;
w = 2*pi.*f;
%
% MAIN CALCULATION
%
% Sets range of search space and resolution
%
x = [6.9:0.001:7.2];
%
% Calculates trial complex E and increments successive trial values
%
for Ei = 1:length(x);
    Ec = Ei + ((Ez-Ei)./(1+(j.*w.*tau))) - (j*conds./(w.*Eo));
    %
    % Calculates rms percentage error over all data points
    %
    delta_Ere = (real(Ec)-real(Em)).*100./real(Em);
    delta_Eim = (imag(Ec)-imag(Em)).*100./imag(Em);
    score = sqrt((sum(delta_Ere.^2)+sum(delta_Eim.^2))/(2*length(Ec)));
    %
    % Keeps the lowest score and best solution
    %
    if score < Max_score
        Max_score = score;
        Best_score = score;
        Best_Ec=Ec;
        Best_Ei=Ei;
    else
        end
    end
    %
    % RESULTS OUTPUT
    disp RESULTS
    Best_Ei
    Best_score
    Best_Ec
    %
    toc

```

**CCfit.m**

```

% A program to find parameter values of a single term Cole-Cole
% function providing the best fit to measured permittivity data.
%
clear all
tic
%
% INPUT DATA
%
f = [60e9 77e9 94e9];
Em = [15.76-j*16.00 11.55-j*6.09 8.78-j*5.54];
%
% SET A FEW CONSTANTS
%
Eo = 8.854191e-12;
Max_score = 100;
%
% MAIN CALCULATION
%
% Sets range of search space and resolution
%
a = [10:0.1:50];           % static permittivity
b = [1:0.1:20];           % infinite permittivity
c = [5e9:1e8:30e9];       % relaxation frequency
d = [0:0.01:2.0];         % static conductivity
e = [0:0.01:1.0];         % alpha parameter
%
% Calculates successive trial values
%
for m = 1:length(a);
for n = 1:length(b);
for o = 1:length(c);
for p = 1:length(d);
for q = 1:length(e);
    Ez = a(m);
    Ei = b(n);
    fc = c(o);
    cond = d(p);
    alpha = e(q);

    tau = (2*pi*fc)^-1;
    w = 2*pi.*f;

    Ec = Ei + ((Ez-Ei)./(1+(j.*w.*tau).^(1-alpha))) - (j*cond./(w.*Eo));
    %
    % Calculates rms percentage error over all data points
    %
end;
end;
end;
end;
end;

```

```

delta_Ere = (real(Ec)-real(Em)).*100./real(Em);
delta_Eim = (imag(Ec)-imag(Em)).*100./imag(Em);
score = sqrt((sum(delta_Ere.^2)+sum(delta_Eim.^2))/(2*length(Ec)));
%
% Keeps the lowest score and best solution
%
if score < Max_score
    Max_score = score;
    Best_score = score;
    Best_Ec=Ec;
    Best_Ei=Ei;
    Best_Ez=Ez;
    Best_fc=fc;
    Best_conds=conds;
    Best_alpha=alpha;
else
    end
end
end
end
end
end
%
% RESULTS OUTPUT
%
disp RESULTS
Best_Ei
Best_Ez
Best_fc
Best_conds
Best_alpha
Best_score
Best_Ec
%
toc

```

**Trise.m**

```
% To solve the model for surface temperature rises.  
%  
% USER INPUTS  
%  
C1 = 46.99e-3;  
C2 = 78.74e-3;  
tau = 3.574;  
%  
% MAIN CALCULATION  
%  
t = 0:0.1:30;  
Tsur = (C1.*sqrt(t))-(C2.*(1-(exp(t/tau)).*(erfc(sqrt(t./tau)))));  
%  
% PLOT RESULTS  
%  
figure(1)  
hold on  
grid on  
plot(t,Tsur,'b-')  
xlabel('Time, seconds')  
ylabel('Temperature Rise, degrees')
```

THIS PAGE INTENTIONALLY LEFT BLANK